

DNA-mediated Arrangement of Chromophores **- Potential Use for Diagnostic Applications**

Inauguraldissertation
der Philosophisch-naturwissenschaftlichen Fakultät
der Universität Bern

vorgelegt von
Sarah Maria Biner
aus St.Niklaus (VS)



Leiter der Arbeit:
Prof. Dr. Robert Häner
Departement für Chemie und Biochemie der Universität Bern

DNA-mediated Arrangement of Chromophores

- Potential Use for Diagnostic Applications

Inauguraldissertation
der Philosophisch-naturwissenschaftlichen Fakultät
der Universität Bern

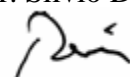
vorgelegt von
Sarah Maria Biner
aus St.Niklaus (VS)

Leiter der Arbeit:
Prof. Dr. Robert Häner
Departement für Chemie und Biochemie der Universität Bern

Von der Philosophisch-naturwissenschaftlichen Fakultät angenommen.

Bern, den 16. März 2012

Der Dekan:
Prof. Dr. Silvio Decurtins



This work was supported by the University of Bern and the Swiss National Science Foundation.

*Für meine Eltern,
Liliane & Berni*

und für

Dani

*Nimm es als Vergnügen,
und es ist Vergnügen.
Nimm es als Qual,
und es ist Qual.*
(ind. Weisheit)

ACKNOWLEDGEMENT

First of all I would like to thank *Prof. Dr. Robert Häner* for giving me the opportunity to do my Ph.D. work in his research group. Especially for his confidence, his support and that he gave me the chance to join conferences and contribute to meetings.

Special thanks go to *Prof. Dr. Dipl. Ing. Ronald Micura* from the Institute of Organic Chemistry at the Center for Molecular Biosciences at the Leopold Franzens University of Innsbruck for being my co-referee and examiner and to *Prof. Dr. Andreas Türlér* from the Department of Chemistry & Biochemistry at University of Berne and the Laboratory for Radiochemistry and Environmental Chemistry at the Paul Scherrer Institute in Villigen who kindly agreed to supervise and chair my final examination.

Many thanks go to the team of *Prof. Dr. Rolf Jaggi* from the Department of Clinical Research at the University of Bern for their contribution to the applicability studies.

Sincere thanks go to *Daniel Wenger* for teaching, instructing and supporting me with numerous helpful and enriching discussions over the last four years as well as for the critical and careful reading of my thesis. Many thanks go to *Simon M. Langenegger* for his interest in molecular beacons, to *Cyril A. Fuhrer* for many valuable discussions and to *Anna-Barbara Gerber* for her support and help during the past.

Many thanks go to *Martin Rauber*, *Dominic Kummer* and *Markus Probst* for giving me the opportunity to supervise them. In addition, I would like thank all the past and current members of *the Häner and the Leumann group* for help, support and good times.

Furthermore, special thanks go to the team of *Dr. Stefan Schürch* for their analytical service, *Prof. Dr. Peter Bigler* and the NMR- team, the “*Ausgabe*”-team, the *technical and electronic support team*, the *administration desks* and the team from the library.

Äs ganz es speziells MERCI geit an mini Famili und Fröinde, wa mich in all der Ziit immär unnerschtiizt und mer kholfu hent und ohni di das apa nid eso weeri üsser cho wies jetzu isch.

Im speziellu ds'erwäänu sind minä Brüedär, wa der Ziit hie am DCB en familiärä Astrich gigää het, mini Studiukollegä, wa di eimaalig Ziit unvergässlich hent gmacht und natiirli wellti ich öi minum Fröind dum Dani merci sägu, ver eifach alles.

Finally, I would like to thank those who I forgot to mention here, but who in one way or the other have contributed to the present thesis.

LIST OF PUBLICATIONS

- ❖ Ivan Trkulja, Sarah M. Biner, Simon M. Langenegger and Robert Häner, **A Molecular Probe for the Detection of Homopurine sequences**, *ChemBioChem* **2007**, 8, 25-27.

- ❖ Robert Häner, Sarah M. Biner, Simon M. Langenegger, Tao Meng and Vladimir L. Malinovskii, **A Highly Sensitive, Excimer-Controlled Molecular Beacon**, *Angew. Chem. Int. Ed.* **2010**, 49, 1227–1230.

- ❖ Sarah M. Biner, Dominic Kummer, Vladimir L. Malinovskii and Robert Häner, **Signal Control by Self-Assembly of Fluorophores in a Molecular Beacon – A Model Study**, *Org. Biomol. Chem.* **2011**, 9, 2628-2633.

- ❖ Sarah M. Biner and Robert Häner, **A Two-Color, Self-Controlled Molecular Beacon**, *ChemBioChem* **2011**, 12, 2733-2736.

- ❖ Markus Probst, Daniel Wenger, Sarah M. Biner, Robert Häner, **The DNA Three-way Junction as a Mould for Tripartite Chromophore Assembly**, *Org. Biomol. Chem.* **2012**, 10, 755-759.

- ❖ Sarah M. Biner and Robert Häner, **Triplex-Mediated Molecular Assembly of Polyaromatic Base Surrogates**, *manuscript in preparation*.

TABLE OF CONTENTS

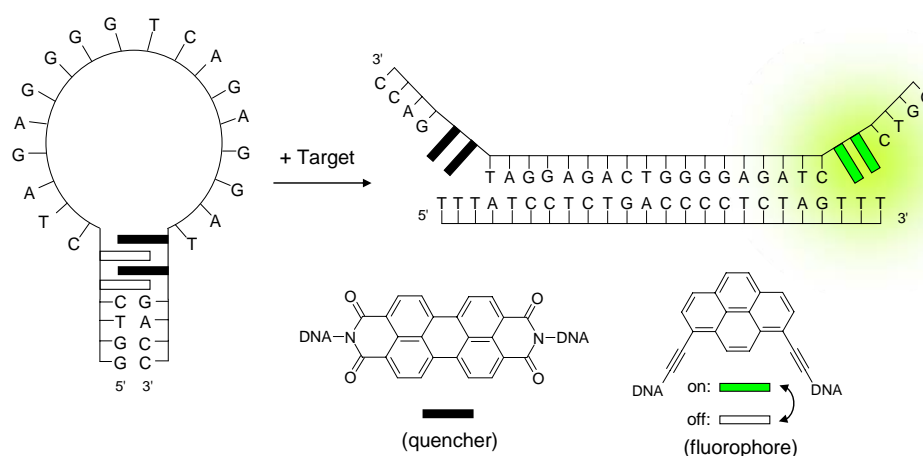
SUMMARY	1
1. GENERAL INTRODUCTION	
1.1 DNA – A Historical Overview	3
1.2 The Double Helix – A Closer Look.....	9
1.3 Structural Elements	16
1.4 Tertiary Structural Elements.....	18
1.4.1 Triplex Structures	19
1.4.2 Quadruplex Structures	22
1.4.3 Branched Structures.....	23
1.5 Molecular Beacons	26
1.5.1 Signal Control System.....	32
1.6 Aim of the Work.....	37
1.7 Importance of the Work.....	38
1.8 References	39
2. A HIGHLY SENSITIVE, EXCIMER-CONTROLLED MOLECULAR BEACON	
2.1 Abstract.....	43
2.2 Introduction	43
2.3 Investigation of a donor-acceptor based MB.....	45
2.3.1 Spectroscopic investigation of the MB by fluorescence measurements.....	46
2.3.2 Selectivity study of the MB	47
2.3.3 Investigation of the donor-acceptor based signal control system.....	48
2.3.4 Sensitivity study of the excimer-controlled MB.....	51
2.4 Conclusion.....	53
2.5 Experimental Part.....	54
2.6 References	57
3. SIGNAL CONTROL BY SELF-ASSEMBLY OF FLUOROPHORES IN A MOLECULAR BEACON – A MODEL STUDY	
3.1 Abstract.....	61
3.2 Introduction	61
3.3 Investigation of the multichromophoric detection system.....	64
3.4 Conclusion.....	75
3.5 Experimental Part.....	77
3.6 References	80

4.	PRELIMINARY STUDIES FOR DIAGNOSTIC APPLICATIONS OF AN EXCIMER-CONTROLLED MOLECULAR BEACON	
4.1	Abstract.....	85
4.2	Introduction	85
4.3	Application as probes in qPCR.....	87
4.3.1	Spectroscopic comparison of the two hybridization probes	88
4.4	Direct rRNA hybridization assays.....	91
4.5	Conclusion.....	96
4.6	Experimental Part	97
4.7	References	99
5.	TRIPLE HELIX MEDIATED ARRANGEMENT OF CHROMOPHORES	
5.1	Abstract.....	103
5.2	Introduction	103
5.3	Spectroscopic behaviour of triple-helical mediated chromophoric complexes	105
5.4	Conclusion.....	119
5.5	Experimental Part	120
5.6	References	122
6.	A TWO-COLOR, SELF-CONTROLLED MOLECULAR BEACON	
6.1	Abstract.....	125
6.2	Introduction	125
6.3	Investigation of a triple-helical stem design.....	127
6.4	Conclusion.....	136
6.5	Experimental Part	137
6.6	References	139
7.	TRIPLEX-MEDIATED MOLECULAR ASSEMBLY OF POLYAROMATIC BASE SURROGATES	
7.1	Abstract.....	143
7.2	Introduction	143
7.3	Investigation of the chromophoric arrangement by spectroscopic measurements	146
7.4	Conclusion.....	154
7.5	Experimental Part	155
7.6	References	157

8.	ORGANIZATION OF OLIGOPYRENE FOLDAMERS IN A BI- SEGMENTAL DNA STRAND DESIGN	
8.1	Abstract.....	161
8.2	Introduction	161
8.3	Spectroscopic study of bi-segmental, double- and triple-stranded structures	163
8.4	Conclusion.....	173
8.5	Experimental Part.....	175
8.6	References	177
9.	OUTLOOK	179
APPENDIX.....		183
A.1	List of Abbreviations.....	185
A.2	List and Collection of the Publications presented in this Work	189
A.3	Curriculum Vitae.....	205
A.4	Erklärung.....	207

SUMMARY

The projects presented in this work are based on the incorporation of polyaromatic, non-nucleosidic building blocks into a DNA framework. The artificial base surrogates are pyrene derivatives and perylenediimide moieties. The interactions and spectroscopic properties of these chromophores are highly interesting and perfectly suitable for the design of signal control systems. Since the bright fluorescence emission of a pyrene dimer can be completely quenched by perylenediimide molecules. First, a molecular beacon with two electron-rich 1,8-dialkynylpyrene units and two electron-poor 3,4,9,10-perylenetetracarboxylic diimide (PDI) building blocks was synthesized and studied (*Chapter 2*). The excellent efficiency of fluorescence suppression renders this type of hybridization probe into a highly sensitive tool for molecular diagnostics. Beside that, this donor-acceptor based molecular beacon is able to differentiate targets by a single mismatch militates in favour of high selectivity.



To gain further information of how these polyaromatic units interact and ensure the above mentioned properties additional stem designs were investigated (*Chapter 3* and *Chapter 6*). The stem design is of crucial importance for a successful creation of a useful molecular beacon. The probe-target hybrid has to have a higher stability as the duplex formed in the stem. Otherwise no detection of target sequences is performed. Additionally, the stem was kept as short as possible up to a stemless version to prevent undesirable base-pairing. In another

approach, the double-helical stem was replaced by a triplex forming structure. There, both chromophores (alkynylpyrene and perylenediimide derivatives) emit fluorescence and quench each other mutually.

The formation of higher ordered structures like triple helices can be visualized with the same donor-acceptor pair (*Chapter 7* and *Chapter 8*). The transitions from a triple-helical structure to a duplex and finally to a random coil structure can be followed based on different interactions between the incorporated artificial base surrogates and the corresponding fluorescence read-out. The strong stacking interactions between these polyaromatic molecules can be further utilized for the construction of DNA architectures (*Outlook*).

1. General Introduction

1.1 DNA – A Historical Overview

Besides the opening of the *Suez Canal*, the construction start of the *Neuschwanstein castle* or the publication of the first *Nature* issue, important contributions in science were done in the year 1869.^[1;2] The periodic system of the elements was developed independently by a German scientist *Lothar Meyer* and a Russian chemist *Dimitrij I. Mendelejew*.^[3] In late 1869, the Swiss physiological chemist *Friedrich Miescher* (**Figure 1.1**) submitted a manuscript containing the description of a new substance called *nuclein*.^[4;5] This macromolecule was isolated from the nuclei of leukocyte cells gained from pus. Later *Miescher* extracted nuclein from salmon spermatozoa, which was easily available and cheap. The isolation and recognition of nuclein leads him to the scientist who discovered DNA.

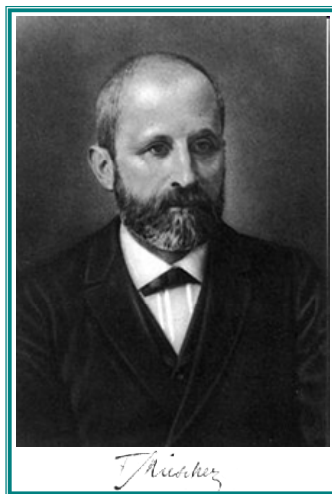


Figure 1.1. *Friedrich Miescher* (1844 – 1895).^[5]

It so happened that in the same year the scientist *Phoebus Aaron Levene* was born (**Figure 1.2**).^[6] He was a natural product chemist who discovered ribose and deoxyribose in RNA and DNA respectively, as well as the phosphate-base-sugar unit known as *nucleotide*. Unfortunately he is now known for his wrongly interpreted “*tetranucleotide hypothesis*”.^[7] At the time of *Levene* proteins were thought to contain the genetic information of cells. This was the state of the art till *Oswald Avery* (**Figure 1.2**) and his co-workers aduced the coherence of

DNA concerning its significance in heredity by the *Avery–MacLeod–McCarty* experiment.^[8;9] Prior to the findings of DNA as the genetic material the scientist *William Astbury* (Figure 1.2) produced first X-ray diffraction patterns of DNA in 1937.^[10;11] He was a pioneer in studying biological molecules with X-ray diffraction measurements. These data already showed the regularity of the structure and were used later by *Linus Pauling* (Figure 1.2) for his interpretation of the DNA structure.^[12;13]



Figure 1.2. From left to right: *Pheobus Aaron Levene* (1869 – 1940),^[6] *Oswald Theodore Avery* (1877 – 1955),^[8] *William Astbury* (1898 – 1961)^[10] and *Linus Pauling* (1901 – 1994).^[12]

However, it should take a few more years until a final structure determination was claimed. In the same year *Rudolf Signer*, a Bernese chemist started to work with DNA as a highly molecular substance (Figure 1.3).^[14;15] He developed an apparatus able to measure molecules based on an optical method. With the flow birefringence method *Signer* investigated polymers, determined the size and performed molecular weight calculations of macromolecules.^[15-19]

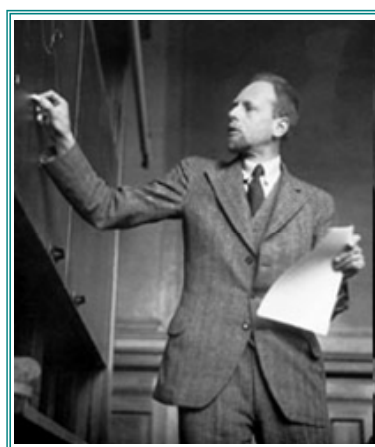


Figure 1.3. *Rudolf Signer* (1903 – 1990).^[14]

His results describe DNA as a rod-like structure where the bases are arranged perpendicular to the longitudinal axis of the molecule. However, he generally became known for his extraction of intact high quality DNA samples.

A few grams of such a high quality sample were given to *Maurice Wilkins* who was working in the lab of *Sir John Turton Randall* at the King's College in London.^[14] Not only *Maurice Wilkins* but also *Rosalind Franklin* performed investigations, X-ray diffraction measurements and interpretations in *Randall's* lab based on *Signer's* samples (Figure 1.4). Conflicts between the researchers lead to parallel studies of DNA.^[20-22] *Rosalind Franklin* and her PhD student *Raymond Gosling* discovered the existence of an A- and B-form of DNA differing only in the water content. Moreover, the DNA X-ray diffraction photographs taken by *Rosalind Franklin* were the best pictures at the time.^[23] The spirit of competition present between *Franklin* and *Wilkins* was noticeable for all. *Maurice Wilkins* got the help of *Herbert R. Wilson* and *Alex Strokes* in evaluating the obtained data. Beyond that he was in close contact with a researcher at the Cavendish Laboratory in Cambridge namely *Francis Crick*.

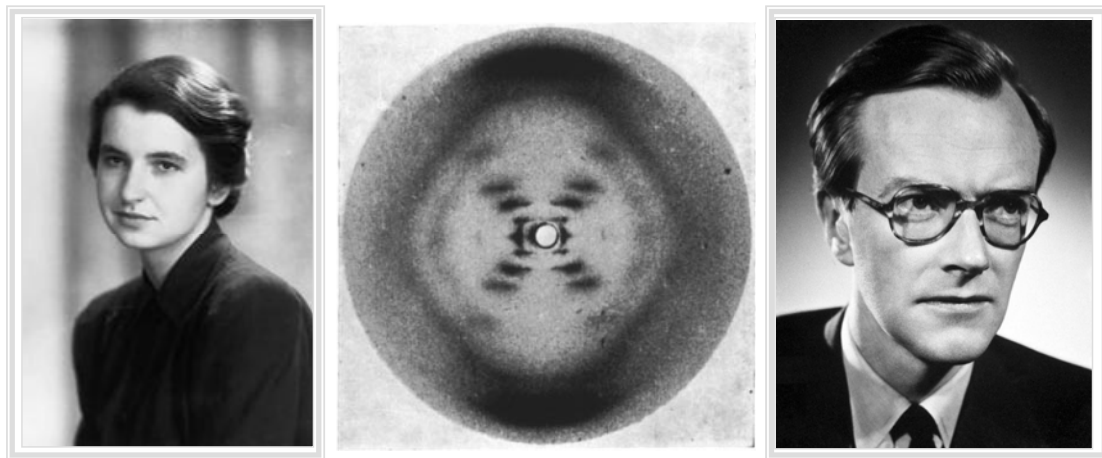


Figure 1.4. A portrait of *Rosalind Franklin* (1920 – 1958),^[24] X-ray diffraction photograph of DNA from calf thymus (by *R. Franklin* and *R. Gosling*)^[23] and a portrait of *Maurice Wilkins* (1916 – 2004).^[24]

By 1950, *Erwin Chargaff* determined that the amount of adenine (A) bases are equal to the amount of thymine (T) residues, whereas guanine (G) bases are present equally to cytosine (C) bases.^[25] These findings lead to the today's known *Chargaff's – Rules*.

This was an important impact for *Francis Crick* who was trying to solve the DNA structure together with *James D. Watson* in the lab of *Max F. Perutz* (Figure 1.5). It was a competition against time as it was known that *Linus Pauling* himself was trying to solve this structural problem too.^[20]



Figure 1.5. A photograph of *Francis Crick* (left, 1916 - 2004) and *James Watson* (right, 1928).^[20]

The rest of the story became history. *Linus Pauling* proposed a triple-helical structure of DNA with the phosphate groups in the inside of the helix which turned out not to be the correct structure.^[13] *Francis Crick* and *James Watson* published a double-helical structure of the DNA molecule based on data from *Rosalind Franklin*.^[26] The *Nobel Prize in Physiology or Medicine* (Figure 1.6) in 1962 was awarded to *Francis Crick*, *James Watson* and *Maurice Wilkins* "for their discoveries concerning the molecular structure of nucleic acids and its significance for information transfer in living material".^[27]



Figure 1.6. The Nobel Medal for Physiology or Medicine, front side (left) and back side (right).^[27]

After the discovery of the DNA structure the question about the implications of such a double-helical antiparallel arrangement arised. It was *Francis Circk*, who continued his work concerning the question of the biological importance. He called it the *central dogma* which explains the way from DNA to RNA and finally leading to proteins including how information is transferred (Figure 1.7). In 1959 the *Nobel Prize* for the discovery of the mechanisms in biological synthesis of RNA and DNA was awarded to the scientists *Severo Ochoa* and *Arthur Kornberg*.^[27]

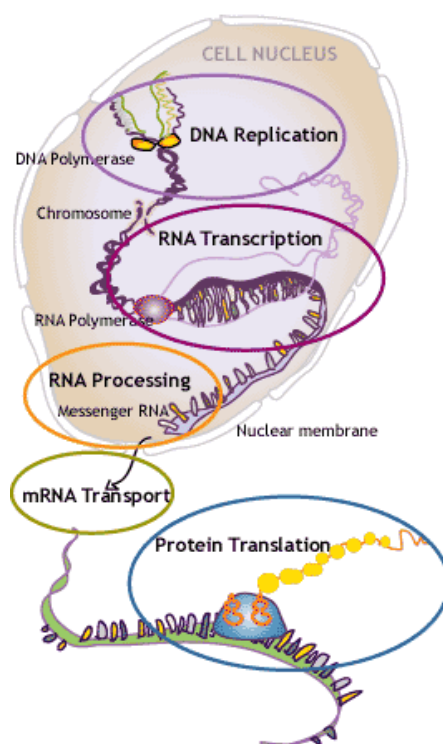


Figure 1.7. A schematic representation of the DNA – RNA – protein pathway.^[27]

An increasing interest in the chemical synthesis of DNA lead to the development of certain oligonucleotide synthesis approaches. The chemical biologist *Har Gobind Khorana* (Figure 1.8) established the phosphodiester approach and successfully synthesized oligonucleotide sequences.^[28;29]



Figure 1.8. A photograph of *Har Gobind Khorana* (1922 - 2011).^[30]

In 1968, he was awarded with the *Nobel Prize in Physiology or Medicine* together with *Marshall W. Nirenberg* and *Robert W. Holley* for their work in “*the interpretation of the genetic code and its function in protein synthesis*”.^[27] Nevertheless, his research on the chemical synthesis of oligonucleotide sequences influenced other researches such as *Marvin H. Caruthers*. Together with *Hubert Koester* he developed the automated solid phase synthesis of oligonucleotides using the *phosphoramidite chemistry*.^[31-33] Since then, further improvements and optimizations of the *phosphoramidite chemistry* were done. Today the synthesis of fully natural oligonucleotides, the incorporation of partially modified nucleotides and even completely artificial building blocks can be proceeded based on solid phase synthesis.

1.2 The Double Helix – A Closer Look

The deoxyribonucleic acid (DNA) is built up based on four different nucleobases: adenine (**A**), thymine (**T**), guanine (**G**) and cytosine (**C**). In ribonucleic acid (RNA) the thymine base is replaced by uracil (**U**).^[34;35] The pyrimidine bases (**C**, **T**, **U**) are linked via the *N1* to the *C1'* of a ribose unit similar to the purine bases (**G**, **A**) that are linked via the *N9* to the sugar residue. This *N-glycosidic bond* leads to the formation of *nucleosides* (Figure 1.9).

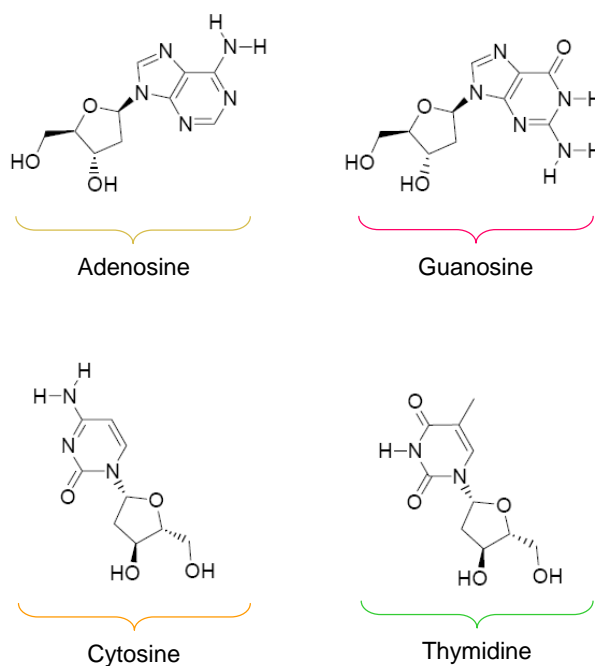


Figure 1.9. The four DNA nucleosides. The top row shows the nucleosides with purine nucleobases and below the pyrimidine base containing nucleosides.

A *nucleotide* is formed by adding a phosphate group to the *C5'* of the ribose unit in DNA and RNA. The connection of nucleotides occurs between the *C5'* from one nucleotide to the *C3'* of another *via* phosphodiester bonds. As a result, the polymer possesses a polarity based on a developed 5'-3' direction of the macromolecule (Figure 1.10). Due to the phosphate groups the backbone is negatively charged at physiological conditions so the formed polymer is a polyanion.

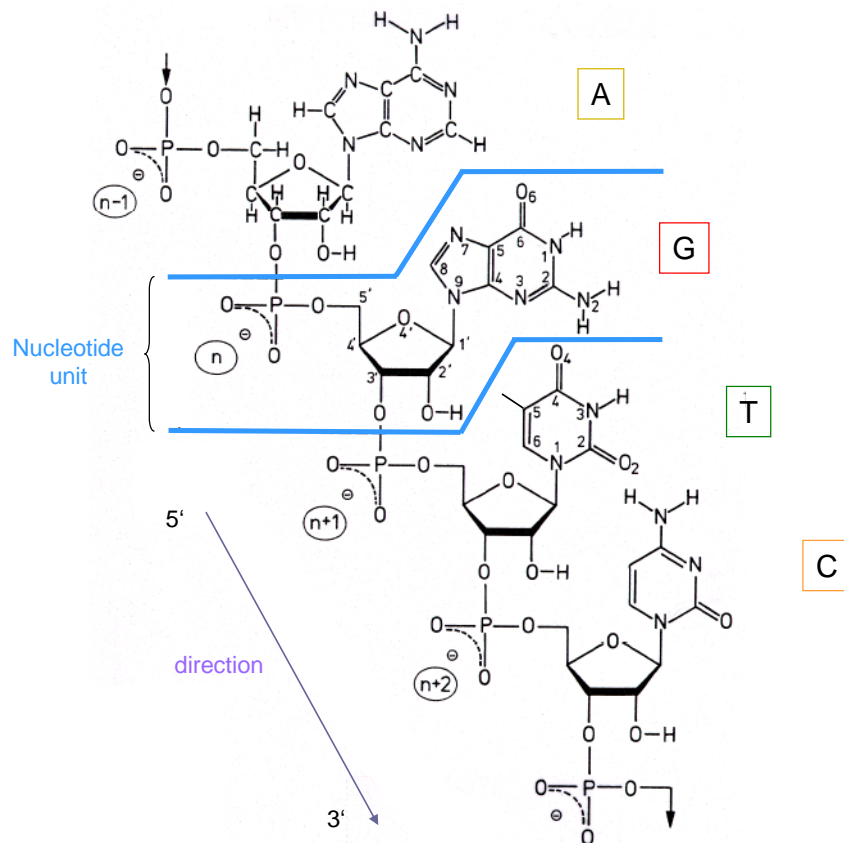


Figure 1.10. DNA nucleotides connected via phosphodiester bonds in a 5'–3' direction. (Illustration adapted from reference ^[36])

Base-pairing takes place between either an **A-T** or a **G-C** pair, the so-called *Watson-Crick* base pairs (**Figure 1.11**). The base pairs differ in number of *hydrogen bonds* whereas an **A-T** pair forms two hydrogen bonds and a **G-C** pair creates three hydrogen bonds.^[26]

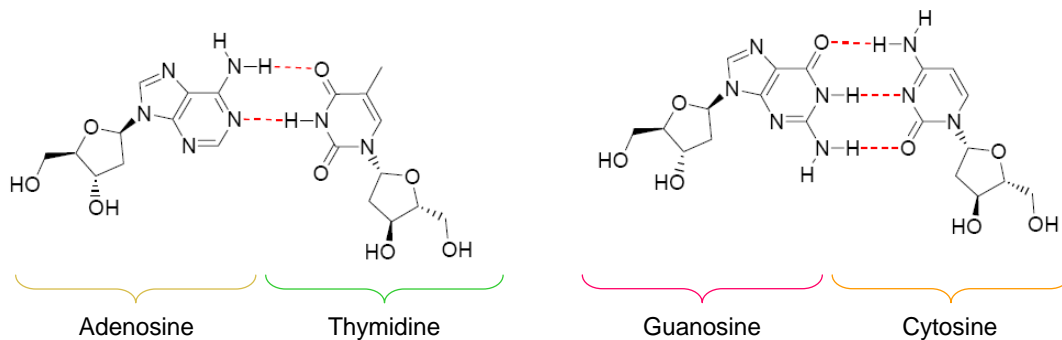


Figure 1.11. *Watson-Crick* base pairs: **A-T** pair (left) and **G-C** pair (right).

Consequently, a double-helical structure is formed with distinct characteristics (Figure 1.12). The two strands are aligned in an *antiparallel* manner, a 5'-3' strand pairs with a 3'-5' oriented strand.^[26] Besides the hydrogen bondings of the base pairs π - π interactions between the bases lead to stacking of the aromatic units and introduces further structural stabilization.

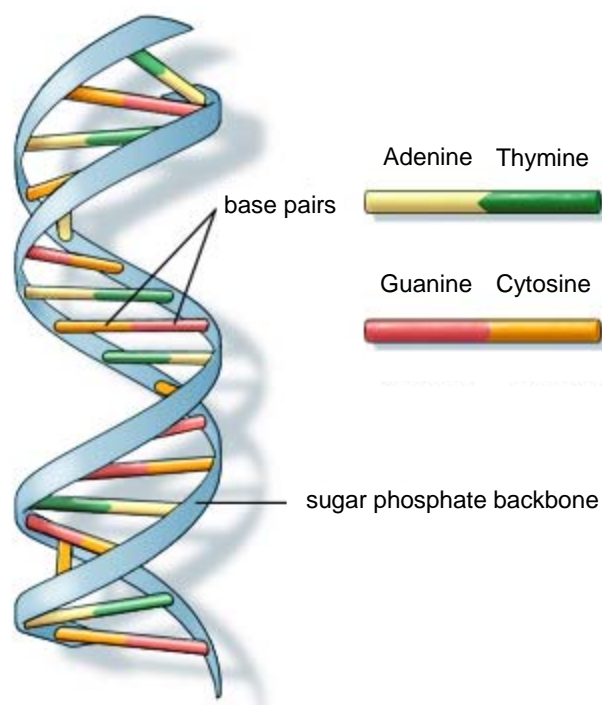


Figure 1.12. Illustration of a DNA duplex.
(Illustration adapted from reference ^[37])

Particular parameters are important in how the structure is built up and looks like. First, the *N-glycosidic bond* between the nucleobase and the sugar moiety can adapt two different conformations (Figure 1.13).^[36] The rotational freedom allows either a *syn*- or an *anti*-form of the bond. In the *syn*-form the base is positioned above the pentose unit whereas in the *anti*-form the base is turned and faces the opposite side.

The sugar moiety itself can occur in different conformations (Figure 1.14). The ribofuranose is a five-membered, non-planar ring. The so-called *sugar pucker* contains the conformations that can be adapted by this pentose unit. The two main forms are either the *C2'-endo* also called south conformation (*S*) or the *C3'-endo*, north conformation (*N*).

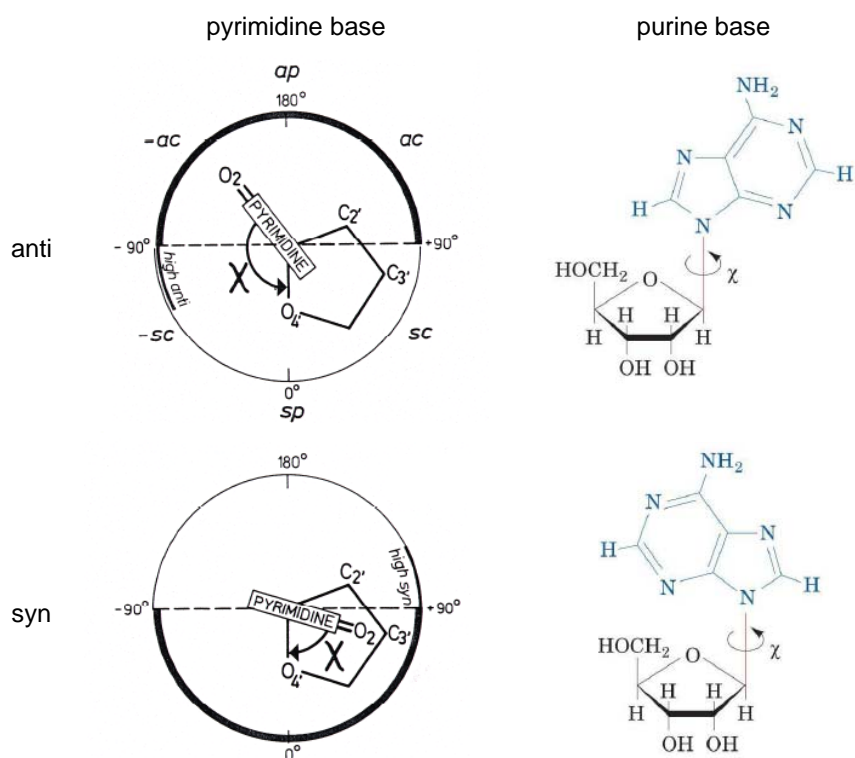


Figure 1.13. *Anti*- and *syn*-conformation of the *N*-glycosidic bond. A general example for pyrimidine bases (left row) and adenosine (right) representing the purine nucleobases. (Illustration adapted from references ^[36] and ^[38])

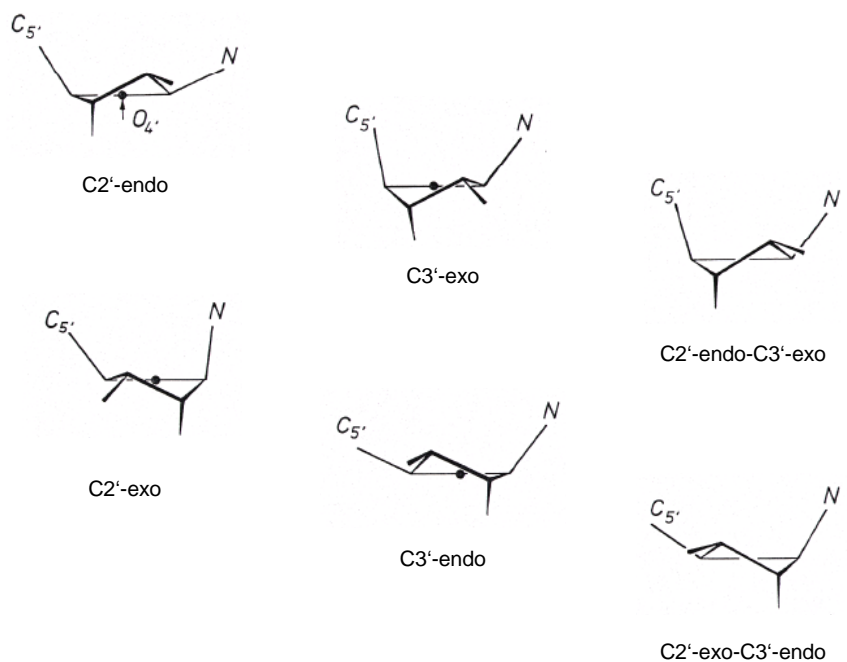


Figure 1.14. Different conformers of the ribofuranose moiety. (Illustration adapted from reference ^[36])

The nucleobases and base pairs can be oriented in different ways. Important parameters concerning the pairing and motions are summarized in [Figure 1.15](#). One differentiates between *rotations* and *translations*.

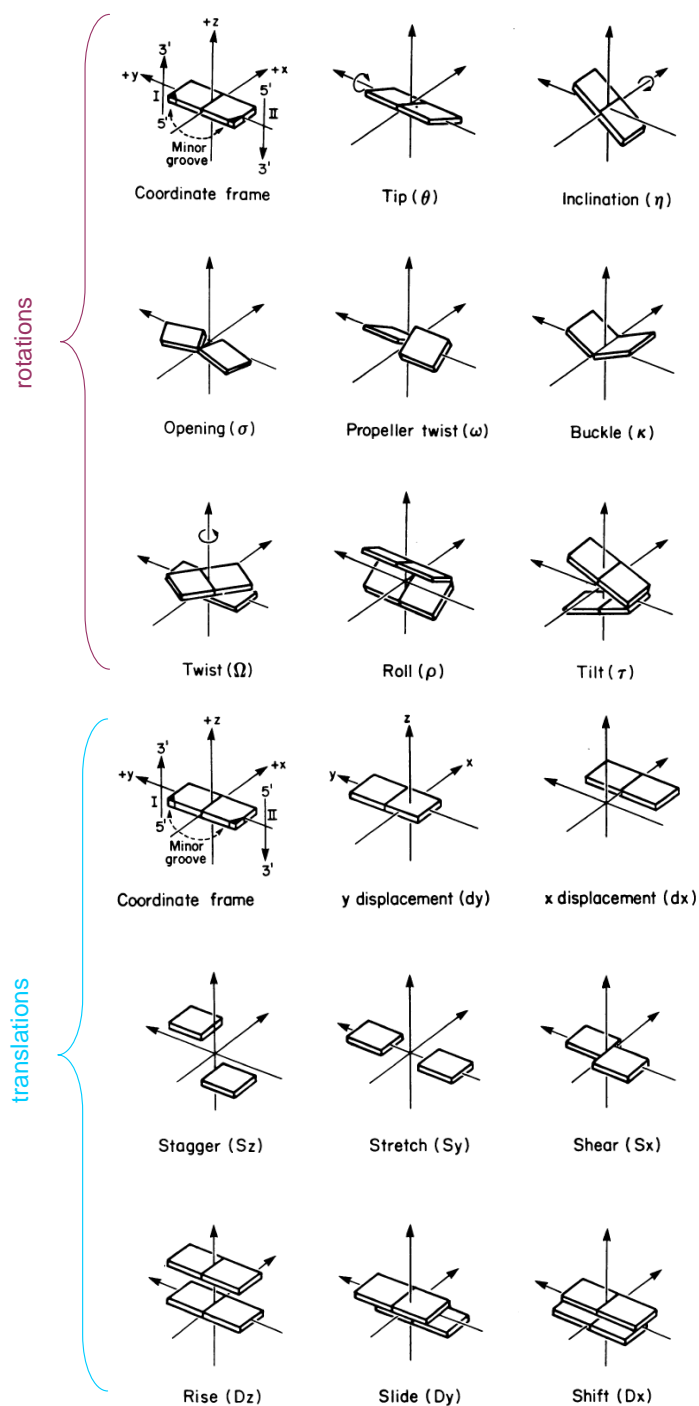


Figure 1.15. Definitions of various *rotation* (top) and *translation* (bottom) motions of nucleobases and base pairs. (Illustration adapted from references ^[39])

The combination of these characteristics leads to a double-helical structure with two grooves differing in width and depth. Depending on their size, the grooves are named *minor* or *major groove* (Figure 1.16).

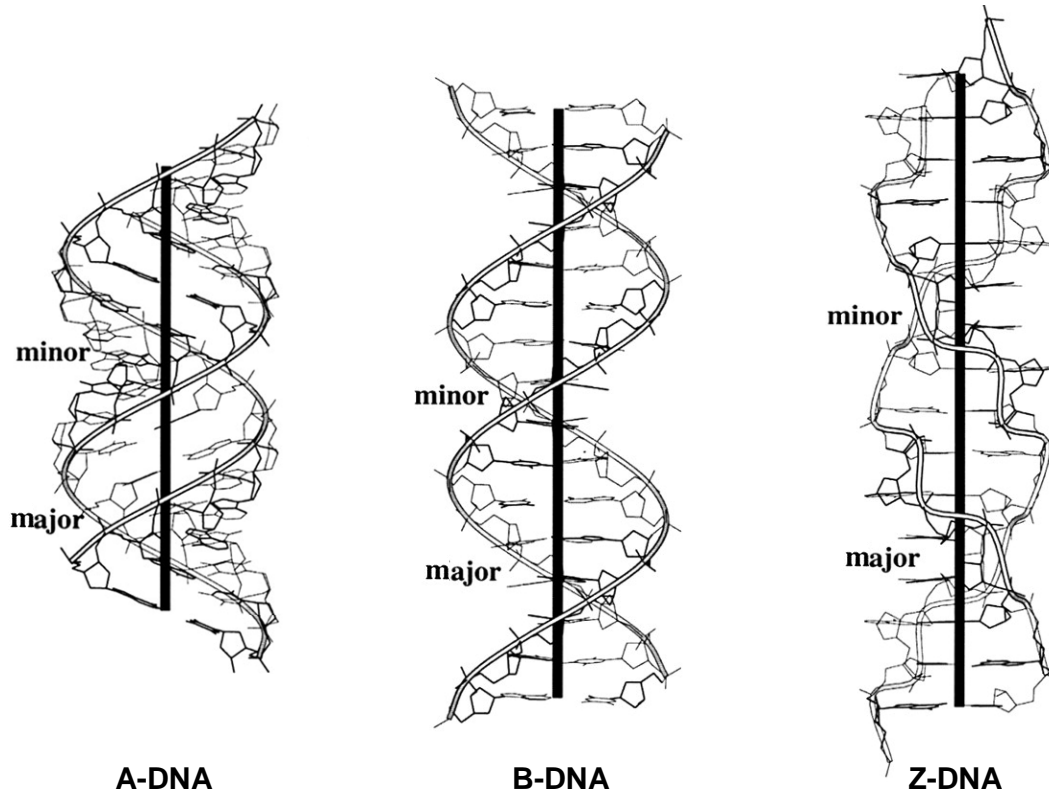


Figure 1.16. Illustration of the three main conformers of a double-stranded DNA: *A-DNA*, *B-DNA* and *Z-DNA*. (Illustration adapted from reference ^[40])

The DNA structure exists in mainly three different forms, represented in Figure 1.16. Depending on the water content, the structural conformer adapts either a fully hydrated form called *B-DNA* or a dehydrated form, namely *A-DNA*.^[23] The third of the three main conformers is called *Z-DNA*. This structure occurs under high ionic strength preferably in a purine/pyrimidine motif. One of the main characteristic of DNA structures is the helical sense of the structure. The *A*- and *B-DNA* adopt a right-handed structure whereas a left-handed arranged structure is taken by *Z-DNA*.

The *major groove* in the A-conformation is *narrow* and *deep* opposite to the *wide* form in a B-DNA. This is completely different for Z-DNA structures. Here, the *major groove* has a *convex* surface and the *minor groove* adapts a *narrow* and *deep* form. Similar to those of B-DNA, but not comparable with the *minor groove* formed within A-DNA. There the *minor groove* is wide and shallow.

There are ten *base pairs per turn* in the B-conformation, eleven in the A- and twelve in the Z-conformation. Together with the *rise per base pair*, that is 2.9 Å for A-DNA, 3.4 Å for B-DNA and 3.7 Å for Z-DNA, the different *itches* of the conformers are configured. The *average twist angle per base pair* around the helical axis differs between the conformers. The base pairs in the B-DNA are twisted by 36° and 31° in the A-DNA. The Z-conformation possesses a average twist angle of -30° per base pair.

Figure 1.17 shows illustrations of the three main DNA conformers from the top view along the axis. The *helical diameters* differ from 26 Å for the A-conformation, to 20 Å for a B-DNA structure and 18 Å for the Z-DNA helices.

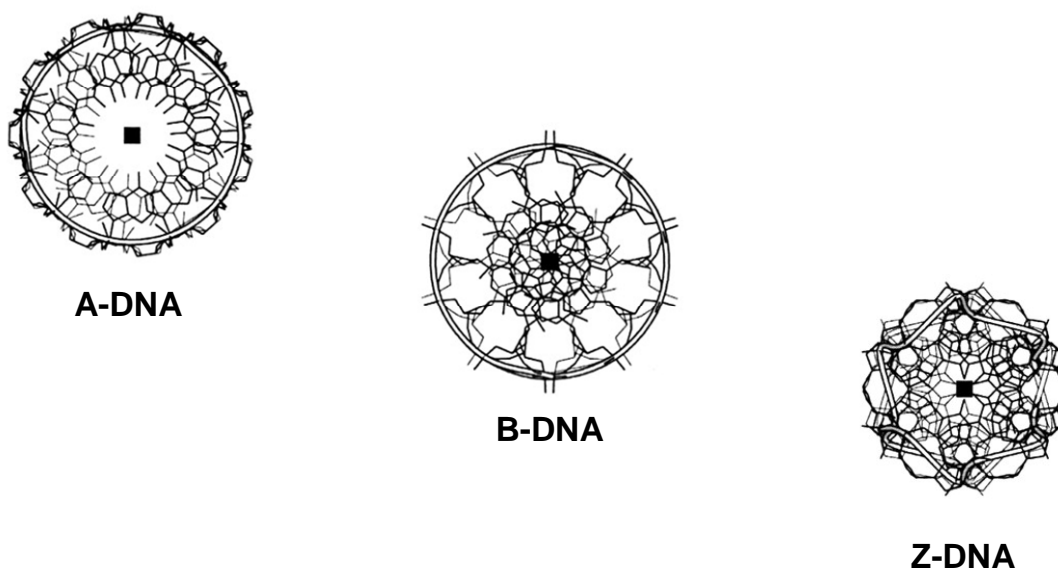


Figure 1.17. Top view illustrations of the three main conformers: A-DNA, B-DNA and Z-DNA. (Illustration adapted from reference ^[40])

Selected parameters of the nucleic acid structures are summarized in Table 1.1 below. The list contains information about the three main conformers A-DNA, B-DNA and Z-DNA. Whereas the B-DNA is the most important structure for the projects presented herein.

Table 1.1. List of selected structural parameters of the three main DNA conformers.

	B-DNA	A-DNA	Z-DNA
Helix sense	right-handed	right-handed	left-handed
Rotation per base pair	36°	31°	-30°
Base pairs per turn	10	11	12
Rise per base pair	3.4 Å	2.9 Å	3.7 Å
Pitch per turn of helix	34 Å	32 Å	45 Å
Helix diameter	20 Å	26 Å	18 Å
Major groove	wide and deep	narrow and deep	convex surface
Minor groove	narrow and deep	wide and shallow	narrow and deep
Sugar pucker	C2'-endo	C3'-endo	C3'-endo (purines) C2'-endo (pyrimidines)
Glycosidic bond	anti	anti	syn (purines) anti (pyrimidines)

1.3 Structural Elements

Nucleic acids can also adopt double-helical structures in the presence of no complete base-pairing. If there are additional nucleotides in one strand of the duplex compared to the other strand, so-called *bulges* can be formed. [Figure 1.18](#) shows the schematic representation of such bulges.

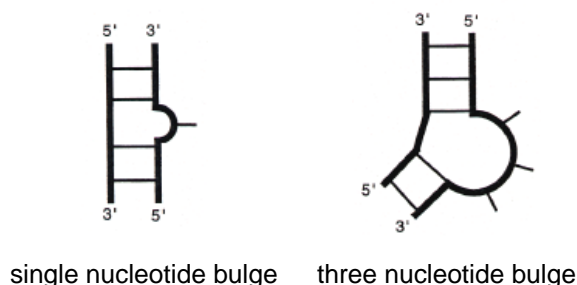


Figure 1.18. Different forms of structural bulges. (Illustration adapted from reference ^[41])

The structural arrangement of an additional nucleotide can be either *stacked into* the helical arrangement or *looped out*. Further, the additional nucleotide can interfere upon *stacking* interactions within the groove (Figure 1.19).

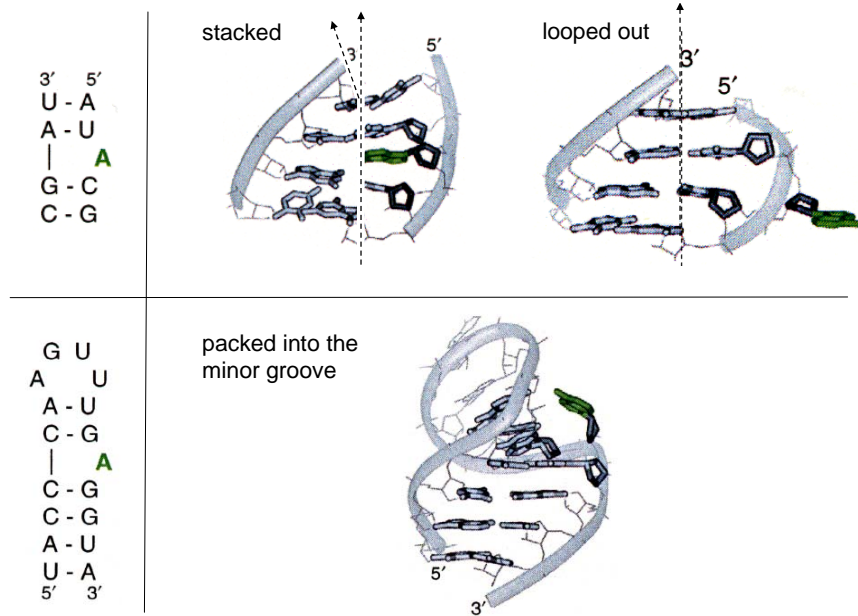


Figure 1.19. Different forms of structural *bulges* in RNA. (Illustration adapted from reference [42])

In the presence of unpairing nucleotides, a *mismatch pair*, the formation of loops occurs. The additional number of nucleotides per strand can be equal or different. Consequently *symmetric* or *asymmetric loops* are formed (Figure 1.20).

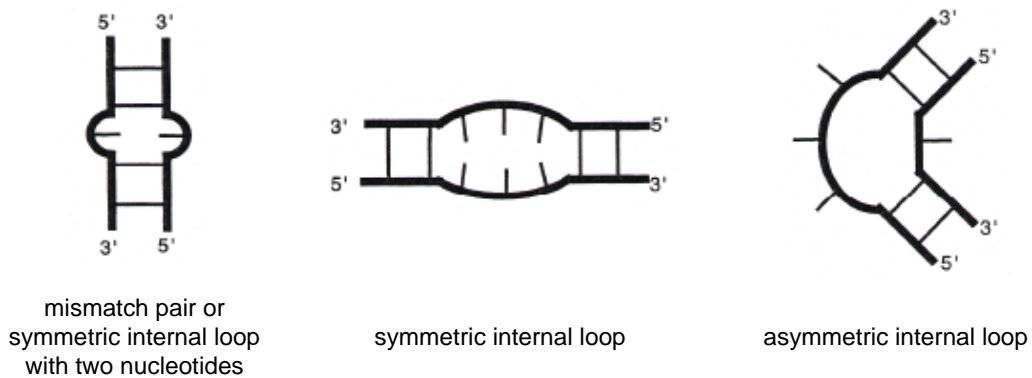


Figure 1.20. Different forms of loops. (Illustration adapted from reference [41])

A *hairpin* structure occurs if the additional nucleotides form a loop and the remaining bases at both ends form a duplex (Figure 1.21). This *stem-loop* feature is of special importance for this work.

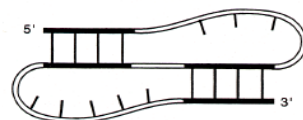


hairpin loop

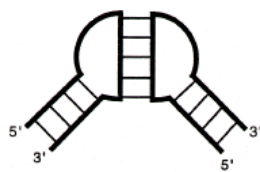
Figure 1.21. A hairpin loop or stem-loop structure. (Illustration adapted from reference ^[41]).

1.4 Tertiary Structural Elements

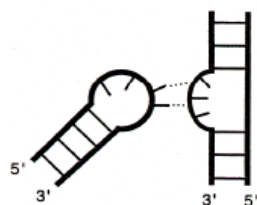
Next to the secondary structures, also tertiary structural elements exist. For example, single strands can form multiple intramolecular stem parts leading to a *pseudoknot* structure (Figure 1.22). Also interactions between two secondary structures like two hairpins (*kissing hairpins*) or a hairpin and a bulge structure (*hairpin loop – bulge contact*) can occur.



pseudoknot



kissing hairpins



hairpin loop – bulge contact

Figure 1.22. Examples for tertiary structures. (Illustration adapted from reference ^[41])

1.4.1 Triplex Structures

Under specific conditions, a double-helical structure with *Watson-Crick* base pairs can form a base triplet with an additional single strand (*Hoogsteen* base pairs).^[43-48] There are two different main motifs, a *parallel* and an *antiparallel* motif. For the *parallel* or *pyrimidine binding* motif the third strand or *Hoogsteen* strand is parallel to the polypurine strand and simply consists of pyrimidine bases: C+GC and TAT (Figure 1.23).^[49;50]

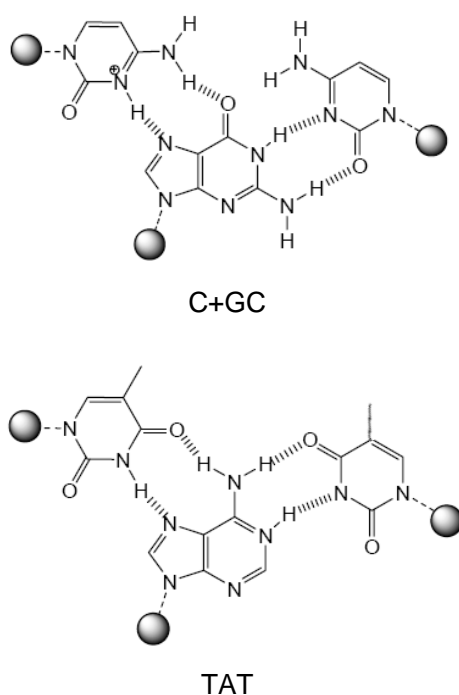


Figure 1.23. Parallel or pyrimidine binding motif of base triplets. (Illustration adapted from reference ^[51])

The *antiparallel* or *purine binding* motif is based on *reversed Hoogsteen* base pairs between the double-helical structure and the third strand.^[45] Here, the *Hoogsteen* strand is antiparallel to the polypurine strand: G-GC, A-AT and T-AT (Figure 1.24).

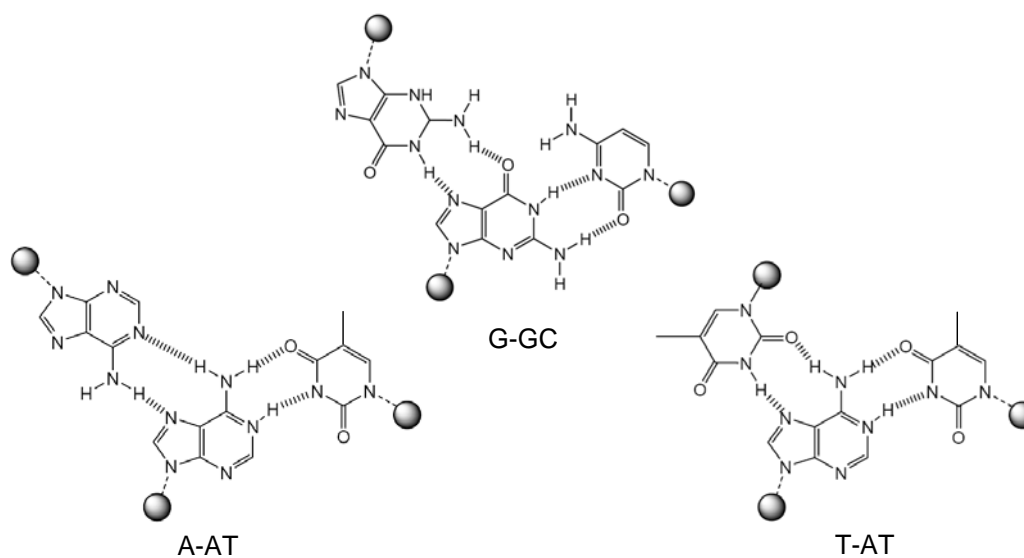


Figure 1.24. Antiparallel or purine binding motif of base triplets. (Illustration adapted from reference ^[51])

Figure 1.25 shows two different examples how triple-helical structures can be formed. In general, besides the well-known triplex structures (Figure 1.26) with a *parallel* or *antiparallel* motif, base triplets exist also in areas of *loop helix contacts*.

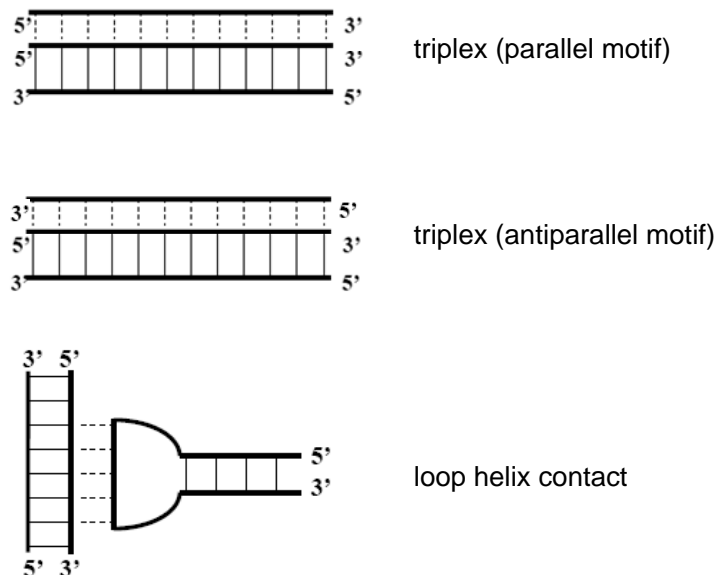


Figure 1.25. Examples of triple-helical structure formation. (Illustration adapted from reference ^[41])

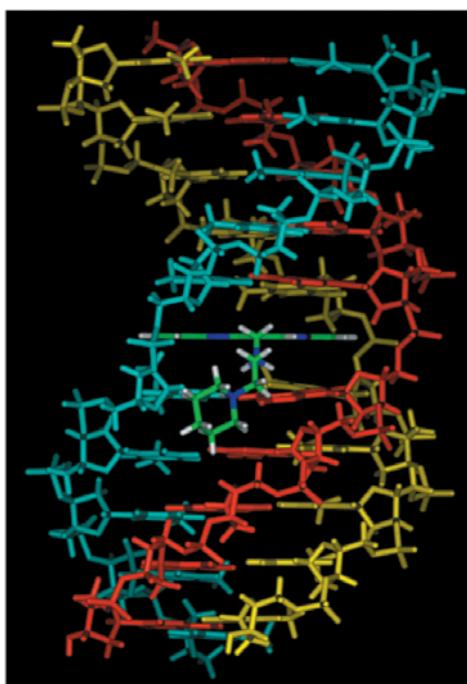


Figure 1.26. Schematic illustration of a triplex (top)^[52] and a energy-minimized model of a triple helical DNA composed of TAT triplets with and intercalated amino-p-quinacridine compound (bottom).^[53]

1.4.2 Quadruplex Structures

The self-association of guanine-rich sequences is based on *Hoogsteen* hydrogen bonds leading to the formation of planar structures containing four guanine bases (*G-tetrad* or *G-quartet*).^[54-56] This structural motif is stabilized by cations placed inside its cavity (Figure 1.27).

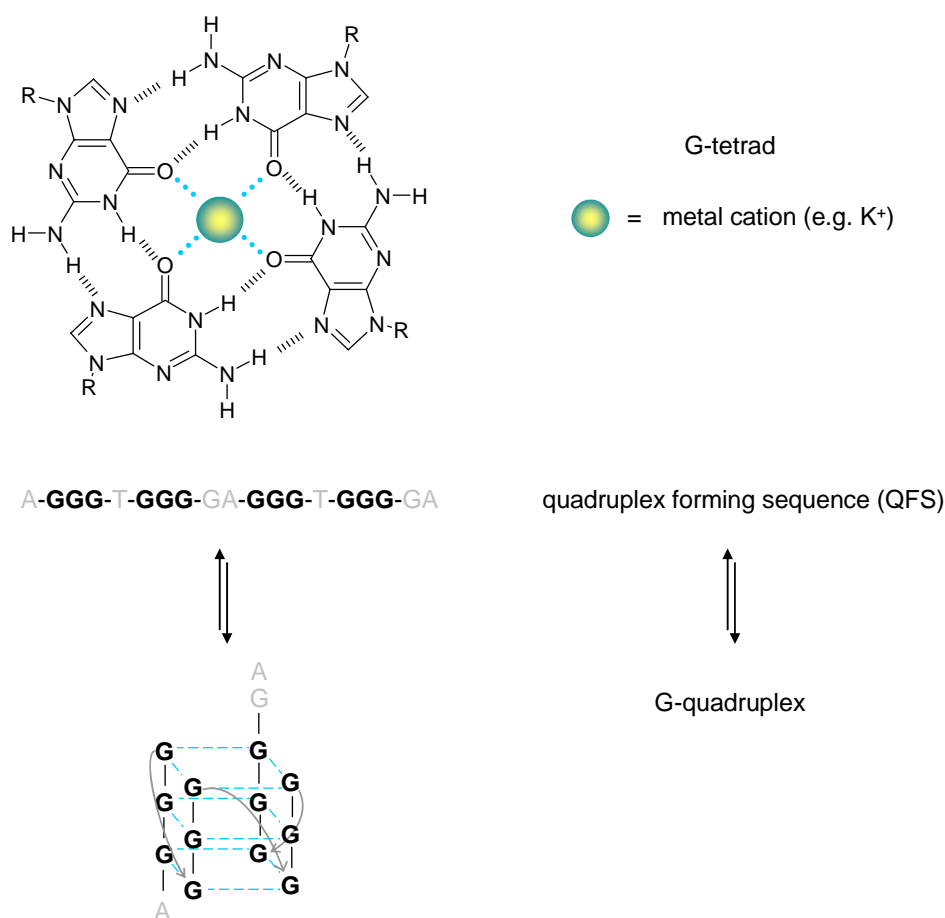


Figure 1.27. Illustration of a G-tetrad (top), an example of a quadruplex forming sequence (middle) and a G-quadruplex structure (bottom). (Illustration adapted from reference^[57])

The G-tetrads can stack on each other and form four-stranded higher ordered structures. The example shown in Figure 1.27 is an intramolecular or *unimolecular* G-quadruplex. Further, *bi-* and *tetramolecular* quadruplexes can be formed.^[55] A selection of different topologies is

presented in Figure 1.28. As a simplification, squares represent G-tetrades and the nucleic acid sequence is illustrated with arrows.

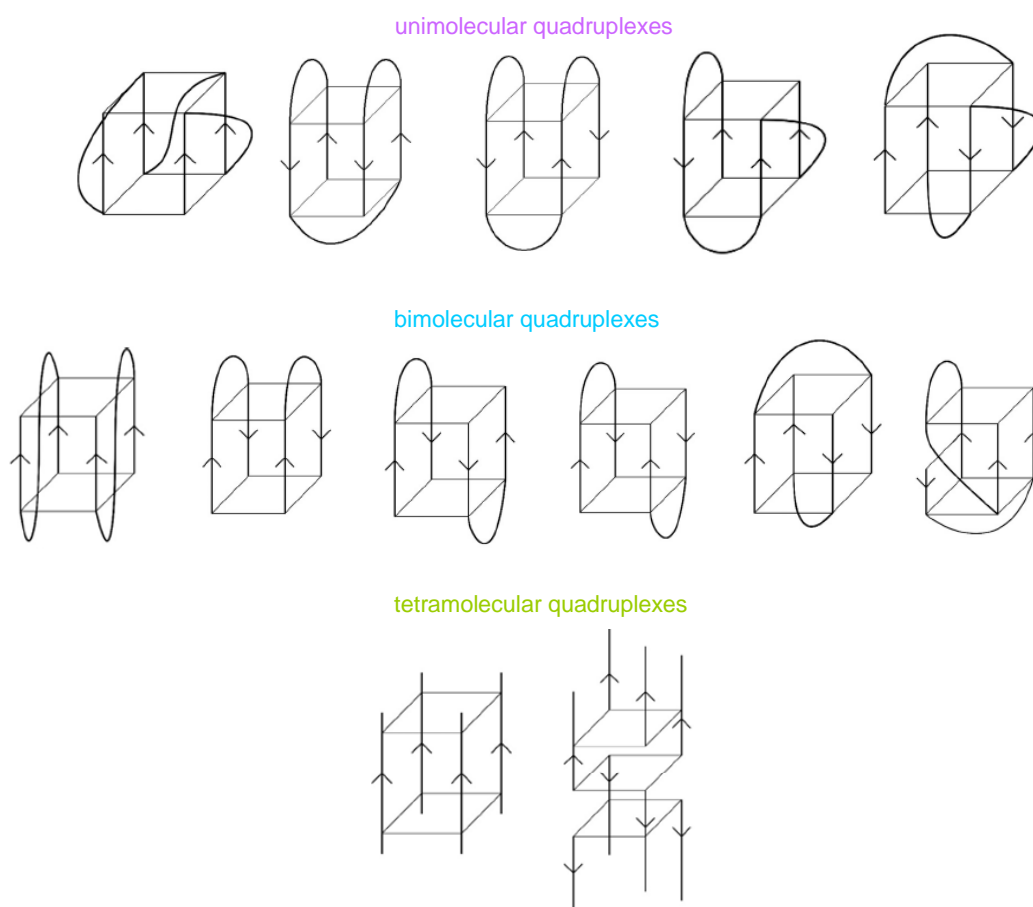


Figure 1.28. G-quadruplex topologies: unimolecular (top), bimolecular (middle) and tetramolecular (bottom) structures. (Illustration adapted from reference ^[55])

In nature, G-quadruplex structure occurs in genomic DNA regions important for regulatory processes, such as promoters and telomers. Consequently, G-quadruplexes gain a lot of interest in the area of anticancer agent research.^[58;59]

1.4.3 Branched Structures

Each structural element depends on the primary structure of the strand, the sequence design. For the formation of branched structures, the characteristics of base-pairing are utilized.

There, multiple strands form double-helical structures containing branch points.^[60-73] Figure 1.29 shows an illustration of branched structures with three, four and five double helical structures as arm sequences. Construction of *six-arm junctions* (or *six-way junctions*) does exist as well.

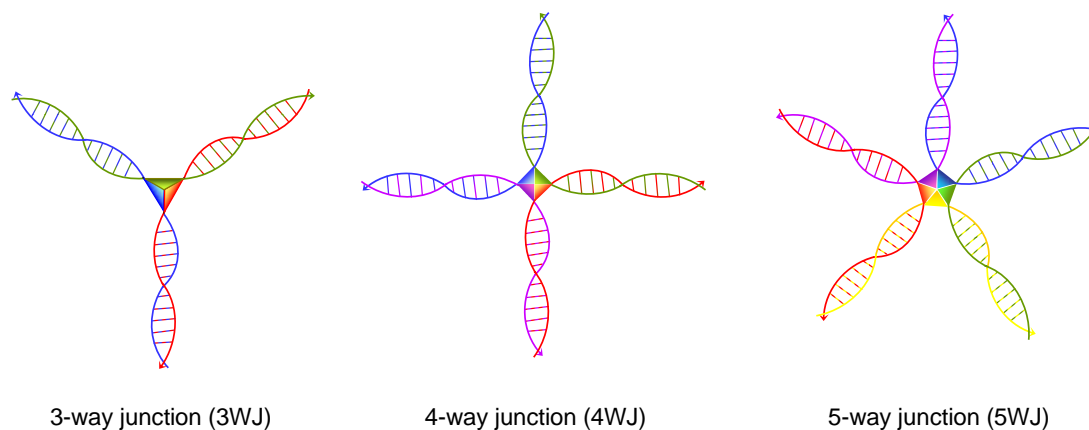


Figure 1.29. Schematic illustration of differently branched junctions. From left to right: a three-way junction (3WJ), a four-way junction (4WJ) and a five-way junction (5WJ).

The negatively charged phosphate groups are in close proximity to each other so strong repulsive forces occur. Multivalent cations such as Mg^{2+} or Fe^{2+} can neutralize and consequently stabilize the structure.^[66]

The exceptional behaviour of DNA to form double-helical structures of complementary strands is the basis for the construction of DNA arrays. Two complementary overhanging sequences (sticky ends) will form a double helix, so a *bis-3-way junction* can be created upon ligation of two *3-way junctions* as it is shown in Figure 1.30.

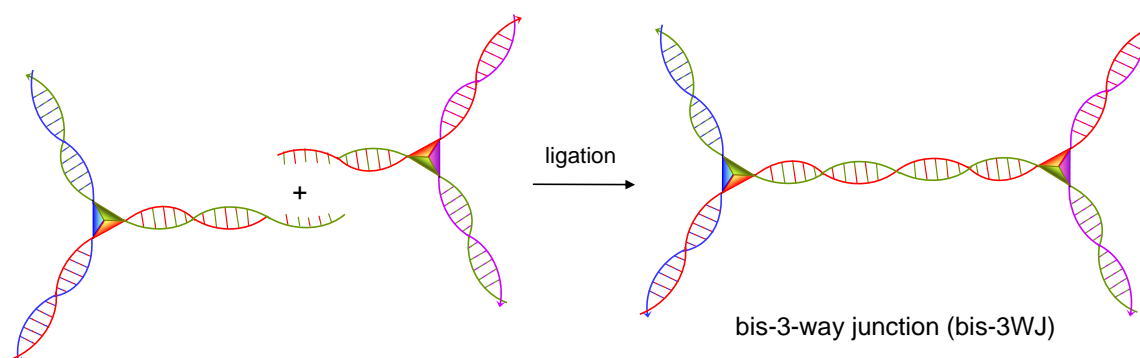


Figure 1.30. Schematic illustration of a *bis-3-way junction* (bis-3WJ) upon ligation of two 3WJs.

Similar DNA architectures can be built up with multiple branched structures like six arm junctions. The branch point lays in the centre of an octahedron-like geometry of the subunit (Figure 1.31).^[74] The sticky ends “connect” the subunits with each other and higher ordered structures like cubes can be constructed.

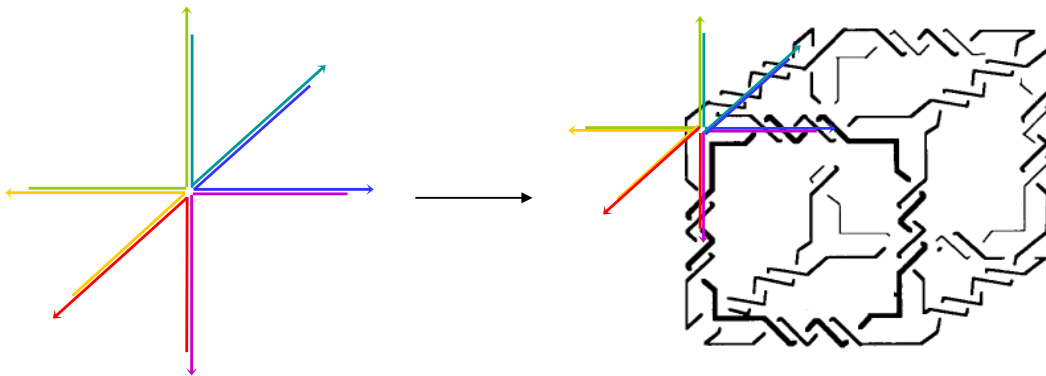


Figure 1.31. DNA nano-architectures with multiple branched junctions as subunits. (Illustration adapted from reference ^[74])

There are many more junctions and their application as subunits studied as it is summarized here. Nevertheless, the aim was to give a brief insight in the field of nano-architectures built up with branched DNA structures, as it will be a part of the project presented in the outlook chapter.

1.5 Molecular Beacons

In 1996, *Sanjay Tyagi* and *Fred Russel Kramer* published a novel nucleic acid hybridization probe, the *molecular beacon*.^[75] A single stranded oligonucleotide sequence with fully modified base surrogates on both ends, 5' and 3' of the strand (Figure 1.32). The primary structure is designed in a way that a *hairpin* structure is formed. The *loop* of the structure contains the *probe sequence*, which is complementary to a demanded target sequence. Further, the nucleotides adjacent to the loop sequence (*arm sequences*) hybridize and form the *stem* of the *stem-and-loop* structure. Consequently, the artificial base surrogates are located closely to each other. This pair of artificial building blocks is build up based on a *fluorophore* unit and a *quencher* moiety.

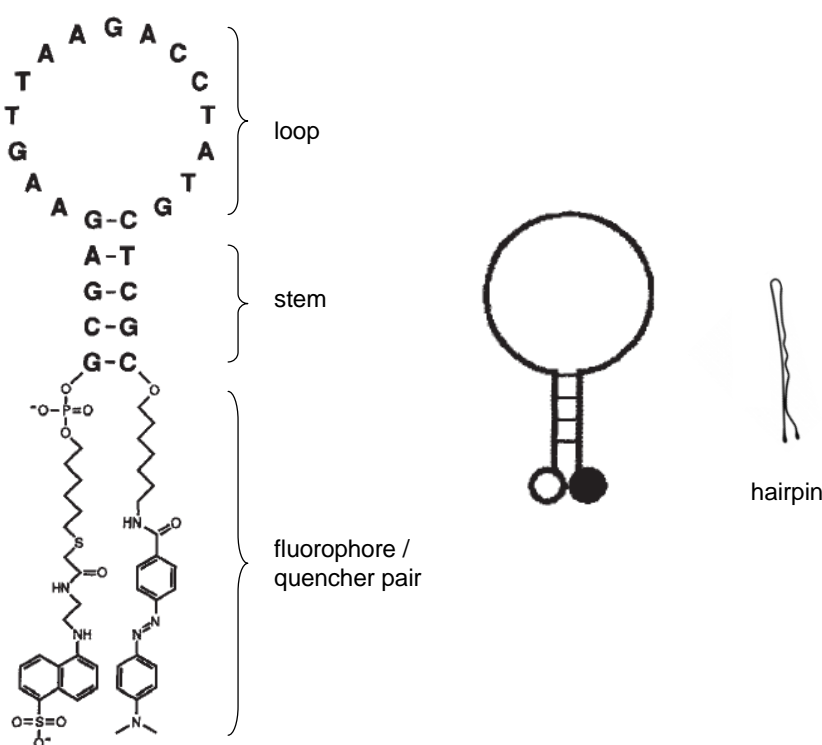


Figure 1.32. Structure (left) and illustration (right) of a molecular beacon. The fluorophore (EDANS, left) and the quencher unit (DABCYL, right) with their linkers are located at the 5'- and 3'-end. (Illustration adapted from reference^[75])

In the *closed form*, fluorescence of the fluorophore is quenched due to fluorescence resonance energy transfer (FRET).^[76] The excited fluorophore transfers the energy to the quencher, that releases the energy as heat.^[77;78] In the ideal case a complete quenching occurs and no fluorescence signal is detected. A dissociation of the stem leads to a separation of the FRET-pair and fluorescence is restored. This takes place either by heating so the stem duplex “melts” or upon hybridization to an oligonucleotide strand containing the target sequence. The hybrid formed between the target and the probe sequence in the loop (*probe-target-hybrid*) is more stable than the hybrid formed by the two arm sequences. Therefore, the molecular beacon undergoes a conformational change, fluorescence is restored and signal detection is ensured (Figure 1.33).

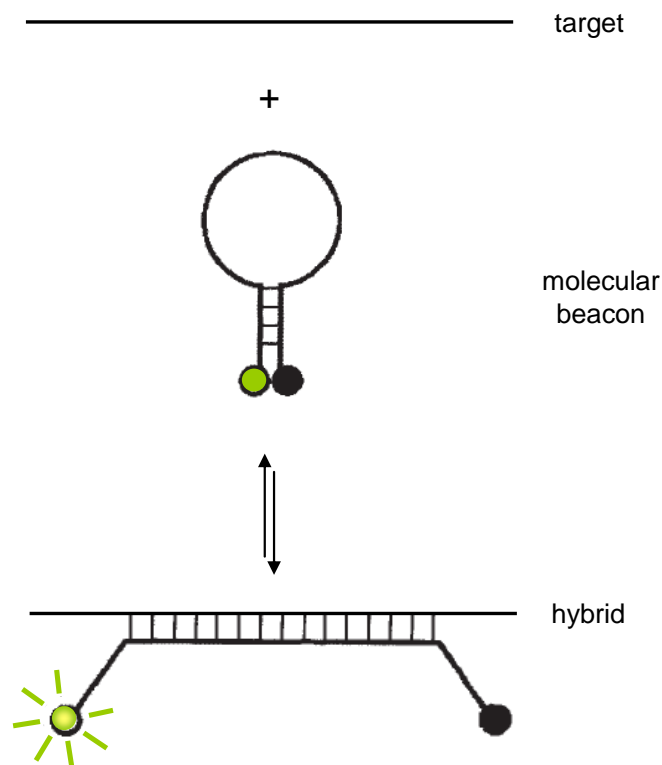


Figure 1.33. Schematic illustration of the hybridization of a molecular beacon with a target sequence and the emission of fluorescence. (Illustration adapted from reference ^[75])

These characteristics enable the use of molecular beacons (MBs) in hybridization assays. No signal is generated in absence of target. The probe-target hybrids can be detected by

fluorescence emission measurements so there is no need to isolate the hybrids for experimental evaluation. In amplification assays, the increase of specific sequences can be followed in *real-time* as it is performed in polymerase chain reactions (PCRs).^[79] Furthermore, these probes can discriminate single nucleotide mismatches. The high *specificity* is based on the two different stable physical states of a MB.^[80] In the absence of target sequences, the probe is in its *closed form* so a stable *stem-and-loop* structure is formed and the energy is kept inside the stem duplex. Whereas in the presence of target sequences, more stable *probe-target* hybrids are originated. In summary, MB enables signal generation only in presence of target otherwise it is “dark”. Further, this probe is very specific and able to discriminate single mismatched sequences with desired color read-out due to specific fluorophores.

The detection of different targets at the same time can be assured in *multiplex assays* based on the presence of several MB probes. Each MB contains the corresponding probe sequence and a specific FRET-pair (*multicolor molecular beacons*).^[81;82] The emission of different wavelengths leads to an independent detection of the different targets (Figure 1.34).

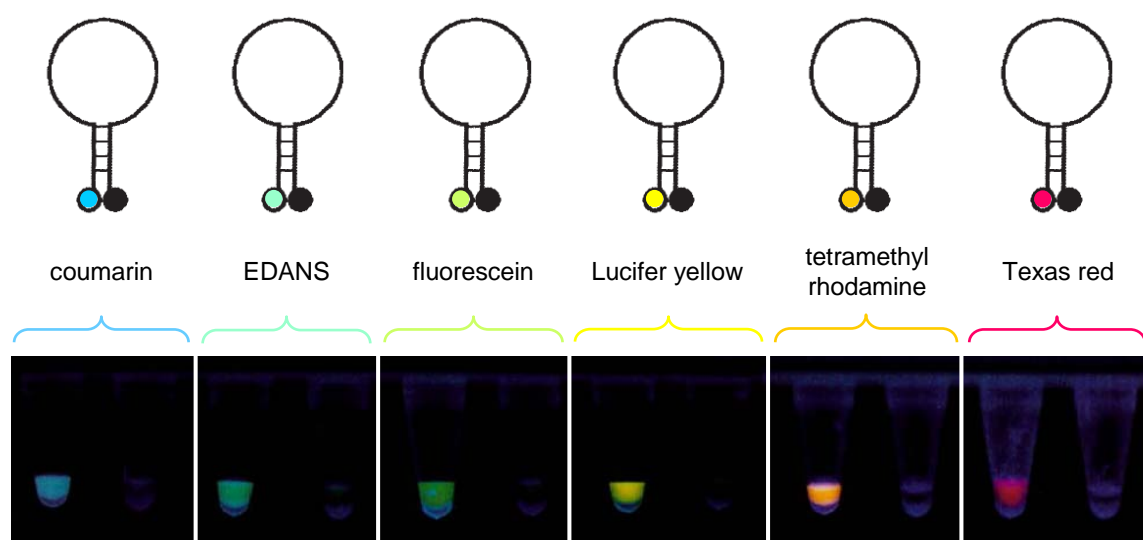


Figure 1.34. A selection of multicolor molecular beacons. The left sample tubes contain the probe and the matched target sequence emitting fluorescence of the corresponding fluorophore mentioned on top and the right tubes contain the probe without target. (Illustration adapted from reference ^[81])

Such multicolor hybridization assays allow the parallel detection of several target sequences in real-time. Allele discrimination of four probes is shown in Figure 1.35. There, time-dependent fluorescence measurements were performed. The probes were excited differently, each at its maximal excitation wavelength and the data were collected at the emission maxima. There is a clear discrimination of the four target sequences written in the data box.

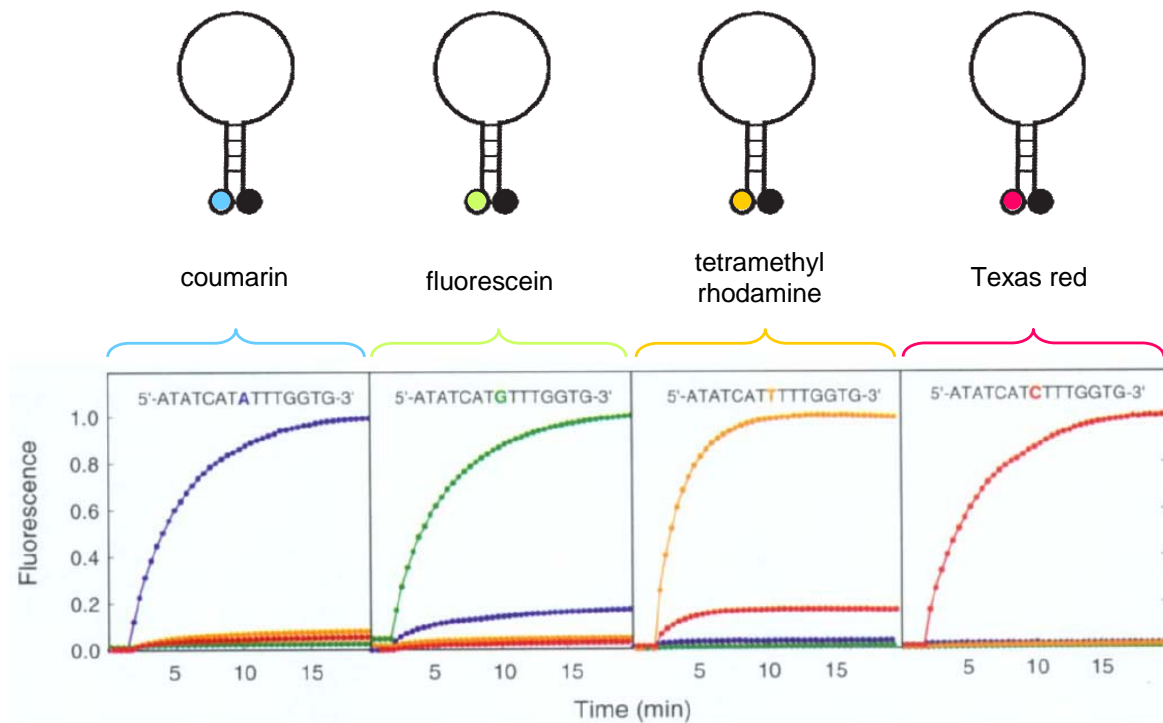


Figure 1.35. Single mismatch discrimination assay with four different MBs. Detection of signal only occurs if the fully matched target (in the data box) was added to the probe and consequently characteristic fluorescence was restored. (Illustration adapted from reference^[81])

Next to the *conventional* and *multicolor* MBs, Sanjay Tyagi and Fred R. Kramer have developed together with Salvatore A. E. Marras a *wavelength-shifting* MB probe.^[83] *Wavelength-shifting* MBs fluoresce in a variety of different colors, but are excited by one wavelength or common monochromatic light source. One fluorophore (*harvester-fluorophore*) absorbs the energy and transfers it to another fluorophore (*emitter-fluorophore*). The *harvester-fluorophore* is able to absorb energy of a bright range of a monochromatic light source, whereas the *emitter-fluorophore* has the ability to absorb the emitted energy from the *harvester-fluorophore*. The quencher unit is chosen to successfully

quench the signal emitted by the *harvester-fluorophore*. In the closed form, the absorbed energy of the *harvester-fluorophore* is transmitted to the quencher molecule and will be released radiationless or as heat. Upon hybridization to a target sequence, the quencher and fluorophore units dissociate. The absorbed energy can now successfully transferred to the *emitter-fluorophore*. The characteristic wavelength is emitted and signal generation is ensured (Figure 1.36).

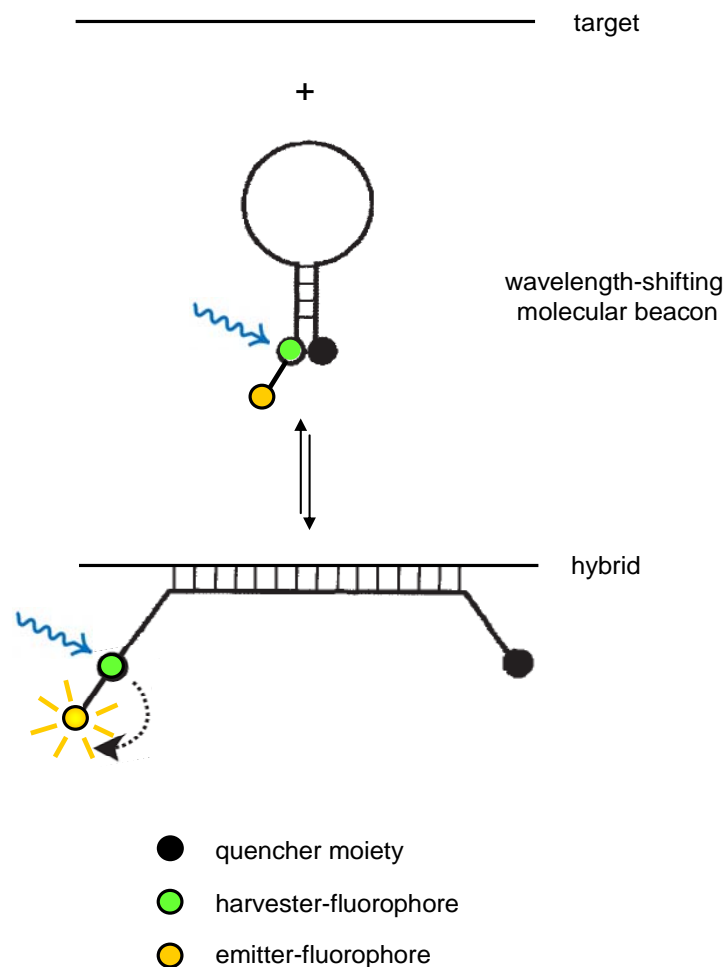


Figure 1.36. Schematic representation of a wavelength-shifting MB with a quencher, a harvester-fluorophore and an emitter-fluorophore. (Illustration adapted from reference ^[83])

Since the invention of the molecular beacon in 1996, different approaches were investigated to improve or redesign hybridization probes based on the principle of the beacon. One approach is presented in this thesis and further works are mentioned in the corresponding introductory part. Nevertheless, none of these probes could even touch the commercial success of the conventional MB from *Fred Russell Kramer* and *Sanjay Tyagi* (Figure 1.37) until today.



Figure 1.28. A photograph of *Salvatore A. E. Marras*, *Fred Russell Kramer* and *Sanjay Tyagi* (from left to right).^[84]

1.5.1 Signal Control Systems

Signal generation and signal quenching are crucial aspects for successful MB probes. The generation of the signal is predicted by fluorescence. A fluorescent chromophore is excited at a certain wavelength at which a maximum in absorbance is obtained. The *Jablonski diagram* in Figure 1.38 shows the origination of fluorescence on a simple example.

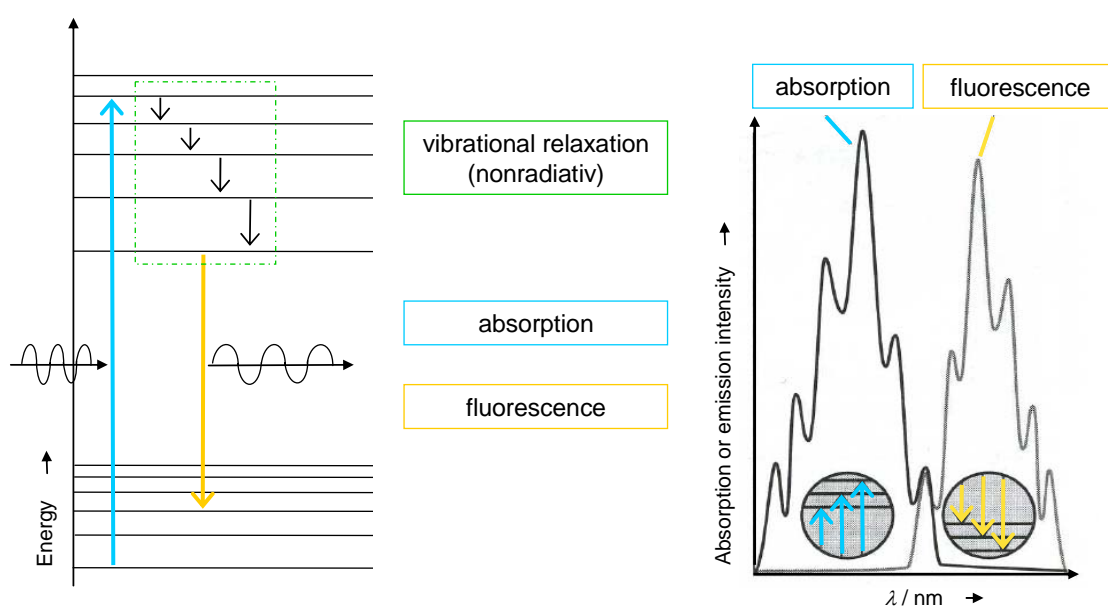
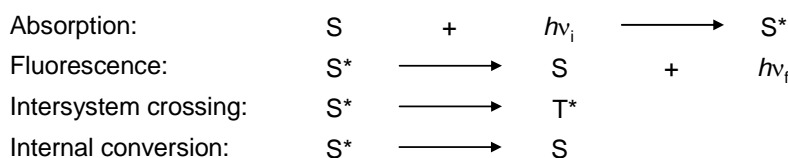
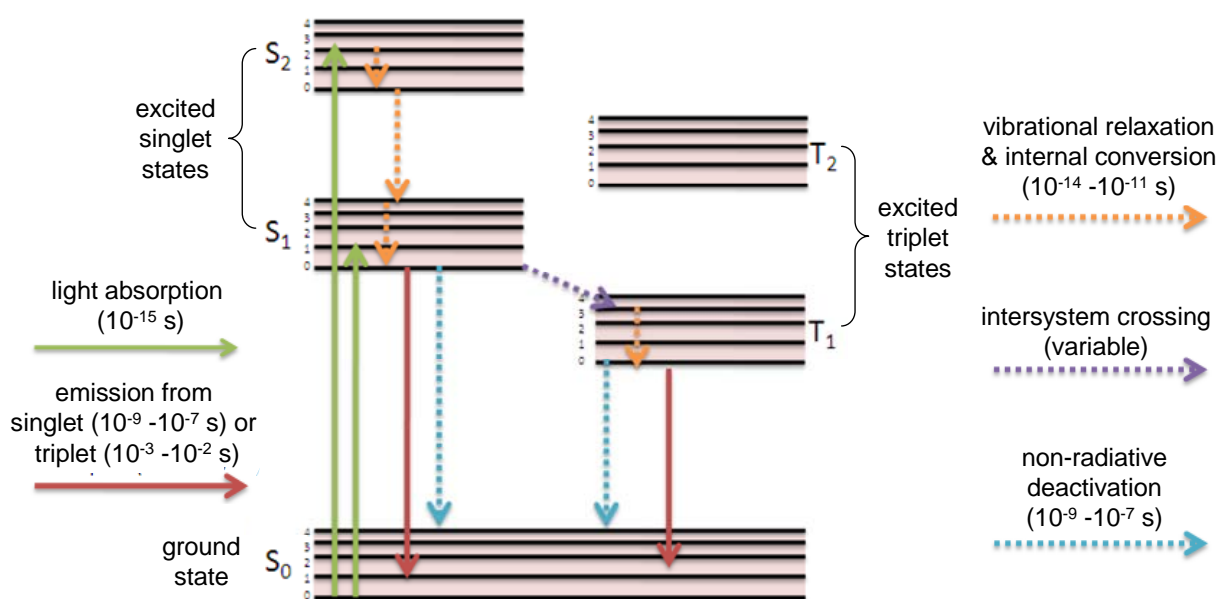


Figure 1.38. Left: Simple example of a Jablonski diagram. Right: Combined absorption and fluorescence spectra. The fluorescence spectrum is a mirror image of the absorption with the corresponding structural pattern. (Illustration adapted from reference ^[85])

The molecular *electronic* and *vibrational energy* levels are illustrated with vertical lines and the *transitions* are represented with arrows. The dedicated wavelength is of higher energy than the finally released energy shown with the differently waved arrows in the scheme. A more detailed illustration is summarized in Figure 1.39. Upon *irradiation* or *light absorption* the molecule is lifted up into an *excited electronic state*. This gained energy is released partially by collisions with neighbouring molecules leading to a *vibrational relaxation*, *internal conversion* or *non-radiative deactivation*. Further, *intersystem crossing* to excited triplet states can occur. If the excited state has a sufficient lifetime, the excess of energy is released by *photons* and consequently *radiation* can be observed.



S = absorbing species
 S^* = excited singlet state
 T^* = excited triplet state

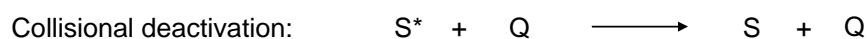
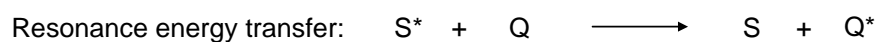
h = Planck's constant [6.62608×10^{-34} Js]
 ν = frequency [Hz]
 $h\nu_i$ and $h\nu_f$ = energy of the incident and fluorescent photon

Figure 1.39. Example of a Jablonski diagram with the processes involved in signal generation. (Illustration adapted from reference ^[86])

A bright fluorescence signal is useless if there is no quencher able to “control” the signal. In general, two different ways of quenching, respectively energy transfers are mainly used: *dynamic* and *static quenching*. *Fluorescence resonance energy transfer* (FRET) or *resonance energy transfer* (RET) as well as *collisional* and *electron-transfer* quenching are mechanisms of *dynamic quenching* whereas *static quenching* includes the formation of a *ground-state complex*.^[76;85;87]

Dynamic quenching:

Common mechanisms for dynamic quenching of excited states can be summarized with the equations listed below:



In which S^* is an excited singlet state compared to S in the ground state, Q is a quencher with the corresponding excited state Q^* . S^+ , S^- , Q^- and Q^+ are the charged species of the singlet state and the quencher unit.^[85]

Successful energy transfer (FRET and RET) depends on certain conditions. The distance between the *donor* and the *acceptor* molecule should be in the range of 20-70 Å (*Förster distance*). Further, the *relative orientation* of the molecules to each other (parallel) and the *spectral overlapping* of the emission spectrum of the donor molecule and the absorbance spectrum of the acceptor unit have to be guaranteed (Figure 1.40).

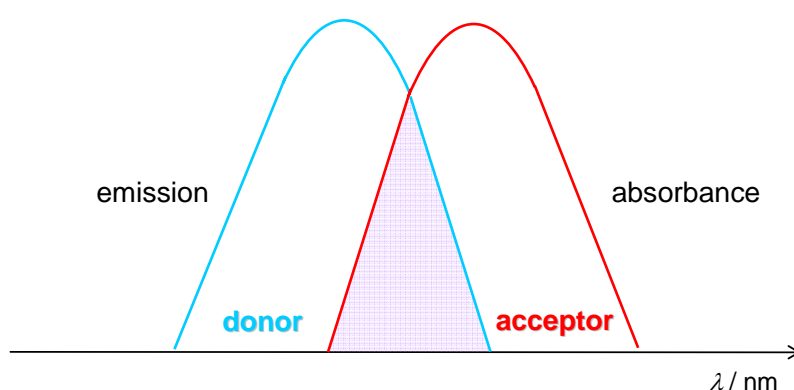


Figure 1.40. Illustration of the required spectral overlap of the donor emission spectra and the acceptor absorbance spectra.

Here, excitation of the donor molecule leads to emission of photons that can be directly absorbed by the acceptor molecule. Table 1.2 shows a list with common donor-acceptor pairs for FRET (FRET pairs).

Table 1.2. Selection of FRET pairs.^[88]

Donor	Acceptor
Fluorescein	Tetramethylrhodamine or Fluorescein
IAEDANS	FITC or 5-(Iodoacetamido)fluorescein
EDANS	Dabcyl
Tryptophan	IAEDANS or Dansyl or Pyrene
Dansyl	Fluorescein
Naphthalene	Dansyl
Pyrene	Coumarin
B-Phycoerythrin	Cy5

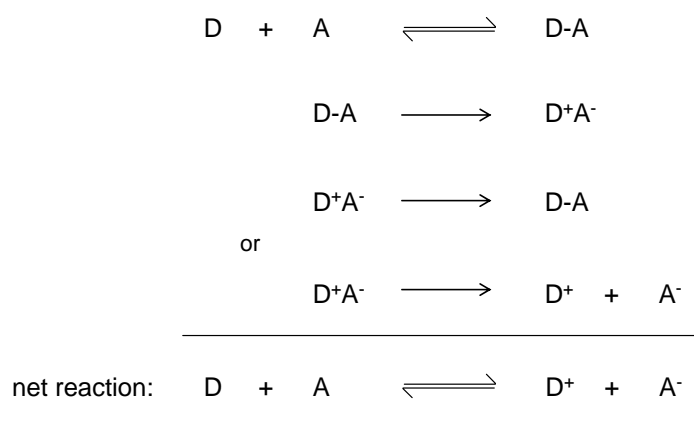
A common used quencher in assays is Dabcyl, 4-(4-dimethylaminophenyl) diazenylbenzoic acid. This acceptor molecule is able to quench the chromophores introduced in the multicolor molecular beacon experiments above and more (Table 1.3).^[81]

Table 1.3. Donor chromophores for multicolor MB assays, the maximal emission wavelength λ_{em} , the quenching efficiency $Q\%$ with the acceptor unit Dabcyl.^[81]

Donor	λ_{em} [nm]	$Q\%$	Acceptor
◆ Coumarin	475	99.3	◆ Dabcyl
◆ EDANS	491	99.5	
◆ Fluorescein	515	99.9	
◆ Lucifer yellow	523	99.2	
◆ Tetramethylrhodamine	575	98.7	
◆ Texas red	615	99.1	
◆ BODIPY	525	95.0	
◆ Eosin	543	98.2	

Collisional quenching is based on an internal exchange of energy from an excited species to an acceptor molecule upon collision (quencher, preferably a heavy species such as an iodide ion).^[85] The quencher releases the gained energy in a non-radiative process and decays back to its ground state.

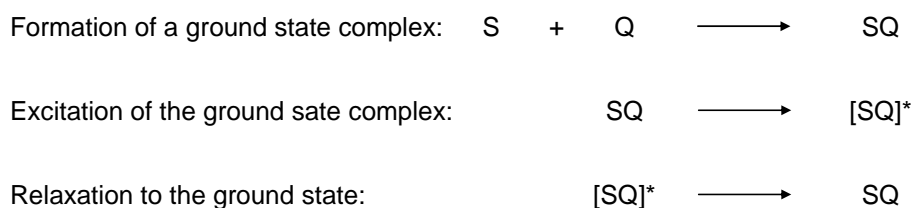
Quenching through *electron transfer* can be summarized in a very simplified way with the following mechanism:



D and **A** are the donor and acceptor moieties forming a donor-acceptor **D-A** complex in an assumed equilibrium. In a next step electron transfer takes place within the **D-A** complex and either a regeneration of a **D-A** complex is formed or separation through dissociation of the charged species occurs.

Static quenching:

The main difference of *dynamic* and *static quenching* is that in the first case a single species (**S**) is excited and in the other one a non-fluorescent ground state complex (**SQ**) between a donor (**S**) and an acceptor (**Q**) is formed and excited, leading to an *exciplex* generation (excited complex, [**SQ**]*) that decays back to the ground state complex.^[85;87]



Compared to *dynamic quenching*, *static (or contact) quenching* is temperature dependent due to the interactions of the donor-acceptor complex. The stacking interactions are mainly based on hydrophobic forces and electrostatic effects. Therefore, the complex possesses unique spectroscopic properties.

However, a clear separation between *dynamic* and *static quenching* of a system is often not possible because many systems generate these processes simultaneously.

1.6 Aim of the Work

The first part of this thesis aims at the development of hybridization probes based on the molecular beacon design using polyaromatic base surrogates as signal control system. Two important basic elements of the working principle had to be fulfilled:

- generation of a strong fluorescence signal
- reliable control of the signal through complete quenching in the native form

In our group, pyrene derivatives are well investigated and appreciated for their ability to form excimers. Especially dialkynylpyrene building blocks generate a bright excimer signal in the range of 450 - 600 nm. Besides that, this derivative possesses appropriate spectroscopic characteristics that enable the investigation of molecular aggregation and disaggregation by *UV/Vis* and *circular dichroism* measurements. This bright excimer signal requires a reliable quencher moiety. A previous study about perylenediimide building blocks in our group led to the resolution of choosing this base surrogate for quenching. Next, undesired base-pairing on the part of bases within the arm sequence has to be prevented. Consequently, additional stem designs had to be investigated up to a complete leave of the stem (stemless probe).

Second, the arrangement of the chosen base surrogates in a DNA framework was studied to investigate the interactions of these polyaromatic molecules and the outcoming characteristic properties. The formation of multichromophoric complexes was studied in a double-helical as well as in a triple-helical DNA design.

1.7 Importance of the Work

This work shows the unique properties of a donor-acceptor complex build up with dialkynylpyrene and perylenediimide derivatives. Based on the spectroscopic properties of these polyaromatic base surrogates, their behaviour within a DNA framework and consequently the influence of the neighbouring nucleotides on the chromophores could be studied. Together with the probe design of a molecular beacon, a highly sensitive and robust hybridization probe was developed. Further, stacking interactions between the chromophores lead to an increase in thermal stability of a natural duplex predestined for the minimization of the natural stem part of the molecular beacon to increase the specificity of the hybridization probe by preventing undesired base-pairing. The use of such a donor-acceptor complex as signal generation and control system enables a high sensitivity, selectivity and in dedicated cases a two-color read-out.

1.8 References

- [1] www.historyorb.com
- [2] www.nature.com
- [3] www.rsc.org/Education/Teachers/Resources/periodictable
- [4] www.fmi.ch/about/history/friedrichmiescher
- [5] www.fml.tuebingen.mpg.de
- [6] R. D. Simoni, R. L. Hill, M. Vaughan, *J.Biol.Chem.* **2002**, 277, 23-24.
- [7] P. A. Levene, *J.Biol.Chem.* **1919**, 40, 415-424.
- [8] www.dnalc.org/view/16378-Gallery-17-Oswald-Avery-around-1930.html
- [9] O. T. Avery, C. M. MacLeod, M. McCarty, *J.Exp.Med.* **1944**, 79, 137-158.
- [10] www.leeds.ac.uk/library/spcoll/digiteach.htm
- [11] W. T. Astbury, *Trans.Faraday Soc.* **1933**, 29, 193-205.
- [12] www.admissions.caltech.edu/about/history
- [13] L. Pauling, R. B. Corey, *Proc.Natl.Acad.Sci.USA* **1952**, 39, 84-97.
- [14] M. Meili, *UNIPRESS* **2003**, 119, 5-7.
- [15] M. Meili, *Chimia* **2003**, 57, 735-740.
- [16] H. Staudinger, R. Signer, *Helv.Chim.Acta* **1928**, 11, 1047-1051.
- [17] R. Signer, *Z.Physik.Chem.A* **1930**, 150, 257-284.
- [18] R. Signer, H. Gross, *Helv.Chim.Acta* **1934**, 17, 335-351.
- [19] R. Signer, H. Schwander, *Helv.Chim.Acta* **1949**, 32, 853-859.
- [20] J. Watson, *Die Doppelhelix*, 20. Auflage, Rowohlt Taschenbuch Verlag, Reinbek bei Hamburg **2007**.
- [21] F. Crick, *What Mad Pursuit*, Basic Books, Inc., Publishers, New York **1988**.
- [22] A. Sayre, *Rosalind Franklin and DNA*, W. W. Norton and Company Inc., New York, **1975**.
- [23] R. E. Franklin, R. G. Gosling, *Nature* **1953**, 171, 740-741.
- [24] <http://kingscollections.org/exhibitions/archives/dna>
- [25] E. Chargaff, R. Lipshitz, C. Green, M. E. Hodes, *J.Biol.Chem.* **1951**, 192, 223-230.
- [26] J. D. Watson, F. H. C. Crick, *Nature* **1953**, 171, 737-738.
- [27] www.nobelprize.org

- [28] H. G. Khorana, *Science* **1979**, 614-625.
- [29] H. G. Khorana, G. M. Teuer, J. G. Moffat, E. H. Pol, *Chem.Ind. (London)*, **1956**, 1523-1523.
- [30] U. L. RajBhandary, *Nature* **2011**, 480, 322-322.
- [31] S. L. Beaucage, M. H. Caruthers, *Tetrahedron Lett.* **1981**, 22, 1859-1862.
- [32] M. H. Caruthers, M. D. Matteuci, *J.Am.Chem.Soc.* **1981**, 103, 3185-3191.
- [33] N. D. Sinha, J. Biernat, J. McManus, H. Koester, *Nucl.Acids Res.* **1984**, 11, 4539-4557.
- [34] P. A. Levene, *J.Am.Chem.Soc.* **1901**, 23, 486-487.
- [35] P. A. Levene, H. S. Simms, *J.Biol.Chem.* **1925**, 65, 519-534.
- [36] W. Saenger, *Principles of nucleic acid structures*, Springer Verlag, **1984**.
- [37] www.news-medical.net/health/What-is-DNA.aspx
- [38] www.siumed.edu
- [39] S. Diekman, *Workshop: Definitions and nomenclature of nucleic acid structure parameters, EMBO J.* **1989**, 8, 1-4.
- [40] nar.oxfordjournals.org
- [41] R. Häner, *Lecture: Principles of Nucleic Acids - Structure, Synthesis and Intercalation*, **2010**.
- [42] T. Hermann, D. Patel, *Structure* **2000**, 10, R47-R54.
- [43] G. Felsenfeld, D. R. Davies, A. Rich, *J.Am.Chem.Soc.* **1957**, 79, 2023-2024.
- [44] G. Felsenfeld, A. Rich, *Biochim.Biophys.Acta* **1957**, 26, 457-468.
- [45] K. Hoogsteen, *Acta Crystallogr.* **1959**, 12, 822-823.
- [46] T. Le Doan; L. Perrouault, D. Praseuth, N. Habhoub, J. L. Decout, N. T. Thuong, J. Lhomme, C. Hélène, *Nucl.Acids Res.* **1987**, 15, 7749-7760.
- [47] M. D. Frank-Kamenetskii, C. M. Mirkin, *Annu.Rev.Biochem.* **1995**, 64, 65-95.
- [48] R. Zain, J. S. Sun, *Cell.Mol.Life Sci.* **2003**, 60, 862-870.
- [49] D. Vlieghe, L. Van-Meervelt, A. Dautant, B. Gallois, G. Précigoux, O. Kennard, *Science* **1996**, 273, 1702-1705.
- [50] S. Rhee, Z. Han, K. Liu, H. T. Miles, D. R. Davies, *Biochemistry* **1999**, 38, 16810-16815.
- [51] A. Mayer, *Inauguraldissertation der Phil.-nat. Fakultät der Universität Bern*, **2005**.

-
- [52] www.biochemsoctrans.org
- [53] M.-P. Teulade-Fichou, D. Perrin, A. Boutorine, D. Polverari, J.-P. Vigneron, J.-M. Lehn, J.-S. Sun, T. Garestier, C. Hélène, *J.Am.Chem.Soc.* **2001**, 123, 9283–9292.
- [54] J. T. Davis, *Angew.Chem.Int.Ed.* **2004**, 43, 668-698.
- [55] S. Burge, *Nucl.Acids Res.* **2006**, 34, 5402-5415.
- [56] B. Armitage, *Nat.Chem.Biol.* **2007**, 3, 203-204.
- [57] www.chem.cmu.edu/groups/army/index_files/Page855.html
- [58] L. H. Hurley, *Nature Reviews Cancer*, **2002**, 2, 188-200.
- [59] A. Siddiqui-Jain, C. L. Grand, D. J. Bearss, *Proc.Natl.Acad.Sci. USA* **2002**, 99, 11593-11598.
- [60] L. R. Bell, B. Byers, *Proc.Natl.Acad.Sci. USA* **1979**, 76, 3445-3449.
- [61] N. C. Seeman, *J.Theor.Biol.* **1982**, 99, 237-247.
- [62] N. R. Kallenbach, R. I. Ma, N. C. Seeman, *Nature (London)* **1983**, 305, 829-831.
- [63] J. H. Chen, M. E. A. Curchill, T. D. Tullius, N. R. Kallenbach, N. C. Seeman, *Biochemistry* **1988**, 85, 6032-6038.
- [64] A. I. H. Murchie, R. M. Clegg, E. von Kitzing, D. R. Duckett, S. Diekmann, D. M. J. Lilley, *Nature (London)* **1989**, 341, 763-766.
- [65] D. R. Duckett, A. I. H. Murchie, D. M. J. Lilley, *EMBO J.* **1990**, 9, 583-590.
- [66] D. R. Duckett, D. M. J. Lilley, *EMBO J.* **1990**, 9, 1659-1664.
- [67] N. C. Seeman, *DNA Cell Biol.* **1991**, 10, 475-486.
- [68] Y. Wang, J.E. Muller, B. Kemper, N. C. Seeman, *Biochemistry* **1991**, 30, 5667-5674.
- [69] M. Lu, Q. Guo, N. R. Kallenbach, *Biochemistry* **1991**, 30, 5815-5820.
- [70] J. Chen, N. C. Seeman, *Nature (London)* **1991**, 350, 631-633.
- [71] T. J. Fu, N. C. Seeman, *Biochemistry* **1993**, 32, 3211-3220.
- [72] D. M. J. Lilley, R. M. Clegg, *Annu.Rev.Biophys.Biomol.Struct.* **1993**, 22, 299-328.
- [73] S. Zhang, T. J. Fu, N. C. Seeman, *Biochemistry* **1993**, 32, 8062-8067.
- [74] N. C. Seeman, N. R. Kallenbach, *Annu.Rev.Biophys.Biomol.Struct.* **1994**, 23, 53-86.
- [75] S. Tyagi, F. R. Kramer, *Nat.Biotechnol.* **1996**, 14, 303-308.
- [76] T. Förster, *Naturwissenschaften* **1946**, 33, 166-175.
- [77] S. A. E. Marras, F. R. Kramer, S. Tyagi, *Nucl.Acids Res.* **2002**, 30, e122.
- [78] www.molecular-beacons.org

- [79] H.H. El-Hajj, S. A. Marras, S. Tyagi, E. Shashkina, M. Kamboj, T. E. Kiehn, M. S. Glickman, F. R. Kramer, D. Alland, *J.Clin.Microbiol.* **2009**, 47, 1190-1198.
- [80] G. Bonnet, S. Tyagi, A. Libchaber, F. R. Kramer, *Proc.Natl.Acad.Sci.USA* **1999**, 96, 6171-6176.
- [81] S. Tyagi, D. P. Bratu, F. R. Kramer, *Nat.Biotechnol.* **1998**, 16, 49-53.
- [82] S. A. E. Marras, F. R. Kramer, S. Tyagi, *Genet.Anal.* **1999**, 14, 151-156.
- [83] S. Tyagi, S. A. E. Marras, F. R. Kramer, *Nat.Biotechnol.* **2000**, 18, 1191-1196.
- [84] www.umdj.edu
- [85] P. Atkins, J. de Paula, *Physical Chemistry for the life Science*, Oxford University Press, Oxford **2006**.
- [86] www.photochemistry.wordpress.com
- [87] K. Wang, Z. Tang, C. J. Yang, Y. Kim, X. Fang, W. Li, Y. Wu, C. D. Medley, Z. Cao, J. Li, P. Colon, H. Lin, W. Tan, *Angew.Chem.Int.Ed.* **2008**, 47, 2-17.
- [88] FluoProbes® *BioDirectory of Fluorescence*, **2005**.

2. A Highly Sensitive, Excimer-Controlled Molecular Beacon

Published in: Robert Häner, Sarah M. Biner, Simon M. Langenegger, Tao Meng, and Vladimir L. Malinovskii, *Angew.Chem.Int.Ed.* **2010**.

2.1 Abstract

Non-nucleosidic chromophores in the stem of a molecular beacon inhibit excimer fluorescence through the formation of a donor–acceptor complex. The excellent reduction of the background fluorescence allows the detection of DNA and RNA targets in the presence of a significant excess of the probe.

2.2 Introduction

Molecular beacons (MBs) are widely used hairpin probes for the specific detection of DNA and RNA targets.^[1-8] First proposed by Tyagi and Kramer,^[1] the concept of a MB is based on the interaction between a fluorescent and a quenching molecule. In the absence of the target, the MB adopts a hairpin structure resulting in close proximity of the two terminally attached chromophores and, hence, fluorescence quenching, whereas hybridization of the target to the MB loop region leads to spatial separation of fluorophore and quencher and concomitant signal appearance. The choice of the stem is a crucial aspect in the design of MBs. Its stability must be finely tuned to ensure close proximity of the dyes in the native form (→ low *background* signal) and, at the same time, allow efficient hybridization with the target (→ high *sensitivity*). Additionally, it should not take part in unintended target hybridization, which might adversely affect *selectivity*, or interfere with formation of the hairpin structure, e.g. by binding to the loop sequence which may also lead to an increase in background or a loss in signal intensity. Several types of stem-modified beacons were presented to address

these issues.^[9-15] Incomplete fluorescence quenching in the hairpin form is a well-recognized drawback and different directions were described to overcome this problem, including the use of time-resolved fluorescence techniques,^[16] wavelength-shifted^[17-19] or super-quenched beacons,^[20] the formation of triple-helical stems^[21;22] or stemless PNA beacons.^[23] In this chapter, a molecular beacon is proposed, in which signal control is accomplished by formation of a donor-acceptor (D-A) complex.^[24-28] As illustrated in **Figure 2.1**, the stem contains pairs of non-nucleosidic pyrene derivatives (**Y**) and perylenediimides (PDIs, **E**) that can interact in an interstrand stacking mode.^[29-31]

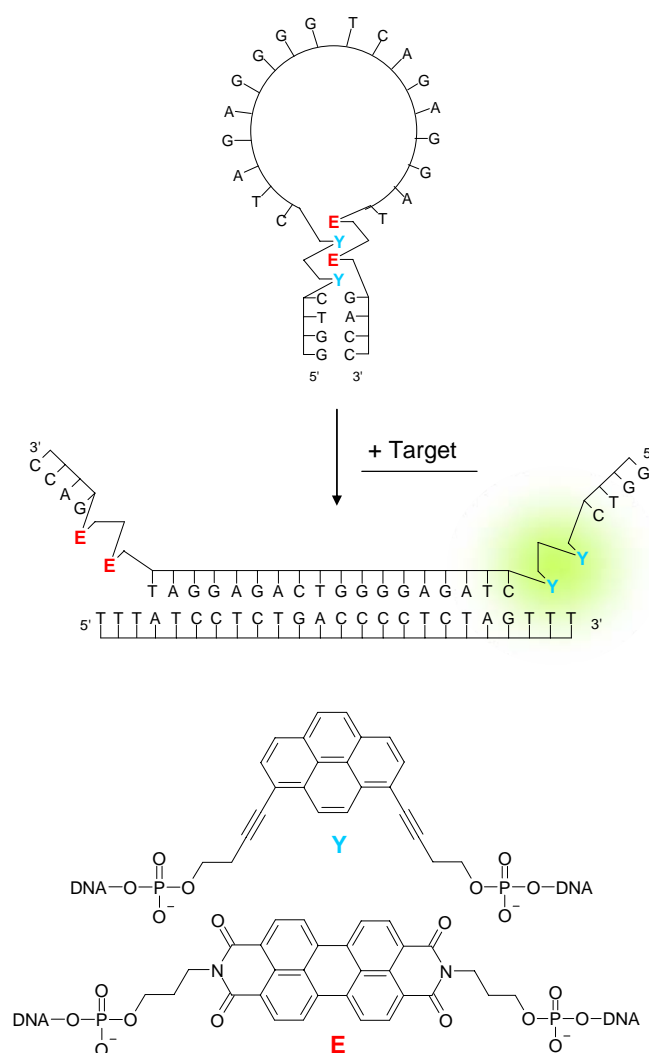


Figure 2.1. Illustration of an excimer-controlled MB; excimer formation between 1,8-dialkynylpyrenes (**Y**) is prevented by the formation of a D-A complex with 3,4,9,10-perylenetetracarboxylic diimide PDI (**E**) in the native form (stem-loop-structure).

In the native structure this leads to efficient signal suppression whereas the hybridized form is characterized by an excimer signal^[32-35] produced by the two adjacent pyrene derivatives.^[36] Additionally, the formation of a D-A complex helps keeping the number of natural bases in the stem minimal thus reducing the chances of unwanted base pairing interactions.

2.3 Investigation of a donor-acceptor based MB

Certain oligonucleotide sequences have been synthesized to investigate the D-A based MB. The oligomers used in this study are listed in Table 2.1. An 18-mer probe sequence was chosen arbitrarily. Four target sequences (DNA and RNA) were tested with either a completely matching sequence or each with a single mismatch. The two pairs of pyrene derivatives and PDIs are located immediately adjacent to either side of the loop region. 1,8-Dialkynylpyrene **Y** is used because it forms a strongly fluorescent excimer with both a large extinction coefficient and a high quantum yield.^[37;38] Moreover, the extension of the pyrene aromatic core with two triple bonds renders this pyrene a particularly electron-rich component for a D-A complex. With four additional base pairs, the stem is of comparable length to that in conventional MBs (5-7 base pairs). D-A interstrand stacking interactions between the electron-rich alkynylpyrenes (**Y**) and the electron-poor PDIs (**E**) support a highly stable secondary structure. This interaction prevents excimer formation and fluorescence emission.

Table 2.1. MB, DNA and RNA target sequences.

MB1	5'	GGT	CYY	CTA	GAG	GGG	TCA	GAG	GAT	EEG	ACC
TD1	3'	TTT	GAT	CTC	CCC	AGT	CTC	CTA	TTT		
TD2	3'	TTT	<u>T</u> AT	CTC	CCC	AGT	CTC	CTA	TTT		
TD3	3'	TTT	GAT	CTC	<u>A</u> CC	AGT	CTC	CTA	TTT		
TD4	3'	TTT	GAT	CTC	CCC	<u>A</u> TT	CTC	CTA	TTT		
TR1	3'	UUU	GAU	CUC	CCC	AGU	CUC	CUA	UUU		
TR2	3'	UUU	<u>U</u> AU	CUC	CCC	AGU	CUC	CUA	UUU		
TR3	3'	UUU	GAU	CUC	<u>A</u> CC	AGU	CUC	CUA	UUU		
TR4	3'	UUU	GAU	CUC	CCC	<u>A</u> UU	CUC	CUA	UUU		

The non-nucleosidic building blocks 1,8-dialkynylpyrene (**Y**) and PDI (**E**) are highlighted in bold and the mismatches are underlined.

2.3.1 Spectroscopic investigation of the MB by fluorescence measurements

The quality of the probe was first analyzed by steady-state fluorescence spectroscopy. Thereby emission spectra of the **MB1** probe in its native form (closed) and in presence of the fully matched target DNA strand were studied. Upon titration of the fully matched target DNA **TD1**, a strong excimer signal at around 520 nm is generated, which increases linearly up to 1.0 equivalent ($R^2 = 0.997$) of target before leveling off (Figure 2.2). A signal-to-background (S/B)^[39] ratio of 434 and a quenching efficiency (Q) of 99.8% were determined (for more details see *Experimental part*).

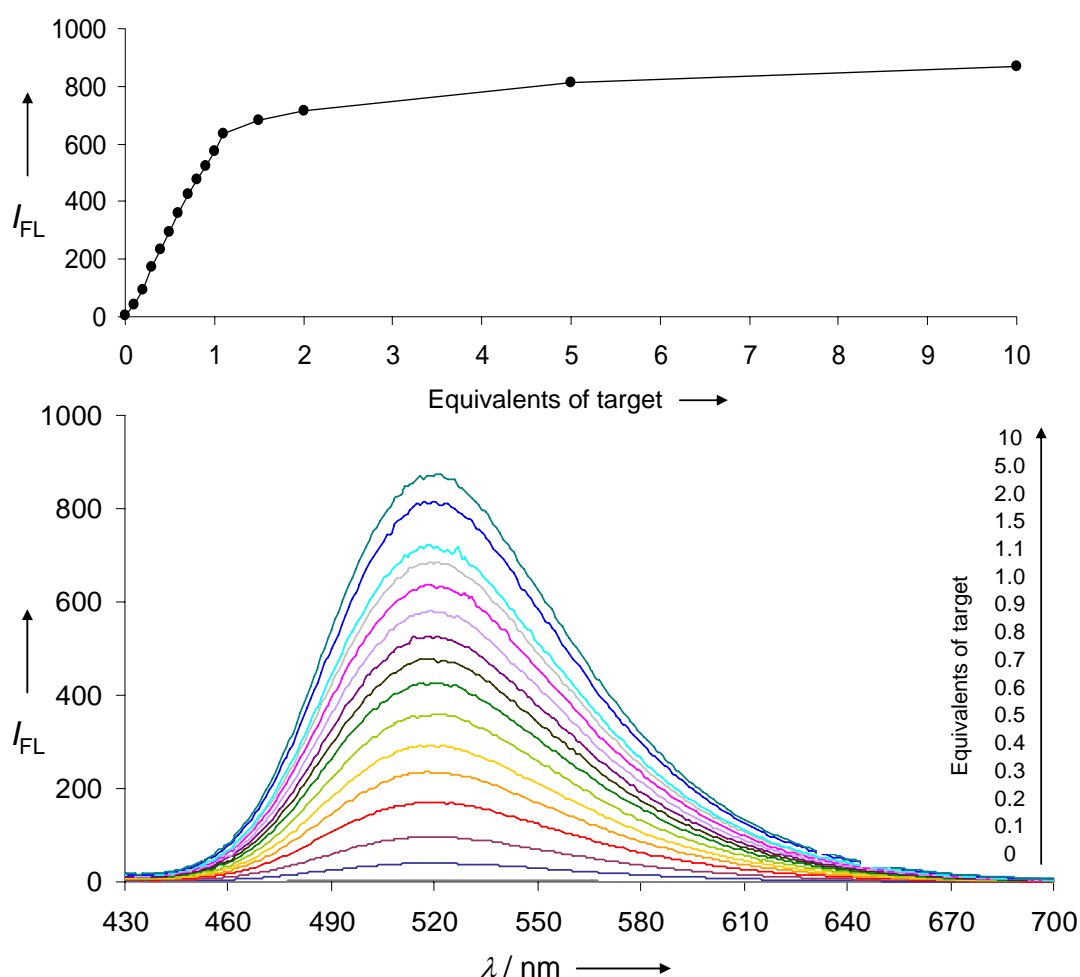


Figure 2.2. Fluorescence read-out obtained with **MB1** (1.0 μM) on hybridization with **TD1** (0 to 10 eq., steps as indicated). Conditions: λ_{ex} : 370 nm, PMT voltage: 600 V, ex/em slit widths: 10/5 nm, 10 mM sodium phosphate buffer pH 7.0, 100 mM NaCl, 37°C, top: concentration-dependent signal intensities obtained at 520 nm.

2.3.2 Selectivity study of the MB

The excimer-controlled **MB1** efficiently differentiates between matched and mismatched DNA and RNA targets. Mismatches located near the middle of the target sequence or at the pyrene-bearing end were tested (sequences see Table 2.1). Temperature-variable fluorescence curves (Figure 2.3) show a loss of signal intensity with all mismatched targets at substantially lower temperatures than with the matched target (Table 2.2).

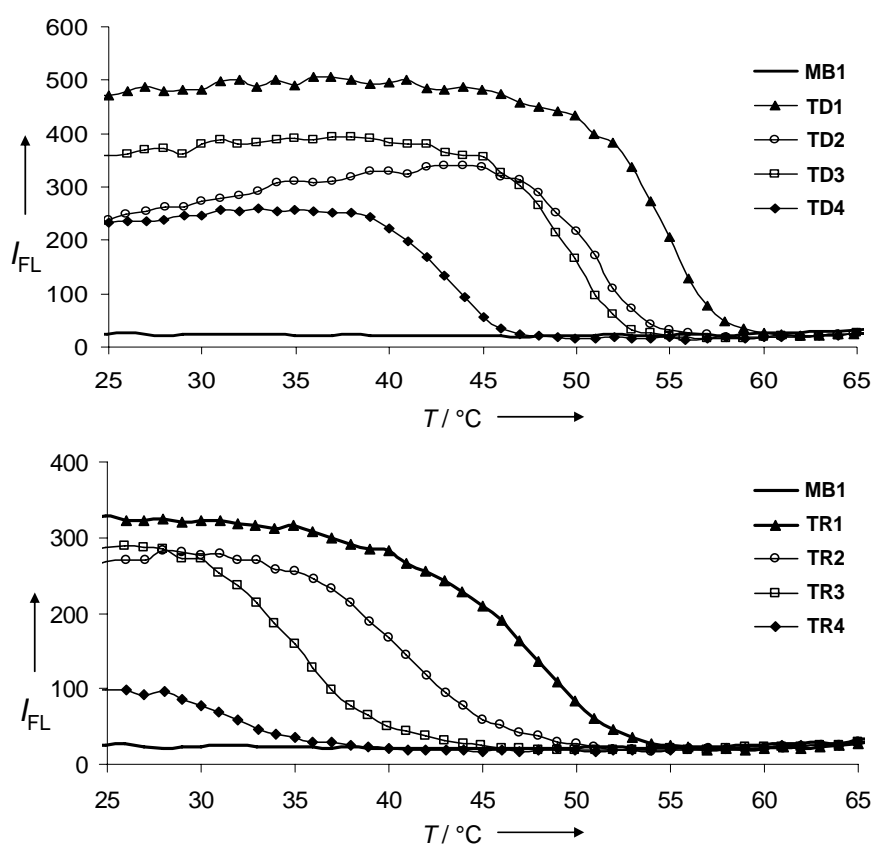


Figure 2.3. **MB1** excimer signal intensities gained in the presence of 1.0 equivalent of matched and mismatched DNA (top: **TD1-TD4**) and RNA (bottom: **TR1-TR4**) targets. Conditions: **MB1** 0.1 μM , 0.1 μM **TDn** resp. **TRn**, 10 mM sodium phosphate buffer, pH 7.0, 100 mM NaCl, λ_{ex} : 370 nm, λ_{em} : 520 nm, ex/em slit widths: 5/5 nm; PMT voltage: 800 V, performance of three ramps (90-20 $^\circ\text{C}$ / 20-90 $^\circ\text{C}$ / 90-20 $^\circ\text{C}$), heating/cooling rate: 0.5 $^\circ\text{C}/\text{min}$, only heating ramps are shown.

Table 2.2. Melting temperatures of **MB1** hybridized to DNA and RNA targets obtained from fluorescence measurements.

DNA hybrid ^[a]	T_m (°C) ^[b]	RNA hybrid ^[a]	T_m (°C) ^[b]
MB1*TD1	55	MB1*TR1	47
MB1*TD2	51	MB1*TR2	41
MB1*TD3	50	MB1*TR3	35
MB1*TD4	44	MB1*TR4	28

[a] conditions see [Figure 2.3](#); [b] estimated error $\pm 1^\circ\text{C}$.

2.3.3 Investigation of the donor-acceptor based signal control system

The quantum yield of excimer fluorescence (Φ) of **MB1** in the presence of 1.0 equivalent of DNA target **TD1** is 0.12. Together with the high absorptivity for the two bis-alkynylpyrenes ($\epsilon \sim 70^3 000 \text{ L mol}^{-1} \text{ cm}^{-1}$)^[37] this translates to a brightness of approximately $8400 \text{ L mol}^{-1} \text{ cm}^{-1}$. Spectral overlap between excimer emission and PDI absorbance is excellent and may, therefore, lead to a partial reduction in signal intensity by mean of a FRET mechanism. This potential signal loss however, is compensated by the high bis-pyrenyl absorptivity.

Fluorescence quenching in conventional MBs is described in the literature as dynamic (FRET mechanism) or static (ground state complex) quenching.^[40;41] Both *static* and *dynamic* quenching are often incomplete resulting in a large background signal, which is a major drawback for the detection of target molecules at low concentrations.^[2;6] In the present type of beacon, the excimer signal from the **YY** dimer that appears in the open form is entirely cancelled in the hairpin structure due to formation of a D-A complex **EY EY** in the stem with two PDIs ([Figure 2.4](#)).^[42-44]

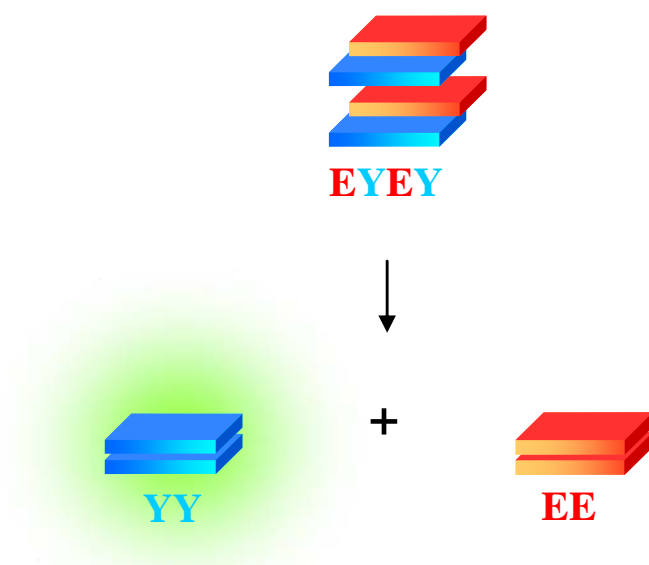


Figure 2.4. Simplified illustration of the chromophoric complex in the closed form (top) and in the open form (bottom). The perylenediimide (**E**) moieties are illustrated in red whereas the alkynylpyrene (**Y**) units are shown in blue and upon dimerization a green highlight representing the excimer formation is charted.

Based on the spectroscopic data formation of an **EY EY** complex seems most likely. UV/Vis and circular dichroism (CD) spectroscopy indicate the stacking of PDI and alkynylpyrene units (Figure 2.5). PDIs are involved in stacking interactions over the whole temperature range as indicated by the vibronic band pattern.^[45] The 0→1 transition (507 nm to 500 nm, blue-shift upon increasing temperature) is over the whole temperature range the higher signal indicating an aggregation of the PDI molecules. But, direct PDI-PDI (**EE**) interactions in a helical arrangement are unlikely because of very weak exciton coupled CD in the closed form.

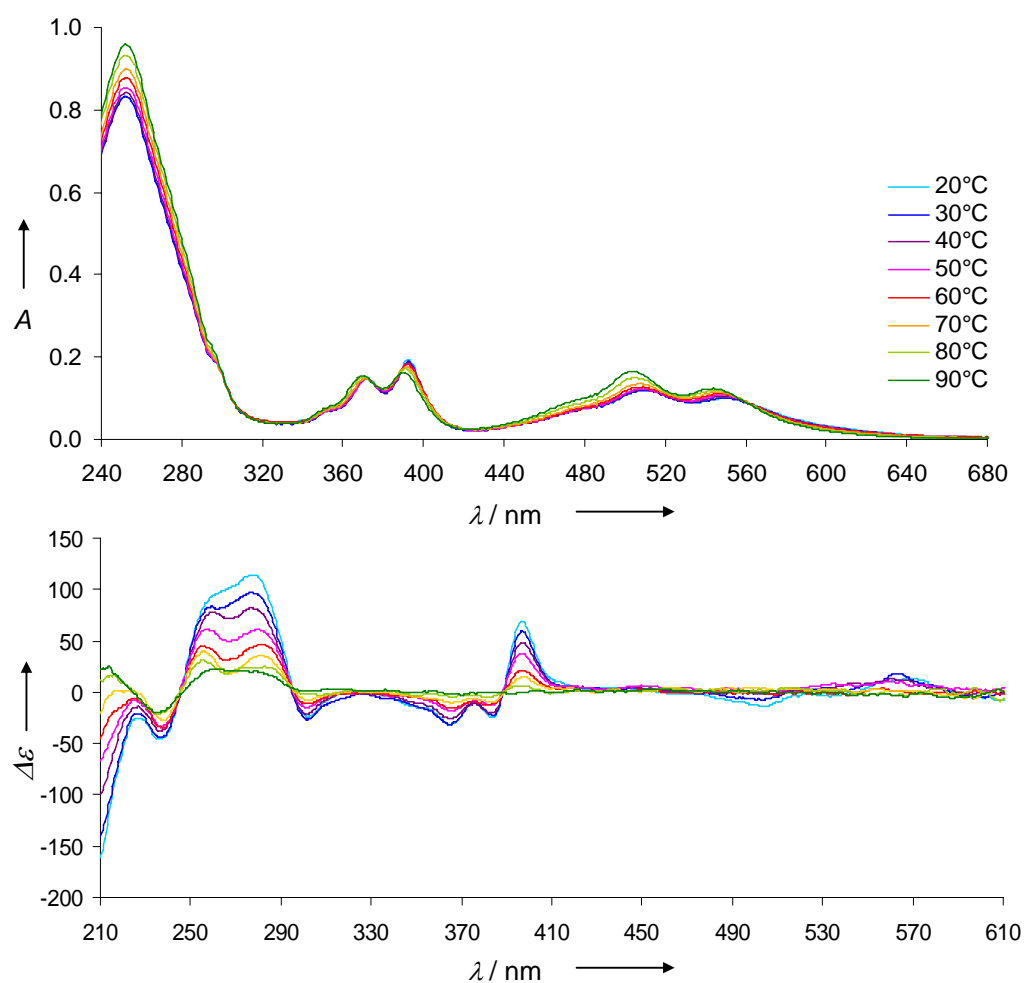


Figure 2.5. Temperature-dependent absorbance (top) and CD (bottom) spectra of **MB1**. Conditions: **MB1** 2.0 μM , 10 mM sodium phosphate buffer pH 7.0, 100 mM NaCl, equilibration time: 10 min.

The vibronic band pattern of the alkynylpyrenes differs from the previously reported pyrene dimeric stacks leading to the suggestion of a change in aggregation upon increasing temperature (**Y/Y** to **YY**).^[37]

In the presence of the target (open form) the two PDI units are in direct proximity, and this accompanied by an increase in the CD couplet (Figure 2.6) and an aggregated state of the alkynylpyrenes shown in the corresponding characteristic vibronic band pattern. Taken together, these data suggest that an **EY₂E** complex is dominant in the closed form of the beacon.

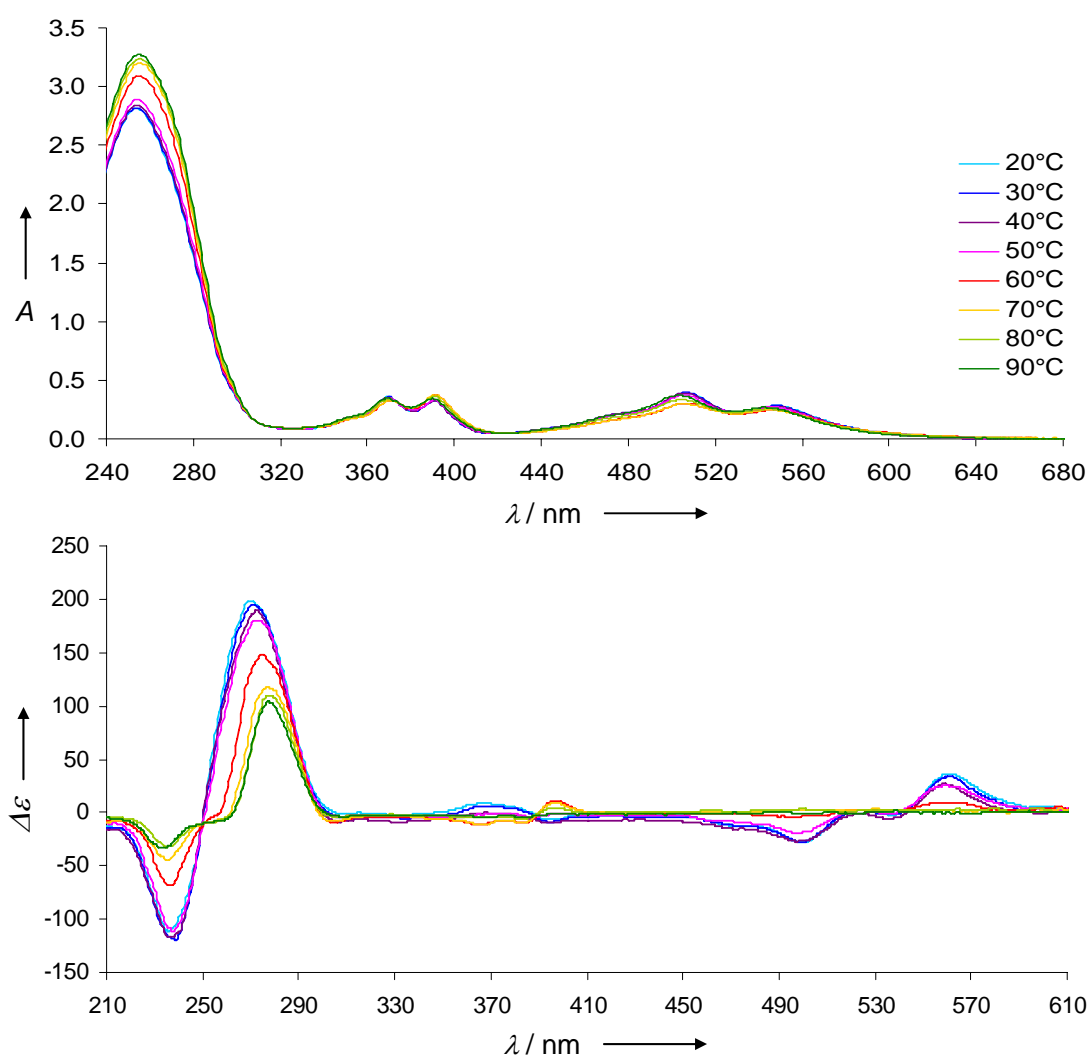


Figure 2.6. Temperature-dependent absorbance (top) and CD (bottom) spectra of hybrid **MB1*TD1**. Conditions: **MB1** 5.0 μM , **TD1** 6.0 μM , 10 mM sodium phosphate buffer pH 7.0, 100 mM NaCl, equilibration time: 10 min.

2.3.4 Sensitivity study of the excimer-controlled MB

As mentioned, fluorescence in the present beacon is suppressed by physical separation of the two alkynylpyrenes. This chromophoric system results in very robust signal characteristics: high signal intensity, largely red-shifted emission, and low background fluorescence. These features allow the detection of the DNA target **TD1** at low nanomolar concentrations (Figure 2.7). In the presence of 0.1 μM **MB1**, a resolved signal is still obtained at 0.001 μM (nM-

range) target concentration. Thus, the target is detectable at a concentration corresponding to 1% of beacon concentration. The calculated detection limit corresponds to a value of 0.3 nM.^[15] To the best of our knowledge such sensitivity has not been reported for molecular beacons in a simple hybridization assay.

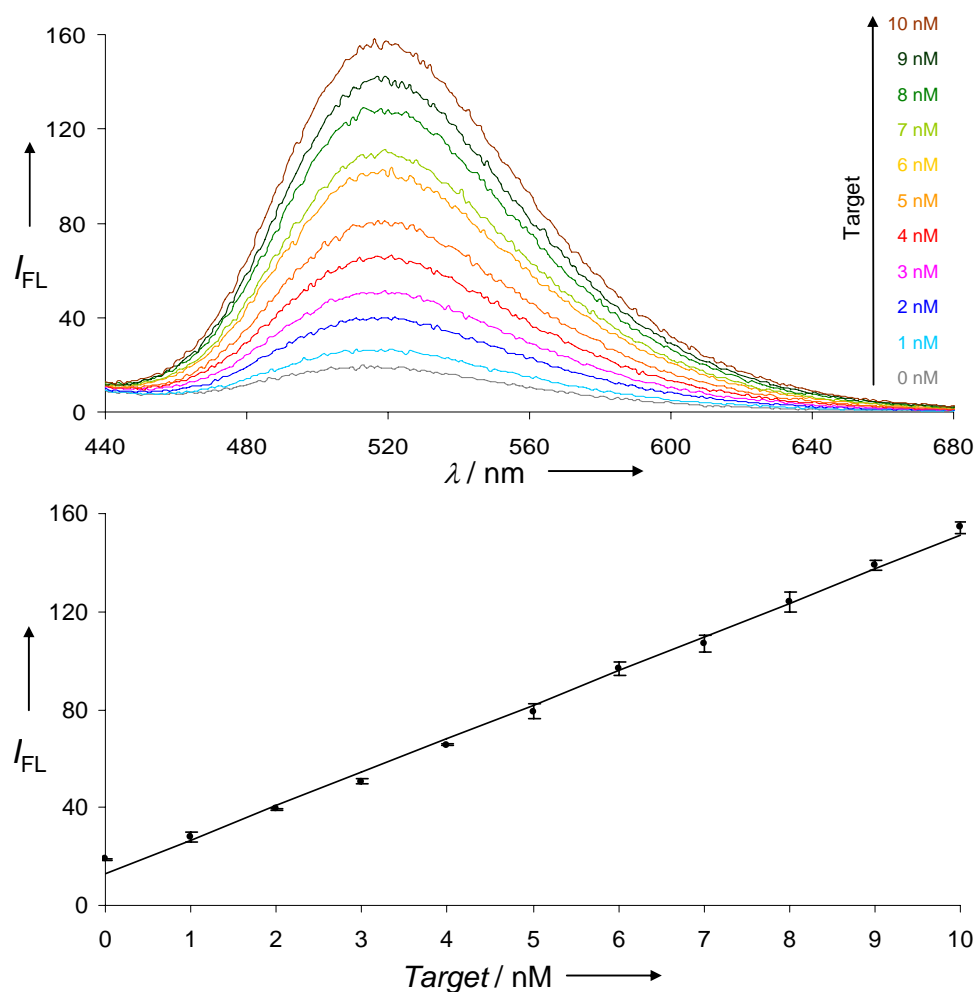


Figure 2.7. Top: fluorescence intensities obtained with **MB1** (0.1 μM) in the presence of 1 to 10 nM DNA target **TD1** in three independent triplicate experiments. The lower graph shows the 1-10 nM concentration range ($R^2 = 0.996$); Conditions: 10 mM sodium phosphate buffer pH 7.0, 100 mM NaCl, λ_{ex} : 370 nm, ex/em slit widths: 10/5 nm, PMT voltage: 800 V, Temp.: 37°C, equilibration time: 10 min.

2.4 Conclusion

In conclusion, an excimer-controlled molecular beacon in which the interaction between two pairs of non-nucleosidic chromophores (alkynylpyrene and perylenediimide) located in the stem is used for signal control (Figure 2.8). Excimer fluorescence is effectively inhibited by formation of a D-A complex between alkynylpyrene and PDI units that prevent the formation of an excited alkynylpyrene dimer. The high efficiency of excimer inhibition allows target detection in the presence of a large excess of beacon probe. In combination with the bright excimer fluorescence of the alkynylpyrene used, this enables the detection of target sequences at low nanomolar concentrations. The excellent sensitivity renders this type of beacon attractive for cellular imaging as well as for screening applications without prior amplification.

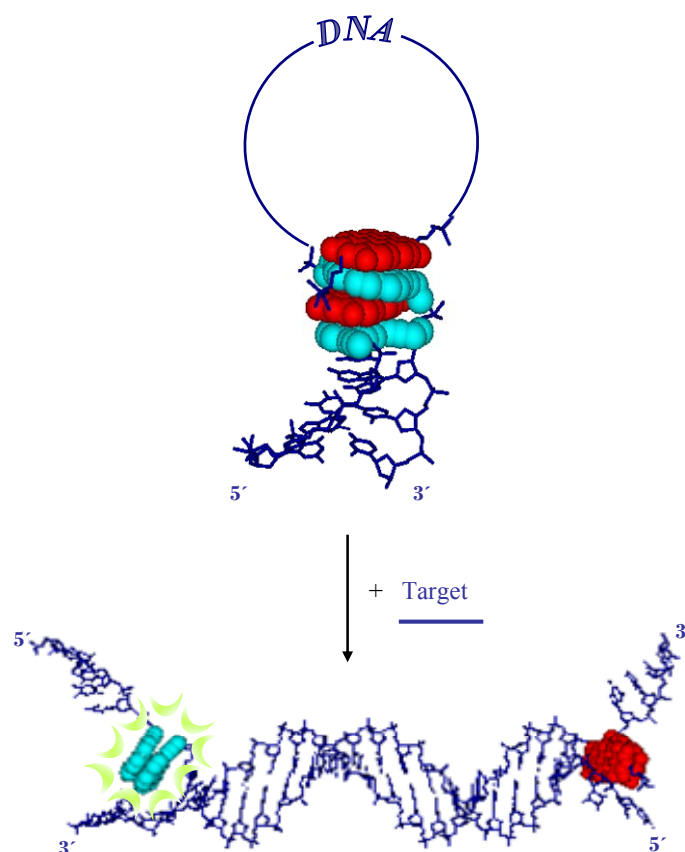


Figure 2.8. Model of **MB1** in closed form and hybrid **MB1*TD1** with a schematically representation of an excimer signal.

2.5 Experimental Part

Oligonucleotide synthesis. The required alkynylpyrene^[37] and PDI^[44] building blocks were synthesized according to published procedures. Commercial natural nucleoside phosphoramidites were used for oligonucleotide synthesis. Oligonucleotides **TD1-TD4** and **TR1-TR4** were purchased from *Microsynth*, Balgach, Switzerland. **MB1** was prepared *via* automated oligonucleotide synthesis by a standard synthetic procedure (2 min coupling time; ‘trityl-off’ mode) on a 394-DNA/RNA synthesizer (*Applied Biosystems*), except for the coupling step of the PDI phosphoramidite, which was performed manually by pushing forth and back the coupling solution through the synthesis column using a syringe at either end. Cleavage from the solid support and final deprotection was done by treatment with 30% NH₄OH solution at 55°C overnight.

Oligonucleotide purification and mass determination. Purification was done by reverse phase HPLC (LiChrospher 100 *RP-18*, 5µm, Merck; *Shimadzu LC-20AT*); eluent *A* = (Et₃NH)OAc (0.1 M, pH 7.4); eluent *B* = MeCN; elution at 30°C; gradient 5 – 20% *B* over 20 min. Mass spectrometry was performed with a Sciex QSTAR pulsar (hybrid quadrupole time-of-flight mass spectrometer, *Applied Biosystems*); ESI-TOF MS (negative mode, acetonitrile/H₂O/triethylamine) ([Table 2.3](#)).

Table 2.3. Specification of the modified oligonucleotide **MB1**.

	<i>molecular formula</i>	<i>HPLC t_R [min]</i>	<i>calcd. avg. mass</i>	<i>found avg. mass</i>
MB1	C ₃₆₃ H ₃₉₃ N ₁₁₂ O ₁₇₆ P ₂₉	18.7	10039.0	10039.6

Oligonucleotide analysis. Temperature-dependent UV/Vis spectra were carried out on a *Varian Cary-100 Bio-UV/Vis* spectrophotometer equipped with a *Varian Cary-block* temperature controller and data were collected with *Varian WinUV* software. CD spectra were recorded on a *JASCO J-715* spectrophotometer using quartz cuvettes with an optic path of 1 cm. Fluorescence spectra were recorded on a *Varian Cary Eclipse* fluorescence spectrophotometer equipped with a *Varian Cary-block* temperature controller using 1 cm x 1

cm quartz cuvettes. For the three independent measurements in the nanomolar range acryl cuvettes (10x10x48 mm) from *Sarstedt* were used. *Varian Eclipse* software was applied to investigate the fluorescence of **MB1**. Experiments containing RNA targets were prepared in RNase free solutions and vessels.

Determination of signal-to-background ratios and quenching efficiencies. The signal-to-background (S/B) ratio and quenching efficiency (Q%) values were determined according to the formulas below (Table 2.4).^[39] Values were obtained for **MB1** in the presence of 1.0, 2.0 and 5.0 equivalents of target **TD1**:

$$S/B = (F_{\text{hybrid}} - F_{\text{buffer}}) / (F_{\text{MB}} - F_{\text{buffer}})$$

$$Q\% = 100 \times \{1 - ((F_{\text{MB}} - F_{\text{buffer}}) / (F_{\text{hybrid}} - F_{\text{buffer}}))\}$$

Table 2.4. S/B and Q% values for **MB1**.

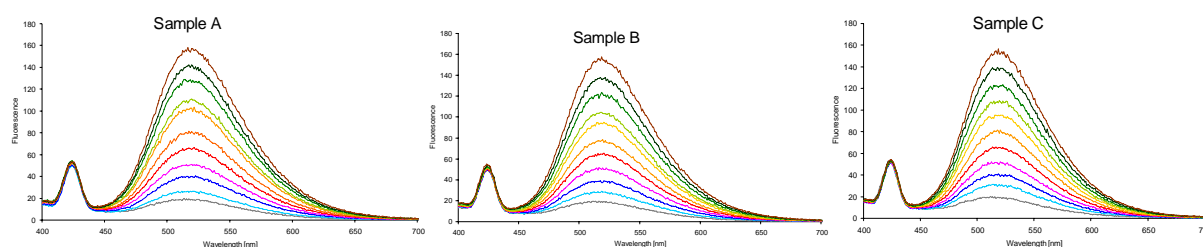
# of eq. TD1	1.0	2.0	5.0
signal-to-background	309	385	434
Q%	99.7	99.7	99.8

Quantum yield determination. The quantum yield Φ was determined by a comparative method employing quinine sulphate dihydrate as fluorescence standard as described previously in a publication by Häner and co-workers.^[46] Suitable **MB1** (1.0 μM) and **TD1** (1.1 μM) concentrations were chosen to ensure absorbance in the range of 0.1. Fluorescence measurements were performed with an excitation wavelength λ_{ex} of 364 nm. The calculated quantum yield is 0.12.

Determination of the limit of detection. The limit of detection was determined by three independent measurements. The titration experiments were performed with a **MB1** concentration of 0.1 μM and a target titration (**TD1**) from 0-10 nM at 37°C. The equilibration

time was set to 10 min. The arisen data lead to a linear regression (trend line), a standard deviation calculation and to the corresponding limit of detection (LOD) of 0.3 nM.

Statistical analysis of the spectroscopic response. Independent triplicate titration experiments were performed to execute a calculation of errors (Figure 2.9). The measurements were operated in acryl cuvettes at 37°C with an equilibration time of 10 min. A trend line equation with the corresponding coefficient of determination R^2 was determined.



Target conc. [nM]	sample A	sample B	sample C	average value	σ	$3x\sigma$
0	18.39602	19.04127	19.25273	18.89667	0.44628	1.33885
1	26.18906	28.06826	29.80412	28.02048	1.80800	
2	39.79875	39.14737	38.77082	39.23898	0.52005	
3	50.25163	49.87439	51.85114	50.65905	1.04947	
4	65.79274	65.29522	65.18909	65.42568	0.32228	
5	80.20857	75.87321	81.61073	79.23084	2.99111	
6	99.63212	95.10946	95.51110	96.75089	2.50328	
7	109.91760	103.24870	107.55230	106.90620	3.38107	
8	128.17600	120.38750	122.46440	123.67597	4.03313	
9	141.36290	137.10030	138.52470	138.99597	2.17003	
10	156.97050	154.20500	151.95120	154.37557	2.51399	

Figure 2.9. Concentration-dependent signal intensities gained for **MB1** at 520 nm with error bars based on three independent experiments performed in acryl cuvettes. Conditions: **MB1** 0.1 μ M, **TD1** 0-10 nM, 10 mM sodium phosphate buffer, pH 7.0, 100 mM NaCl, λ_{ex} : 370 nm, ex/em slit widths: 10/5 nm. Sample without target was heated to 90°C and cooled down to 20°C prior to measurement, equilibration time:10 min, Temp.: 37°C.

2.6 References

- [1] S. Tyagi, F. R. Kramer, *Nat.Biotechnol.* **1996**, 14, 303-308.
- [2] R. T. Ransinghe, T. Brown, *Chem.Commun.* **2005**, 5487-5502.
- [3] A. P. Silverman, E. T. Kool, *Trends Biotechnol.* **2005**, 23, 225-230.
- [4] S. A. E. Marras, S. Tyagi, F. R. Kramer, *Clin.Chim.Acta* **2006**, 363, 48-60.
- [5] N. Venkatesan, Y. J. Seo, B. H. Kim, *Chem.Soc.Rev.* **2008**, 37, 648-663.
- [6] K. M. Wang, Z. W. Tang, C. Y. J. Yang, Y. M. Kim, X. H. Fang, W. Li, Y. R. Wu, C. D. Medley, Z. H. Cao, J. Li, P. Colon, H. Lin, W. H. Tan, *Angew.Chem.Int.Ed.* **2009**, 48, 856-870.
- [7] W. H. Tan, K. M. Wang, T. J. Drake, *Curr.Opin.Chem.Biol.* **2004**, 8, 547-553.
- [8] P. Santangelo, N. Nitin, G. Bao, *Ann.Biomed.Eng.* **2006**, 34, 39-50.
- [9] O. Seitz, *Angew.Chem.Int.Ed.* **2000**, 39, 3249-3252.
- [10] H. Kuhn, V. V. Demidov, J. M. Coull, M. J. Fiandaca, B. D. Gildea, M. D. Frank-Kamenetskii, *J.Am.Chem.Soc.* **2002**, 124, 1097-1103.
- [11] C. Crey-Desbiolles, D. R. Ahn, C. J. Leumann, *Nucl.Acids Res.* **2005**, 33, e77.
- [12] L. Wang, C. Y. J. Yang, C. D. Medley, S. A. Benner, W. H. Tan, *J.Am.Chem.Soc.* **2005**, 127, 15664-15665.
- [13] Y. Saito, Y. Shinohara, S. S. Bag, Y. Takeuchi, K. Matsumoto, I. Saito, *Tetrahedron* **2009**, 65, 934-939.
- [14] Y. Ueno, A. Kawamura, K. Takasu, S. Komatsuzaki, T. Kato, S. Kuboe, Y. Kitamura, Y. Kitade, *Org.Biomol.Chem.* **2009**, 7, 2761-2769.
- [15] E. Socher, D. V. Jarikote, A. Knoll, L. Roglin, J. Burmeister, O. Seitz, *Anal.Biochem.* **2008**, 375, 318-330.
- [16] P. Conlon, C. J. Yang, Y. Wu, Y. Chen, K. Martinez, Y. Kim, N. Stevens, A. A. Marti, S. Jockusch, N. J. Turro, W. Tan, *J.Am.Chem.Soc.* **2008**, 130, 336-342.
- [17] S. Tyagi, S. A. E. Marras, F. R. Kramer, *Nat.Biotechnol.* **2000**, 18, 1191-1196.
- [18] P. Zhang, T. Beck, W. H. Tan, *Angew.Chem.Int.Ed.* **2001**, 40, 402-405.
- [19] A. Tsourkas, M. A. Behlke, Y. Q. Xu, G. Bao, *Anal.Chem.* **2003**, 75, 3697-3703.
- [20] C. J. Yang, H. Lin, W. Tan, *J.Am.Chem.Soc.* **2005**, 127, 12772-12773.
- [21] T. N. Grossmann, L. Roglin, O. Seitz, *Angew.Chem.Int.Ed.* **2007**, 46, 5223-5225.

- [22] Y. Xiao, K. J. I. Plakos, X. H. Lou, R. J. White, J. R. Qian, K. W. Plaxco, H. T. Soh, *Angew.Chem.Int.Ed.* **2009**, 48, 4354-4358.
- [23] E. Socher, L. Bethge, A. Knoll, N. Jungnick, A. Herrmann, O. Seitz, *Angew.Chem.Int.Ed.* **2008**, 47, 9555-9559.
- [24] C. A. Hunter, J. K. M. Sanders, *J.Am.Chem.Soc.* **1990**, 112, 5525-5534.
- [25] W. Y. Zhang, W. R. Dichtel, A. Z. Stieg, D. Benitez, J. K. Gimzewski, J. R. Heath, J. F. Stoddart, *Proc.Nat.Acad.Sci.(USA)* **2008**, 105, 6514-6519.
- [26] F. Würthner, *Chem.Commun.* **2004**, 1564-1579.
- [27] J. J. Reczek, B. L. Iverson, *Macromolecules* **2006**, 39, 5601-5603.
- [28] Z. Merican, K. D. Johnstone, M. J. Gunter, *Org.Biomol.Chem.* **2008**, 6, 2534-2543.
- [29] S. M. Langenegger, R. Häner, *Bioorg.Med.Chem.Lett.* **2006**, 16, 5062-5065.
- [30] S. M. Langenegger, R. Häner, *Chem.Commun.* **2004**, 2792-2793.
- [31] V. L. Malinovskii, F. Samain, R. Häner, *Angew.Chem.Int.Ed.* **2007**, 46, 4464-4467.
- [32] F. M. Winnik, *Chem.Rev.* **1993**, 93, 587-614.
- [33] F. Samain, V. L. Malinovskii, S. M. Langenegger, R. Häner, *Bioorg.Med.Chem.* **2008**, 16, 27-33.
- [34] R. Häner, F. Samain, V. L. Malinovskii, *Chem.Eur.J.* **2009**, 15, 5701-5708.
- [35] V. A. Galievsky, V. L. Malinovskii, A. S. Stasheuski, F. Samain, K. A. Zachariasse, R. Häner, V. S. Chirvony, *Photochem.Photobiol.Sci.* **2009**, 8, 1448-1454.
- [36] For alternative approaches using pyrene excimer formation in molecular beacons, see:
- a) K. Fujimoto, H. Shimizu, M. Inouye, *J.Org.Chem.* **2004**, 69, 3271-3275.
- b) I. Trkulja, S. M. Biner, S. M. Langenegger, R. Häner, *ChemBioChem* **2007**, 8, 25-27.
- c) K. Yamana, Y. Ohshita, Y. Fukunaga, M. Nakamura, A. Maruyama, *Bioorg.Med.Chem.* **2008**, 16, 78-83.
- d) P. Conlon, C. J. Yang, Y. Wu, Y. Chen, K. Martinez, Y. Kim, N. Stevens, A. A. Marti, S. Jockusch, N. J. Turro, W. Tan, *J.Am.Chem.Soc.* **2008**, 130, 336-342.
- e) S. Thurley, L. Roglin, O. Seitz, *J.Am.Chem.Soc.* **2007**, 129, 12693-12695.
- f) E. Mayer, L. Valis, C. Wagner, M. Rist, N. Amann, H. A. Wagenknecht, *ChemBioChem* **2004**, 5, 865-868.
- g) I. V. Astakhova, V. A. Korshun, J. Wengel, *Chem.Eur.J.* **2008**, 14, 11010-11026.

- h) thiazole orange as fluorophore: S. Berndl, H.A. Wagenknecht, *Angew.Chem.Int.Ed.* **2009**, 48, 2418-2421.
- i) exciplex-based probe: A. Gbaj, L. Walsh, M. C. Rogert, A. Sardarian, E. V. Bichenkova, L. L. Etchells, D. Whitcombe, K. T. Douglas, *Biosci.Reports* **2008**, 28, 1-5.
- j) ends-free molecular beacons: Y. Saito, Y. Shinohara, S. S. Bag, Y. Takeuchi, K. Matsumoto, I. Saito, *Tetrahedron* **2009**, 65, 934-939.
- k) H. Kashida, T. Takatsu, T. Fujii, K. Sekiguchi, X. G. Liang, K. Niwa, T. Takase, Y. Yoshida, H. Asanuma, *Angew.Chem.Int.Ed.* **2009**, 48, 7044-7047.
- [37] H. Bittermann, D. Siegemund, V. L. Malinovskii, R. Häner, *J.Am.Chem.Soc.* **2008**, 130, 15285-15287.
- [38] S. Uno, C. Dohno, H. Bittermann, V. L. Malinovskii, R. Häner, K. Nakatani, *Angew.Chem.Int.Ed.* **2009**, 48, 7362-7365.
- [39] J. A. M. Vet, S. A. E. Marras, in *Oligonucleotide Synthesis: Methods and Applications*, Humana Press Inc., Totowa, NJ **2004**, 273-290.
- [40] S. A. E. Marras, F. R. Kramer, S. Tyagi, *Nucl.Acids Res.* **2002**, 30, e122.
- [41] T. Förster, *Naturwissenschaften* **1946**, 33, 166-175.
- [42] C. A. Hunter, K. R. Lawson, J. Perkins, C. J. Urch, *J.Chem.Soc. Perkin Trans.2* **2001**, 651-669.
- [43] E. A. Meyer, R. K. Castellano, F. Diederich, *Angew.Chem.Int.Ed.* **2003**, 42, 1210-1250.
- [44] N. Bouquin, V. L. Malinovskii, R. Häner, *Chem.Commun.* **2008**, 1974-1976.
- [45] R. Carmieli, T. A. Zeidan, R. F. Kelley, Q. Mi, F. D. Lewis, M. R. Wasielewski, *J.Phys.Chem.A* **2009**, 113, 4691-4700.
- [46] S. Werder, V. L. Malinovskii, R. Häner, *Org.Lett.* **2008**, 10, 2011-2014.

3. Signal Control by Self-Assembly of Fluorophores in a Molecular Beacon – A Model Study

Published in: Sarah M. Biner, Dominic Kummer, Vladimir L. Malinovskii and Robert Häner, *Org.Biomol.Chem.* **2011**.

3.1 Abstract

Pyrene excimer fluorescence is efficiently regulated through formation of π -stacked aggregates between dialkynylpyrene (**Y**) and perylenediimide (**E**) residues located in the stem region of a molecular beacon (MB). The building blocks form organized, multichromophoric complexes in the native form. Hybridization to the target results in a conformational reorganization of the chromophores. The nature of the aggregates was investigated by changing the number of chromophores and natural base pairs in the beacon stem. The formation of different types of complexes (**EY EY** \rightarrow **YEY** \rightarrow **EY**) is revealed by characteristic spectroscopic changes. The data show that signal control is an intrinsic property of the interacting chromophores. The directed assembly of non-nucleosidic chromophores can be used for the generation of an *on/off* switch of fluorescence signal. The concept may find applications in various types of light-based input/output systems.

3.2 Introduction

Molecular beacons (MBs) are hairpin-shaped oligonucleotide probes, in which the loop region contains the target recognition sequence and the stem part enables the generation of a fluorescent diagnostic signal.^[1-4] The composition of the stem represents an essential aspect for the successful design of a MB. The stability of the stem has to be balanced to ensure the complete suppression of fluorescence in the closed form and, on the other hand, an efficient formation of the target-beacon complex.^[4-8] Fluorescence quenching in hairpin-type MBs is

based on the formation of a non-fluorescent ground state complex between fluorophore and quencher or *via* resonance energy transfer (FRET), corresponding to *static* and *dynamic* quenching, respectively.^[9;10] Incomplete quenching of the signal in the closed form is one of the major drawbacks of MBs for highly sensitive applications. Therefore, the development of new fluorophores and/or quenchers^[11-21] as well as innovative fluorophore-quencher systems is in continuous progress.^[18;22-31] Improved spectroscopic properties as well as hybridization behaviour were also observed with stem-modified MBs.^[32-38]

In the course of the group internal work on non-nucleosidic DNA building blocks,^[39-47] it was shown that alkynyl- and triazole-substituted pyrenes^[48-50] possess excellent fluorescence properties. Large extinction coefficients and quantum yields result in a high brightness of these fluorophores. Excimer fluorescence of these pyrenes is nearly environment independent^[50] and may, therefore, be used as a robust output signal in sensor applications.^[51;52] As described in *chapter 2*, the placement of two 3,4,9,10-perylenetetracarboxylic diimide (PDI) units opposite to two 1,8-dialkynylpyrenes (**Figure 3.1**) lead to very efficient suppression of the excimer signal.^[26;53] The very low background observed with this stem design opens the possibility of using the beacon in a considerable excess over the target, which is often not possible due to incomplete quenching.

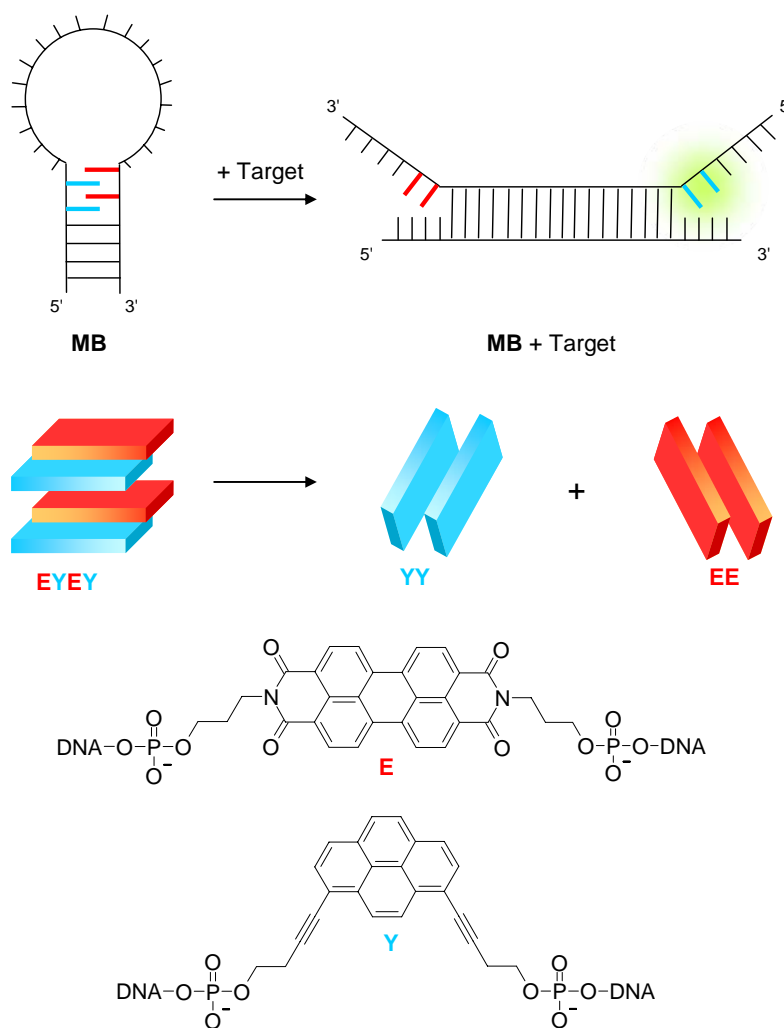


Figure 3.1. Illustration of signal control through self-assembly of aromatic chromophores in a MB. Generation of the fluorescence signal is regulated by conformational rearrangement of multichromophoric assembly of alkynylpyrene (**Y**) and PDI (**E**) building blocks.

This chapter provides an extended study on the origin of this remarkable signal suppression. The present type of MB possesses a detection system based on the formation of a donor-acceptor (D-A) type complex between alkynylpyrenes and PDI units (Figure 3.1)^[26] The combination of this chromophore complex with natural base pairs renders this stem a valuable module for fluorogenic detection systems. Control of fluorescence is based on specific interactions between the two types of chromophores. The organization of this multichromophoric complex is the reason for the excellent signal control. Since this type of π -stacked architecture^[54-69] can also be applied to other sensor systems, we studied the

chromophore organization in more detail. This chapter demonstrates that the supramolecular self-assembly of donor-acceptor π -aggregates serves as a highly reliable and robust system for the control of fluorescence and represents an alternative to the classic MB design.

3.3 Investigation of the multichromophoric detection system

For this study of PDI-alkynylpyrene interaction, a set of MBs (**MB1** to **MB5**) varying in the composition of the stem was synthesized (Table 3.1). Both chromophores, alkynylpyrene and PDI, possess a strong absorptivity and exhibit a high sensitivity towards stacking interactions which can conveniently be followed by changes in the relative vibronic band intensities ($A^{0\rightarrow0}/A^{0\rightarrow1}$ transitions).^[49;70-72] Since the longest wavelength absorption of the two different chromophores appears in separate regions of the UV/Vis spectra (dialkynylpyrene, **Y**: 330-420 nm; PDI, **E**: 420-650 nm) conformational changes and aggregation processes can be followed for each type of the chromophores independently.

Table 3.1. Sequences of molecular beacons (**MB1** to **MB5**) and targets (**TD1** to **TD4**).

MBs	MB1	5'	GGTC YY	CTA	GAG	GGG	TCA	GAG	GAT	EEGACC
	MB2	5'	TC YY	CTA	GAG	GGG	TCA	GAG	GAT	EEGA
	MB3	5'	YY	CTA	GAG	GGG	TCA	GAG	GAT	EE
	MB4	5'	TC YY	CTA	GAG	GGG	TCA	GAG	GAT	EGA
	MB5	5'	GGTCT Y	CTA	GAG	GGG	TCA	GAG	GAT	EAGACC
Targets	TD1	3'	TTT	GAT	CTC	CCC	AGT	CTC	CTA	TTT
	TD2	3'	TTT	<u>T</u> AT	CTC	CCC	AGT	CTC	CTA	TTT
	TD3	3'	TTT	GAT	CTC	<u>A</u> CC	AGT	CTC	CTA	TTT
	TD4	3'	TTT	GAT	CTC	CCC	<u>A</u> TT	CTC	CTA	TTT

The chromophores alkynylpyrene (**Y**) and PDI (**E**) are highlighted in bold and the mismatches are underlined.

Figure 3.2 shows the changes in vibronic band intensities between open (presence of 1.2 eq. of **TD1**) and closed (absence of target) form of **MB1**, **MB4** and **MB5**. In **MB1** a high degree of PDI stacking (420-650 nm) is revealed by the strong intensity of the 0 \rightarrow 1 transition in the open form, in which the PDI units are in close proximity. In the closed form, the PDI-PDI

interaction is significantly reduced. This suggests the formation of a different molecular complex.

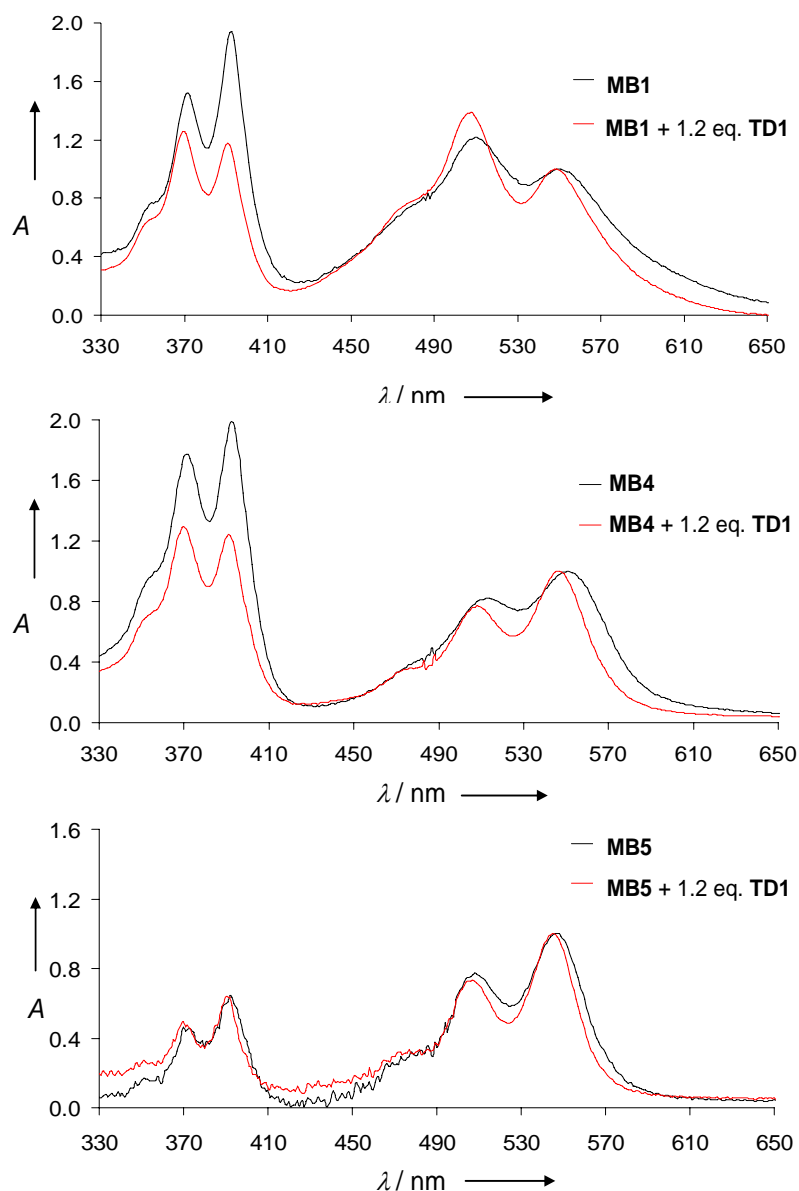


Figure 3.2. Normalized UV/Vis absorption spectra at 20°C of **MB1** (top), **MB4** (middle) and **MB5** (bottom), MB (black) and with 1.2 equivalents of the target **TD1** (red), normalized at the 0 \rightarrow 0 transition of PDI.

The same pattern is observed in the pyrene area (330-420 nm): the vibronic band intensity ratio varies strongly between open and closed form, showing pronounced pyrene-pyrene interactions in the presence of the target. Intensity ratios of the vibronic bands are listed in [Table 3.2](#). These observations are compatible with interstrand stacking interactions between PDI and dialkynylpyrene units in an alternating mode (**EY EY**) in the stem part of the closed beacon. These findings correlate with the well-described effects of hydrophobic stacking interactions between PDI derivatives in a polar environment.^[73-76] Furthermore, they are in best agreement with the described distance dependence of vibronic band ratios in DNA-PDI constructs.^[77]

Table 3.2. Absorption ratios of the 0→0 to the 0→1 transition at 20°C.^[a]

	$A^{0\rightarrow0}/A^{0\rightarrow1}$ alkynylpyrene ^[b]		$A^{0\rightarrow0}/A^{0\rightarrow1}$ PDI ^[c]	
	No target	1.2 eq. TD1	No target	1.2 eq. TD1
	(closed)	(open)	(closed)	(open)
MB1	1.28	0.94	0.84	0.72
MB2	1.19	0.90	0.74	0.71
MB3	1.19	1.06	0.76	0.73
MB4	1.12	0.96	1.22	1.31
MB5	1.39	1.29	1.30	1.36

[a] Conditions: 100 mM NaCl, 10 mM sodium phosphate buffer, pH 7.0;
 [b] 330-420 nm; [c] 420-650 nm.

The same qualitative behaviour was also observed for beacons **MB2** and **MB3** ([Table 3.2](#)). In **MB4** and **MB5** ([Figure 3.2](#)), which contain only a single PDI, the ratio of $A^{0\rightarrow0}/A^{0\rightarrow1}$ transitions indicates non-aggregated PDIs in both, closed and open form. Therefore, one can conclude that the significant increase of the 0→1 transition is primarily due to PDI-PDI and not to PDI-pyrene interactions. Pyrene aggregation is observed for all beacons containing two adjacent alkynylpyrenes in the open form. The pyrene vibronic band ratios observed for **MB4** suggest that the same conclusions as for the PDI building blocks can also be drawn for the pyrene building block, *i.e.* the pyrene 0→1 transition is most sensitive to pyrene-pyrene interactions, but not for pyrene-PDI interactions ([see Figure 3.2, MB5](#)). The results support

the model shown in Figure 3.1, in which mixed aggregates (**EY****EY**) are present in the closed form and, upon opening of the stem part, self-aggregates (**EE** and **YY**) are formed.

Further insight into chromophore organization was obtained by circular dichroism (CD) spectroscopy. Temperature-dependent spectroscopy of **MB2** (Figure 3.3) shows a signal signature for the pyrene units [394 nm (+), 382 nm (-) and 362 nm (-)] and the PDI building blocks [561 nm (+), 499 nm (-)]. The spectra at long wavelengths show a positive bisignate signal characteristic for an exciton coupling^[78;79] between the PDI units. The signal of the alkynylpyrene building blocks at shorter wavelengths indicates that exciton coupling also takes place between the alkynylpyrene units. However, the CD signal originating from alkynylpyrene interactions is different from the one observed previously in a DNA hybrid in which two alkynylpyrenes were placed in close contact leading to a **YY** interaction.^[49] This difference in CD signature can be attributed to the separation of the alkynylpyrenes by PDI units that leads to an alternating **EY****EY** π -stack. The CD signatures in the 300-600 nm region gradually disappear with increasing temperature.

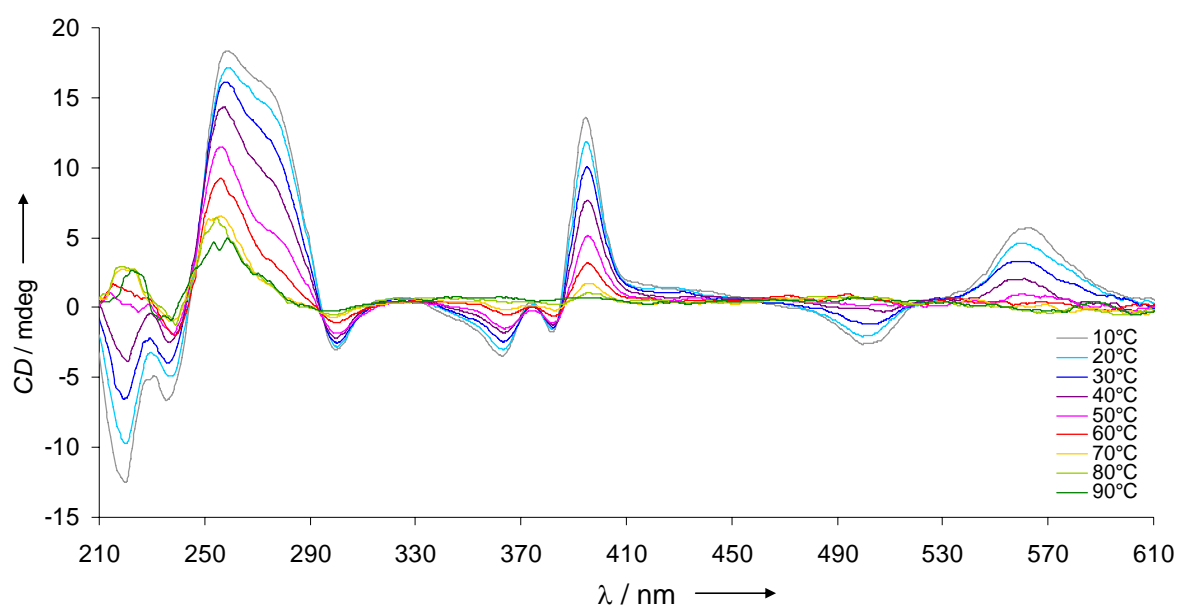


Figure 3.3. Temperature-dependent CD spectroscopy of **MB2**. Conditions: **MB2** 5.0 μ M, 10 mM sodium phosphate buffer, pH 7.0, 100 mM NaCl, equilibration time: 10 min.

The spectra of **MB1** in the presence and the absence of target **TD1** at 20°C are shown in [Figure 3.4](#). Addition of the target **TD1** leads to gradual change of this alkynylpyrene CD signal (from $A = +100$ to $A = -15$), whereas the strength of the PDI couplet is increasing (from $A = +26$ to $A = +64$). This finding is explained by the strong hydrophobic PDI interactions in aqueous environment.

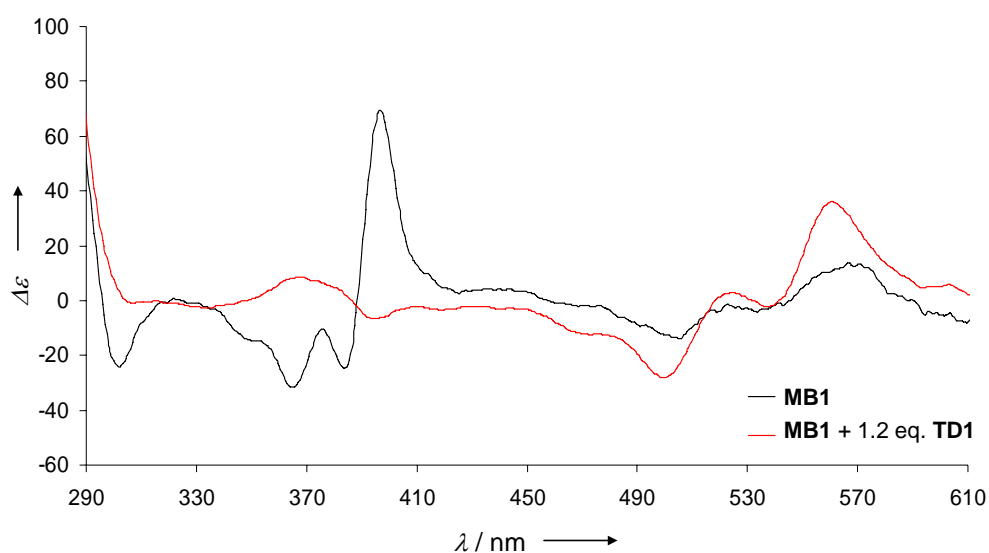


Figure 3.4. CD spectra of **MB1** (black) and with 1.2 eq. of target **TD1** (red). Conditions: 10 mM sodium phosphate buffer, pH 7.0, 100 mM NaCl, Temp.: 20°C.

The formation of **EY EY** aggregates follows the well-documented pattern of donor-acceptor (D-A) π -interactions,^[60;80-84] such as arene-perfluoroarene^[85-89] or pyrene-naphthalenediimide aromatic interactions.^[90-95] The present alkynylpyrene-PDI aggregation seems to proceed after this motif.

A worthy goal in the design of MBs consists in the reduction of the stem to a minimal length. The difference between **MB1** and **MB2** is a reduction of the stem length from four to two natural base pairs. [Figure 3.5](#) shows the fluorescence curves of **MB1** and **MB2** obtained upon hybridization to the target. The quenching efficiency (Q%) in the absence of the target is approx. 97% ([Table 3.3](#)), which is excellent in view of the shortness and simplicity of the stem.

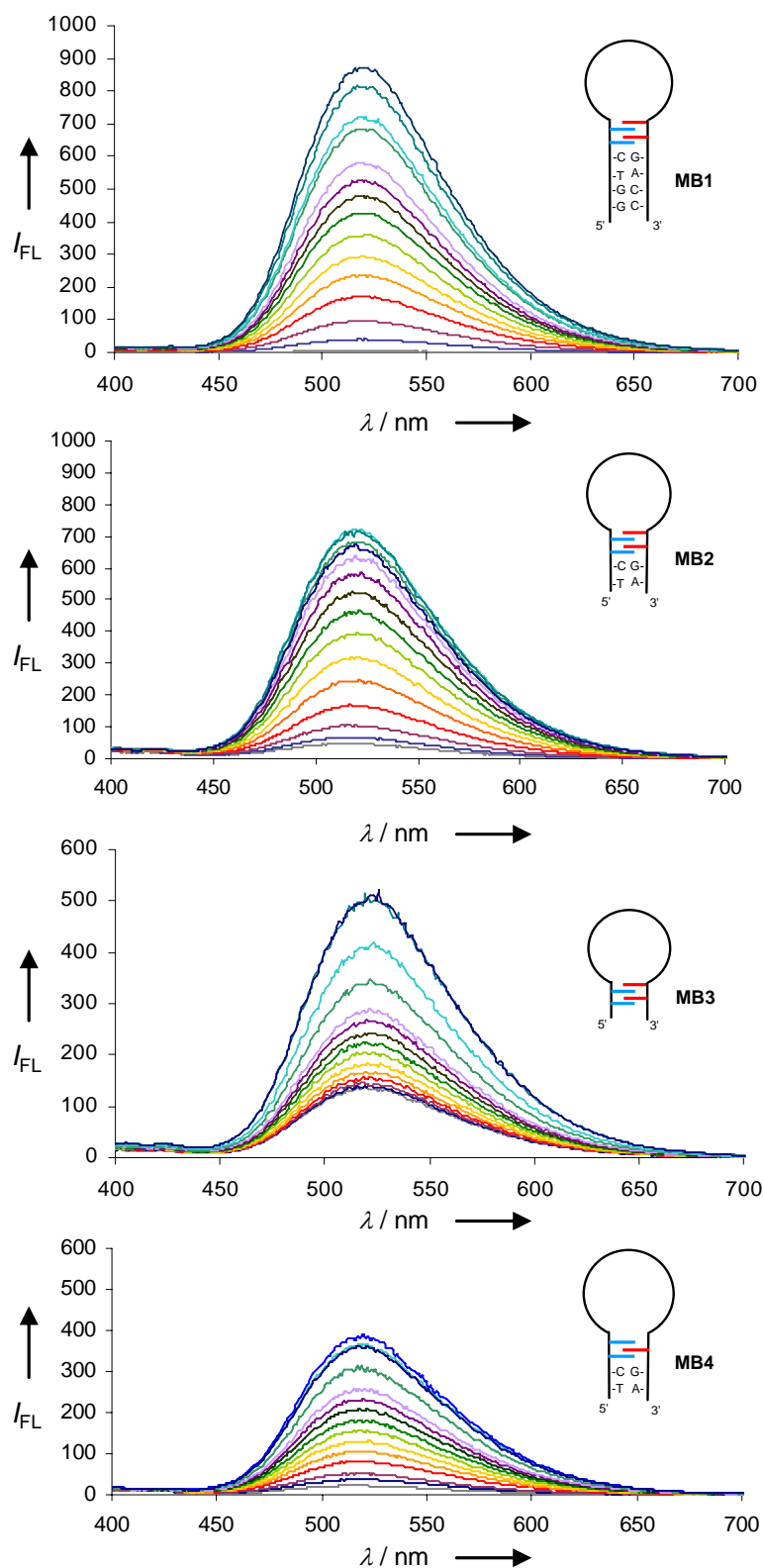


Figure 3.5. Fluorescence read-out of MB1 to MB4. Conditions: MB1, MB2, MB3, MB4 1.0 μM , TD1 0 to 10 eq. (lines correspond to: 0, 0.1, 0.2, 0.3, 0.4, 0.5, 0.6, 0.7, 0.8, 0.9, 1.0, 1.5, 2.0, 5.0, 10 eq.), 10 mM sodium phosphate buffer, pH 7.0, 100 mM NaCl, λ_{ex} : 370 nm, Temp.: 37°C, no equilibration time.

Table 3.3. Quenching efficiency (Q%) values for **MB1** to **MB5** in presence of 1.0 eq. target **TD1**^[a]

	MB1 ^[26]	MB2	MB3	MB4	MB5
Q%	99.7	97.2	53.1	91.5	36.9

[a] Conditions: 10 mM sodium phosphate buffer, pH 7.0, 100 mM NaCl, λ_{ex} : 370 nm, Temp.: 37°C, values were determined at emission maxima.

In addition, **MB2** exhibited a mismatch discrimination comparable to **MB1** (Figure 3.6) when hybridized to target oligomers **TD1** to **TD4**.

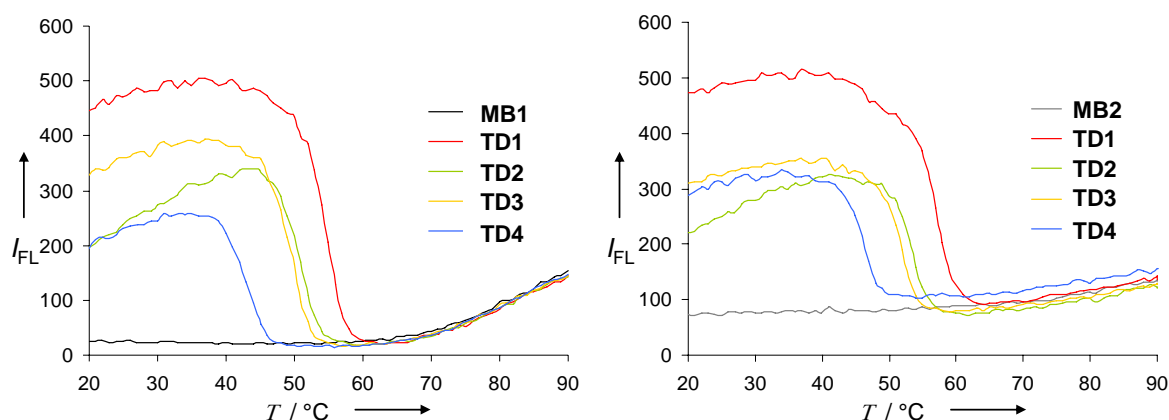


Figure 3.6. **MB1** (left) and **MB2** (right) excimer signal intensities obtained in the presence of 1 eq. of matched and mismatched DNA targets **TD1** to **TD4**. Conditions: **MB1** resp. **MB2** 0.1 μM , **TD1** to **TD4** 0.1 μM , 10 mM sodium phosphate buffer, pH 7.0, 100 mM NaCl, λ_{ex} : 370 nm, λ_{em} : 520 nm (excimer), ex/em slit widths: 5/5 nm, PMT voltage: 800 V, performance of three ramps (90-20°C / 20-90°C / 90-20°C), heating/cooling rate: 0.5°C/min, only heating ramps are shown.

Further simplification was tested with **MB3** containing no natural base pairs in the stem. Formation of a stem-loop structure can be expected through intramolecular stacking interactions between the two alkynylpyrene and PDI building blocks that are located at the ends of the oligomer. UV/Vis spectra show PDI and dialkynylpyrene aggregation also for this beacon (Figure 3.7).

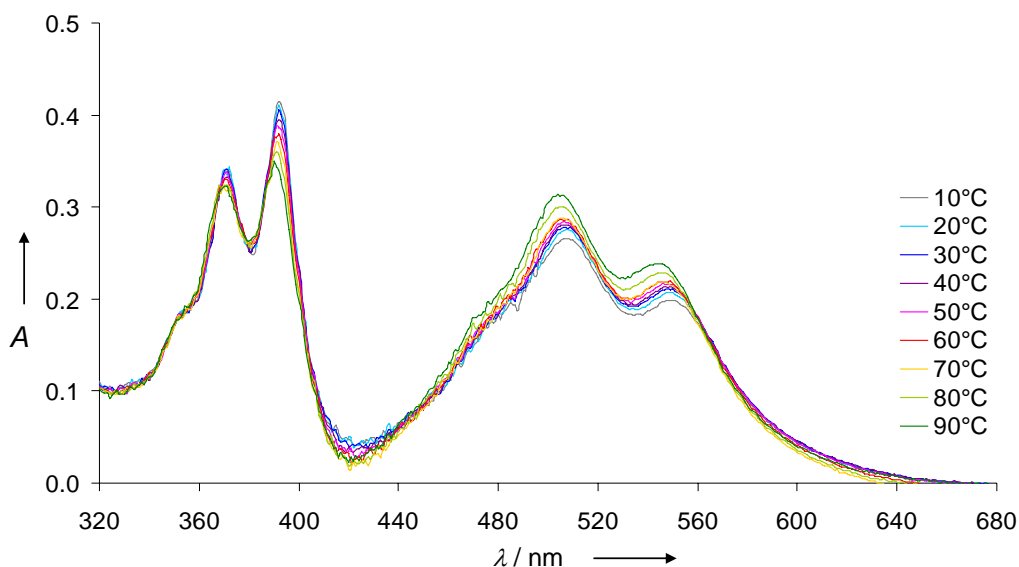


Figure 3.7. Temperature-dependent absorbance spectra of **MB3**. Conditions: **MB3** 2.0 μM , 10 mM sodium phosphate buffer, pH 7.0, 100 mM NaCl, equilibration time: 10 min.

However, the degree of quenching in the absence of the target is greatly diminished (Figure 3.5) as well as the concentration-dependent fluorescent read-out (Figure 3.8).

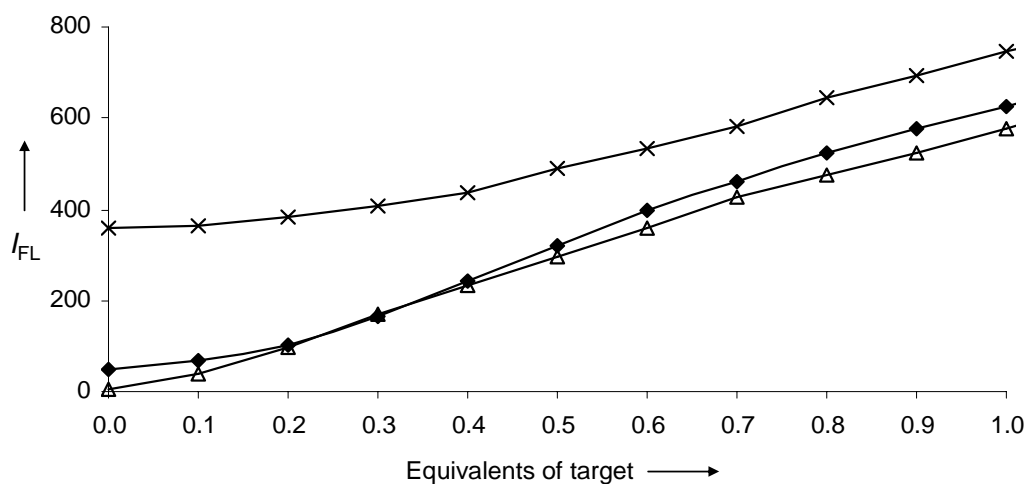


Figure 3.8. Concentration-dependent fluorescence read-out at 520 nm gained with **MB1** (Δ), **MB2** (\blacklozenge) and **MB3** (\times). Conditions: **MB1**, **MB2** and **MB3** 1.0 μM , **TD1** 0 to 1.0 eq. in 0.1 steps, 10 mM sodium phosphate buffer, pH 7.0, 100 mM NaCl, λ_{ex} : 370 nm, λ_{em} : 520 nm (excimer), ex/em slit widths: 10/5 nm, PMT voltage: 600 V, Temp.: 37°C.

Furthermore, the CD spectra (Figure 3.9) exhibit a remarkable temperature-dependent behaviour in the PDI area (410-610 nm). These changes may well be due to PDI-mediated formation of dimers or larger aggregates at low temperature. It is likely that individual molecules associate *intermolecularly* through stacking interactions between the PDI and/or alkynylpyrene residues located at their ends. The formation of interstrand assemblies of DNA conjugates through interaction of sticky ends formed with porphyrine^[66] or PDI^[67] derivatives was recently demonstrated. The intensity of the broad, unstructured band between 410 nm and 510 nm is significantly reduced on increasing the temperature, which may indicate thermal disaggregation. Therefore, the broadening of this band is attributed to partial intermolecular PDI aggregation.

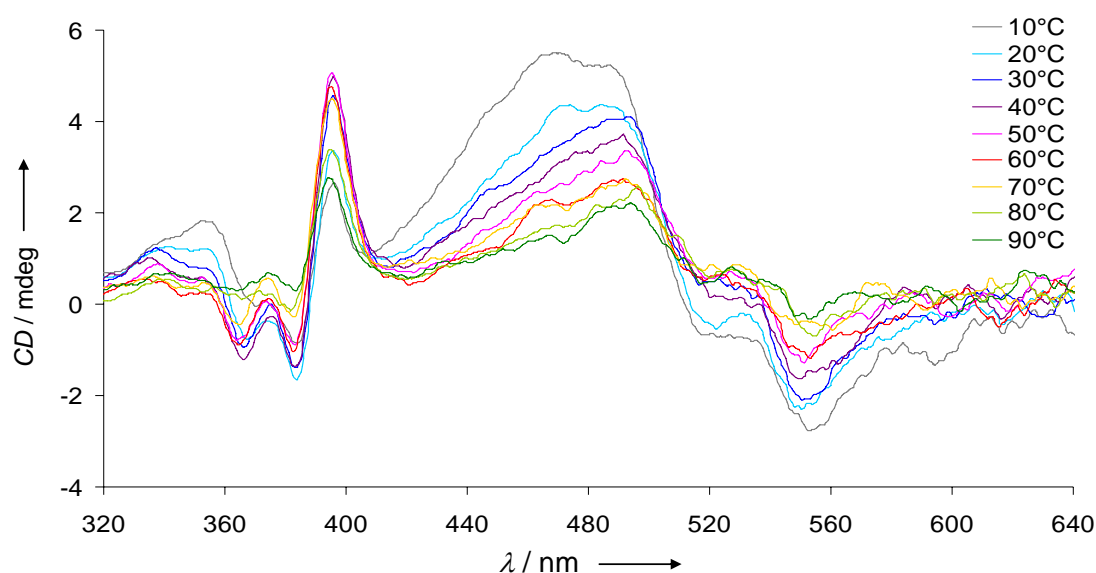


Figure 3.9. Temperature-dependent CD spectroscopy of **MB3** from 10°C to 90°C in 10°C increments. Conditions: **MB3** 5.0 μM , 10 mM sodium phosphate buffer, pH 7.0, 100 mM NaCl, equilibration time 10 min.

In the presence of target **TD1** (Figure 3.10), substantial temperature-dependent CD changes are observed in the pyrenyl area of **MB3**. The negative Cotton-effect in the alkynylpyrene signature including an intense negative signal at ~ 390 nm indicates a change in the aggregation state of the building blocks. These changes may have their origin in competing intra- and intermolecular aggregation of the stemless beacon: at low temperature, interactions between PDI and alkynylpyrene sticky ends are predominate and

at high temperature, after dissociation from the target, the pyrenes adopt the same **EYE(Y)** conformation as observed with the beacons containing additional base pairs (**MB1** and **MB2**). In the PDI region, the CD spectrum shows a negative Cotton-effect and a broadening of the band at shorter wavelengths. These observations can be due to a dangling PDI unit at the 3'-end of the stem while the PDI closer to the loop region can interact as described above with the two alkynylpyrenes. These findings support the general formation of a donor-acceptor interaction among the chromophores in **MB3** but they also suggest that this type of (stemless) beacon is less suitable for practical use due to the increased competition between inter- and intramolecular stacking of the aromatic chromophores.

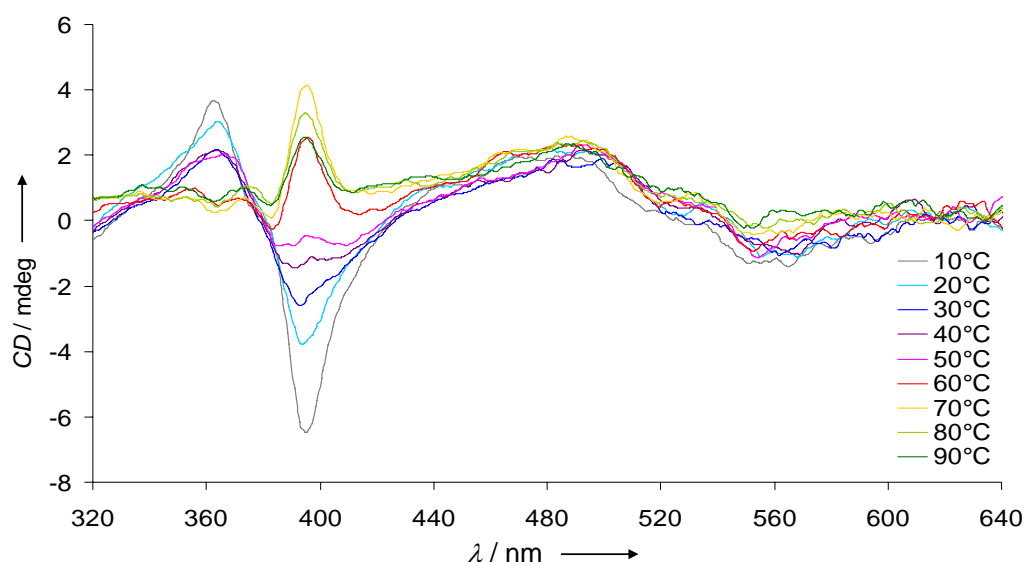


Figure 3.10. Temperature-dependent CD spectra of **MB3** in presence of 1.2 eq. **TD1** from 10°C to 90°C in 10°C increments. Conditions: **MB3** 5.0 μM, 6.0 μM **TD1**, 10 mM phosphate buffer, pH 7.0, 100 mM NaCl, equilibration time: 10 min.

The fluorescence data obtained with **MB4** (Figure 3.5 and Figure 3.11) are quite remarkable. This probe contains only a single PDI yet the excimer signal is largely suppressed in the closed form (Table 3.3). The excellent signal control can be attributed to the formation of a **Y E Y** (donor-acceptor-donor, D-A-D) complex.

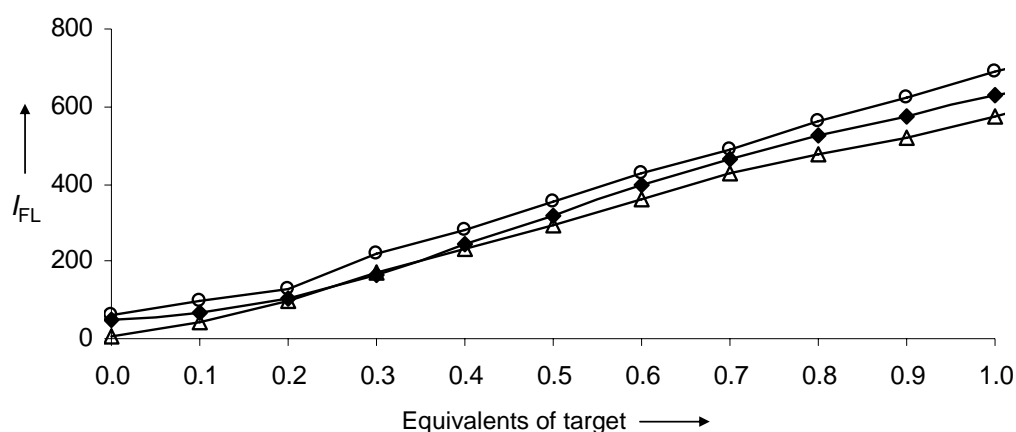


Figure 3.11. Concentration-dependent fluorescence read-out obtained at 520 nm for **MB1** (Δ), **MB2** (\blacklozenge) and **MB4** (\circ). Conditions: **MB1**, **MB2** and **MB4** 1.0 μM , **TD1** 0 to 1.0 eq. in 0.1 steps, 10 mM sodium phosphate buffer, pH 7.0, 100 mM NaCl, λ_{ex} : 370 nm, λ_{em} : 520 nm (excimer), ex/em slit widths: 10/5 nm, PMT voltage: 600 V, Temp.: 37°C.

MB5 contains only a single pyrene and a single PDI and allows, therefore, a direct comparison between monomer and excimer based sensing systems. The findings reveal the high value of the pyrene excimer read-out. In comparison to beacons **MB1** to **MB4**, which are all based on excimer formation, **MB5** shows i) a very weak (monomer) signal (**Figure 3.12**) and ii) very poor signal quenching in the absence of the target (**Table 3.3**).

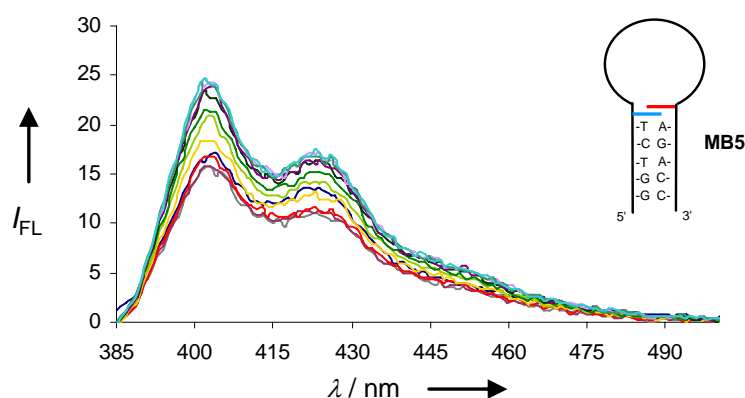


Figure 3.12. Fluorescence read-out of **MB5**. Conditions: **MB5** 0.1 μM , **TD1** 0 to 2.0 eq., (lines correspond to: 0, 0.1, 0.2, 0.3, 0.4, 0.5, 0.6, 0.7, 0.8, 0.9, 1.0, 1.5, 2.0, 5.0, 10 eq.), 10 mM sodium phosphate buffer, pH 7.0, 100 mM NaCl, λ_{ex} : 370 nm, ex/em slit widths: 10/5 nm, PMT voltage: 600 V, Temp.: 37°C.

The UV/Vis and CD data obtained for **MB1**, **MB2** and **MB3** were quite similar despite significantly differing numbers of natural bases in the stem. This indicates that the organization of the PDI/pyrene complex is an intrinsic property of the chromophoric building blocks and largely independent from the DNA part. Therefore, in the context of supramolecular chemistry, the loop of the MB may be regarded as a flexible linker between the components of the directed assembly. The target sequence serves as an external factor that induces a conformational reorganization of the supramolecular complex under isothermal conditions. Furthermore, it should also be mentioned that this study allows the direct comparison of optical properties and stacking interactions of both types of chromophores (pyrene and PDI) in a single experiment at equal conditions. The UV/Vis and CD effects are comparable for the two types of compounds. Pyrene interactions lead to pronounced fluorescence signals while the PDI aggregates are basically non-fluorescent.

3.4 Conclusion

The data demonstrated that the directed assembly of non-nucleosidic chromophores can be used for the generation of an *on/off* switch for a diagnostic signal. Pyrene excimer fluorescence is efficiently regulated by formation of π -stacked aggregates between alkynylpyrenes and PDI residues located in the stem region of the MB. By varying of the numbers of alkynylpyrene (**Y**) and PDI (**E**) residues it could be shown that the the two types of chromophores interact in a donor-acceptor way of stacking in the closed form. The formation of various types complexes (**EY EY** \rightarrow **YEY** \rightarrow **EY**) is revealed by characteristic changes in CD, UV/Vis and fluorescence spectra. Conformational changes induced by target recognition leads to direct pyrene-pyrene interaction and, thus, efficient excimer fluorescence. Highest quenching efficiency was obtained with two PDIs placed opposite two alkynylpyrenes in **MB1** and **MB2**. A single PDI, however, showed also surprisingly strong excimer signal inhibition (**MB4**). A longer stem gave better quenching efficiencies (**MB1** vs. **MB2** vs. **MB3**). Finally, the approach of using aromatic π -stacking works largely better for the control of excimer than of monomer suppression (e.g. **MB1** vs. **MB5**). The data show that signal control is an intrinsic property of the interacting

chromophores. Therefore, the concept described herein, represents a functional module that may find applications not only in MBs but also in other *input/output* systems using light as the source of information.^[96-98]

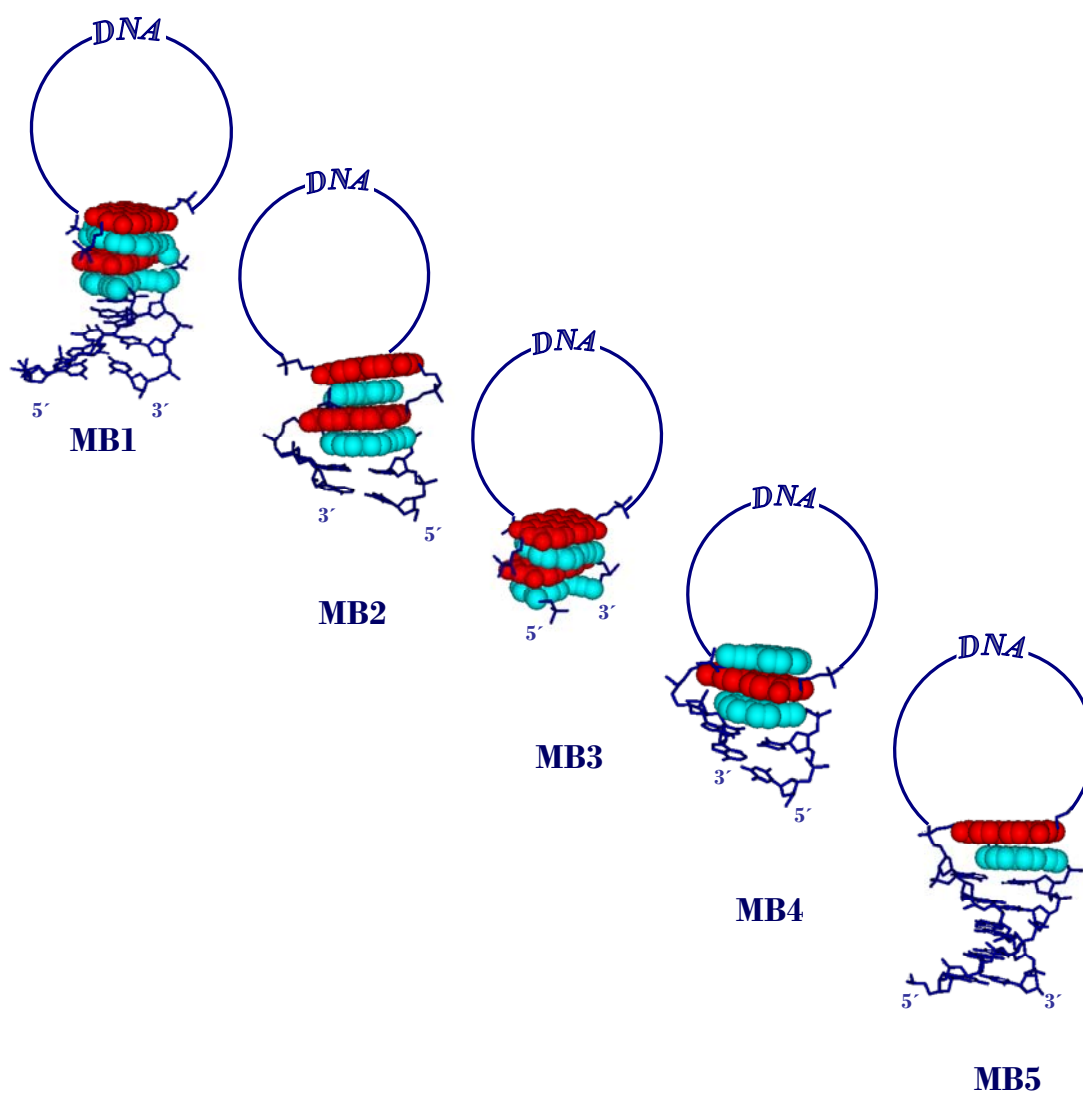


Figure 3.13. Model of **MB1** to **MB5** in the closed form with donor-acceptor complexes highlighted in red (PDI) and cyan (alkynylpyrene).

3.5 Experimental Part

Oligonucleotide synthesis. The non-nucleosidic building blocks alkynylpyrene^[49] and PDI^[99] were synthesized according to published procedures. Nucleosid phosphoramidites were purchased from SAFC (*Proligo Reagents*). Oligonucleotide **TD1** was purchased from Microsynth, Balgach, Switzerland. **MB1** to **MB5** were prepared *via* automated oligonucleotide synthesis by an adapted synthetic procedure on a 394-DNA/RNA synthesizer (*Applied Biosystems*). Cleavage from the solid support and final deprotection was done by treatment with 30% NH₄OH solution at 55°C overnight and for oligomer **MB3** at 80°C for two days.

Oligonucleotide purification and mass determination. Purification was performed by reverse phase HPLC (LiChrospher 100 *RP-18*, 5µm, Merck; *Shimadzu LC-20AT* for **MB1** and *Kontron Instruments* device for **MB2 – MB5**). For all oligonucleotide sequences: eluent A = (Et₃NH)OAc (0.1 M, pH 7.4), B = MeCN ([Table 3.4](#)).

Table 3.4. Purification performance and retention times t_R .

	Elution temperature	Elution gradient	Elution time	t_R
MB1	30°C	5 – 20 %	20 min	18.7 min
MB2	60°C	5 – 40 %	30 min	23.1 min
MB3	60°C	5 – 50 %	30 min	22.7 min
MB4	60°C	5 – 40 %	30 min	22.8 min
MB5	60°C	5 – 30 %	30 min	22.5 min

Mass spectrometry was performed with a Sciex QSTAR pulsar (hybrid quadrupole time-of-flight mass spectrometer, *Applied Biosystems*); ESI-TOF MS (negative mode, acetonitrile/H₂O/triethylamine) ([Table 3.5](#)).

Table 3.5. Specification of modified oligonucleotides **MB1** to **MB5**.

	<i>molecular formula</i>	<i>calcd. avg. mass</i>	<i>found avg. mass</i>
MB1	C ₃₆₃ H ₃₉₃ N ₁₁₂ O ₁₇₆ P ₂₉	10039.0	10039.6
MB2	C ₃₂₅ H ₃₄₅ N ₉₆ O ₁₅₂ P ₂₅	8802.1	8802.6
MB3	C ₂₈₆ H ₂₉₆ N ₈₁ O ₁₂₈ P ₂₁	7566.3	7565.8
MB4	C ₂₉₅ H ₃₂₄ N ₉₄ O ₁₄₄ P ₂₄	8233.6	8232.8
MB5	C ₃₂₉ H ₃₈₀ N ₁₁₇ O ₁₇₆ P ₂₉	9687.4	9680.8

Oligonucleotide analysis. Temperature-dependent UV/Vis spectra were carried out on a *Varian Cary-100 Bio-UV/Vis* spectrophotometer equipped with a *Varian Cary-block* temperature controller and data were collected with *Varian WinUV* software. CD spectra were recorded on a *JASCO J-715* spectrophotometer using quartz cuvettes with an optic path of 1 cm. Fluorescence spectra were recorded on a *Varian Cary Eclipse* fluorescence spectrophotometer equipped with a *Varian Cary-block* temperature controller using 1 cm x 1 cm quartz cuvettes. *Varian Eclipse* software was used to investigate the fluorescence data. All measurements were performed in 10 mM phosphate buffer pH 7.0 and 100 mM NaCl.

Determination of signal-to-background ratios and quenching efficiencies. The signal-to-background (S/B) and quenching efficiency (Q%) values were determined according to the formulas below ([Table 3.6](#) and [Table 3.7](#)).^[100]

$$S/B = (F_{\text{hybrid}} - F_{\text{buffer}}) / (F_{\text{MB}} - F_{\text{buffer}})$$

$$Q\% = 100 \times \{1 - ((F_{\text{MB}} - F_{\text{buffer}}) / (F_{\text{hybrid}} - F_{\text{buffer}}))\}$$

Table 3.6. S/B ratios and quenching efficiency (Q%) values for **MB1** to **MB5** in presence of 1.0 eq. target **TD1**.^[a]

	MB1 ^[b]	MB2 ^[b]	MB3 ^[c]	MB4 ^[c]	MB5 ^[d]
S/B	309	35.6	2.1	11.8	1.6
Q%	99.7	97.2	53.1	91.5	36.9

[a] Conditions: 10 mM sodium phosphate buffer, pH 7.0, 100 mM NaCl, λ_{ex} : 370 nm, PMT voltage: 600 V, Temp.: 37°C, [b] **MB1** and **MB2**: 1.0 μM , ex/em slit widths: 10/5 nm, [c] **MB3** and **MB4**: 1.0 μM , ex/em slit widths: 5/5 nm, [d] **MB5**: 0.1 μM , ex/em slit widths: 10/5 nm.

Table 3.7. Quenching efficiency (Q%) values for **MB1** to **MB5** in presence of 1.0, 3.0 and 5.0 eq. target **TD1**^[a]

	MB1 + 1.0 eq. T1	MB1 + 2.0 eq. T1	MB1 + 5.0 eq. T1
Q%	99.7	99.7	99.8
	MB2 + 1.0 eq. T1	MB2 + 2.0 eq. T1	MB2 + 5.0 eq. T1
Q%	97.2	97.6	97.5
	MB3 + 1.0 eq. T1	MB3 + 2.0 eq. T1	MB3 + 5.0 eq. T1
Q%	53.1	66.9	73.5
	MB4 + 1.0 eq. T1	MB4 + 2.0 eq. T1	MB4 + 5.0 eq. T1
Q%	91.5	93.9	94.2
	MB5 + 1.0 eq. T1	MB5 + 2.0 eq. T1	
Q%	36.9	37.6	

[a] see conditions [Table 3.6](#).

3.6 References

- [1] S. Tyagi, F. R. Kramer, *Nat.Biotechnol.* **1996**, 14, 303-308.
- [2] R. T. Ranasinghe, T. Brown, *Chem.Commun.* **2005**, 5487-5502.
- [3] B. Juskowiak, *Anal.Bioanal.Chem.* **2010**.
- [4] K. M. Wang, Z. W. Tang, C. Y. J. Yang, Y. M. Kim, X. H. Fang, W. Li, Y. R. Wu, C. D. Medley, Z. H. Cao, J. Li, P. Colon, H. Lin, W. H. Tan, *Angew.Chem.Int.Ed.* **2009**, 48, 856-870.
- [5] A. P. Silverman, E. T. Kool, *Trends Biotechnol.* **2005**, 23, 225-230.
- [6] S. A. E. Marras, S. Tyagi, F. R. Kramer, *Clin.Chim.Acta* **2006**, 363, 48-60.
- [7] N. Venkatesan, Y. J. Seo, B. H. Kim, *Chem.Soc.Rev.* **2008**, 37, 648-663.
- [8] P. Santangelo, N. Nitin, G. Bao, *Ann.Biomed.Eng.* **2006**, 34, 39-50.
- [9] S. A. E. Marras, F. R. Kramer, S. Tyagi, *Nucl.Acids Res.* **2002**, 30, e122.
- [10] T. Förster, *Naturwissenschaften*, **1946**, 33, 166-175.
- [11] K. Fujimoto, H. Shimizu, M. Inouye, *J.Org.Chem.* **2004**, 69, 3271-3275.
- [12] P. Conlon, C. J. Yang, Y. Wu, Y. Chen, K. Martinez, Y. Kim, N. Stevens, A. A. Marti, S. Jockusch, N. J. Turro, W. Tan, *J.Am.Chem.Soc.* **2008**, 130, 336-342.
- [13] E. Socher, L. Bethge, A. Knoll, N. Jungnick, A. Herrmann, O. Seitz, *Angew.Chem.Int.Ed.* **2008**, 47, 9555-9559.
- [14] I. V. Astakhova, V. A. Korshun, J. Wengel, *Chem.Eur.J.* **2008**, 14, 11010-11026.
- [15] V. V. Filichev, I. V. Astakhova, A. D. Malakhov, V. A. Korshun, E. B. Pedersen, *Chem.Eur.J.* **2008**, 14, 9968-9980.
- [16] H. Kashida, T. Takatsu, T. Fujii, K. Sekiguchi, X. G. Liang, K. Niwa, T. Takase, Y. Yoshida, H. Asanuma, *Angew.Chem.Int.Ed.* **2009**, 48, 7044-7047.
- [17] Y. Ueno, A. Kawamura, K. Takasu, S. Komatsuzaki, T. Kato, S. Kuboe, Y. Kitamura, Y. Kitade, *Org.Biomol.Chem.* **2009**, 7, 2761-2769.
- [18] Y. Saito, Y. Shinohara, S. S. Bag, Y. Takeuchi, K. Matsumoto, I. Saito, *Tetrahedron* **2009**, 65, 934-939.
- [19] R. Varghese, H. A. Wagenknecht, *Org.Biomol.Chem.* **2010**, 8, 526-528.
- [20] U. Forster, C. Grunewald, J. W. Engels, J. Wachtveitl, *J.Phys.Chem.B* **2010**, 114, 11638-11645.

- [21] K. Giessler, H. Griesser, D. Gohringer, T. Sabirov, C. Richert, *Eur.J.Org.Chem.* **2010**, 3611-3620.
- [22] T. N. Grossmann, L. Roglin, O. Seitz, *Angew.Chem.Int.Ed.* **2007**, 46, 5223-5225.
- [23] J. N. Wilson, Y. J. Cho, S. Tan, A. Cuppoletti, E. T. Kool, *ChemBioChem* **2008**, 9, 279-285.
- [24] I. Trkulja, S. M. Biner, S. M. Langenegger, R. Häner, *ChemBioChem* **2007**, 8, 25-27.
- [25] I. V. Nesterova, S. S. Erdem, S. Pakhomov, R. P. Hammer, S. A. Soper, *J.Am.Chem.Soc.* **2009**, 131, 2432-2433.
- [26] R. Häner, S. M. Biner, S. M. Langenegger, T. Meng, V. L. Malinovskii, *Angew.Chem.Int.Ed.* **2010**, 49, 1227-1230.
- [27] M. E. Ostergaard, J. Maity, B. R. Babu, J. Wengel, P. J. Hrdlicka, *Bioorg.Med.Chem.Lett.* **2010**, 20, 7265-7268.
- [28] Y. V. Gerasimova, A. Hayson, J. Ballantyne, D. M. Kolpashchikov, *ChemBioChem* **2010**, 11, 1762-1768.
- [29] S. P. Sau, T. S. Kumar, P. J. Hrdlicka, *Org.Biomol.Chem.* **2010**, 8, 2028-2036.
- [30] Y. N. Teo, J. N. Wilson, E. T. Kool, *J.Am.Chem.Soc.* **2009**, 131, 3923-3933.
- [31] F. Seela, S. A. Ingale, *J.Org.Chem.* **2010**, 75, 284-295.
- [32] L. Wang, C. Y. J. Yang, C. D. Medley, S. A. Benner, W. H. Tan, *J.Am.Chem.Soc.* **2005**, 127, 15664-15665.
- [33] C. Crey-Desbiolles, D. R. Ahn, C. J. Leumann, *Nucl.Acids Res.* **2005**, 33, e77.
- [34] K. Yamana, Y. Ohshita, Y. Fukunaga, M. Nakamura, A. Maruyama, *Bioorg.Med.Chem.* **2008**, 16, 78-83.
- [35] P. P. Sheng, Z. Y. Yang, Y. M. Kim, Y. R. Wu, W. H. Tan, S. A. Benner, *Chem.Commun.* **2008**, 5128-5130.
- [36] J. Chen, T. W. B. Liu, P. C. Lo, B. C. Wilson, G. Zheng, *Bioconjug.Chem.* **2009**, 20, 1836-1842.
- [37] K. Matsumoto, Y. Shinohara, S. S. Bag, Y. Takeuchi, T. Morii, Y. Saito, I. Saito, *Bioorg.Med.Chem.Lett.* **2009**, 19, 6392-6395.
- [38] L. Bethge, I. Singh, O. Seitz, *Org.Biomol.Chem.* **2010**, 8, 2439-2448.
- [39] S. M. Langenegger, R. Häner, *Helv.Chim.Acta* **2002**, 85, 3414-3421.
- [40] S. M. Langenegger, R. Häner, *Chem.Commun.* **2004**, 2792-2793.

- [41] S. M. Langenegger, R. Häner, *ChemBioChem* **2005**, 6, 2149-2152.
- [42] S. M. Langenegger, R. Häner, *Bioorg.Med.Chem.Lett.* **2006**, 16, 5062-5065.
- [43] V. L. Malinovskii, F. Samain, R. Häner, *Angew.Chem.Int.Ed.* **2007**, 46, 4464-4467.
- [44] I. Trkulja, R. Häner, *J.Am.Chem.Soc.* **2007**, 129, 7982-7989.
- [45] R. Häner, F. Samain, V. L. Malinovskii, *Chem.Eur.J.* **2009**, 15, 5701-5708.
- [46] R. Häner, F. Garo, D. Wenger, V. L. Malinovskii, *J.Am.Chem.Soc.* **2010**, 132, 7466-7471.
- [47] D. Wenger, V. L. Malinovskii, R. Häner, *Chem.Commun.* **2011**, 47, 3168-3170.
- [48] V. L. Malinovskii, R. Häner, *Eur.J.Org.Chem.* **2006**, 3550-3553.
- [49] H. Bittermann, D. Siegemund, V. L. Malinovskii, R. Häner, *J.Am.Chem.Soc.* **2008**, 130, 15285-15287.
- [50] S. Werder, V. L. Malinovskii, R. Häner, *Org.Lett.* **2008**, 10, 2011-2014.
- [51] V. A. Galievsky, V. L. Malinovskii, A. S. Stasheuski, F. Samain, K. A. Zachariasse, R. Häner, V. S. Chirvony, *Photochem.Photobiol.Sci.* **2009**, 8, 1448-1454.
- [52] S. Uno, C. Dohno, H. Bittermann, V. L. Malinovskii, R. Häner, K. Nakatani, *Angew.Chem.Int.Ed.* **2009**, 48, 7362-7365.
- [53] N. Bouquin, V. L. Malinovskii, R. Häner, *Chem.Commun.* **2008**, 1974-1976.
- [54] C. A. Hunter, J. K. M. Sanders, *J.Am.Chem.Soc.* **1990**, 112, 5525-5534.
- [55] E. A. Meyer, R. K. Castellano, F. Diederich, *Angew.Chem.Int.Ed.* **2003**, 42, 1210-1250.
- [56] J. Rebek, *Acc.Chem.Res.* **2009**, 42, 1660-1668.
- [57] H. J. Schneider, *Angew.Chem.Int.Ed.* **2009**, 48, 3924-3977.
- [58] N. Sakai, J. Mareda, S. Matile, *Acc.Chem.Res.* **2008**, 41, 1354-1365.
- [59] J. D. Badjic, A. Nelson, S. J. Cantrill, W. B. Turnbull, J. F. Stoddart, *Acc.Chem.Res.* **2005**, 38, 723-732.
- [60] J. K. Klosterman, Y. Yamauchi, M. Fujita, *Chem.Soc.Rev.* **2009**, 38, 1714-1725.
- [61] V. L. Malinovskii, D. Wenger, R. Häner, *Chem.Soc.Rev.* **2010**, 39, 410-422.
- [62] S. Grimme, *Angew.Chem.Int.Ed.* **2008**, 47, 3430-3434.
- [63] I. Trkulja, R. Häner, *Bioconjug.Chem.* **2007**, 18, 289-292.
- [64] F. Samain, V. L. Malinovskii, S. M. Langenegger, R. Häner, *Bioorg.Med.Chem.* **2008**, 16, 27-33.

- [65] K. I. Shaikh, C. S. Madsen, L. J. Nielsen, A. S. Jorgensen, H. Nielsen, M. Petersen, P. Nielsen, *Chem.Eur.J.* **2010**, 16, 12904-12919.
- [66] A. Mammana, G. Pescitelli, T. Asakawa, S. Jockusch, A. G. Petrovic, R. R. Monaco, R. Purrello, N. J. Turro, K. Nakanishi, G. A. Ellestad, M. Balaz, N. Berova, *Chem.Eur.J.* **2009**, 15, 11853-11866.
- [67] P. P. Neelakandan, Z. Pan, M. Hariharan, Y. Zheng, H. Weissman, B. Rybtchinski, F. D. Lewis, *J.Am.Chem.Soc.* **2010**, 132, 15808-15813.
- [68] A. W. I. Stephenson, N. Bomholt, A. C. Partridge, V. V. Filichev, *ChemBioChem* **2010**, 11, 1833-1839.
- [69] I. Bouamaied, T. Nguyen, T. Ruhl, E. Stulz, *Org.Biomol.Chem.* **2008**, 6, 3888-3891.
- [70] H. Langhals, R. Ismael, *Eur.J.Org.Chem.* **1998**, 1915-1917.
- [71] A. D. Q. Li, W. Wang, L. Q. Wang, *Chem.Eur.J.* **2003**, 9, 4594-4601.
- [72] Y. Zheng, H. Long, G. C. Schatz, F. D. Lewis, *Chem.Commun.* **2005**, 4795-4797.
- [73] W. Wang, L. S. Li, G. Helms, H. H. Zhou, A. D. Q. Li, *J.Am.Chem.Soc.* **2003**, 125, 1120-1121.
- [74] T. E. Kaiser, V. Stepanenko, F. Würthner, *J.Am.Chem.Soc.* **2009**, 131, 6719-6732.
- [75] M. A. Abdalla, J. Bayer, J. O. Radler, K. Müllen, *Angew.Chem.Int.Ed.* **2004**, 43, 3967-3970.
- [76] F. Würthner, C. Thalacker, S. Diele, C. Tschierske, *Chem.Eur.J.* **2001**, 7, 2245-2253.
- [77] T. A. Zeidan, M. Hariharan, K. Siegmund, F. D. Lewis, *Photoch.Photobio.Sci.* **2010**, 9, 916-922.
- [78] N. Berova, K. Nakanishi, R. W. Woody, *Circular Dichroism - Principles and Applications*, 2nd ed. Wiley-VCH, New York **2000** .
- [79] N. Berova, L. Di Bari, G. Pescitelli, *Chem.Soc.Rev.* **2007**, 36, 914-931.
- [80] D. B. Amabilino, J. F. Stoddart, *Chem.Rev.* **1995**, 95, 2725-2828.
- [81] K. M. Guckian, B. A. Schweitzer, R. X. F. Ren, C. J. Sheils, D. C. Tahmassebi, E. T. Kool, *J.Am.Chem.Soc.* **2000**, 122, 2213-2222.
- [82] C. A. Hunter, K. R. Lawson, J. Perkins, C. J. Urch, *J.Chem.Soc. Perkin Trans.2*, **2001**, 651-669.
- [83] J. J. Reczek, B. L. Iverson, *Macromolecules* **2006**, 39, 5601-5603.

- [84] A. L. Sisson, N. Sakai, N. Banerji, A. Furstenberg, E. Vauthey, S. Matile, *Angew.Chem.Int.Ed.* **2008**, 47, 3727-3729.
- [85] F. Cozzi, F. Ponzini, R. Annunziata, M. Cinquini, J. S. Siegel, *Angew.Chem.Int.Ed Engl.* **1995**, 34, 1019-1020.
- [86] G. W. Coates, A. R. Dunn, L. M. Henling, D. A. Dougherty, R. H. Grubbs, *Angew.Chem.Int.Ed Engl.* **1997**, 36, 248-251.
- [87] A. P. West, S. Mecozzi, D. A. Dougherty, *J.Phys.Org.Chem.* **1997**, 10, 347-350.
- [88] F. Ponzini, R. Zaghera, K. Hardcastle, J. S. Siegel, *Angew.Chem.Int.Ed.* **2000**, 39, 2323-2325.
- [89] G. Mathis, J. Hunziker, *Angew.Chem.Int.Ed.Engl.* **2002**, 41, 3203-3205.
- [90] N. S. S. Kumar, M. D. Gujrati, J. N. Wilson, *Chem.Commun.* **2010**, 46, 5464-5466.
- [91] H. M. Colquhoun, Z. X. Zhu, D. J. Williams, *Org.Lett.* **2003**, 5, 4353-4356.
- [92] B. W. Greenland, S. Burattini, W. Hayes, H. M. Colquhoun, *Tetrahedron* **2008**, 64, 8346-8354.
- [93] T. Murase, K. Otsuka, M. Fujita, *J.Am.Chem.Soc.* **2010**, 132, 7864-7865.
- [94] S. Bhosale, A. L. Sisson, P. Talukdar, A. Furstenberg, N. Banerji, E. Vauthey, G. Bollot, J. Mareda, C. Roger, F. Wurthner, N. Sakai, S. Matile, *Science* **2006**, 313, 84-86.
- [95] S. V. Bhosale, C. H. Jani, S. J. Langford, *Chem.Soc.Rev.* **2008**, 37, 331-342.
- [96] V. Balzani, A. Credi, F. M. Raymo, J. F. Stoddart, *Angew.Chem.Int.Ed.* **2000**, 39, 3349-3391.
- [97] W. R. Browne, B. L. Feringa, *Nat.Nanotech.* **2006**, 1, 25-35.
- [98] E. R. Kay, D. A. Leigh, F. Zerbetto, *Angew.Chem.Int.Ed.* **2007**, 46, 72-191.
- [99] N. Rahe, C. Rinn, T. Carell, *Chem.Commun.* **2003**, 2119-2121.
- [100] J. A. M. Vet, S. A. E. Marras, in *Oligonucleotide Synthesis: Methods and Applications*, Humana Press Inc. Totowa, NJ **2004**, 273-290.

4. Preliminary Studies for Diagnostic Applications of an Excimer-Controlled Molecular Beacon

In collaboration with Prof. Rolf Jaggi, Department of Clinical Research, University of Bern.

4.1 Abstract

The design of the highly sensitive, excimer-controlled molecular beacon presented in *chapter 2* allows a selective and sensitive detection of DNA and RNA targets. This quality characteristic implements the probe into an interesting tool for nucleic acid hybridization assays.

4.2 Introduction

The invention of the molecular beacon proposed by Tyagi and Kramer,^[1] more than ten years ago, was probably initiated by the need of a technique for quantitative determination of nucleic acids in real-time which allows, with comparatively low cost and efforts, a reliable and rapid detection procedures. Nowadays, molecular beacons (MBs) are widely spread in different research fields. Such probes can be applied in assays concerning DNA binding proteins,^[2] the investigation of DNA-protein interactions,^[3-6] the detection of proteins^[7-10] and enzymes,^[11] DNA^[12-15] and RNA^[16-18] related assays, as well as analytical methods in environmental chemistry,^[19] elemental analysis^[20] and the investigation of special chemical processes.^[21-23] Not only applicability in almost any environment, but also simplification in handling makes this probe design so useful and interesting.

In the polymerase chain reaction (PCR),^[24] molecular beacons are used to detect, monitor and quantify the accumulation of DNA or RNA sequences during each cycle.^[25-30] Even if no accumulation step is performed MBs can be applied, due to their high sensitivity

towards targets.^[31-34] and the detection of the demanded target can be visualized and followed in real time.^[22, 35-45]

This chapter summarizes preliminary data obtained with donor-acceptor based MBs in hybridization assays. First, the applicability in quantitative PCR (qPCR) measurements was tested with an excimer-controlled MB in comparison with a FRET pair-based probe. Second, the possible use in detecting **18S rRNA** as a target was investigated, which often deals as an internal standard in PCR experiments. The well studied stem design of the MB in *chapter 2* (**MB1**) forms the basis of the probes used in this study. All probes have a four base pairs and a donor-acceptor (D-A) complex stem design in common and differ only in the target detection sequence in the loop region (**Figure 4.1**).

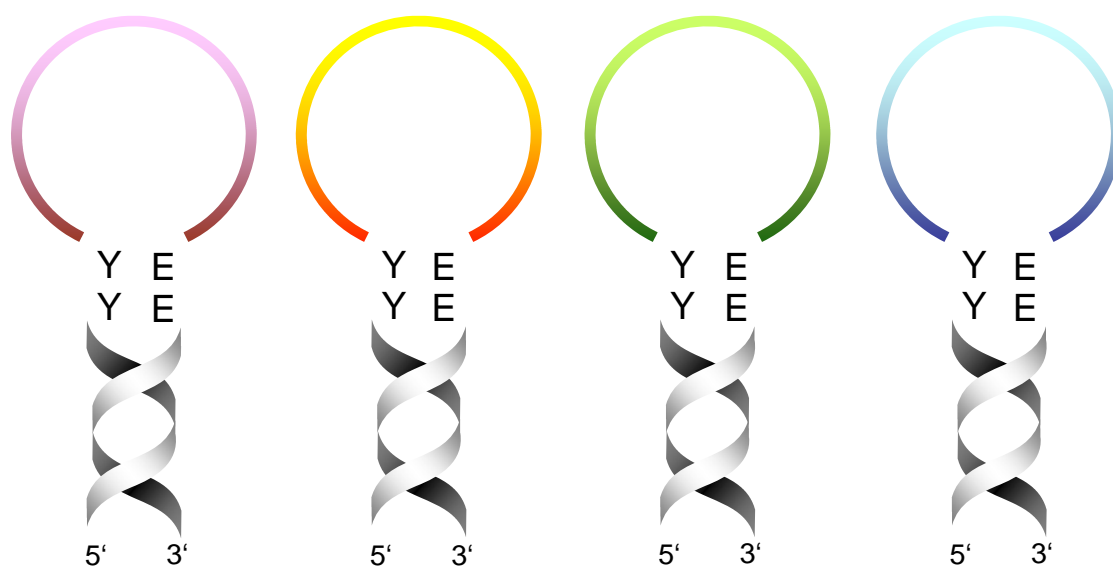


Figure 4.1. Schematic representation of the four excimer-controlled MBs with different target detection sequences in the loop illustrated with the four different loop colors; excimer formation between pyrene derivatives (**Y**) is prevented by donor-acceptor (D-A) complex formation with PDI (**E**) in the native form of the probe (stem-loop-structure).

4.3 Application as probes in qPCR

The novelty in performing qPCR is the real-time monitoring of the amplification process.^[46] Therefore, different methods can be used like binding dyes (e.g. EtBr) or hybridization probes. Molecular beacons are such hybridization probes applied in real-time PCR and enable an accurate detection. In respect of applicability, a D-A based beacon was tested in comparison with a commercially available, target optimized probe containing a **FAM - BHQ-1** FRET pair (Figure 4.2). The oligonucleotide sequences investigated in this study are listed in Table 4.1. The D-A system includes the signal generation design of beacon **MB1**, studied in detail in chapter 2.

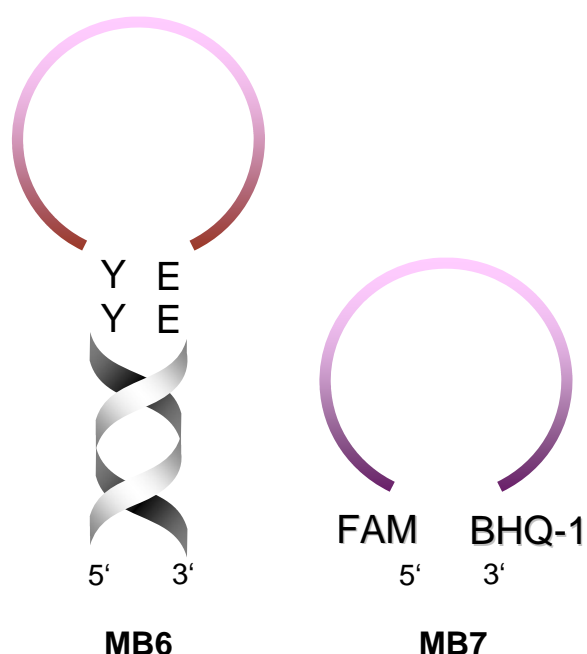


Figure 4.2. Illustration of the two molecular beacons: a D-A based, excimer-controlled MB **MB6** and probe **MB7**, containing **FAM – BHQ-1** as a FRET pair.

Table 4.1. Sequences of **MB6**, **MB7** and the fully matched target DNA **TD5**.

MB6	5' GGTC YY CCC GAC CCG GGG AGG TAG TG EEGACC
MB7	5' FAM CCC GAC CCG GGG AGG TAG TG BHQ
TD5	3' TTT GGG CTG GGC CCC TCC ATC AC TTT

Y: 1,8-dialkynylpyrene; **E:** perylenediimide (PDI); **FAM:** 6-carboxy-fluorescein; **BHQ-1:** Black Hole Quencher™.

4.3.1 Spectroscopic comparison of the two hybridization probes

To test if the D-A based MB passes all requirements for real application a comparative study has to be performed. The excimer-controlled probe **MB6** and the commercially available, FRET-based probe **MB7** were analyzed by fluorescence spectroscopy. The two alkynylpyrene units in **MB6** generate an excimer signal in the open form, whereas the two PDI building blocks prevent a dimerization of the alkynylpyrene moieties in the closed form by formation of an altering D-A complex (**EY EY**). **MB7** on its part ensures signal control on the basis of an adjusted FRET pair, whereas **FAM** is the fluorophore and **BHQ-1** acts as the quencher unit (Figure 4.3).

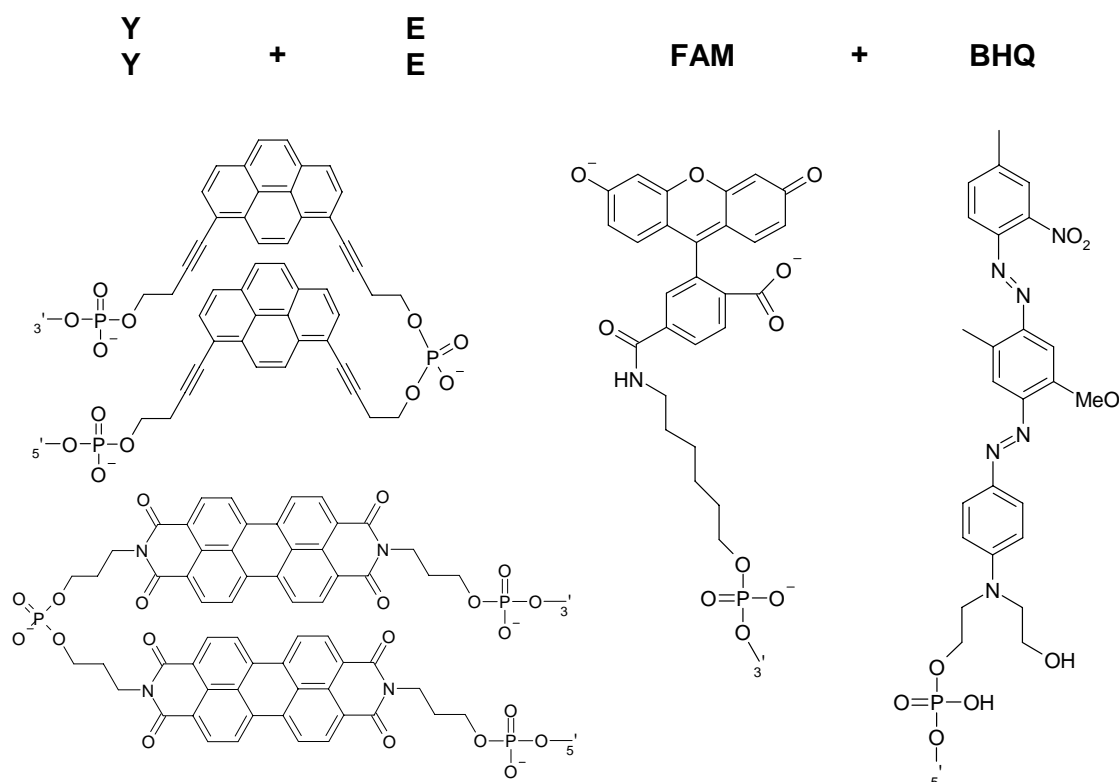


Figure 4.3. Structures of the 1,8-dialkynylpyrene (**Y**) and the 3,4,9,10-perylenetetracarboxylic diimide (PDI, **E**) building blocks forming a D-A complex **EY EY** in the closed form of the probe and the FRET-pair 6-carboxy-fluorescein (**FAM**) and the Black Hole Quencher -1 (**BHQTM**).

First, thermal denaturation curves for both probes **MB6** and **MB7** were recorded to follow the conformational change of the molecular beacons (closed to open form) upon detecting the emission read-outs (Figure 4.4). The melting temperature (T_m) values of **MB6** and **MB7** differ in approximately 15°C. The stem of **MB6** contains four base pairs in addition to the donor-acceptor complex **EY EY**, resulting in a relatively high T_m value. Is a lower T_m value demanded, this probe design offers the possibility to shorten the stem and in consequence decrease the T_m value. Nevertheless, a high T_m value assures a signal generation only in presence of the complementary target and not due to thermal dissociation of the stem.

The fluorescence emission from 50°C on shows a clear difference between the commercially available probe and the donor-acceptor based probe. A fluorescence signal starts to appear with probe **MB7** whereas **MB6** develops the excimer signal not until 70°C as well as the increase in signal constitution and signal intensity of **MB7** seems more pronounced compared to **MB6**. The dissociation of the end-standing FRET pair is initiated before the disaggregating of the electron-rich alkynylpyrene and the electron-poor PDI building blocks, elucidating the observed differences.

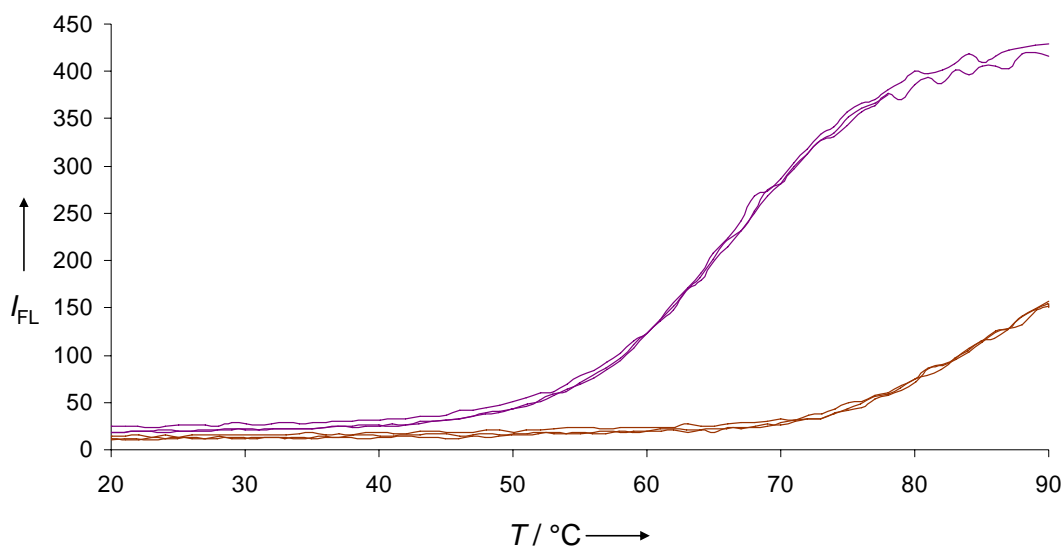


Figure 4.4. Temperature-dependent fluorescence read-out of **MB6** (brown) and **MB7** (violet). Conditions: **MB6** resp. **MB7** 0.1 μ M, 10 mM sodium phosphate buffer, pH 7.0, 100 mM NaCl, λ_{ex1} : 370 nm (**MB6**), λ_{ex2} : 492 nm (**MB7**), λ_{em} : 520 nm, ex/em slit widths: 5/5 nm, PMT voltage: 800 V, performance of three ramps (90-20°C / 20-90°C / 90-20°C), heating/cooling rate: 0.5°C/min.

After adding the complementary fully matched target DNA **TD5** another temperature-dependent fluorescence measurement was performed. The data obtained with (1.2 eq.) and without target **TD5** are combined in Figure 4.5. Beside the differences in intensity another non-conformance can be observed. A signal, based on **MB6**, below 70°C is just generated in presence of target **TD5**. As mentioned before, no temperature induced signal generation due to the strong donor-acceptor interactions of alkynylpyrene and PDI units occurs. Elsewise with **MB7**, where a signal generation at certain temperatures can not simply assigned to probe target hybridization apart from signal intensity. So, **MB6** can be used up to 70°C without the appearance of false positive results.

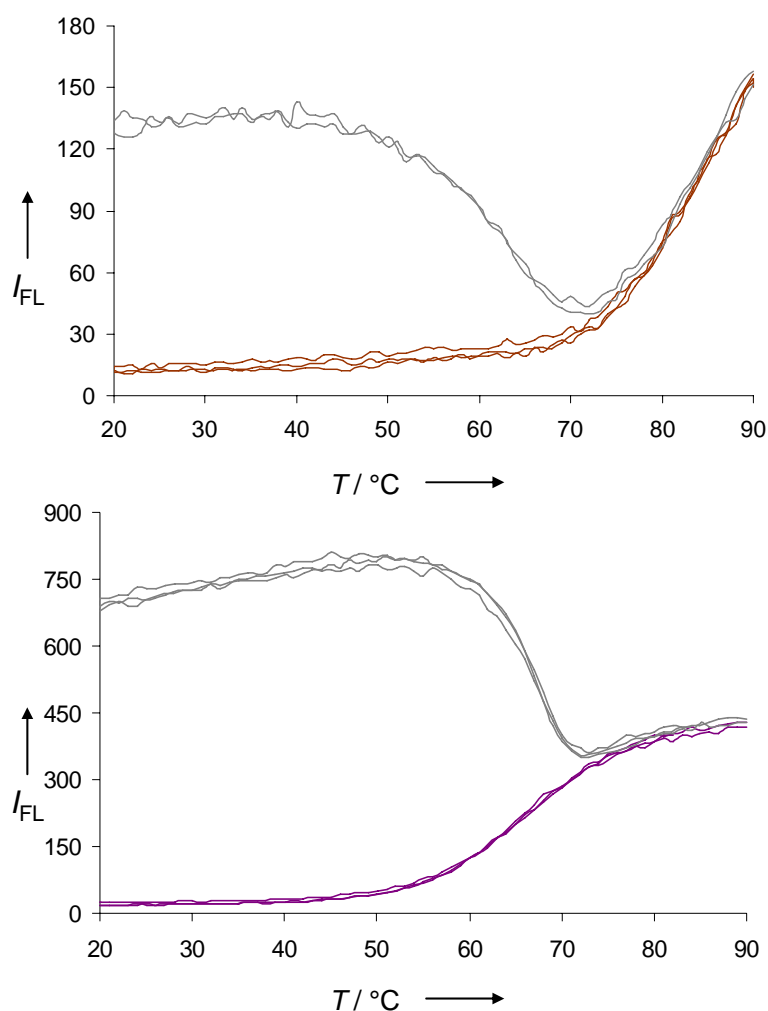


Figure 4.5. Temperature-dependent fluorescence read-out of **MB6** (brown) and **MB6*TD5** (grey) on top as well as **MB7** (violet) and **MB7*TD5** (grey) at the bottom. Conditions: **MB6** resp. **MB7** 0.1 μM , 1.2 eq. **TD5**, see Figure 4.4.

Upon titration experiments the sensitivity of **MB6** compared to **MB7** was investigated. [Figure 4.6](#) shows the normalized fluorescence read-out for the titration of 0 to 1.0 equivalents of the fully matched DNA target to **MB6** and **MB7**. The background signal (at 0 eq. **TD5**) is higher for the donor-acceptor based probe **MB6** compared to the data obtained for **MB7**. The sensitivity below 0.4 equivalents of target seems to be higher for the FRET based probe **MB7** than for **MB6**. Another difference is the increase in signal intensity perceptible on the slope of the straight line indicating a faster response of **MB7**. Nevertheless, **MB6** shows a gradual increase in signal generation and should therefore as well fulfill the demanded requirements for the use in qPCR experiments.

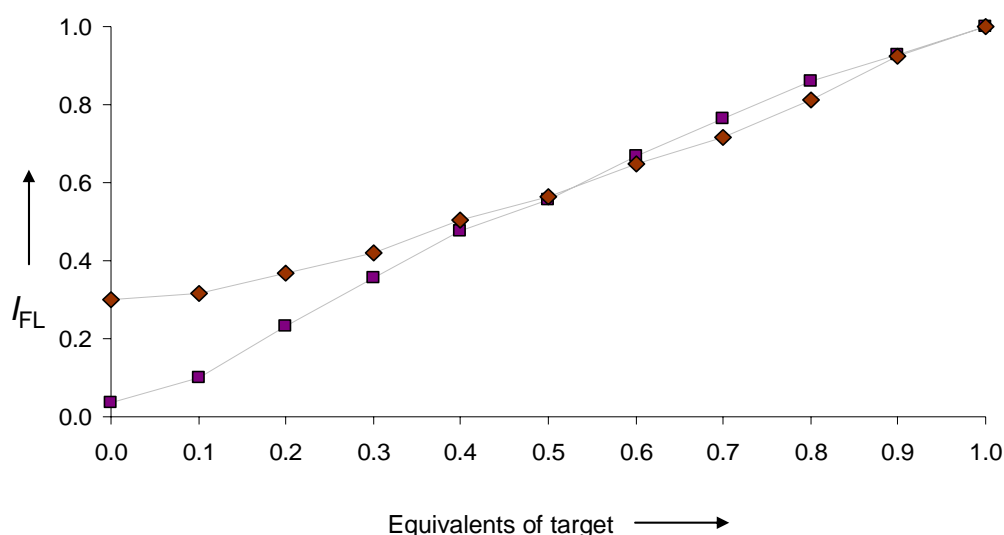


Figure 4.6. Normalized fluorescence read-out obtained for **MB6** (♦) and **MB7** (■) on hybridization with target DNA **TD5** (0 to 1.0 eq. in 0.1 steps) Conditions: **MB6** resp. **MB7** 0.1 μ M, 10 mM sodium phosphate buffer, pH 7.0, 100 mM NaCl, λ_{ex1} : 370 nm (**MB6**), λ_{ex2} : 492 nm (**MB7**), λ_{em} : 520 nm, ex/em slit widths: 5/5 nm, PMT voltage: 600 V.

4.4 Direct rRNA hybridization assays

The observed features of an excimer-controlled MB based on a D-A complex for signal generation presented in *chapter 2* lead us to further applicability studies. Due to high sensitivity and selectivity of the probe, a potential application in RNA hybridization assays

was taken into consideration. Therefore, three highly conserved regions in the **18S rRNA** sequence were chosen as targets. These sequences are of different length and should provide good access for detection. The complementary sequences were the base for the loop sequences of the hybridization probes **MB8**, **MB9** and **MB10** (Figure 4.7). The oligomers used for this study are listed in Table 4.2.

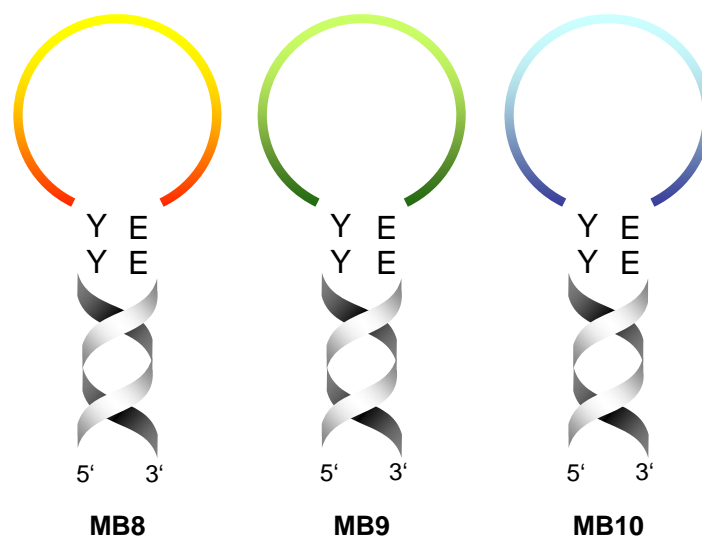


Figure 4.7. Schematic representation of the three D-A based, excimer-controlled hybridization probes **MB8**, **MB9** and **MB10** with different target detection sequences in the loop.

Table 4.2. Sequences of **MB8**, **MB9** and **MB10** with the corresponding fully matched target sequences **TD6**, **TD7** and **TD8**.

MB8	5'GGT CYY AAT ATA CGC TAT TGG AGC TGG AAT TAC EEG ACC
TD6	3'TTT TTA TAT GCG ATA ACC TCG ACC TTA ATG TTT
MB9	5'GGT CYY CCA AGA TCC AAC TAC GAG CTT EEG ACC
TD7	3'TTT GGT TCT AGG TTG ATG CTC GAA TTT
MB10	5'GGT CYY CGG TGG CTC GCC TCG EEG ACC
TD8	3'TTT GCC ACC GAG CGG AGC TTT

Y: 1,8-dialkynylpyrene; **E:** 3,4,9,10-perylenetetracarboxylic diimide (PDI).

Before testing the probes with **18S rRNA** target, preliminary titration experiments with DNA targets were performed. **Figure 4.8** shows the fluorescence emission data obtained for the titration experiment with **MB8**. The generated fluorescence signal correlates linearly with the increase in target concentration.

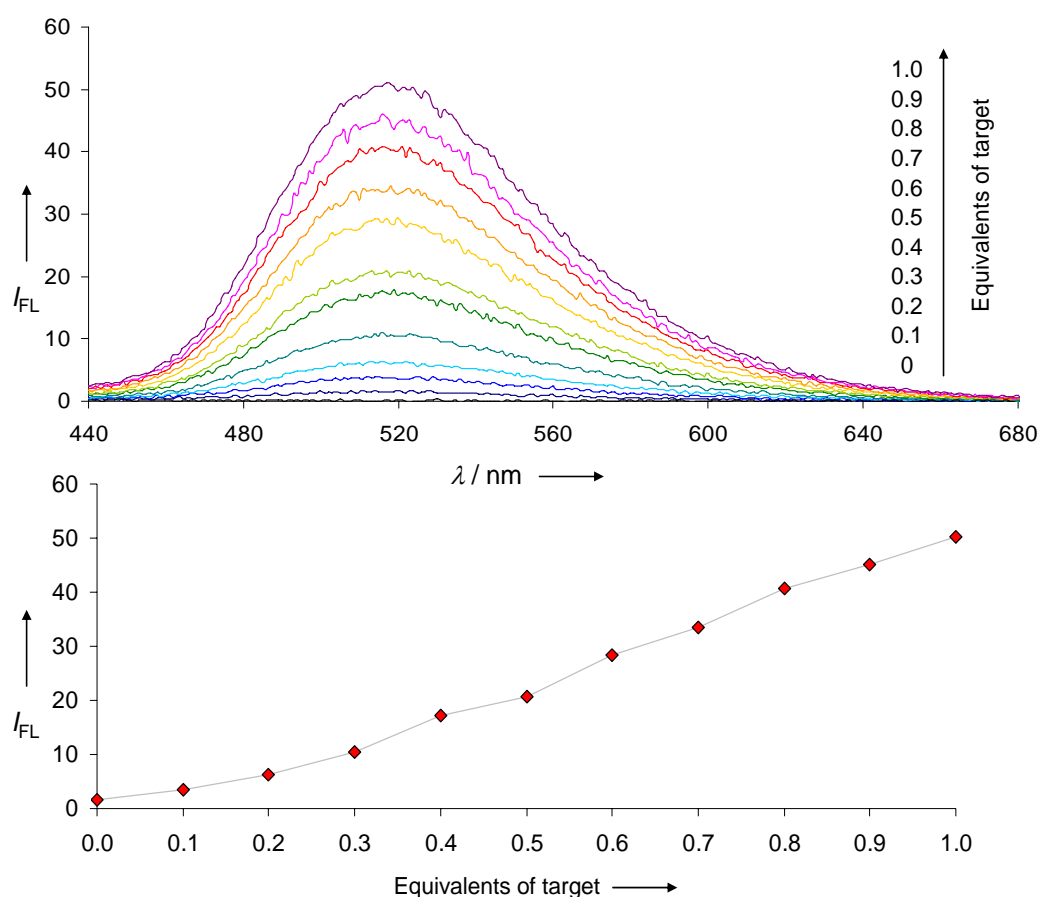


Figure 4.8. Fluorescence read-out obtained for **MB8** on hybridization with DNA target **TD6** (0 to 1.0 eq. in 0.1 steps as indicated) Conditions: **MB8** 0.1 μM , 10 mM sodium phosphate buffer, pH 7.0, 100 mM NaCl, 5.0 mM Mg_2Cl , λ_{ex} : 370 nm, λ_{em} : 520 nm, ex/em slit widths: 5/5 nm, PMT voltage: 600 V, Temp.: 37°C.

This correlation can be represented with a trend line and a corresponding linear equation as it is proceeded in **Figure 4.9**. The linear equation forms the basis of the arising data evaluation for the hybridization assays with **18S rRNA**. The received trend line describes the preliminary calibration line.

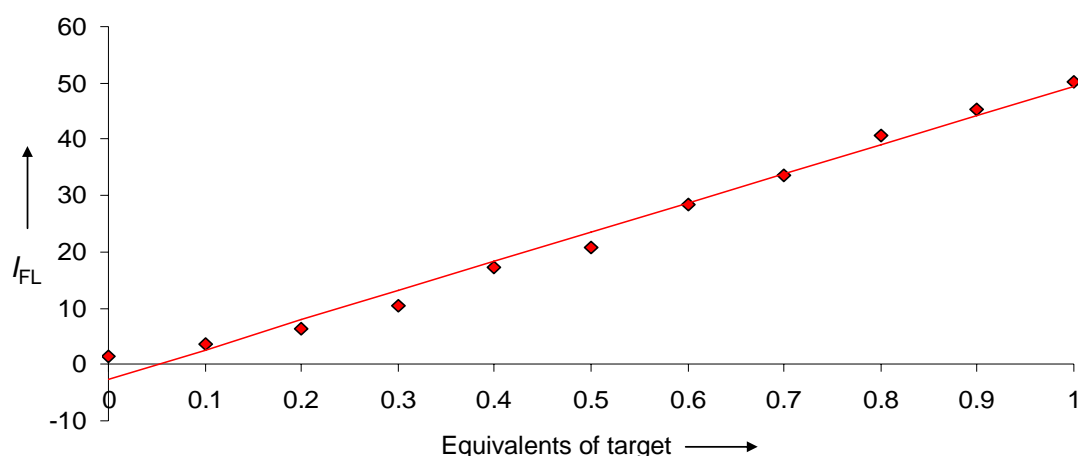


Figure 4.9. Fluorescence read-out obtained for the titration of target **TD6** to **MB8** (see [Figure 4.8](#)) with the corresponding trend line. Linear equation: $y = 51.919x - 2.5308$ with a coefficient of determination $R^2 = 0.9865$.

Further, a time-dependent hybridization experiment was performed, while measuring the fluorescence emission of **MB8**, **MB9** and **MB10** in presence of **18S rRNA** ([Figure 4.10](#)). As a reference, a sample containing only **18S RNA** was tested in parallel.

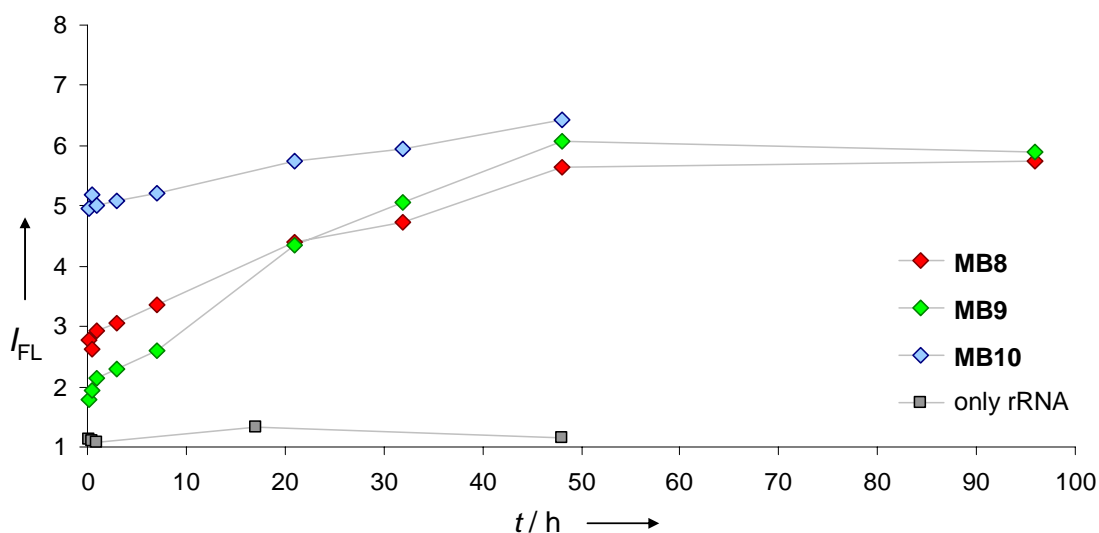


Figure 4.10. Time-dependent fluorescence read-out obtained for **MB8**, **MB9** and **MB10** on hybridization with **18S rRNA** target. Conditions: **MBn** 0.1 μM , **18S rRNA** 0.1 μM , 10 mM sodium phosphate buffer, pH 7.0, 100 mM NaCl, 5.0 mM Mg_2Cl , λ_{ex} : 370 nm, λ_{em} : 520 nm, ex/em slit widths: 5/5 nm, PMT voltage: 600 V, Temp.: 37°C.

To draw conclusion to the amount of detected RNA target, the linear equation ($y = 51.919x - 2.5308$) received in the course of the study is required. To be precise, the performed evaluation of the data can not be taken for granted, due to the assumptions which had to be done and the arising uncertainties that exist. But nevertheless, a first idea of a potential applicability of the D-A based probes can be gained. The calculated concentrations of the detected **18S rRNA** with **MB8** are listed in Table 4.3. The analysis of **MB9** and **MB10** was performed based on the same procedure. The data obtained for **MB10** make further evaluation steps at this point useless. So, a first evaluation of the hybridization assay with **18S rRNA** was performed only for **MB8** and **MB9** (Table 4.4)

Table 4.3. Calculated concentrations of detected **18S rRNA** hybridized to **MB8**.

MB8	<i>y</i>	<i>x</i>
Time [h]	Intensity [a.u.]	<i>nM</i>
0.167	2.780	10.23
0.5	2.631	9.94
1.0	2.922	10.50
3.0	3.044	10.74
7.0	3.347	11.32
21	4.402	13.35
32	4.739	14.00
48	5.653	15.76
96	5.733	15.92
192	7.804	19.91

Table 4.4. Calculated concentrations of detected **18S rRNA** hybridized to **MB9**.

MB9	<i>y</i>	<i>x</i>
Time [h]	Intensity [a.u.]	<i>nM</i>
0.167	1.774	3.07
0.5	1.929	3.41
1.0	2.137	3.87
3.0	2.300	4.23
7.0	2.607	4.91
21	4.346	8.77
32	5.050	10.33
48	6.065	12.58
96	5.890	12.19
192	7.763	16.34

4.5 Conclusion

An excimer-controlled MB with a donor-acceptor (D-A) based signal generation system is used as hybridization probe concerning application in quantitative polymerase chain reaction (PCR) experiments and as detection probe for RNA assays. Preliminary measurements indicate possible applications of D-A based probes in qPCR. The MB was tested in a comparatively study with a commercially available FRET-based probe. The preparatory studies with rRNA as target demonstrate a potential use of D-A based beacons as hybridization probes. However, the data presented in *chapter 4* are just preliminary and further investigations have to be done for final conclusions.

4.6 Experimental Part

Oligonucleotide synthesis. The required alkynylpyrene^[47] and PDI^[48] building blocks were synthesized according to published procedures. Commercial natural nucleoside phosphoramidites were used for oligonucleotide synthesis. Oligonucleotides **MB7** and **TD5** to **TD8** were purchased from *Microsynth*, Balgach, Switzerland. **MB6**, **MB8**, **MB9** and **MB10** were prepared *via* automated oligonucleotide synthesis by an adapted synthetic procedure on a 394-DNA/RNA synthesizer (*Applied Biosystems*). Cleavage from the solid support and final deprotection was done by treatment with 30% NH₄OH solution at 55°C overnight.

Oligonucleotide purification and mass determination. Purification was done by reverse phase HPLC (LiChrospher 100 *RP-18*, 5µm, Merck; *Kontron Instruments* device); eluent *A* = (Et₃NH)OAc (0.1 M, pH 7.4); eluent *B* = MeCN ([Table 4.5](#)).

Table 4.5. Purification performance and retention times (*t_R*s).

	Elution temperature	Elution gradient	Elution time	<i>t_R</i>
MB6	60°C	5 – 40 %	30 min	20.9 min
MB8	60°C	5 – 30 %	30 min	21.6 min
MB9	60°C	5 – 40 %	30 min	21.7 min
MB10	60°C	5 – 30 %	30 min	23.3 min

Mass spectrometry was performed with a Sciex QSTAR pulsar (hybrid quadrupole time-of-flight mass spectrometer, *Applied Biosystems*); ESI-TOF MS (negative mode, acetonitrile/H₂O/triethylamine) ([Table 4.6](#)).

Table 4.6. Molecular formula and masses of the investigated probes.

	<i>molecular formula</i>	<i>calcd. avg. mass</i>	<i>found avg. mass</i>
MB6	C ₃₇₉ H ₄₁₆ N ₁₁₇ O ₁₈₉ P ₃₁	10594.40	10594.30
MB8	C ₄₅₁ H ₅₀₆ N ₁₃₈ O ₂₃₁ P ₃₈	12732.83	12732.19
MB9	C ₃₈₈ H ₄₈₀ N ₁₁₄ O ₁₉₃ P ₃₂	10769.56	10769.88
MB10	C ₃₂₉ H ₃₅₇ N ₈₉ O ₁₆₃ P ₂₆	8971.34	8970.02

Oligonucleotide analysis. Fluorescence spectra were recorded on a *Varian Cary Eclipse* fluorescence spectrophotometer equipped with a *Varian Cary*-block temperature controller using 1 cm x 1 cm quartz cuvettes. *Varian Eclipse* software was used to investigate the fluorescence.

Preliminary DNA titration experiments for MB9 and MB10. Prior to the time-dependent hybridization experiments with RNA, a titration with the fully matched DNA target was performed. Data obtained for **MB9** and **MB10** (for **MB8** see main text) are presented in [Figure 4.11](#).

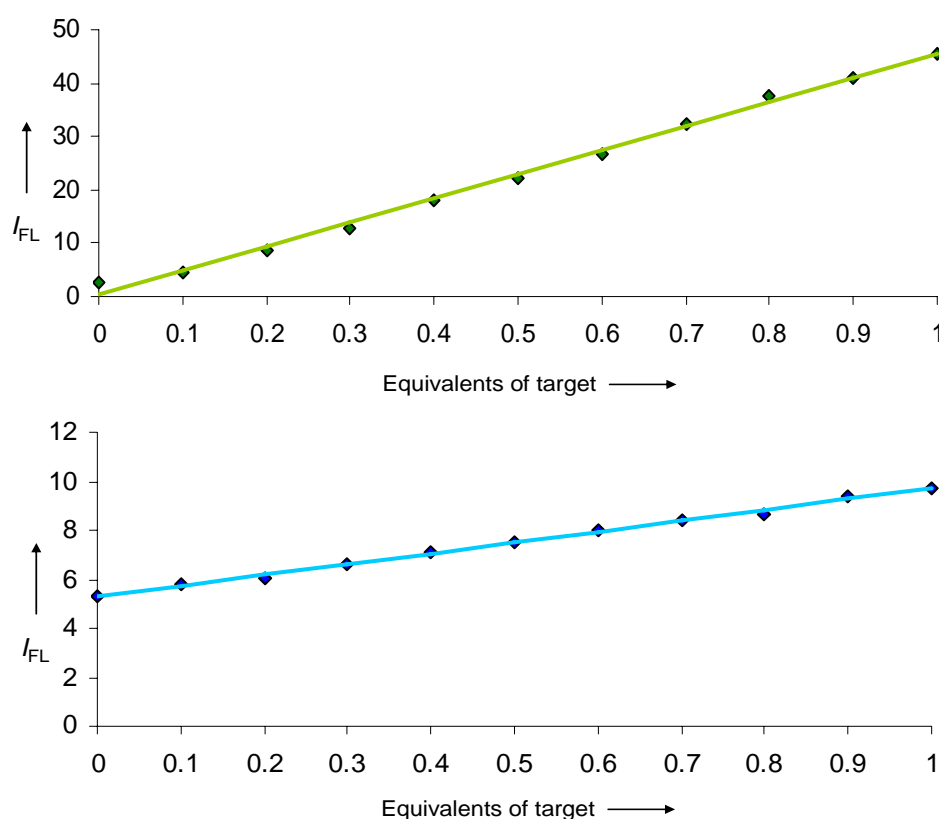


Figure 4.11. Fluorescence read-out obtained for the titration of target **TD7** to **MB9** (top) and **TD8** to **MB10** (bottom) with the corresponding trend line. Conditions: **MB9** respectively **MB10** 0.1 μ M, 10 mM Tris-HCl buffer, pH 7.4, 100 mM NaCl, 5.0 mM Mg_2Cl , λ_{ex} : 370 nm, λ_{em} : 520 nm, ex/em slit widths: 5/5 nm, PMT voltage: 600 V, Temp.: 37°C. **MB9**: Linear equation: $y = 45.116x + 0.3913$ with a coefficient of determination $R^2 = 0.9959$. **MB10**: Linear equation: $y = 4.4605x + 5.2756$ with a coefficient of determination $R^2 = 0.9977$.

4.7 References

- [1] S. Tyagi, F. R. Kramer, *Nat.Biotechnol.* **1996**, 14, 303-308.
- [2] B. Dummitt, Y. H. Chang, *Assay Drug Dev. Technol.* **2006**, 4, 343-349.
- [3] C. J. Yang, H. Lin, W. Tan, *J.Am.Chem.Soc.* **2005**, 127, 12772-12773.
- [4] J. J. Li, X. Fang, S. M. Schuster, W. Tan, *Angew.Chem.Int.Ed.Engl.* **2000**, 39, 1049-1052.
- [5] J. Vitko, I. Rujan, L. A. Androga, I. Mukerji, P. H. Bolton, *Biophys. J.* **2007**, 93, 3210-3217.
- [6] J. Li, Z. C. Cao, Z. Tang, K. Wang, W. Tan, *Methods Mol. Biol.* **2008**, 429, 209-224.
- [7] N. Hamaguchi, A. Ellington, M. Stanton, *Anal.Biochem.* **2001**, 294, 126-131.
- [8] J. J. Li, X. Fang, W. Tan, *Biochem Biophys.Res.Commun.* **2002**, 292, 31-40.
- [9] M. Levy, S. F. Cater, A. D. Ellington, *ChemBioChem.* **2005**, 6, 2163-2166.
- [10] T. Krusinski, A. Laskowska, A. Ozyhar, P. Dobryszycki, *J.Biomol.Screen.* **2008**, 13, 899-905.
- [11] X. Fang, J. J. Li, W. Tan, *Anal.Chem.* **2000**, 72, 3280-3285.
- [12] J. P. Knemeyer, N. Marme, M. Sauer, *Anal.Chem.* **2000**, 72, 3717-3724.
- [13] A. Maksimenko, A. A. Ishchenko, G. Sanz, J. Laval, R. H. Elder, M. K. Saparbaev *Biochem.Biophys.Res.Commun.* **2004**, 319, 240-246.
- [14] J. J. Li, Y. Chu, B. Y. Lee, X. S. Xie, *Nucl.Acids Res.* **2008**, 36, e36.
- [15] Y. W. Lin, H. T. Ho, C. C. Huang, H. T. Chang, *Nucl.Acids Res.* **2008**, 36, 123.
- [16] R. H. Kehlenbach, *Nucl.Acids Res.* **2003**, 31, e64.
- [17] A. A. Marti, S. Jockusch, N. Stevens, J. Ju, N. J. Turro, *Acc.Chem.Res.* **2007**, 40, 402-409.
- [18] L. J. Kuechenmeister, K. L. Anderson, J. M. Morrison, P. M. Dunman, *J. Microbiol. Methods* **2009**, 76, 146-151.
- [19] T. M. Lerga, C. K. O'Sullivan, *Anal.Chim.Acta* **2008**, 610, 105-111.
- [20] M. Rajendran, A. D. Ellington, *Anal.Bioanal.Chem.* **2008**, 390, 1067-1075.
- [21] V. Vijayanathan, T. Thomas, L. H. Sigal, T. J. Thomas, *Antisense Nucl.Acid Drug Dev.* **2002**, 12, 225-233.

- [22] Z. Tang, K. Wang, W. Tan, C. Ma, J. Li, L. Liu, Q. Guo, X. Meng, *Nucl.Acids Res.* **2005**, 33, e97.
- [23] C. J. Yang, J. J. Li, W. Tan, *Methods Mol.Biol.* **2006**, 335, 71-81.
- [24] R. K. Saiki, S. Scharf, F. Faloona, K. B. Mullis, G. T. Horn, H. A. Erlich, N. Arnheim, *Science* **1985**, 230, 1350-1354.
- [25] D. Whitcombe, J. Theaker, S. P. Guy, T. Brown, S. Little, *Nat.Biotechnol.* **1999**, 17, 804-807.
- [26] B. K. Saha, B. Tian, R. P. Bucy, *J.Virol.Methods* **2001**, 93, 33-42.
- [27] D. Summerer, A. Marx, *Angew.Chem.Int.Ed.Engl.* **2002**, 41, 3620-3622.
- [28] K. Petersen, U. Vogel, E. Rockenbauer, K. V. Nielsen, S. Kolvraa, L. Bolund, B. Nexø, *Mol.Cell Probes* **2004**, 18, 117-122.
- [29] X. Li, C. Song, Zhao M, and Li Y, *Anal.Biochem.* **2008**, 381, 5-7.
- [30] C. Song, C. Zhang, M. P. Zhao, *Chem.Asian J.* **2010**, 5, 1146-1151.
- [31] R. J. Strouse, F. Z. Hakki, S. C. Wang, A. W. DeFusco, J. L. Garrett, M. A. Schenerman, *Biopharm.* **2000**, 13, 40-47.
- [32] C. M. Puleo, T. H. Wang, *Lab Chip* **2009**, 9, 1065-1072.
- [33] M. Batish, A. Raj, S. Tyagi, *Methods Mol. Biol.* **2011**, 714, 3-13.
- [34] D. P. Bratu, I. E. Catrina, S. A. E. Marras, *Methods Mol. Biol.* **2011**, 714, 141-157.
- [35] O. Seitz, *Angew.Chem.Int.Ed.Engl.* **2000**, 39, 3249-252.
- [36] J. Liu, P. Feldman, T. D. Chung, *Anal.Biochem.* **2002**, 300, 40-45.
- [37] J. J. Li, W. Tan, *Anal.Biochem.* **2003**, 312, 251-254.
- [38] S. A. E. Marras, B. Gold, F. R. Kramer, I. Smith, S. Tyagi, *Nucl.Acids Res.* **2004**, 32, e72.
- [39] C. Ma, Z. Tang, K. Wang, W. Tan, J. Li, W. Li, Z. Li, X. Yang, H. Li, L. Liu, *Anal.Biochem.* **2006**, 353, 141-143.
- [40] C. Ma, Z. Tang, K. Wang, W. Tan, X. Yang, W. Li, Z. Li, X. Lv, *Anal.Biochem.* **2007**, 363, 294-296.
- [41] H. Q. He, X. H. Ma, B. Liu, X. Y. Zhang, W. Z. Chen, C. X. Wang, S. H. Cheng, *Acta Pharmacol.Sin.* **2007**, 28, 811-817.
- [42] C. Ma, Z. Tang, K. Wang, W. Tan, X. Yang, W. Li, Z. Li, H. Li, X. Lv, *ChemBioChem* **2007**, 8, 1487-1490.

- [43] X. Feng, X. Duan, L. Liu, L. An, F. Feng, S. Wang, *Langmuir* **2008**, 24, 12138-12141.
- [44] C. Ma, Z. Tang, X. Huo, X. Yang, W. Li, W. Tan, *Talanta* **2008**, 76, 458-461.
- [45] S. M. Wu, Z. Q. Tian, Z. L. Zhang, B. H. Huang, P. Jiang, Z. X. Xie, D. W. Pang, *Biosens.Bioelectron.* **2010** 26, 491-496.
- [46] R. Higuchi, C. Fockler, G. Dollinger, R. Watson, *Nat.Biotechnol.* **1993**, 11, 1026-1030.
- [47] H. Bittermann, D. Siegemund, V. L. Malinovskii, R. Häner, *J.Am.Chem Soc.* **2008**, 130, 15285-15287.
- [48] N. Bouquin, V. L. Malinovskii, R. Häner, *Chem.Commun.* **2008**, 1974-1976.

5. Triple Helix Mediated Arrangement of Chromophores

5.1 Abstract

The spectroscopic behaviour of different chromophoric complexes containing alkynylpyrene and PDI building blocks in a triple-helical mediated structure was investigated. The structure is set up by a clamp-type oligonucleotide and a target strand able to form a triple helix in a parallel motif. Investigations were performed with fluorescence spectroscopy, UV/Vis absorbance and circular dichroism (CD) measurements.

5.2 Introduction

The design of bi-molecular^[1-4] triplex structures is based on a target strand (polypurines) and a clamp-type oligonucleotide (polypyrimidines). Bi-molecular triplexes (Figure 5.1) are stabilized by Hoogsteen- as well as Watson-Crick hydrogen bonding. Upon incorporation of a non-nucleosidic, aromatic linker into the polypyrimidine strand an increase in stability can be observed.^[5-8] This increase in stability is induced by additional π -stacking interactions between the aromatic linker and the terminal base triplet. Aromatic perylene- or naphthalene derivatives are able to interact with all three base residues of the terminal base triplet and are therefore predestined as linker units for the clamp-type oligonucleotide.^[7-10]

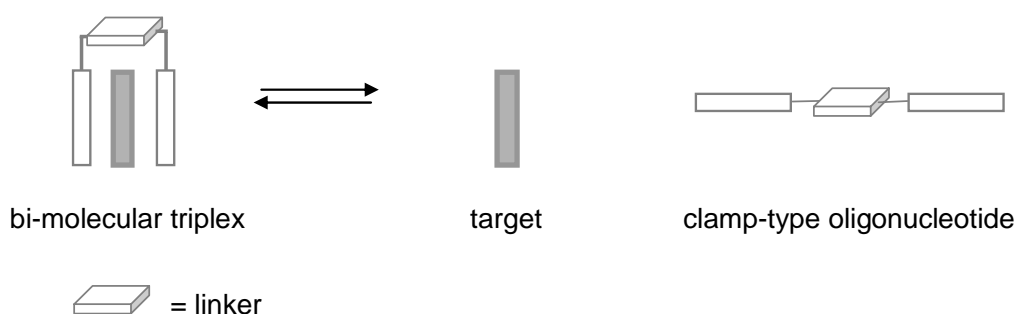


Figure 5.1. Illustration of a bi-molecular triplex motif based on a clamp-type oligonucleotide and a target strand.

The interaction between 3,4,9,10-perylenetetracarboxylic diimide (PDI, **E**)^[11] and 1,8-dialkynylpyrene (**Y**)^[12] building blocks as base surrogates was previously studied in a molecular beacon design (see also *chapter 2* and *chapter 3*).^[13;14] The chromophores were placed adjacent to the loop sequence acting as signal control system. The combination of these two chromophores is the basis for an excimer-controlled molecular beacon, whereas a formation of a donor-acceptor complex of the aromatic building blocks based on π -interactions ensures the signal control.^[15-19] In the closed form no signal is generated and disruption of the complex leads to a dimerization of the alkynylpyrenes and fluorescence of excimer emission is restored.^[11-14] To investigate possible new stem designs for donor-acceptor based probes, a triple helical-mediated arrangement of the chromophores is investigated.

The design is studied with clamp-forming oligonucleotides containing a linker unit (e.g. PDI) and a target strand (polypurine) tethered with either no additional units, additional natural bases, one or two alkynylpyrenes or a PDI building block. [Figure 5.2](#) illustrates the combination of a PDI containing clamp-forming oligonucleotide and a target strand with two terminally attached alkynylpyrene units.

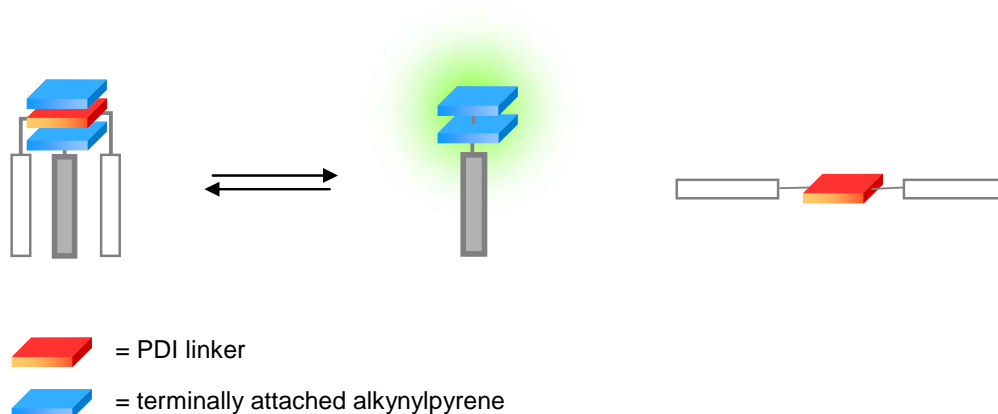


Figure 5.2. Illustration of a triple-helical motif. A red square represents the PDI unit and the alkynylpyrene building blocks are illustrated with blue squares. The formation of an excimer and the resulting signal generation is highlighted in green.

5.3 Spectroscopic behaviour of triple-helical mediated chromophoric complexes

The investigated modified oligonucleotides, non-nucleosidic building blocks and a schematic representation of the triple-helical structure are summarized in Table 5.1 and Figure 5.3.

Table 5.1. Sequences of polypurine (**Cn**) and polypyrimidine (**Tn**) strands.

Clamp type sequences	C1	5' TCT TCT CT E TC TCT TCT
	C2	5' TCT TCT CT E
	C3	5' TCT TCT CT(T) ₆ TC TCT TCT
	C4	5' TCT TCT CT(TTGGTT)TC TCT TCT
Target strands	T1	3' AGA AGA GA YY
	T2	3' AGA AGA GA Y
	T3	3' AGA AGA GA E
	T4	3' AGA AGA GA
	T5	3' AGA AGA GA GGG

The chromophores alkynylpyrene (**Y**) and PDI (**E**) are highlighted in bold.

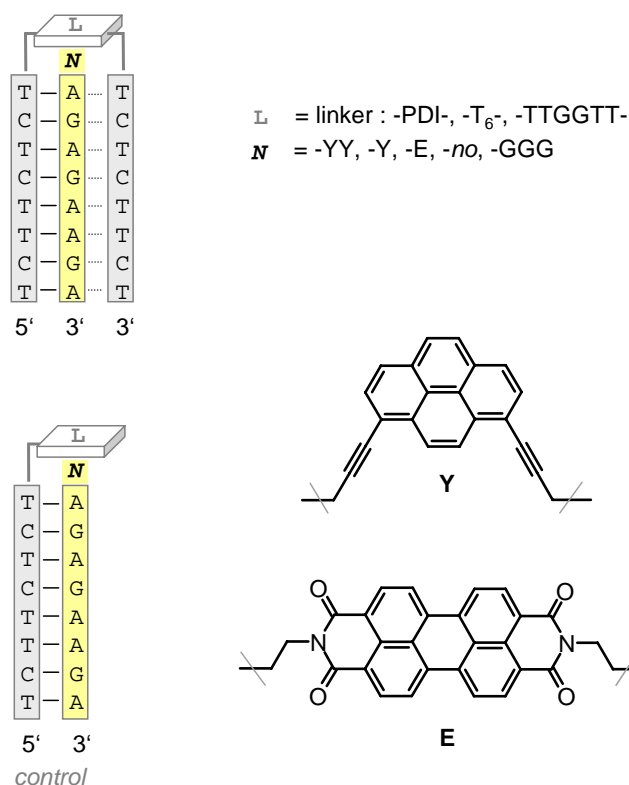


Figure 5.3. List of investigated modified oligonucleotides with alkynylpyrene building blocks (**Y**) and perylenediimide units (**E**) and an illustration of the triplex formed by a clamp-type sequence and a target strand. The Watson-Crick base-pairs are represented by – and the Hoogsteen bonds are illustrated with ---.

To study the influence of the incorporated non-nucleosidic base surrogates on the triplex stability, thermal denaturation experiments were performed (Table 5.2).

Table 5.2. T_m -values of the modified triple helices.

	T_m [°C] ^a	ΔT_m [°C]		T_m [°C] ^a	ΔT_m [°C]
C1*T1	77		C1*T2	78	1
C3*T1	56	21	C1*T4	63	14
C4*T1	55	22	C1*T5	67	10

^aConditions: 1.0 μM single strand concentration, 10 mM sodium acetate buffer, pH 5.0, 100 mM NaCl, 20 mM MgCl_2 . absorbance at 260 nm.

As a reference triplex the combination of the PDI linker containing clamp-type oligonucleotide (**C1**) and the target with two terminally attached alkynylpyrene units (**T1**) was set. Hybrid **C1*T2** (Figure 5.4) is build up with one alkynylpyrene unit compared to hybrid **C1*T1** (Figure 5.5). Nevertheless, the induced stability seems not to be influenced.

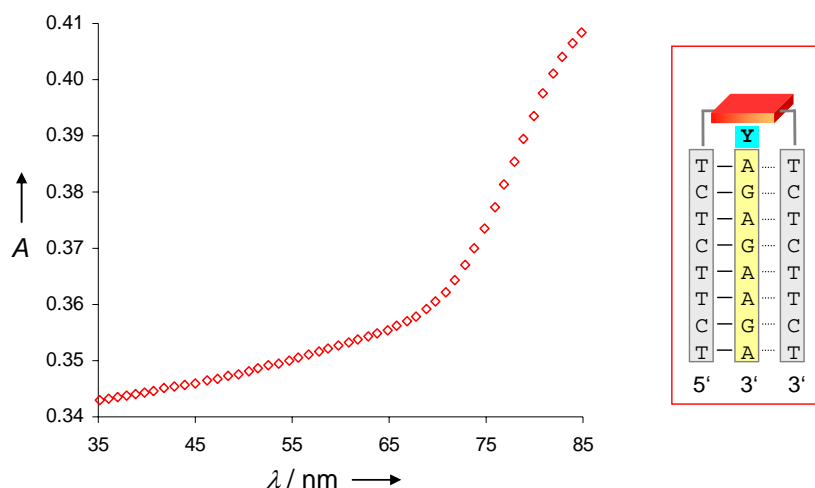


Figure 5.4. Thermal denaturation profile of hybrid **C1*T2** monitored at 260 nm. Conditions: 1.0 μM single strand concentration, 10 mM sodium acetate buffer, pH 5.0, 100 mM NaCl, 20 mM MgCl_2 .

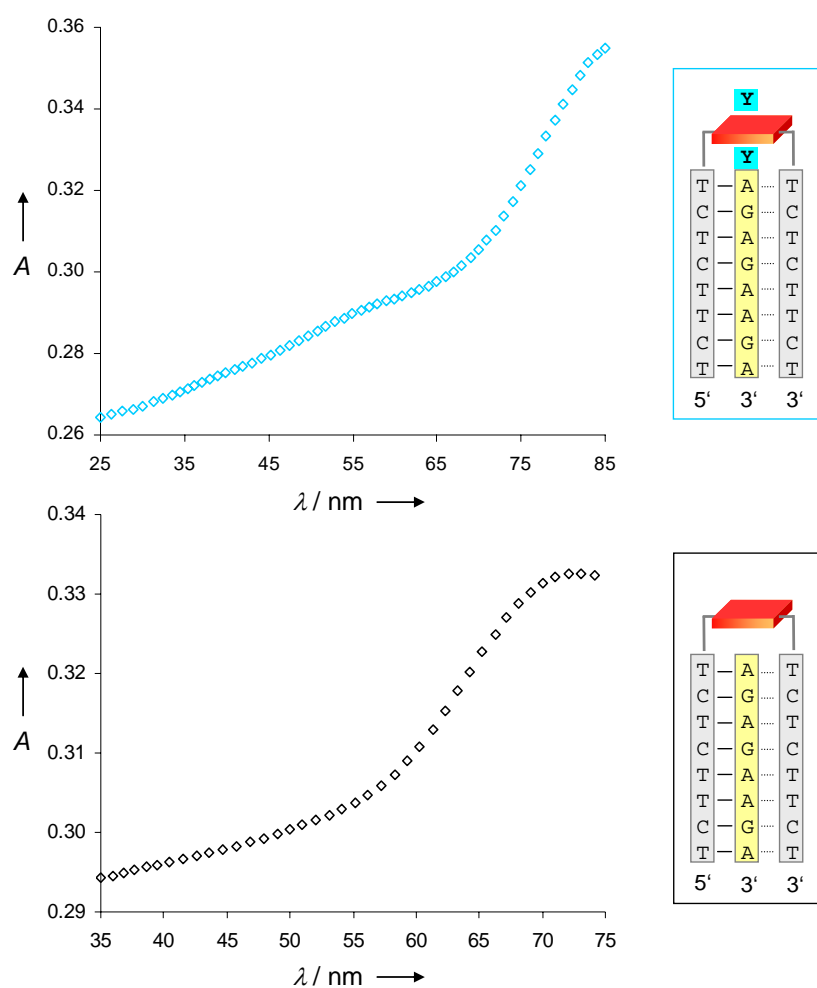


Figure 5.5. Thermal denaturation profiles of hybrids **C1*T1** (top) and **C1*T4** (bottom) monitored at 260 nm. Conditions: 1.0 μM single strand concentration, 10 mM sodium acetate buffer, pH 5.0, 100 mM NaCl, 20 mM MgCl_2 .

The hybrid with the completely matching target sequences without additional bases at the 5'-end (**C1*T4**) (Figure 5.5) has a ΔT_m of approx. 14°C, showing the induced stability effect of the alkynylpyrene units at the 5'-end of the target strand. By replacing the chromophores with three guanosine bases (-GGG-) a destabilization compared to hybrid **C1*T1** can be observed (Figure 5.6).

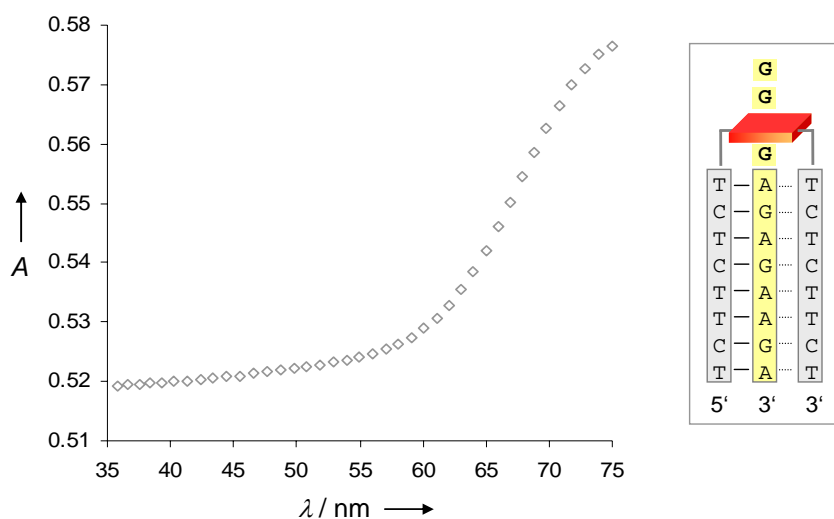


Figure 5.6. Thermal denaturation profile of hybrid **C1*T5** monitored at 260 nm. Conditions: 1.0 μM single strand concentration, 10 mM sodium acetate buffer, pH 5.0, 100 mM NaCl, 20 mM MgCl_2 .

The interaction of the terminally attached alkynylpyrene units with the PDI linker influences the stability of the triplex. The contribution of the PDI linker in combination with the alkynylpyrene units was investigated by substituting the PDI by a T_6 -loop linker (Figure 5.7) or a $-\text{TTGGTT}-$ sequence (Figure 5.8). Both hybrids suffer a loss in stability of approximately 20°C .

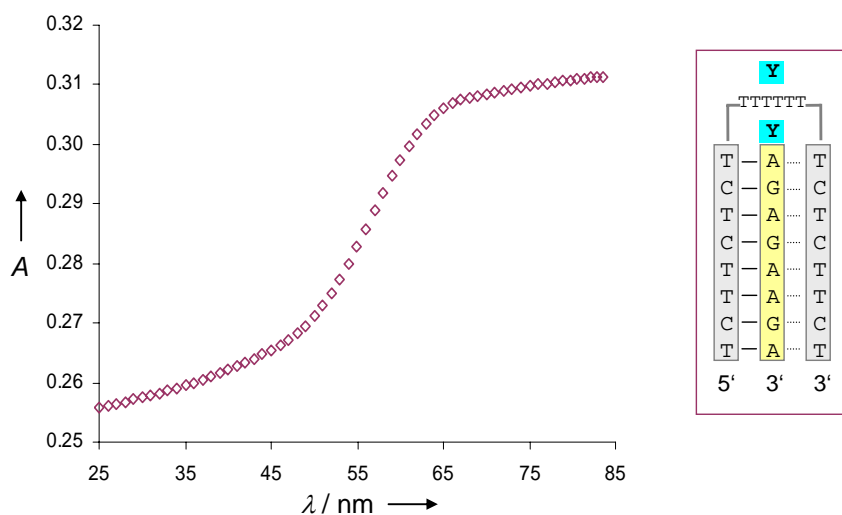


Figure 5.7. Thermal denaturation profile of hybrid **C3*T1** monitored at 260 nm. Conditions: 1.0 μM single strand concentration, 10 mM sodium acetate buffer, pH 5.0, 100 mM NaCl, 20 mM MgCl_2 .

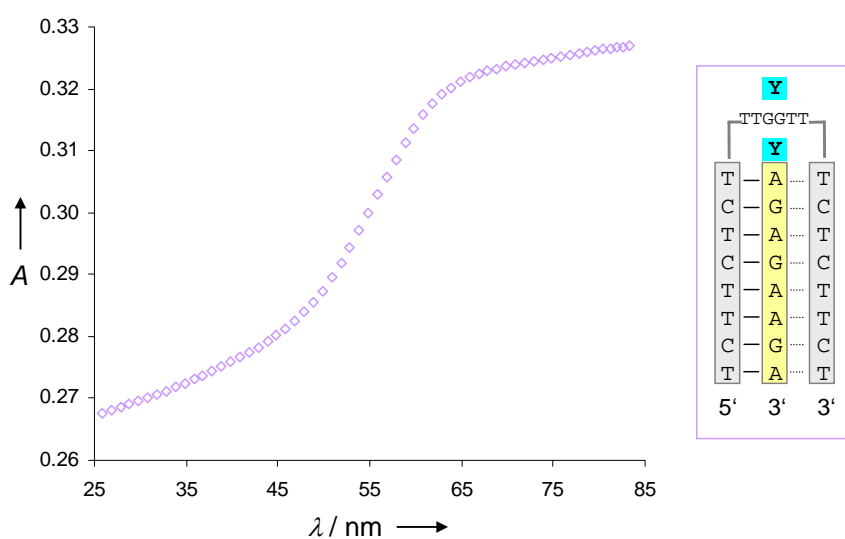


Figure 5.8. Thermal denaturation profile of hybrid **C4*T1** monitored at 260 nm. Conditions: 1.0 μM single strand concentration, 10 mM sodium acetate buffer, pH 5.0, 100 mM NaCl, 20 mM MgCl_2 .

The substantial rise in triplex stability can be credited to the π -stacking interaction between the aromatic base surrogates and the terminal base triplet and to the strong stacking interactions between the electron-poor PDI unit and the electron-rich alkynylpyrene moieties.^[9;13;14]

Stacking interaction and aggregation states can be also studied by fluorescence spectroscopy. The alkynylpyrene building blocks show characteristic monomer and excimer emission upon separation or dimerization.^[12-14] The excimer emission can be successfully quenched with a PDI unit. Upon excitation at 370 nm, hybrid **C1*T1** shows almost no signal (**Figure 5.9** top). After increasing the temperature to 90°C a bright excimer signal at 520 nm appears. The triple-helical structure is disrupted upon increasing temperature and consequently the stacking interaction between the PDI unit and the alkynylpyrenes is vanishing. The pyrene excimer emission can no longer be quenched by the PDI building block. Else wise hybrid **C1*T2** emits monomer fluorescence at 10°C as well as at 90°C. Monomer emission is not completely quenched but rather reduced (**Figure 5.9** bottom).

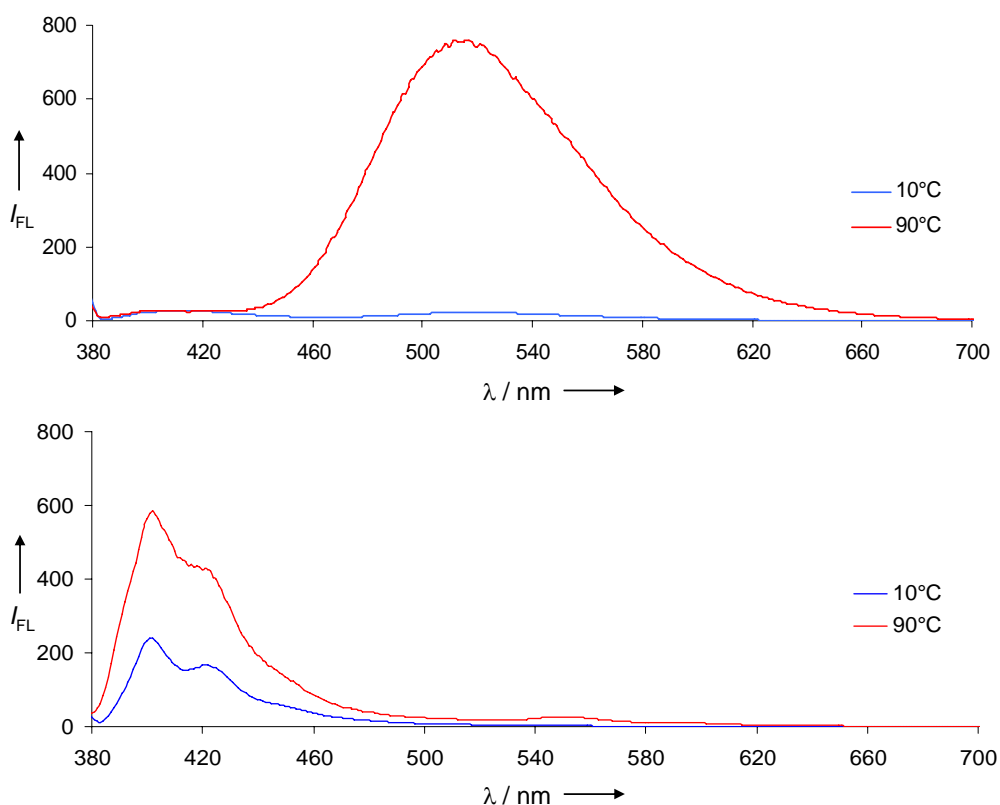


Figure 5.9. Temperature-dependent fluorescence emission spectra of hybrids **C1*T1** (top) and **C1*T2** (bottom). Conditions: 1.0 μM single strand concentration, 10 mM sodium acetate buffer, pH 5.0, 100 mM NaCl, 20 mM MgCl_2 , λ_{ex} : 370 nm, ex/em slit widths: 10/5 nm, PMT voltage: 600 V, equilibration time: 3 min.

As a control, the target strand with two terminally attached alkynylpyrene units was studied in presence of different linker environments. [Figure 5.10](#) summarizes the fluorescence emission data of hybrid **C1*T1**, **C3*T1** and **C4*T1** at 10°C and 90°C. The spectra show a clear difference concerning quenching efficiency. One should be aware that the linker sequence of oligonucleotide **C3** (-T₆-) and **C4** (-TTGGTT-) could form a loop what can end up in a weak interaction between the bases from the linker and the alkynylpyrene units. As a consequence, the quenching would be not efficient as well. Nevertheless, data observed in these measurements show that the PDI unit seems to be an excellent quencher for alkynylpyrene excimer emission in this triple-helical design.

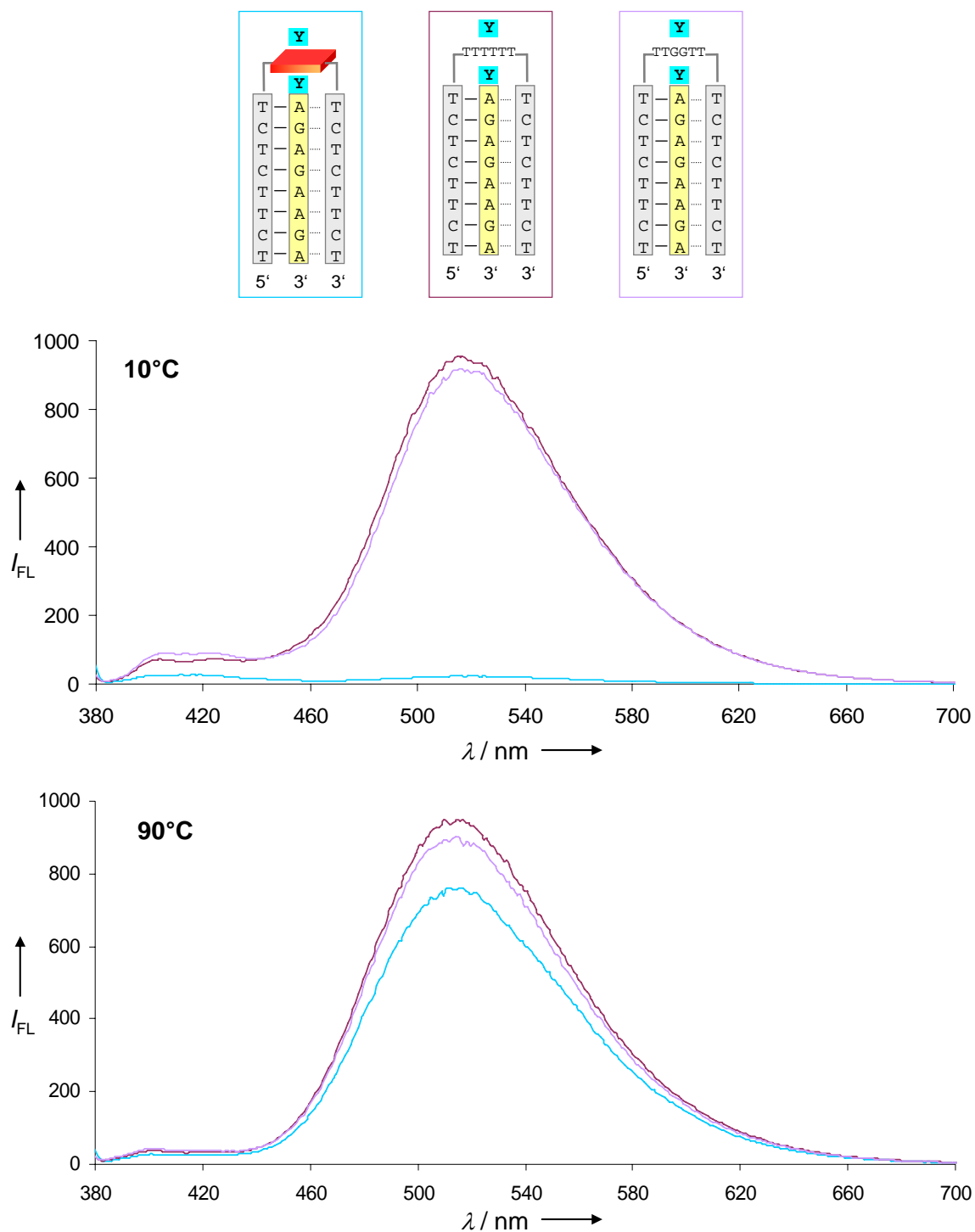


Figure 5.10. Top: illustration of the investigated hybrids **C1*T1**, **C3*T1** and **C4*T1**. Bottom: Temperature-dependent fluorescence emission spectra. Conditions: 1.0 μM single strand concentration, 10 mM sodium acetate buffer, pH 5.0, 100 mM NaCl, 20 mM MgCl_2 , λ_{ex} : 370 nm, ex/em slit widths: 10/5 nm, PMT voltage: 600 V, equilibration time: 3 min.

In this design the PDI unit is placed in between pyrimidine bases which enables the PDI unit to emit fluorescence. On his part, PDI fluorescence can be quenched by neighbouring bases, alkynylpyrenes and also self-quenching can be observed.^[20;21] The polypyrimidine oligomer **C1** exhibits PDI fluorescence upon excitation at 505 nm (Figure 5.11).

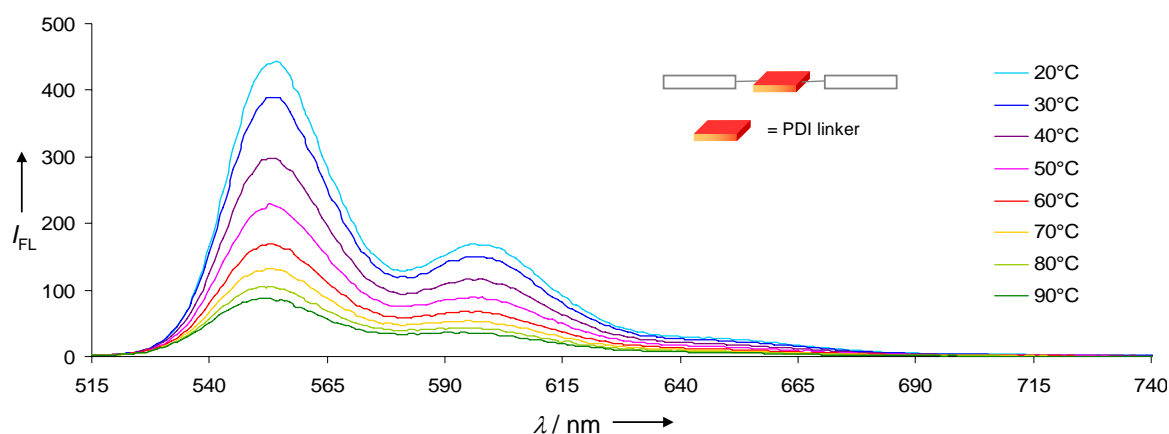


Figure 5.11. Temperature-dependent fluorescence emission spectra of the oligomer **C1**. Conditions: 1.0 μM single strand concentration, 10 mM sodium acetate buffer, pH 5.0, 100 mM NaCl, 20 mM MgCl_2 , λ_{ex} : 505 nm, ex/em slit widths: 5/5 nm, PMT voltage: 600 V, equilibration time: 3 min.

The temperature-dependent emission spectra of hybrid **C1*T1** and **C1*T2** show the quenching effect of the alkynylpyrene units on the PDI fluorescence (Figure 5.12). The monomer fluorescence of PDI (520–690 nm) is nearly completely quenched (Figure 5.13). Although the fluorescence signal intensity is not extremely high.

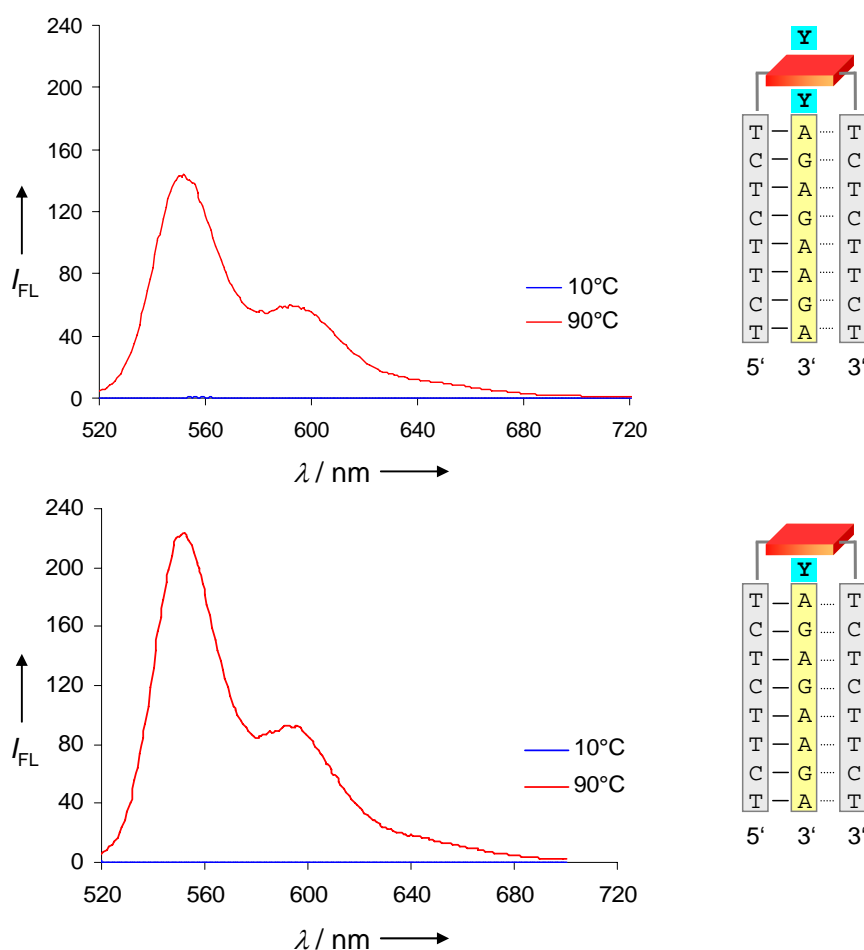


Figure 5.12. Temperature-dependent fluorescence emission spectra of the hybrids **C1*T1** (top) and **C1*T2** (bottom). Conditions: 1.0 μM single strand concentration, 10 mM sodium acetate buffer, pH 5.0, 100 mM NaCl, 20 mM MgCl_2 , λ_{ex} : 505 nm, ex/em slit widths: 10/5 nm, PMT voltage: 600 V, equilibration time: 3 min.

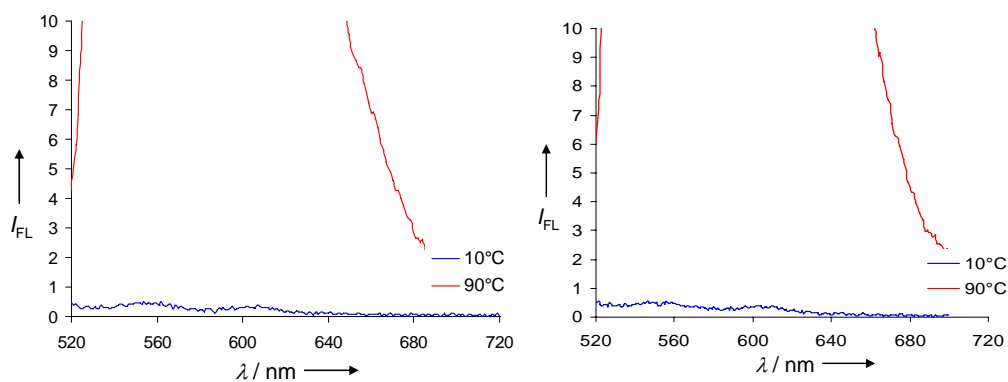


Figure 5.13. Enlarged spectra of the data presented in Figure 5.12 for hybrids **C1*T1** (left) and **C1*T2** (right). Conditions: see Figure 5.12.

Hybrid **C1*T3** contains two PDI building blocks. The additional PDI unit is placed on the 5'-end of the target strand. The fluorescence spectra of oligomer **T3** show only minor emission of the PDI building block. The neighbouring bases are exclusively purine bases known to have quenching properties, especially guanosine bases. These observations can be confirmed with the data obtained for hybrid **C1*T5** (Figure 5.14).

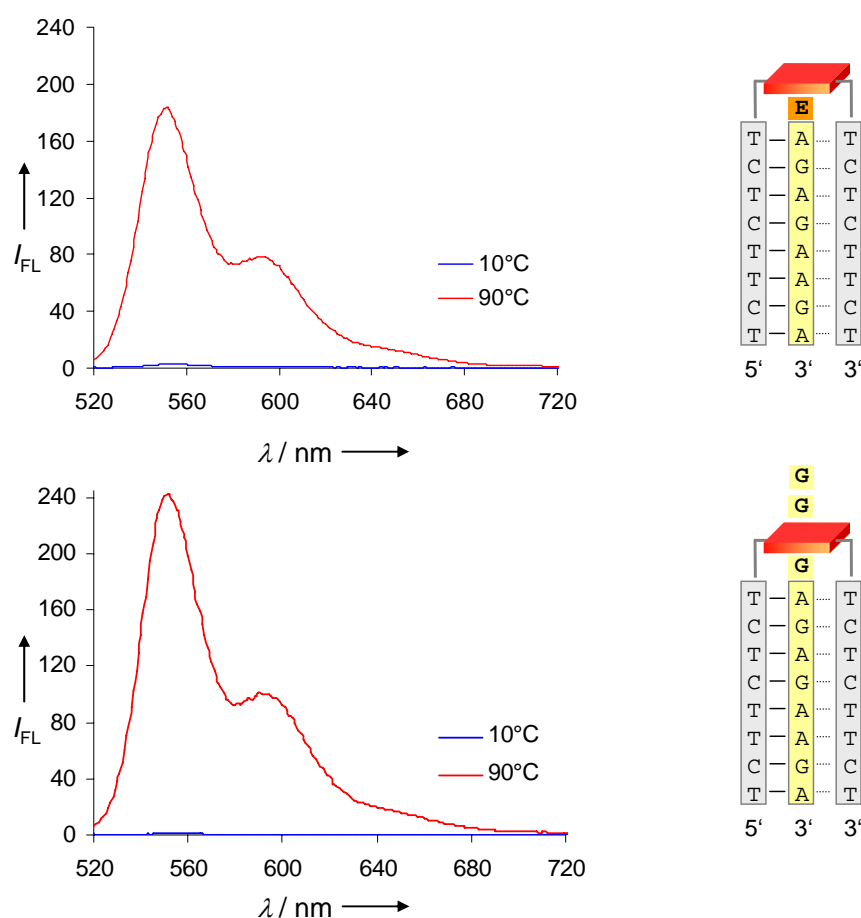


Figure 5.14. Temperature-dependent fluorescence emission spectra of the hybrids **C1*T3** (top) and **C1*T5** (bottom). Conditions: 1.0 μM single strand concentration, 10 mM sodium acetate buffer, pH 5.0, 100 mM NaCl, 20 mM MgCl_2 , λ_{ex} : 505 nm, ex/em slit widths: 10/5 nm, PMT voltage: 600 V, equilibration time: 3 min.

The data verify the quenching of PDI fluorescence by either aromatic building block such as alkynylpyrenes, the self-quenching of PDI and the influence of neighbouring guanosine bases. However, if the target is not elongated but rather completely matching, the fluorescence is only slightly quenched by the next purine base (Figure 5.15). This could also be due to the length of the attached carbon linkers on the PDI building block.

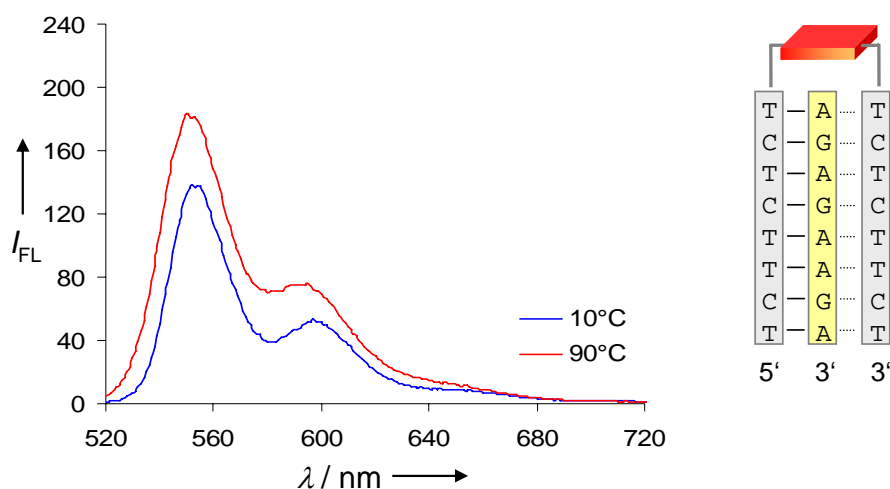


Figure 5.15. Temperature-dependent fluorescence emission spectra of the hybrid **C1*T4**. Conditions: 1.0 μM single strand concentration, 10 mM sodium acetate buffer, pH 5.0, 100 mM NaCl, 20 mM MgCl_2 , λ_{ex} : 505 nm, ex/em slit widths: 10/5 nm, PMT voltage: 600 V, equilibration time: 3 min.

The mutual influence of both chromophores can be also followed by temperature-dependent absorbance measurements. The characteristic signals for the alkynylpyrene building blocks appear between 330–430 nm whereas the PDI unit shows its absorbance signature between 430–610 nm.^[22-29] The shape of the alkynylpyrene signal of hybrid **C1*T1** indicates an aggregated state as the vibronic transition 0-1 is higher in intensity as the A^{0-0} transition. This is not the case in hybrid **C1*T2**, where the signal shows a monomer-like behaviour of the alkynylpyrene units. The PDI signal shows an increase in intensity and a slight blue shift upon increasing the temperature, indicating aggregation interactions with the neighbouring alkynylpyrenes (Figure 5.16).

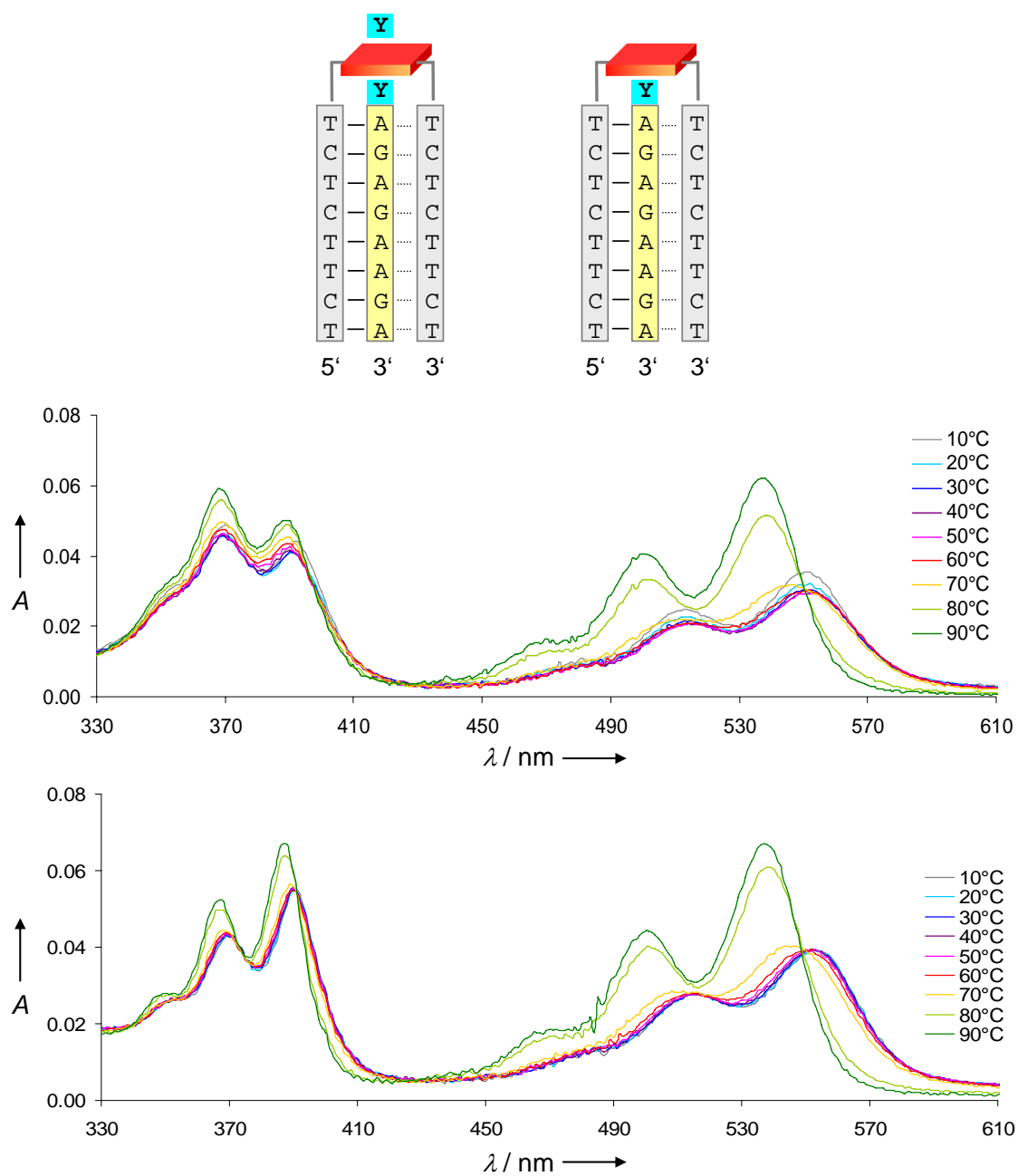


Figure 5.16. Illustration of the investigated hybrids **C1*T1** (left) and **C1*T2** (right). Temperature-dependent UV/Vis read-out of the hybrids **C1*T1** (top) and **C1*T2** (bottom). Conditions: 1.0 μM single strand concentration, 10 mM sodium acetate buffer, pH 5.0, 100 mM NaCl, 20 mM MgCl_2 , equilibration time: 3 min.

Selected CD measurements were performed in a temperature-dependent manner (10-90°C). Figure 5.17 shows the spectra obtained for two hybrids (C1*T1 and C1*T2) and the corresponding composed of single strands (C1, T1 and T2).

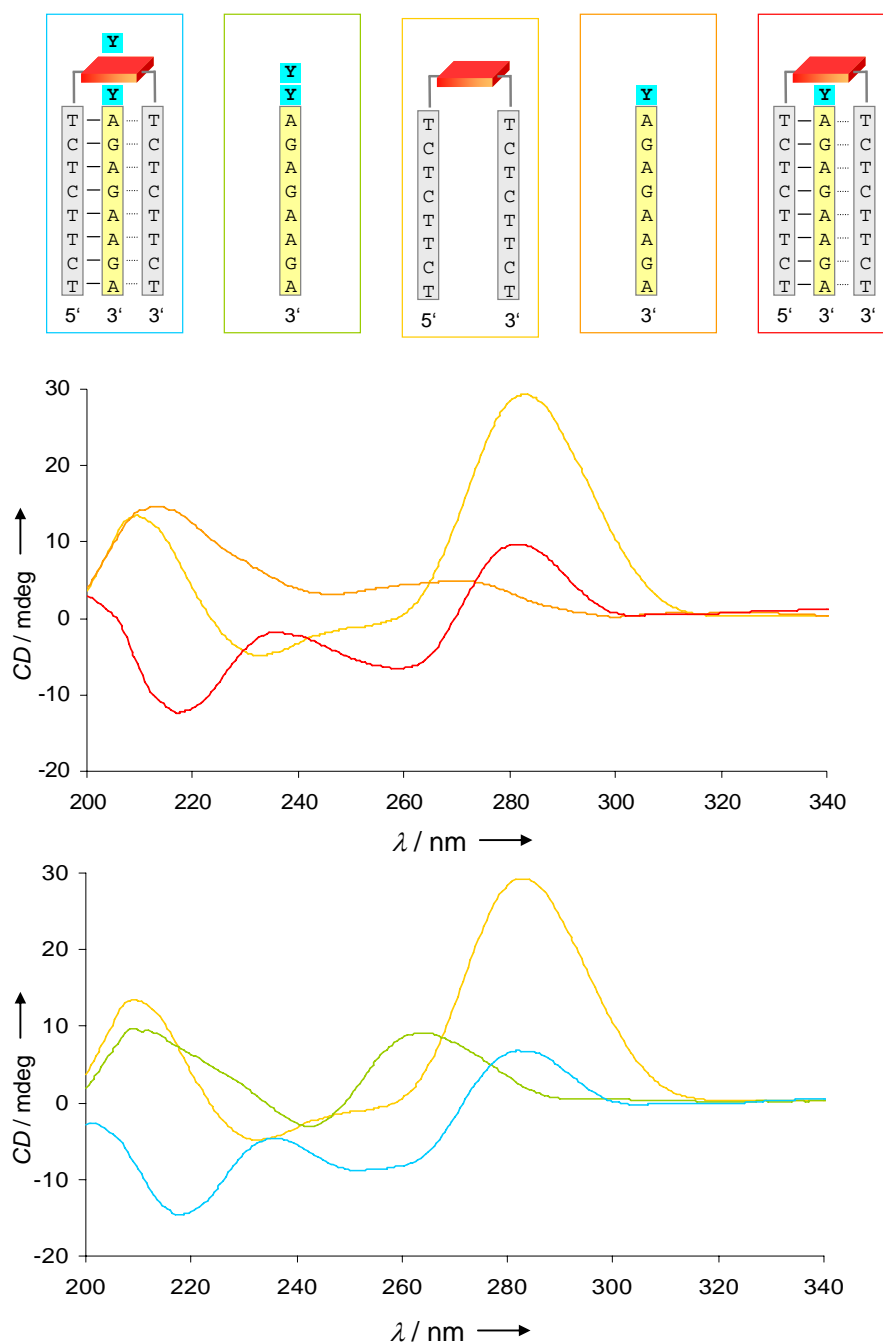


Figure 5.17. Illustration of the investigated hybrids (top), the color of the frame represents the corresponding data in the recorded CD spectra (e.g. blue framed sample → blue spectra). Conditions: 5.0 μM single strand concentration, 10 mM sodium acetate buffer, pH 5.0, 100 mM NaCl, 20 mM MgCl_2 , Temp.: 10°C.

In general, the presence of a negative band at 210-220 nm indicates the existence of a triple helical structure.^[30-32] The spectra observed for the hybrids differ from the sum of the corresponding single strand spectra and confirm the formation of a triplex. Hybrids **C1*T1** and **C1*T2** form triple-helical structures, since both hybrids show a negative band at lower wavelength as well as their spectra are not the sum of the data of their single strands. Hybrid **C1*T3** possesses the same CD characteristics to approve the formation of a triple-helical structure (Figure 5.18). The building block specific CD signatures are not very intense leading to the suggestion of a non-helical arrangement of the chromophores.

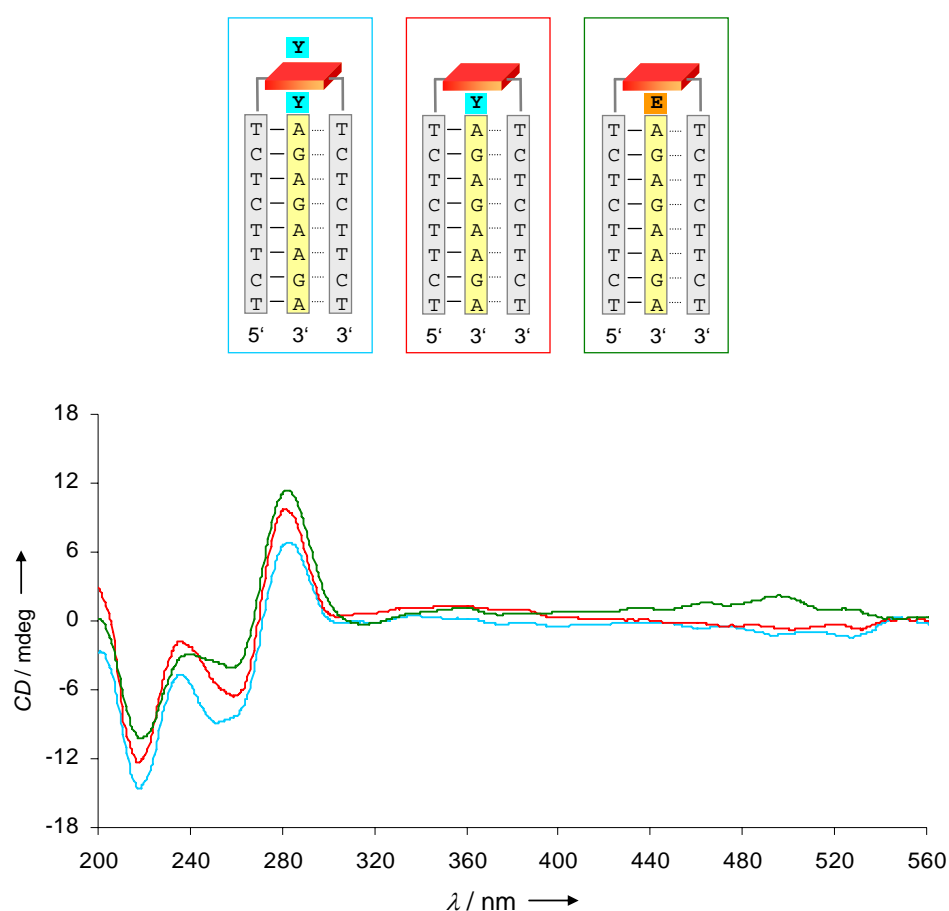


Figure 5.18. Illustration of the PDI linker containing hybrids (top), **C1*T1** (blue), **C1*T2** (red) and **C1*T3** (green). Conditions: 5.0 μ M single strand concentration, 10 mM sodium acetate buffer, pH 5.0, 100 mM NaCl, 20 mM $MgCl_2$, Temp.: 10°C.

5.4 Conclusion

A clamp-type oligonucleotide that contains a PDI linker and a target strand with terminally attached alkynylpyrene units forms a stable triple-helical structure (Figure 5.19). The non-nucleosidic building blocks interact based on π -stacking forces. This induces stability to the structure and offers the possibility to shorten the part with the natural base pairs. The design allows the aromatic moieties to get in close proximity and an aggregation in an altering mode can be provided. Consequently, quenching of the chromophore specific fluorescence could be observed. Not only can the generation of a pyrene excimer (or monomer) signal be ensured, but also fluorescence of the PDI unit. Excimer fluorescence is quenched if the clamp contains one PDI as a non-nucleosidic unit. Replacing of the PDI unit with a T₆-loop or a combination of thymine and guanosine bases results in no quenching of the excimer signal. Alkynylpyrenes, an additional PDI unit, guanosine bases or no additional units at the 5'-end of the target strand influences the fluorescence behaviour of the PDI building block in the polypyrimidine strand. The PDI signal vanishes if the target strand is elongated in any way. The data summarized in this chapter represent the main results of the whole study. Further experiments were performed e.g. the measurements with the “control-clamp”, but no additional insights were gained. Overall, the obtained results lead to a new stem design for a molecular beacon and can be therefore seen as a preparatory study for the probe presented in *chapter 6*.

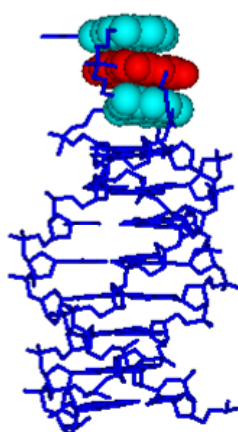


Figure 5.19. Model of hybrid **C1*T1**, chromophores are illustrated in red (PDI) and cyan (alkynylpyrene).

5.5 Experimental Part

Oligonucleotide synthesis. The required alkynylpyrene^[12] and PDI^[11] building blocks were synthesized according to published procedures. Commercial natural nucleoside phosphoramidites were used for oligonucleotide synthesis. Oligonucleotides **C3**, **C4**, **T4**, and **T5** were purchased from *Microsynth*, Balgach, Switzerland. **C1**, **C2**, **T1**, **T2** and **T3** were prepared *via* automated oligonucleotide synthesis by a standard synthetic procedure (2 min coupling time; ‘trityl-off’ mode) on a 394-DNA/RNA synthesizer (*Applied Biosystems*), except for the coupling step of the PDI phosphoramidite, an adapted activating step was proceeded. Cleavage from the solid support and final deprotection was done by treatment with 30% NH₄OH solution at 55°C overnight and for oligomer **C2** at 80°C for two days.

Oligonucleotide purification and mass determination. Purification was done by reverse phase HPLC (LiChrospher 100 *RP-18*, 5µm, Merck; *Kontron Instruments* device); eluent *A* = (Et₃NH)OAc (0.1 M, pH 7.4); eluent *B* = MeCN ([Table 5.3](#)).

Table 5.3. Purification performance and retention times (*t_R*s).

	Elution temperature	Elution gradient	Elution time	<i>t_R</i>
C1	50°C	5 – 40 %	30 min	19.75 min
C2	40°C	5 – 40 %	30 min	21.19 min
T1	50°C	5 – 50 %	30 min	25.25 min
T2	50°C	5 – 50 %	30 min	20.58 min
T3	40°C	5 – 40 %	30 min	21.08 min

Mass spectrometry was performed with a Sciex QSTAR pulsar (hybrid quadrupole time-of-flight mass spectrometer, *Applied Biosystems*); ESI-TOF MS (negative mode, acetonitrile/H₂O/triethylamine) ([Table 5.4](#)).

Table 5.4. Specification of the investigated oligomers.

	<i>Molecular formula</i>	<i>calcd. avg. mass</i>	<i>found avg. mass</i>
C1	C ₁₈₄ H ₂₂₄ N ₄₀ O ₁₁₂ P ₁₆	5283.53	5282.98
C2	C ₁₀₇ H ₁₂₃ N ₂₁ O ₅₉ P ₈	2895.02	2895.46
T1	C ₁₂₈ H ₁₃₁ N ₄₀ O ₄₉ P ₉	3292.41	3292.62
T2	C ₁₀₄ H ₁₁₄ N ₄₀ O ₄₅ P ₈	2892.05	2891.84
T3	C ₁₁₀ H ₁₁₈ N ₄₂ O ₄₉ P ₈	3060.16	3060.42

Oligonucleotide analysis. Temperature-dependent UV/Vis spectra were carried out on a *Varian Cary-100 Bio-UV/Vis* spectrophotometer equipped with a *Varian Cary-block* temperature controller and data were collected with *Varian WinUV* software. Fluorescence spectra were recorded on a *Varian Cary Eclipse* fluorescence spectrophotometer equipped with a *Varian Cary-block* temperature controller using 1 cm x 1 cm quartz cuvettes. *Varian Eclipse* software was used to process the data. CD spectra were recorded on a *JASCO J-715* spectrophotometer using quartz cuvettes with an optic path of 1 cm.

5.6 References

- [1] D. J. Dsouza, E. T. Kool, *J.Biomol.Struct.Dynamics* **1992**, 10, 141-152.
- [2] A. A. Mundt, G. J. Crouch, B. E. Eaton, *Biochemistry* **1997**, 36, 13004-13009.
- [3] A. V. Maksimenko, E. M. Volkov, J. R. Bertrand, H. Porumb, C. Malvy, Z. A. Shabarova, M. B. Gottikh, *Eur.J.Biochem.* **2000**, 267, 3592-3603.
- [4] T M. Chin, C. M. Chang, H. W. Huang, L. L. Lo, *J.Biomol.Struct.Dynamics* **2004**, 22, 35-43.
- [5] M. Durand, K. Chevie, M. Chassignol, N. T. Thoug, J. C. Maurizot, *Nucl.Acids Res.* **1990**, 18(21), 6353-6359.
- [6] M. Salunkhe, T. Wu, R. L. Letsinger, *J.Am.Chem.Soc.* **1992**, 114, 8768-8772.
- [7] S. Bevers, T. P. O'Dea, L. W. McLaughlin, *J.Am.Chem.Soc.* **1998**, 120, 11004-11005.
- [8] I. Trkulja, R. Häner, *Bioconjugate Chem.* **2007**, 18, 289-292.
- [9] I. Trkulja, S. M. Biner, S. M. Langenegger, R. Häner, *ChemBioChem.* **2007**, 8, 25-27
- [10] F. D. Lewis, L. Zhang, R. F. Kelley, D. McCammant, M. R. Wasielewski, *Tetrahedron* **2007**, 63, 3457-3464.
- [11] N. Bouquin, V. L. Malinovskii, R. Häner, *Chem.Commun.* **2008**, 1974–1976.
- [12] H. Bittermann, D. Siegemund, V. L. Malinovskii, R. Häner, *J.Am.Chem.Soc.* **2008**, 130, 15285–15287.
- [13] R. Häner, S. M. Biner, S. M. Langenegger, T. Meng, V. L. Malinovskii, *Angew.Chem.Int.Ed.* **2010**, 49, 1227–1230.
- [14] S. M. Biner, D. Kummer, V. L. Malinovskii, R. Häner, *Org.Biomol.Chem.* **2011**, 9, 2628-2633.
- [15] D. B. Amabilino, J. F. Stoddart, *Chem.Rev.* **1995**, 95, 2725-2828.
- [16] K. M. Guckian, B. A. Schweitzer, R. X. F. Ren, C. J. Sheils, D. C. Tahmassebi, E. T. Kool, *J.Am.Chem.Soc.* **2000**, 122, 2213-2222.
- [17] C. A. Hunter, K. R. Lawson, J. Perkins, C. J. Urch, *J.Chem.Soc. Perkin Trans.2*, **2001**, 651-669.
- [18] J. J. Reczek, B. L. Iverson, *Macromolecules* **2006**, 39, 5601-5603.
- [19] A. L. Sisson, N. Sakai, N. Banerji, A. Furstenberg, E. Vauthey, S. Matile, *Angew.Chem.Int.Ed.* **2008**, 47, 3727-3729.

- [20] J. N. Wilson, C. Younjin, S. Tan, A. Cuppoletti, E. T. Kool, *ChemBioChem* **2008**, 9, 279-285.
- [21] Y. N. Teo, J. N. Wilson, E. T. Kool, *Chem.Eur.J.* **2009**, 15, 11551-11558.
- [22] H. Langhals, R. Ismael, *Eur.J.Org.Chem.* **1998**, 1915-1917.
- [23] F. Würthner, C. Thalacker, S. Diele, C. Tschierske, *Chem.Eur.J.* **2001**, 7, 2245-2253.
- [24] A. D. Q. Li, W. Wang, L. Q. Wang, *Chem.Eur.J.* **2003**, 9, 4594-4601.
- [25] W. Wang, L. S. Li, G. Helms, H. H. Zhou, A. D. Q. Li, *J.Am.Chem.Soc.* **2003**, 125, 1120-1121.
- [26] M. A. Abdalla, J. Bayer, J. O. Radler, K. Müllen, *Angew.Chem.Int.Ed.* **2004**, 43, 3967-3970.
- [27] Y. Zheng, H. Long, G. C. Schatz, F. D. Lewis, *Chem.Commun.* **2005**, 4795-4797.
- [28] T. E. Kaiser, V. Stepanenko, F. Würthner, *J.Am.Chem.Soc.* **2009**, 131, 6719-6732.
- [29] T. A. Zeidan, M. Hariharan, K. Siegmund, F. D. Lewis, *Photoch.Photobio.Sci.* **2010**, 9, 916-922.
- [30] G. Manzini, L. E. Xodo, D. Gasparoto, F. Quadrifoglio, G. A. van der Marel, J. H. van Boom, *J.Mol.Biol.* **1990**, 213, 833-843.
- [31] D. E. Callahan, T. L. Trapane, P. S. Miller, P. O. Tso, L. S. Kan, *Biochemistry* **1991**, 30, 1650-1655.
- [32] N. Berova, K. Nakanishi, R. W. Woody, *Circular Dichroism – Principles and Applications*, Wiley-VCH: New York, **2000**.

6. A Two-Color, Self-Controlled Molecular Beacon

Published in part: Sarah M. Biner and Robert Häner, *ChemBioChem*, **2011**, 12, 2733-2736.

6.1 Abstract

A two-color, self-controlled molecular beacon with non-nucleosidic chromophores in a triplex stem is presented in this chapter. Alkynylpyrene and PDI fluorophores act as mutual quenchers by formation of a donor-acceptor complex in the closed form. Hybridization with the target results in two independent fluorescence signals. The two-color read-out provides a 'self-control' feature, which helps to eliminate false positive signals in imaging and screening applications.

6.2 Introduction

The reliable detection of DNA and RNA sequences is of major interest for the design of future diagnostic tools. The use of hybridization probes, such as molecular beacons (MBs), to quantify or localize genes is widespread in the biological and medicinal sciences.^[1-4] The principle of the classical MB, first proposed by Tyagi and Kramer^[5;6] is based on a stem-loop structure containing terminally attached fluorophore and quencher moieties forming a FRET pair. The interplay of the two dyes is controlled by the secondary structure of the beacon and results in the diagnostic read-out.^[1-3;6-11] The quality of the signal depends on several factors including the sequence of the beacon, the choice of the dye molecules and the stability of the stem-loop structure. Any unwanted dissociation of the fluorophore-quencher pair will directly lead to a loss in *sensitivity* and *specificity* of the beacon. Therefore, the design of the stem is of particular importance for the success of a MB. Several different approaches addressing this issue have been proposed over the past years.^[12-28] In this chapter, a MB with two different fluorophores, 1,8-dialkynylpyrene (**Y**) and 3,4,9,10-perylenetetracarboxylic diimide (PDI,

E),^[25;26;29] arranged in a triple-helical stem is presented.^[30-34] In the closed form, the dyes are engaged in a donor-acceptor(-donor) [**Y-E(-Y)**] interaction^[35-44] resulting in a mutual quenching of the two fluorophores. Binding of the beacon to the target sequence disrupts the triple helix^[13] and generates a two-color fluorescent hybrid. The principle is illustrated representative with **MB11** in Figure 6.1.

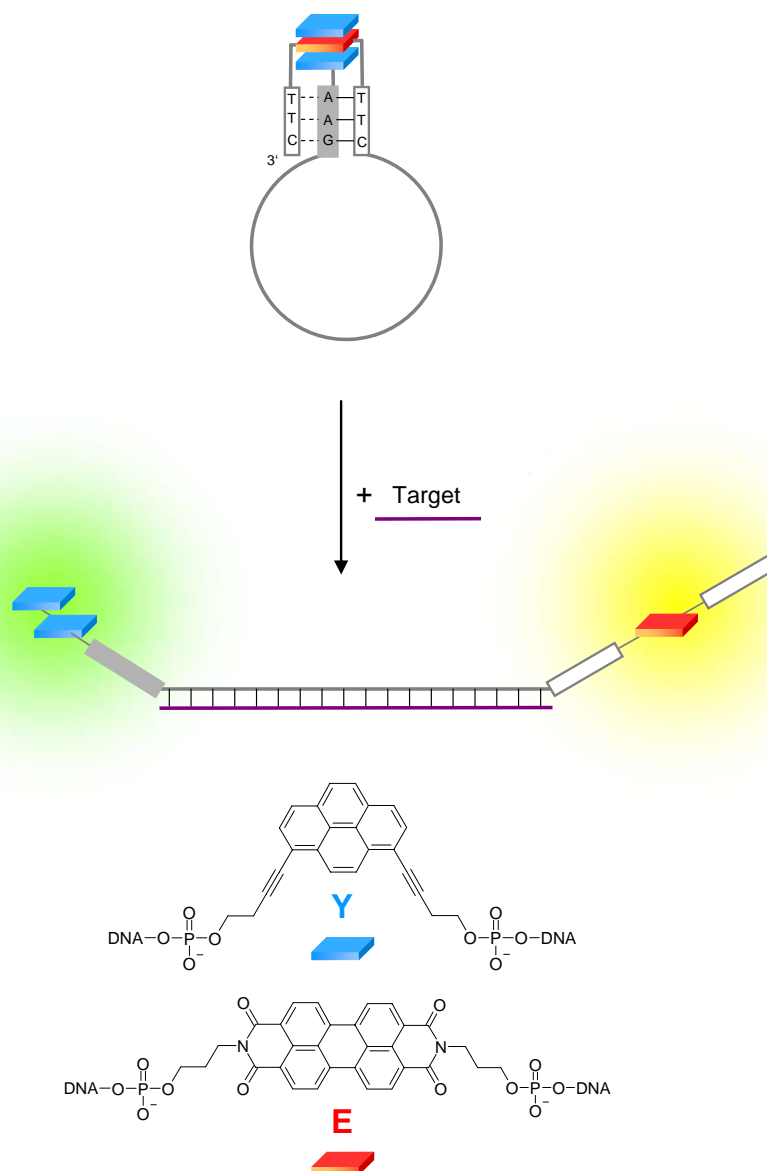


Figure 6.1. Illustration of a dual-labelled, self-controlled MB, here **MB11**. In the native form, a triple-helical stem supports the formation of a non-fluorescent pyrene-PDI-pyrene (**Y-E-Y**) stack. Disruption of the stem generates two fluorescence signals (pyrene excimer and PDI).

6.3 Investigation of a triple-helical stem design

The triple-helical stem design involves the formation of one C+GC and two TAT base triplets. In this setup, the PDI is embedded in a stretch of thymidines, whereas the alkynylpyrenes are attached to the 5'-end of the probe sequence (Table 6.1). **MB11** contains two alkynylpyrenes able to form an excimer, whereas beacon **MB12** poses a single alkynylpyrene and in consequence emits pyrene monomer emission (Figure 6.2).

Table 6.1. Investigated MB and target DNA sequences.

MB11	5' YY AAG CTA GAG GGG TCA GAG GAT CTT E TTC
MB12	5' Y AAG CTA GAG GGG TCA GAG GAT CTT E TTC
TD1	3' TTT GAT CTC CCC AGT CTC CTA TTT
TD3	3' TTT GAT CTC <u>ACC</u> AGT CTC CTA TTT
TD4	3' TTT GAT CTC CCC <u>ATT</u> CTC CTA TTT

The non-nucleosidic building blocks alkynylpyrene (**Y**) and PDI (**E**) are highlighted in bold and the mismatches are underlined.

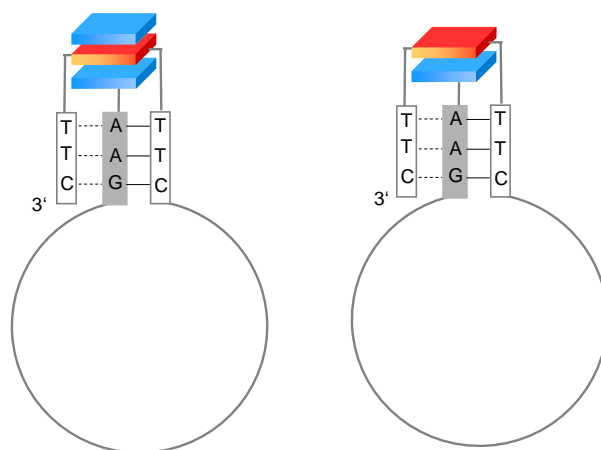


Figure 6.2. Schematic representation of **MB11** (left) and **MB12** (right) in the closed form. The triple-helical stem supports the formation of a non-fluorescent pyrene-PDI-pyrene (**Y-E-Y**) respectively a pyrene-PDI (**Y-E**) stack.

The stacking interaction between PDI and alkynylpyrenes in the closed form is demonstrated by UV/Vis spectroscopy (Figure 6.3). A clear blue-shift upon melting of the triple-helical

stem in the PDI region (440-600 nm) and hyperchromicity for PDI and for alkynylpyrene (320-420 nm) are observed.

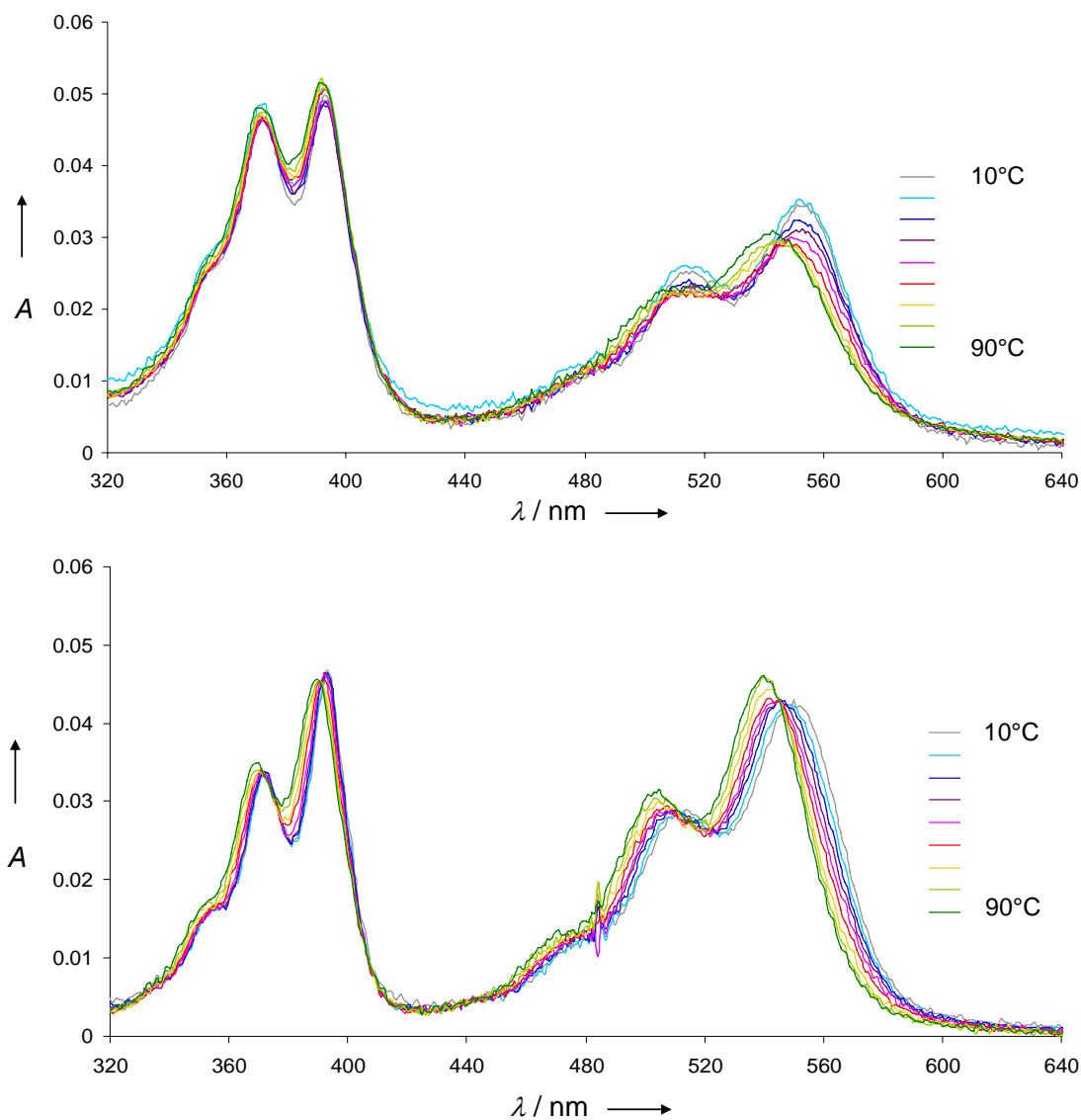


Figure 6.3. Temperature-dependent UV/Vis spectra of **MB11** (top) and **MB12** (bottom) from 10°C to 90°C in 10°C increments. Conditions: **MBn** 1.0 μM , 10 mM sodium acetate buffer pH 5.0, 100 mM NaCl, 20 mM MgCl_2 , equilibration time: 3 min.

The $A^{0 \rightarrow 0}/A^{0 \rightarrow 1}$ ratio for **MB11** shown in Figure 6.4, which serves as a measure for the aggregation state of PDI^[45-49] and alkynylpyrene,^[26;50] changed in accordance with the expectations. A decrease of the ratio indicates that the pyrene building blocks are aggregated.

This is the case when the third strand of the triplex stem (Hoogsteen-strand) is dissociated so that the PDI unit is not in close proximity anymore (as it is shown at approx. 40°C). The pyrene-pyrene interactions are not significantly disturbed.

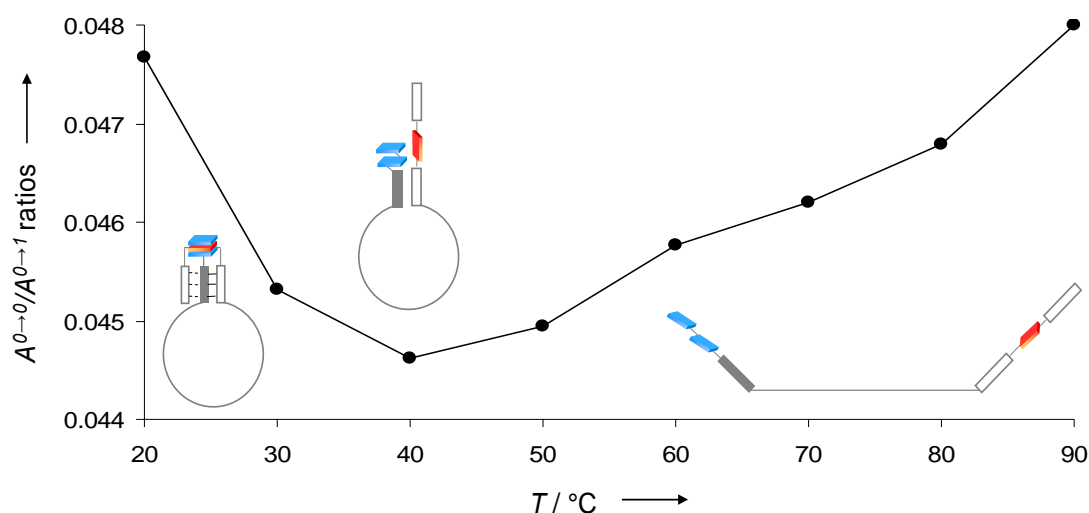


Figure 6.4. Absorption ratios of the 0→0 to the 0→1 transition at different temperatures. Conditions: **MB11** 1.0 μM, 1.2 eq. **TD1**, 10 mM sodium acetate buffer pH 5.0, 100 mM NaCl, 20 mM MgCl₂, equilibration time: 3 min.

The two fluorophores in **MB11** quench each other in the closed form of the MB. Separation of the dyes results in an increase in PDI and alkynylpyrene fluorescence. **Figure 6.5** shows the emission spectra resulting from hybridization of **MB11** with the target DNA **TD1**. The fluorophores exhibit fluorescence proportional to the target concentration. For the alkynylpyrenes (**Figure 6.5** top) both, monomer and excimer fluorescence are observed. The monomer part (380-460 nm) is comparatively large.^[26] This may be due to increased flexibility arising from the terminal location of the two alkynylpyrenes compared to a situation where the pyrene derivatives are located at internal positions.^[26] Nevertheless, the excimer signal (emission maximum 520 nm) grows proportionally with the concentration of the target. The same behaviour is observed for PDI (530-680 nm). Also for this fluorophore, the signal increases with the concentration of the target.

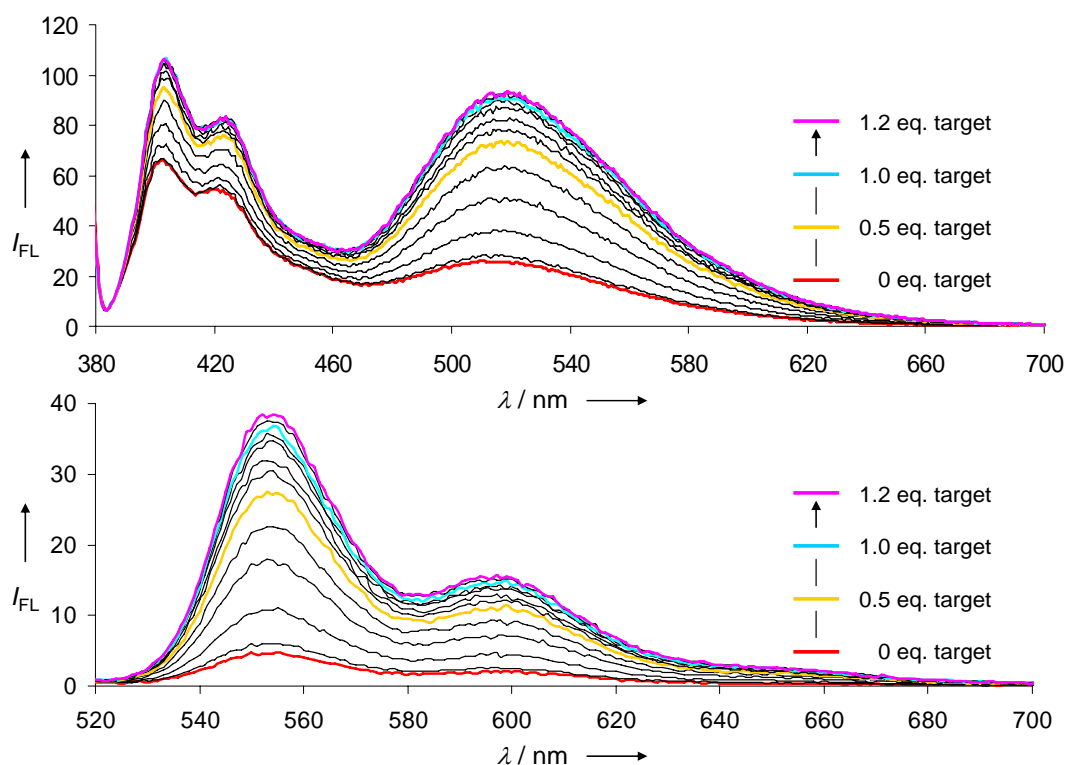


Figure 6.5. Fluorescence intensities obtained for **MB11** on hybridization with **TD1**. Conditions: **MB11** 1.0 μM , 0 to 1.2 eq. **TD1** in 0.1 increments, 10 mM sodium acetate buffer pH 5.0, 100 mM NaCl, 20 mM MgCl_2 , λ_{ex1} : 370 nm (top) and, λ_{ex2} : 505 nm (bottom), ex/em slit widths: 10/5 nm, PMT voltage: 600 V, Temp.: 15°C.

Compared to **MB11**, **MB12** shows no mutual quenching of the two fluorophores in the closed form of the beacon. The increase in alkynylpyrene monomer emission is proportional to the target concentration (Figure 6.6 top). This is a similar behaviour as observed with **MB11** except for the signal intensities. However, the PDI monomer emission seems not to be quenched at all by a single alkynylpyrene unit (Figure 6.6 bottom). In this case, quenching requires the presence of two alkynylpyrenes to ensure a mutual control of signal generation.

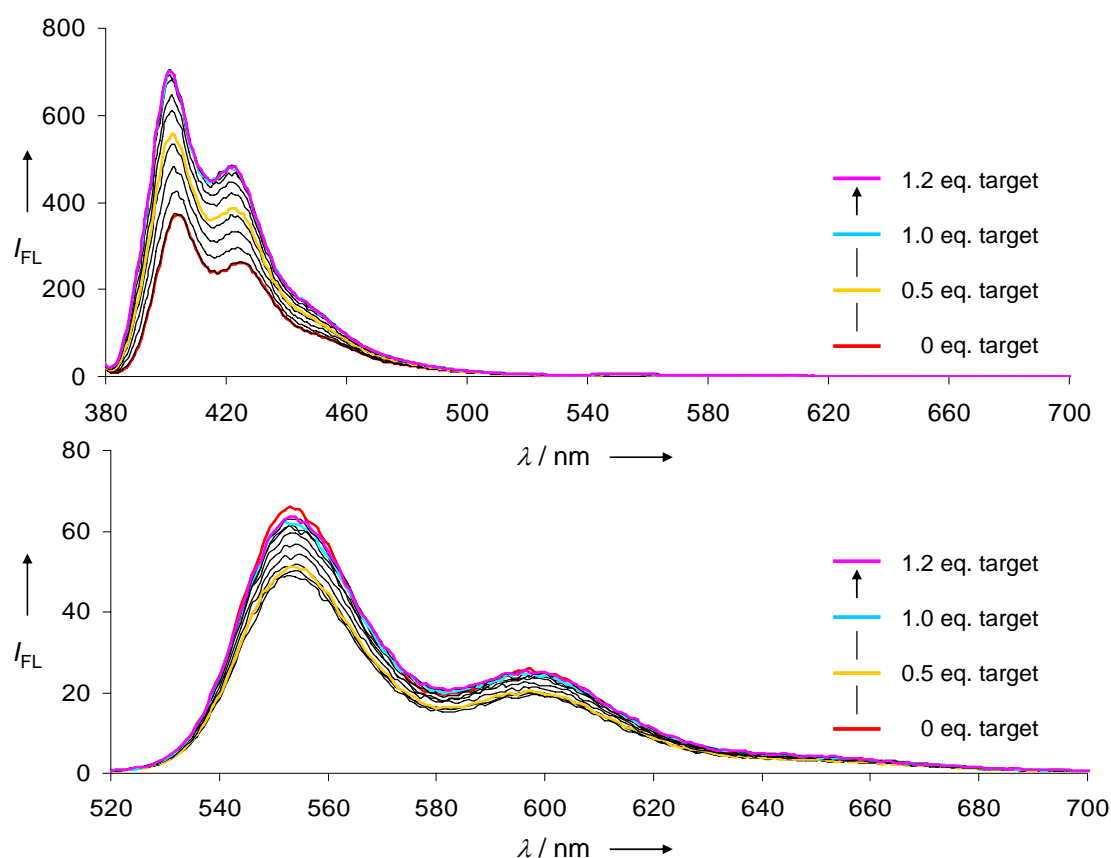


Figure 6.6. Fluorescence intensities obtained for **MB12** on hybridization with **TD1**. Conditions: **MB12** 1.0 μM , 0 to 1.2 eq. **TD1** in 0.1 increments, 10 mM sodium acetate buffer pH 5.0, 100 mM NaCl, 20 mM MgCl_2 , λ_{ex1} : 370 nm (top), λ_{ex2} : 505 nm (bottom), ex/em slit widths: 10/5 nm, PMT voltage: 600 V, Temp.: 15°C.

The quenching behaviour of the single alkynylpyrene containing probe **MB12** is not sufficient and won't be further discussed in detail, as it is performed for **MB11**.

For **MB11**, in the presence of 1.2 equivalents of fully matched target DNA **TD1**, a quantum yield (Φ) of approx. 0.028 is obtained (see Experimental part). This is in strong contrast to mixed sequences, in which context PDI is usually entirely quenched.^[29] In the current design of the triple-helical stem, the PDI is placed in between several thymidines,^[51] which has a similar effect as unnatural insulators.^[52] The simultaneous, hybridization-based appearance of two independent fluorescence signals (alkynylpyrene and PDI) provides an efficient way of

eliminating false positive signals. Thus, the two labels act not only as mutual suppressors in the closed form but also as internal references for each other in the presence of the target.

Thermal denaturation of the beacon shows the expected increase of both signal intensities upon heating (Figure 6.7). Melting of the triple-helical structure leads to the deaggregation of the chromophore stack, resulting in a parallel growth of the alkynylpyrene excimer and PDI signals.

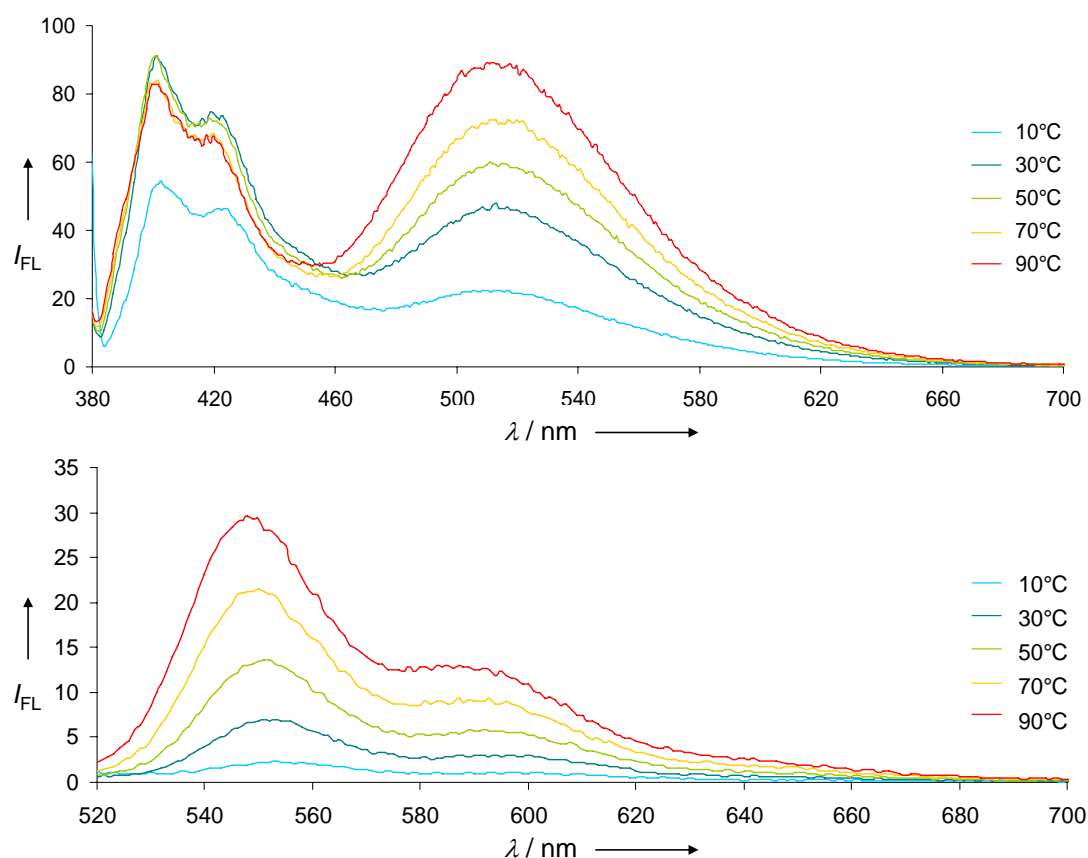


Figure 6.7. Temperature-dependent fluorescence read-out of **MB11**. Conditions: **MB11** 1.0 μM , 10 mM sodium acetate buffer pH 5.0, 100 mM NaCl, 20 Mm MgCl_2 , λ_{ex1} : 370 nm (top) λ_{ex1} : 505 nm (bottom), ex/em slit widths: 10/5 nm, PMT voltage: 600 V, equilibration time: 3 min.

This system represents a self-controlled chromophoric system of two fluorescent labels that function as mutual quenchers. The quenching efficiencies are 64% (pyrene excimer) and 84%

(PDI). **Figure 6.8** shows the target-response curves of beacon **MB11** for the two chromophores. Both signals increase with target concentration and reach a maximum at 1.0 equivalent target concentration.

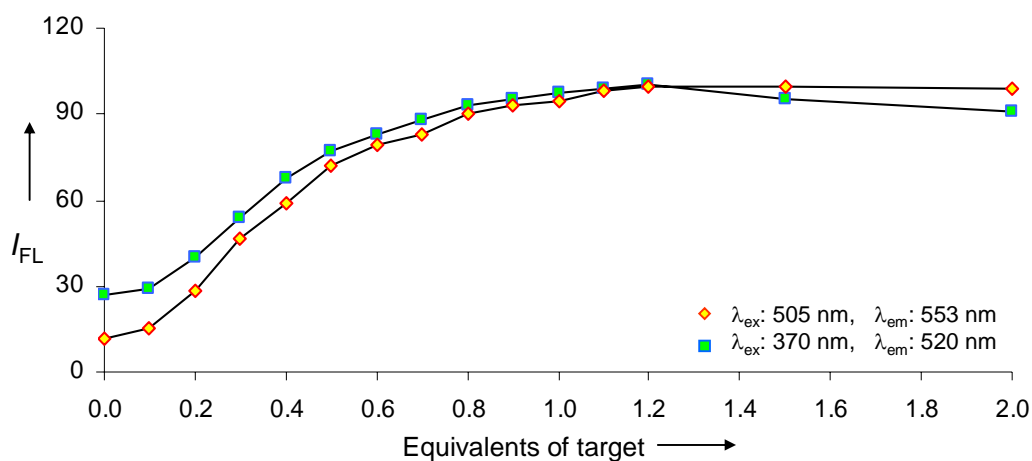


Figure 6.8. Concentration-dependent normalized signal intensities at 520 nm and 553 nm as illustrated in the graph. Conditions: **MB11** 1.0 μ M, 10 mM sodium acetate buffer pH 5.0, 100 mM NaCl, 20 mM $MgCl_2$, ex/em slit widths: 10/5 nm, PMT voltage: 600 V, Temp.: 15°C.

Hybridization kinetics of MBs is an important aspect which has been discussed in the literature.^[53] Triple helix formation^[54] is considerably slower than duplex formation. In order to ensure fast hybridization of the probe to the target, the triple-helical stem was kept as short as possible, that is, three base triplets. As shown in **Figure 6.9**, the signal response is very fast. The signal intensity of both labels reaches 80-90% (PDI: 81%; alkynylpyrene: 86%) of the maximum read-out immediately (<1min) after addition of the fully matched target **TD1** to **MB11** at 20°C.

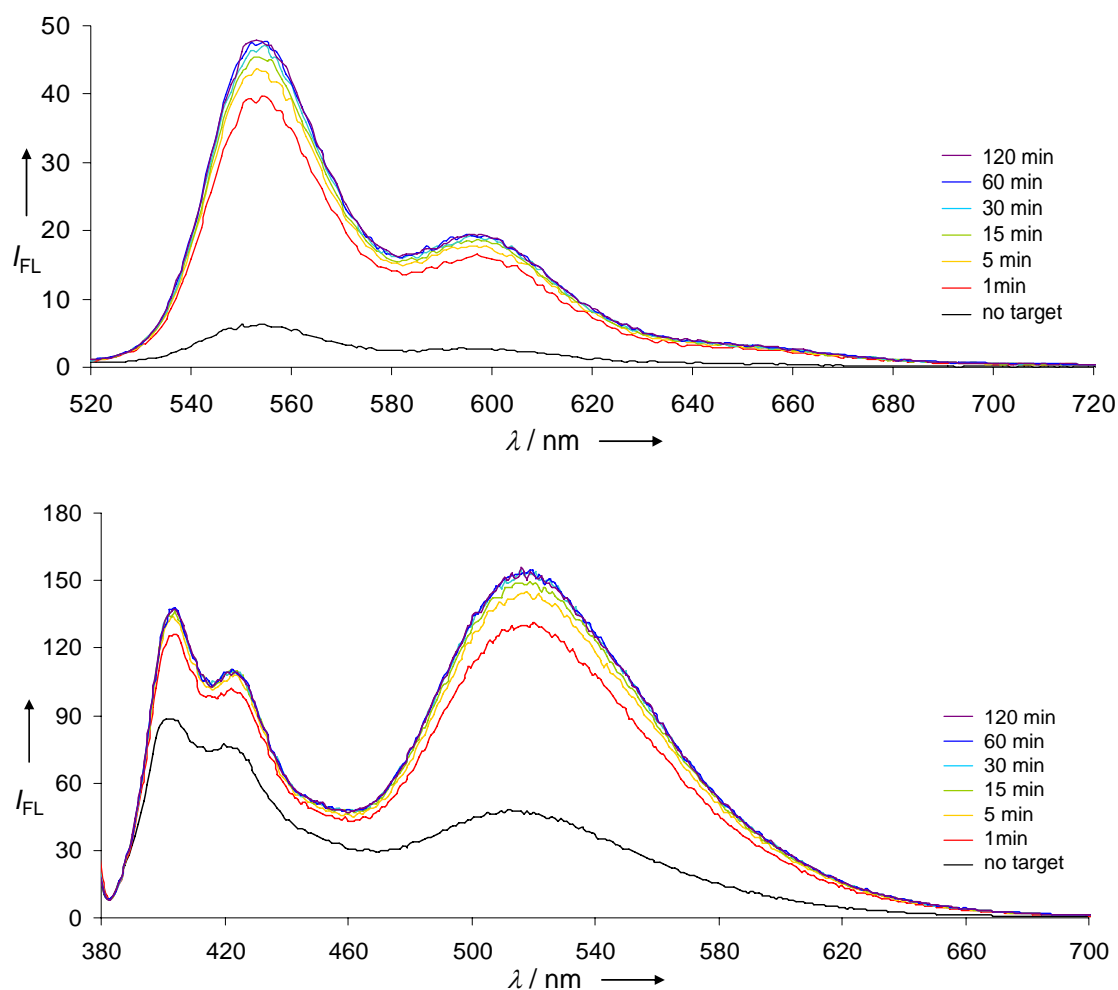


Figure 6.9. Time-dependent fluorescence read-out obtained for **MB11** on hybridization with 1.2 eq. **TD1**. Conditions: **MB11** 1.0 μM , **TD1** 1.2 μM , 10 mM sodium acetate buffer pH 5.0, 100 mM NaCl, 20 mM MgCl_2 , λ_{ex1} : 505 nm (top) and λ_{ex2} : 370 nm (bottom), ex/em slit widths: 10/5 nm, PMT voltage: 600 V, Temp.: 20°C.

The selectivity of the MB was studied by temperature-variable fluorescence measurements in presence of different targets (**Figure 6.10**). The hybrids containing mismatched targets (**TD3** and **TD4**) show a loss in fluorescence intensity at lower temperature than with the completely matched target sequence (**TD1**).

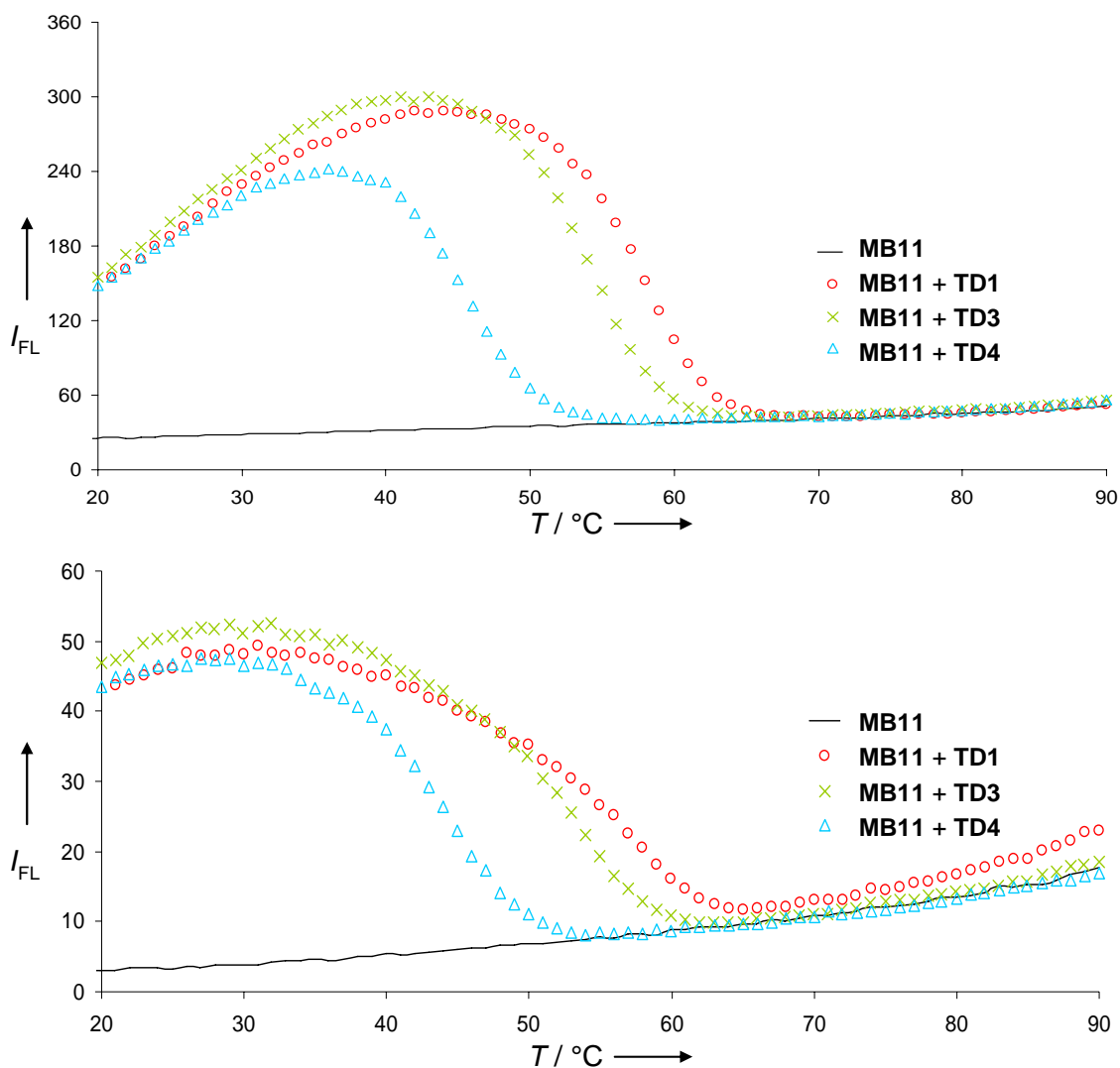


Figure 6.10. Alkynylpyrene excimer emission (top) and PDI fluorescence read-out (bottom) in presence of matched (**TD1**) and mismatched (**TD3**, **TD4**) targets. Conditions: **MB11** 1.0 μM , **TDn** 1.0 μM , 10 mM sodium acetate buffer pH 5.0, 100 mM NaCl, 20 mM MgCl_2 , $\lambda_{\text{ex}1}$: 370 nm (pyrene), $\lambda_{\text{em}1}$: 520 nm (top), $\lambda_{\text{ex}2}$: 505 nm (PDI), $\lambda_{\text{em}2}$: 552 nm (bottom), ex/em slit widths: 10/5 nm, PMT voltage: 600 V, performance of three ramps (90-10°C / 10-90°C / 90-10°C), heating/cooling rate: 0.5°C/min, only heating ramps are shown.

6.4 Conclusion

A MB with a two-color read-out signal has been described. A successful signal control involves a triple-helical stem design with two alkynylpyrenes and one PDI unit. Single incorporation of alkynylpyrene and PDI building blocks lead to insufficient quenching behaviour. In the closed form of **MB11** (Figure 6.11), 1,8-dialkynylpyrene and PDI are arranged in a π -stacked complex and the two chromophores act as mutual fluorescence quenchers. Hybridization of the probe to a target sequence disrupts the chromophore complex resulting in two independent fluorescence signals. The combination of two detectable individual signals and their mutual quenching properties introduces a ‘self-control’ feature which might help to eliminate false positive signals in imaging and screening applications.

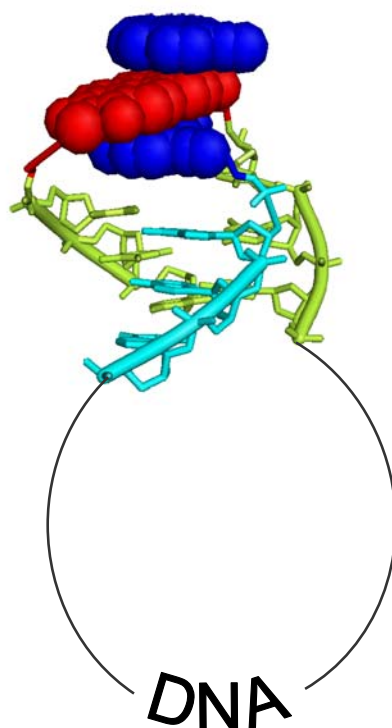


Figure 6.11. Model of **MB11** in the closed form with donor-acceptor complexes in a triple-helical stem design. The chromophores are highlighted in red (PDI) and blue (alkynylpyrene).

6.5 Experimental Part

Oligonucleotide synthesis. The required alkynylpyrene^[50] and PDI^[29] building blocks were synthesized according to published procedures. Commercial natural nucleoside phosphoramidites were used for oligonucleotide synthesis. Oligonucleotides **TD1**, **TD3** and **TD4** were purchased from *Microsynth*, Balgach, Switzerland. **MB11** and **MB12** were prepared *via* automated oligonucleotide synthesis by a standard synthetic procedure (2 min coupling time; ‘trityl-off’ mode) on a 394-DNA/RNA synthesizer (*Applied Biosystems*), except for the coupling step of the PDI phosphoramidite, an adapted activating step was proceeded. Cleavage from the solid support and final deprotection was done by treatment with 30% NH₄OH solution at 55°C overnight.

Oligonucleotide purification and mass determination. Purification was done by reverse phase HPLC (LiChrospher 100 *RP-18*, 5µm, Merck; *Kontron Instruments* device); eluent A = (Et₃NH)OAc (0.1 M, pH 7.4); eluent B = MeCN; elution at 40°C; gradient 5 – 50% B over 30 min. Mass spectrometry was performed with a Sciex Qtrap, (*Applied Biosystems*); *ESI-MS*, Electrospray Low Resolution, negative mode, acetonitrile/H₂O (1:1) + 1% m triethylamine) (Table 6.3).

Table 6.3. Specification of oligonucleotide **MB11** and **MB12**.

	<i>Molecular formula</i>	<i>HPLC t_R [min]</i>	<i>calcd. avg. mass</i>	<i>found avg. mass</i>
MB11	C ₃₄₄ H ₃₈₇ N ₁₀₈ O ₁₇₆ P ₂₉	23.2	9748.6	9748.7
MB12	C ₃₂₀ H ₃₇₀ N ₁₀₈ O ₁₇₂ P ₂₈	18.9	9348.3	9495.4

Oligonucleotide analysis. Temperature dependent UV/Vis spectra were carried out on a *Varian Cary-100 Bio-UV/Vis* spectrophotometer equipped with a *Varian Cary-block* temperature controller and data were collected with *Varian WinUV* software. Fluorescence spectra were recorded on a *Varian Cary Eclipse* fluorescence spectrophotometer equipped with a *Varian Cary-block* temperature controller using 1 cm x 1 cm quartz cuvettes. *Varian Eclipse* software was used to process the data.

Determination of signal-to-background ratio and quenching efficiency. Signal-to-background (S/B) ratio and quenching efficiency (Q%) values were determined according to the following formulas (Table 6.4):

$$S/B = (F_{\text{hybrid}}) / (F_{\text{MB}})$$

$$Q\% = 100 \times \{1 - ((F_{\text{MB}}) / (F_{\text{hybrid}}))\}$$

Values obtained for **MB11** in the presence of 1.2 eq. of target DNA **TD1**:

Table 6.4. S/B ratios and Q% values of **MB11** and **MB12**.

	Alkynylpyrene	PDI
S/B ratio	2.82	6.42
Q%	64.6	84.4

Quantum yield determination. The quantum yield Φ was determined by a comparative method as described previously in a publication by Häner and co-workers,^[56] employing rhodamine 6G in ethanol (Φ : 0.94) as fluorescence standard for the PDI building block. Suitable **MB11** and **TD1** concentrations were chosen to ensure absorbance in the range of 0.1. Fluorescence measurements were performed with two excitation wavelengths for statistical reasons (λ_{ex1} : 523 nm, λ_{ex2} : 505 nm) (Table 6.5).

$$\Phi = \{(Area_{\text{comp}} \times Abs_{\text{ref}}) / (Abs_{\text{comp}} \times Area_{\text{ref}})\} \times \Phi_{\text{ref}}$$

Table 6.5. Quantum yield determination.

	λ_{ex1}	λ_{ex2}
Φ	0.026	0.029

6.6 References

- [1] R. T. Ranasinghe, T. Brown, *Chem. Commun.* **2005**, 5487-5502.
- [2] P. Santangelo, N. Nitin, G. Bao, *Ann. Biomed. Eng.* **2006**, 34, 39-50.
- [3] K. M. Wang, Z. W. Tang, C. Y. J. Yang, Y. M. Kim, X. H. Fang, W. Li, Y. R. Wu, C. D. Medley, Z. H. Cao, J. Li, P. Colon, H. Lin, W. H. Tan, *Angew. Chem. Int. Ed.* **2009**, 48, 856-870.
- [4] B. Juskowiak, *Anal. Bioanal. Chem.* **2011**, 399, 3157-3176.
- [5] S. Tyagi, D. P. Bratu, F. R. Kramer, *Nat. Biotechnol.* **1998**, 16, 49-53.
- [6] S. Tyagi, F. R. Kramer, *Nat. Biotechnol.* **1996**, 14, 303-308.
- [7] A. P. Silverman, E. T. Kool, *Trends Biotechnol.* **2005**, 23, 225-230.
- [8] S. A. E. Marras, S. Tyagi, F. R. Kramer, *Clin. Chim. Acta* **2006**, 363, 48-60.
- [9] N. Venkatesan, Y. J. Seo, B. H. Kim, *Chem. Soc. Rev.* **2008**, 37, 648-663.
- [10] W. H. Tan, K. M. Wang, T. J. Drake, *Curr. Opin. Chem. Biol.* **2004**, 8, 547-553.
- [11] Y. V. Gerasimova, A. Hayson, J. Ballantyne, D. M. Kolpashchikov, *ChemBioChem* **2010**, 11, 1762-1768.
- [12] O. Seitz, *Angew. Chem. Int. Ed.* **2000**, 39, 3249-3252.
- [13] T. N. Grossmann, L. Roglin, O. Seitz, *Angew. Chem. Int. Ed.* **2007**, 46, 5223-5225.
- [14] E. Socher, L. Bethge, A. Knoll, N. Jungnick, A. Herrmann, O. Seitz, *Angew. Chem. Int. Ed.* **2008**, 47, 9555-9559.
- [15] H. Kuhn, V. V. Demidov, J. M. Coull, M. J. Fiandaca, B. D. Gildea, M. D. Frank-Kamenetskii, *J. Am. Chem. Soc.* **2002**, 124, 1097-1103.
- [16] K. R. Fox, T. Brown, *Quart. Rev. Biophys.* **2005**, 38, 311-320.
- [17] L. Wang, C. Y. J. Yang, C. D. Medley, S. A. Benner, W. H. Tan, *J. Am. Chem. Soc.* **2005**, 127, 15664-15665.
- [18] C. Crey-Desbiolles, D. R. Ahn, C. J. Leumann, *Nucl. Acids Res.* **2005**, 33, e77.
- [19] Y. W. Lin, H. T. Ho, C. C. Huang, H. T. Chang, *Nucl. Acids Res.* **2008**, 36.
- [20] Y. Saito, Y. Shinohara, S. S. Bag, Y. Takeuchi, K. Matsumoto, I. Saito, *Tetrahedron* **2009**, 65, 934-939.
- [21] Y. Ueno, A. Kawamura, K. Takasu, S. Komatsuzaki, T. Kato, S. Kuboe, Y. Kitamura, Y. Kitade, *Org. Biomol. Chem.* **2009**, 7, 2761-2769.

- [22] Y. Xiao, K. J. I. Plakos, X. H. Lou, R. J. White, J. R. Qian, K. W. Plaxco, H. T. Soh, *Angew.Chem.Int.Ed.* **2009**, 48, 4354-4358.
- [23] H. Kashida, T. Takatsu, T. Fujii, K. Sekiguchi, X. G. Liang, K. Niwa, T. Takase, Y. Yoshida, H. Asanuma, *Angew.Chem.Int.Ed.* **2009**, 48, 7044-7047.
- [24] I. Trkulja, S. M. Biner, S. M. Langenegger, R. Häner, *ChemBioChem* **2007**, 8, 25-27.
- [25] R. Häner, S. M. Biner, S. M. Langenegger, T. Meng, V. L. Malinovskii, *Angew.Chem.Int.Ed.* **2010**, 49, 1227-1230.
- [26] S. M. Biner, D. Kummer, V. L. Malinovskii, R. Häner, *Org.Biomol.Chem.* **2011**, 9, 2628-2633.
- [27] C. Holzhauser, H. A. Wagenknecht, *Angew.Chem.Int.Ed.* **2011**, 50, 7268-7272.
- [28] J. Ren, H. Qin, J. Wang, N. Luedtke, E. Wang, J. Wang, *Anal.Bioanal.Chem.* **2011**, 399, 2763-2770.
- [29] N. Bouquin, V. L. Malinovskii, R. Häner, *Chem.Commun.* **2008**, 1974-1976.
- [30] G. Felsenfeld, D. R. Davies, A. Rich, *J.Am.Chem.Soc.* **1957**, 79, 2023-2024.
- [31] I. Trkulja, R. Häner, *Bioconjug.Chem.* **2007**, 18, 289-292.
- [32] I. Trkulja, R. Häner, *J.Am.Chem.Soc.* **2007**, 129, 7982-7989.
- [33] N. T. Thuong, C. Hélène, *Angew.Chem.Int.Ed.Engl.* **1993**, 32, 666-690.
- [34] H. E. Moser, P. B. Dervan, *Science* **1987**, 238, 645-650.
- [35] C. A. Hunter, J. K. M. Sanders, *J.Am.Chem.Soc.* **1990**, 112, 5525-5534.
- [36] R. S. Lokey, B. L. Iverson, *Nature* **1995**, 375, 303-305.
- [37] G. Mathis, J. Hunziker, *Angew.Chem.Int.Ed.Engl.* **2002**, 41, 3203-3205.
- [38] S. Bhosale, A. L. Sisson, P. Talukdar, A. Furstenberg, N. Banerji, E. Vauthey, G. Bollot, J. Mareda, C. Roger, F. Würthner, N. Sakai, S. Matile, *Science* **2006**, 313, 84-86.
- [39] J. J. Reczek, B. L. Iverson, *Macromolecules* **2006**, 39, 5601-5603.
- [40] E. A. Meyer, R. K. Castellano, F. Diederich, *Angew.Chem.Int.Ed.* **2003**, 42, 1210-1250.
- [41] W. Y. Zhang, W. R. Dichtel, A. Z. Stieg, D. Benitez, J. K. Gimzewski, J. R. Heath, J. F. Stoddart, *Proc.Nat.Acad.Sci.(USA)* **2008**, 105, 6514-6519.
- [42] Z. Merican, K. D. Johnstone, M. J. Gunter, *Org.Biomol.Chem.* **2008**, 6, 2534-2543.
- [43] J. K. Klosterman, Y. Yamauchi, M. Fujita, *Chem.Soc.Rev.* **2009**, 38, 1714-1725.

- [44] S. Shirai, S. Iwata, T. Tani, S. Inagaki, *J.Phys.Chem.A* **2011**, 115, 7687-7699.
- [45] H. Langhals, *Helv.Chim.Acta* **2005**, 88, 1309-1343.
- [46] F. Würthner, *Chem.Commun.* **2004**, 1564-1579.
- [47] A. D. Q. Li, W. Wang, L. Q. Wang, *Chem.Eur.J.* **2003**, 9, 4594-4601.
- [48] Y. Zheng, H. Long, G. C. Schatz, F. D. Lewis, *Chem.Commun.* **2005**, 4795-4797.
- [49] M. A. Abdalla, J. Bayer, J. O. Radler, K. Müllen, *Angew.Chem.Int.Ed.* **2004**, 43, 3967-3970.
- [50] H. Bittermann, D. Siegemund, V. L. Malinovskii, R. Häner, *J.Am.Chem.Soc.* **2008**, 130, 15285-15287.
- [51] Y. Paukku, G. Hill, *J.Phys.Chem.A* **2011**, 115, 4804-4810.
- [52] a) J. N. Wilson, Y. J. Cho, S. Tan, A. Cuppoletti, E. T. Kool, *ChemBioChem* **2008**, 9, 279-285. b) H. Kashida, K. Sekiguchi, H. Asanuma, *Chem.Eur.J.* **2010**, 16, 11554-11557.
- [53] A. Tsourkas, M. A. Behlke, S. D. Rose, G. Bao, *Nucl.Acids Res.* **2003**, 31, 1319-1330.
- [54] V. N. Soyfer, V. N. Potaman, *Triple-Helical Nucleic Acids*, Springer, New York **1996**.
- [55] N. Rahe, C. Rinn, T. Carell, *Chem.Commun.* **2003**, 2119-2121.
- [56] S. Werder, V. L. Malinovskii, R. Häner, *Org.Lett.* **2008**, 10, 2011-2014.

7. Triplex-Mediated Molecular Assembly of Polyaromatic Base Surrogates

7.1 Abstract

Intramolecular triple helical structures containing polyaromatic base surrogates were studied. The formation of an intramolecular DNA triple helix was “visualized” by alkynylpyrene emission (monomer – excimer). Vice versa the signal is controlled by the structure of the oligonucleotide. This study shows the use of chromophores to follow the formation of intramolecular triple helices and the possible use of a triplex as a mould to investigate chromophoric interactions. The triple-helical structures were investigated by fluorescence spectroscopy, UV/Vis absorbance and circular dichroism (CD) measurements.

7.2 Introduction

The discovery of the double-helical structure of DNA in 1953 by Watson and Crick was a milestone. The fact that DNA forms a double-helical structure is nowadays used in different research fields such as molecular biology, physics (nano-materials) and chemistry.^[1-9] The zipper-like duplex formation allows applications of DNA sequences in many fields, so DNA can act as a frame for modified bases or completely non-nucleosidic building blocks.^[10-17] The arrangement and the influence of these base surrogates on the natural pair can be investigated. Not only the stability can be influenced, but also spectroscopic changes can be observed. In our research group different polyaromatic base surrogates like pyrene, phenanthrene, phenanthroline, fluorene and perylene diimide derivatives and other building blocks were successfully incorporated and studied.^[18-34] After the discovery of three-stranded DNA structures new interesting studies were initiated.^[35-37] Notably, triple-helical structures were investigated with regard on their occurrence and potential biological significance such as triple helix target sites (TTS) that are present in certain promoter regions in the human genome.^[38-41] Triplex-forming oligonucleotides are able to form triple-helical structures upon

binding to TTS sequences and represent an interesting sequence-specific tool for different applications. Further studies introduce the existence of H-DNA.^[37] Intramolecular triple helices suggested to be possibly involved in DNA replication, transcription and recombination. The aim of this study was to investigate the formation of an intramolecular triple helix and in return the aggregation of polyaromatic units inside a triple-helical arrangement could be studied. Therefore non-nucleosidic base surrogates (1,8-dialkynylpyrene and 3,4,9,10-perylenetetracarboxylic diimide) were introduced into an oligonucleotide sequence (Figure 7.1).

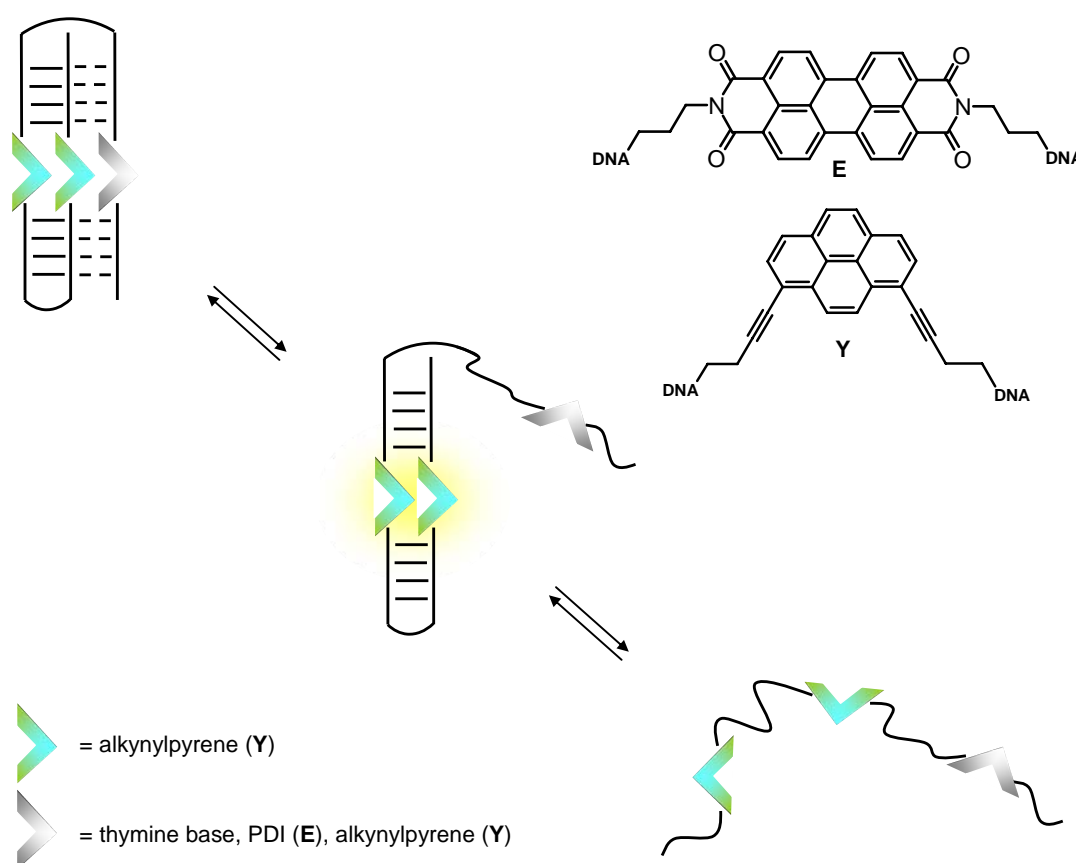


Figure 7.1. Schematic representation of an intramolecular triple helix upon structural dissociation and the structures of the polyaromatic building blocks alkynylpyrene (Y) and perylenediimide (PDI, E).

The selected alkynylpyrene building block offers the possibility to follow a dimerization or separation by fluorescence spectroscopy due to specific emission, either excimer or monomer emission.^[26;28;30;34] To ensure a clear differentiation between monomer and excimer by fluorescence emission measurements a quencher unit has to be introduced in addition to the fluorophores. The modified oligonucleotides used for this study are listed in [Table 7.1](#) and illustrated in [Figure 7.2](#). In oligomer **I1** the quenching ability of a thymine base was studied^[42-46] and in comparison oligomer **I2** was synthesized with a perylenediimide (PDI) unit as quencher.^[25;47] The intramolecular structure was further used to study the molecular arrangement of a monochromophoric complex based on three polyaromatic building blocks such as alkynylpyrenes (oligomer **I3**) or PDI units (oligomer **I4**).

Table 7.1. Sequences of the investigated intramolecular triplex forming oligomers **I1** to **I4**.

I1	5'	AGA	G YA	AGA	TTT	TTC	T TY	CTC	TTT	TTT	TTC	T CT	TTC	T
I2	5'	AGA	G YA	AGA	TTT	TTC	T TY	CTC	TTT	TTT	TTC	T CE	TTC	T
I3	5'	AGA	G YA	AGA	TTT	TTC	T TY	CTC	TTT	TTT	TTC	T CY	TTC	T
I4	5'	AGA	G EA	AGA	TTT	TTC	T TE	CTC	TTT	TTT	TTC	T CE	TTC	T

The polyaromatic chromophores alkynylpyrene (**Y**) and PDI (**E**) are highlighted in bold.

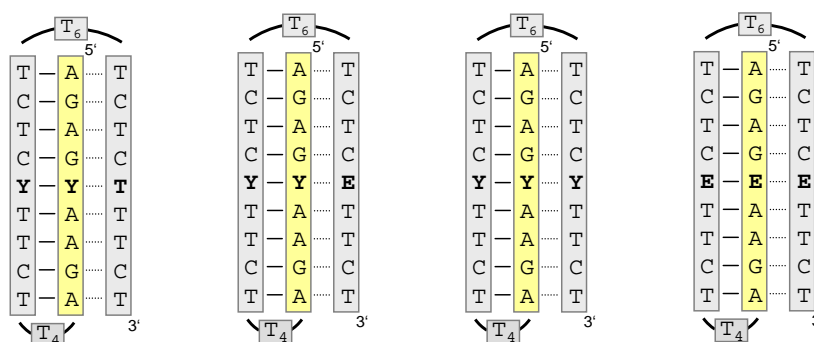


Figure 7.2. Illustration of the intramolecular triple helices and the investigated oligonucleotide sequences with alkynylpyrene building blocks (**Y**) and perylenediimide units (**E**). The Watson-Crick base pairs are represented by – and the Hoogsteen bonds are illustrated with ---.

7.3 Investigation of the chromophoric arrangement by spectroscopic measurements

The intramolecular triple helices were first analyzed by temperature-dependent UV/Vis measurements to study the effect of the Hoogsteen base in the triad (*YYT*, *YYE*, *YYY*, *EEE*). The introduction of non-nucleosidic building blocks in the “centre” of the structure constrains the characteristic smooth transitions observable in thermal denaturation experiments recorded at 260 nm (Figure 7.3). The interaction between the aromatic units hinders a smooth triplex-hairpin and hairpin-random coil transition.

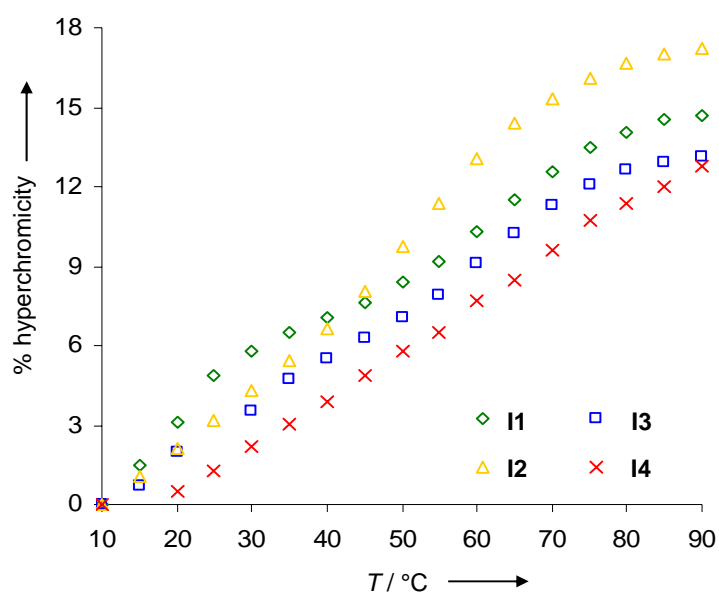


Figure 7.3. Temperature-dependent absorbance measurements of oligomer **I1** (green), **I2** (orange), **I3** (blue) and **I4** (red). Conditions: 1.0 μM single strand concentration, 10 mM sodium cacodylate buffer, pH 7.0, 100 mM NaCl, 20 mM MgCl_2 , equilibration time: 3 min, absorbance was recorded at 260 nm.

The structural transitions can be followed by the characteristic changes in the ratios of the $A^{0\rightarrow0}/A^{0\rightarrow1}$ transitions of the alkynylpyrene building blocks as it is shown for oligomer **I1** in Figure 7.4.^[26;28;30;32;34;48-51]

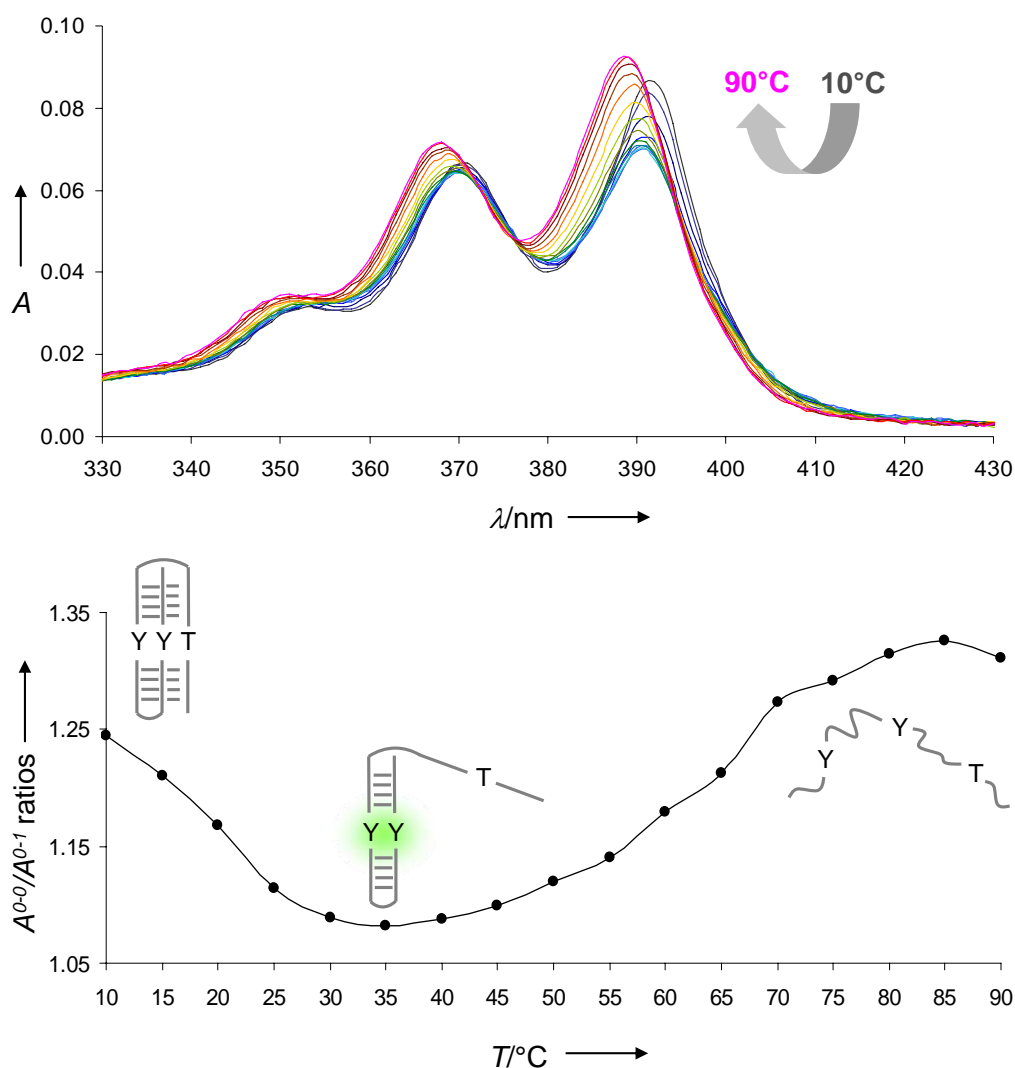


Figure 7.4. Temperature-dependent UV/Vis measurements (330-430 nm) of oligomer **II** (top) and absorption ratios of the 0 \rightarrow 0 to the 0 \rightarrow 1 transitions of the alkynylpyrene building block (bottom). Conditions: 1.0 μ M single strand concentration, 10 mM sodium cacodylate buffer, pH 7.0, 100 mM NaCl, 20 mM MgCl₂, equilibration time: 3 min.

The $A^{0\rightarrow 0}/A^{0\rightarrow 1}$ ratio gives information about the aggregation state of the alkynylpyrene building blocks.^[48-51] Figure 7.4 shows the temperature-dependent aggregation mode of the alkynylpyrene units based on its vibronic band ratios. A decrease of the ratio indicates that the alkynylpyrene building blocks are aggregated (dimer-like structure). This is the case when the third strand of the triplex (Hoogsteen-strand) is dissociated so that the thymine base is not anymore in close proximity (as it is shown at approx. 35°C) and the pyrene-pyrene interaction

is not significantly disturbed. These observations can not be done with oligomer **I2**, where the thymine base is replaced by a PDI unit. (Figure 7.5) There the data indicate certain ground state electronic interactions between the alkynylpyrene units and the PDI building block. The introduction of a third polyaromatic unit offers the possibility of additional π -stacking interactions and influences the coupling between the alkynylpyrene units. Oligomer **I3** with three alkynylpyrene building blocks possesses more monomer-like absorbance spectra. This could be due to an overlapping of partially dimerized alkynylpyrenes and mainly disaggregated alkynylpyrenes.

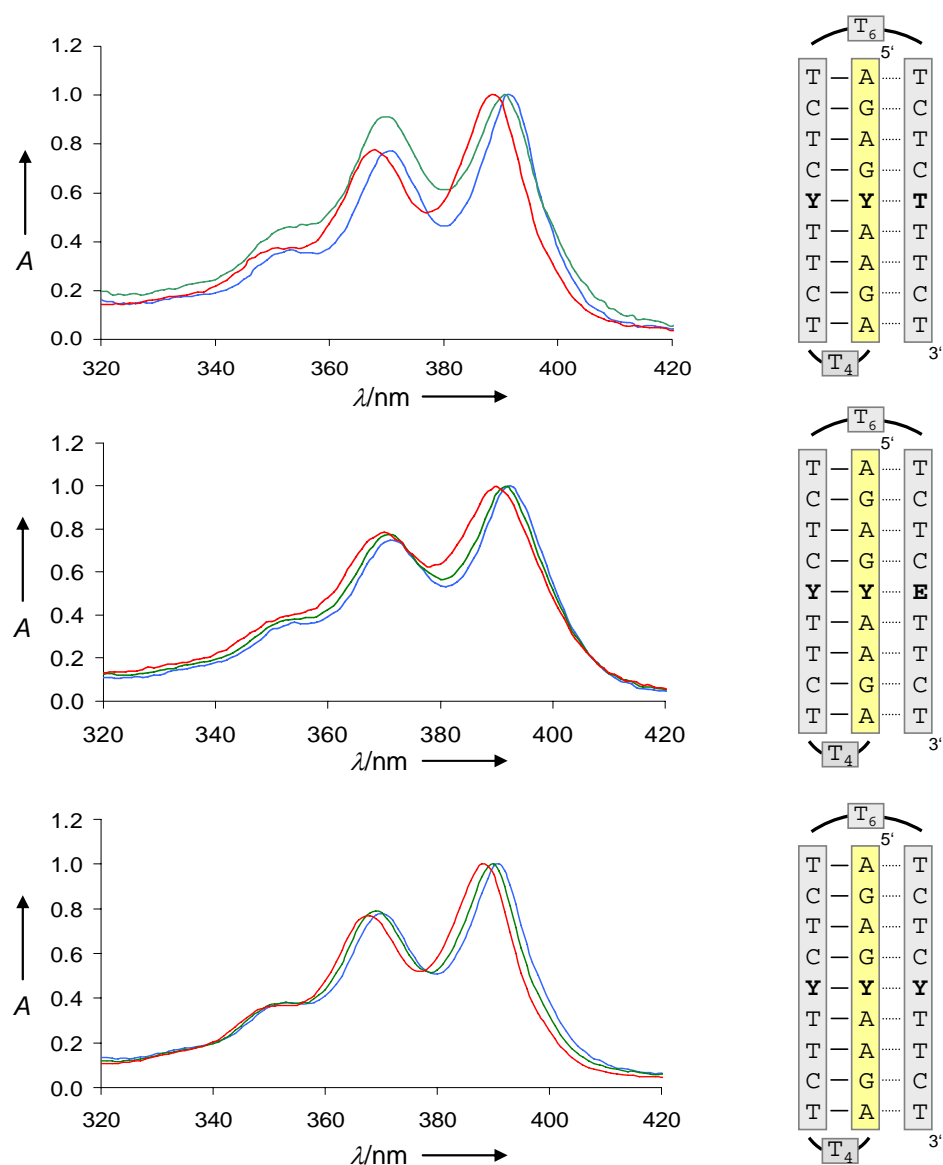


Figure 7.5. Temperature-dependent UV/Vis measurements: 10°C (blue), 40°C (green) and 90°C (red). Data presented for oligomer **I1** (top), **I2** (middle) and **I3** (bottom), normalized at the 0-0 transition. Conditions: see Figures 7.4.

The observed effects from the third unit of the triad (Hoogsteen base) on the two alkynylpyrenes can be confirmed by fluorescence experiments based on characteristic alkynylpyrene emission of fluorescence.^[52-56] The conformational changes introduce the appearance of either monomer or excimer fluorescence as it is illustrated in [Figure 7.6](#).

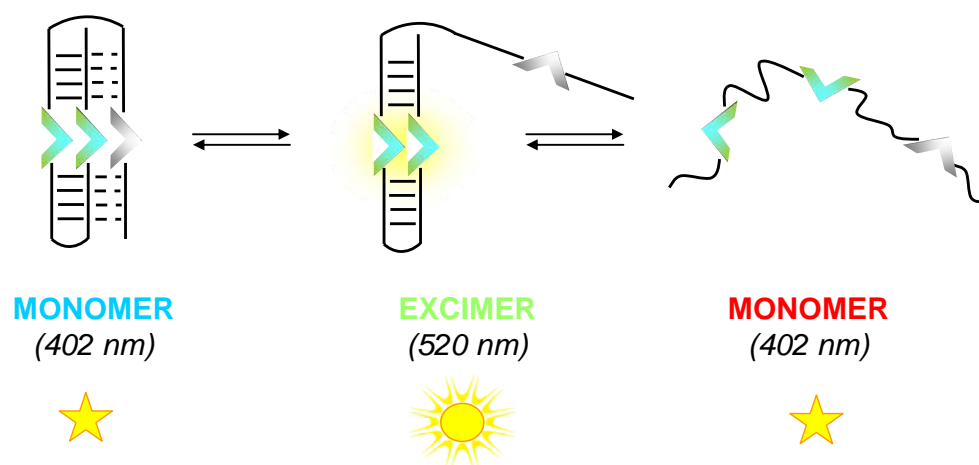


Figure 7.6. Schematic representation of the changes in fluorescence emission of intramolecular triple helices **I1** and **I2** upon structural dissociation.

The presence of an alkynylpyrene-PDI assembly in oligomer **I2** inhibits the formation of an alkynylpyrene dimer and therefore a loss in excimer signal in the fluorescence emission measurements. Else wise in oligomer **I1**, which ensures dimerization (excimer formation) and separation (quenching) of the two alkynylpyrene building blocks based on a thymine base. As it is known in literature pyrimidines, especially thymine, can quench hydrocarbons as well as excimer or exciplex-forming dinucleosides.^[46;57] These observations can be done for oligomer **I1** ([Figure 7.7](#)).

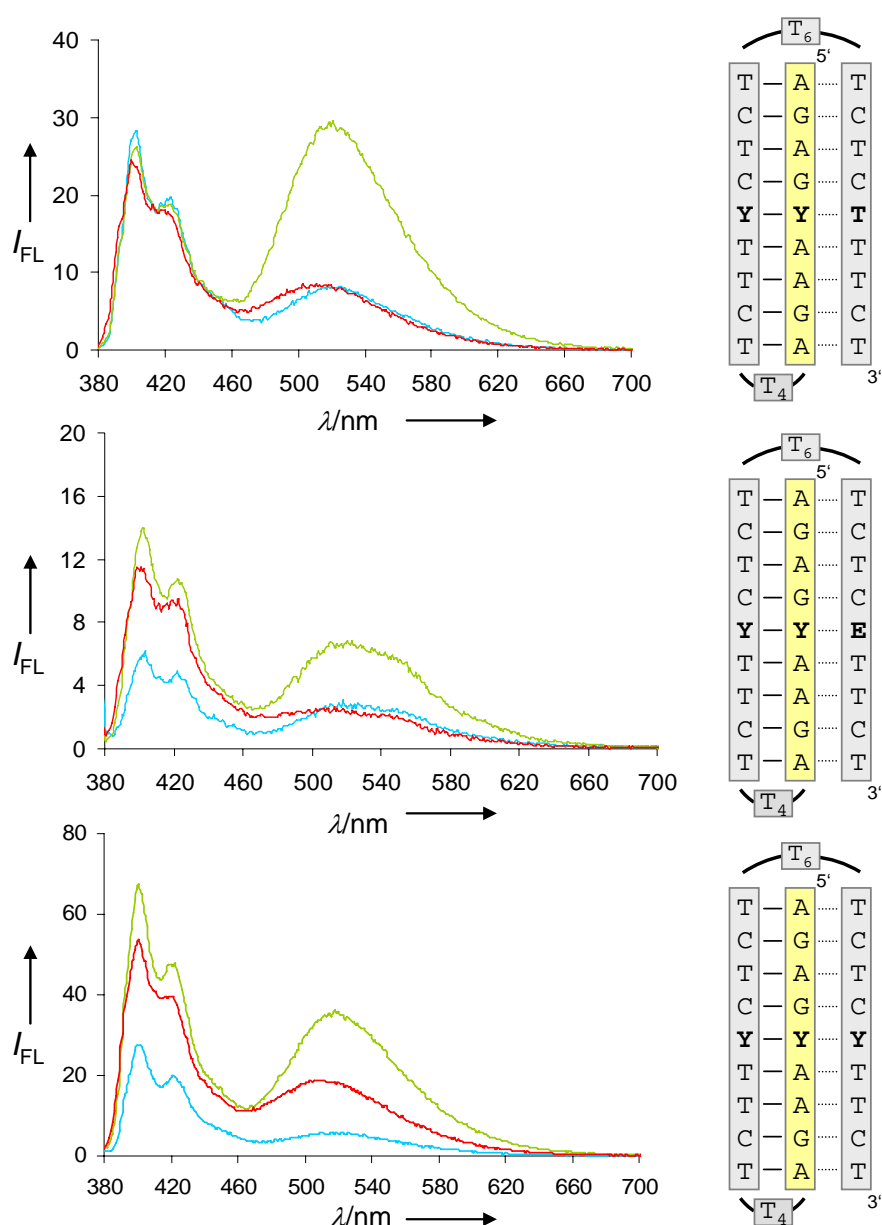


Figure 7.7. Temperature-dependent fluorescence emission measurements of oligomer **I1** (top), **I2** (middle) and **I3** (bottom) at 10°C (blue), 40°C (green) and 90°C (red). Conditions: 0.1 μ M single strand concentration, 10 mM sodium cacodylate buffer, pH 7.0, 100 mM NaCl, 20 mM MgCl₂, λ_{ex} : 370 nm, ex/em slit widths: 5/5 nm, PMT voltage: 600 V, equilibration time: 3 min.

The fluorescence emission data observed for oligomer **I2** show a small shoulder in the excimer signal between 530-580 nm (Figure 7.8). A possible explanation is an exciplex formation between alkynylpyrene and PDI units similarly suggested with the UV/Vis data.

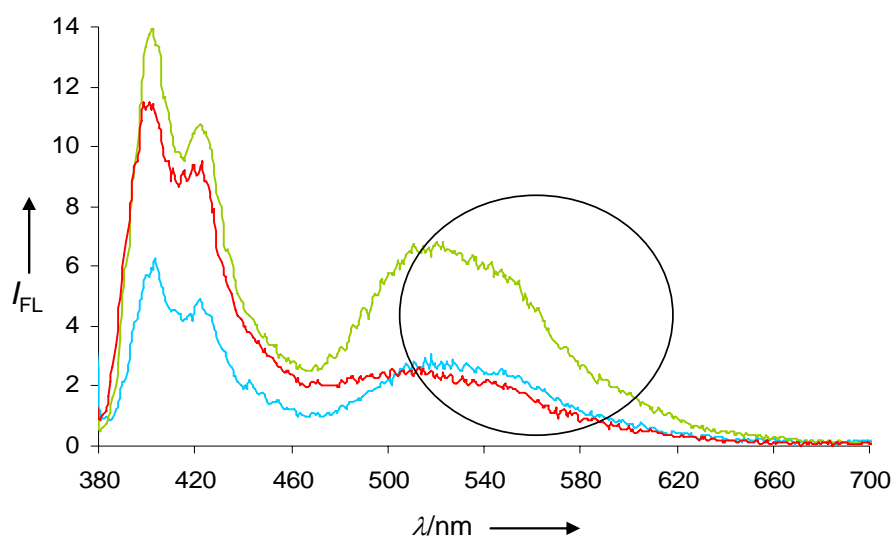


Figure 7.8. Temperature-dependent fluorescence emission measurements of oligomer **I2** at 10°C (blue), 40°C (green) and 90°C (red). Conditions: see Figure 7.7.

The fluorescence excitation spectra of oligomer **I2** confirm the influence on the PDI unit upon excitation at 370 nm (Figure 7.9). The contribution of aggregated alkynylpyrenes is stronger, as the signal intensity at 370 nm is higher than the intensity observed at 390 nm.

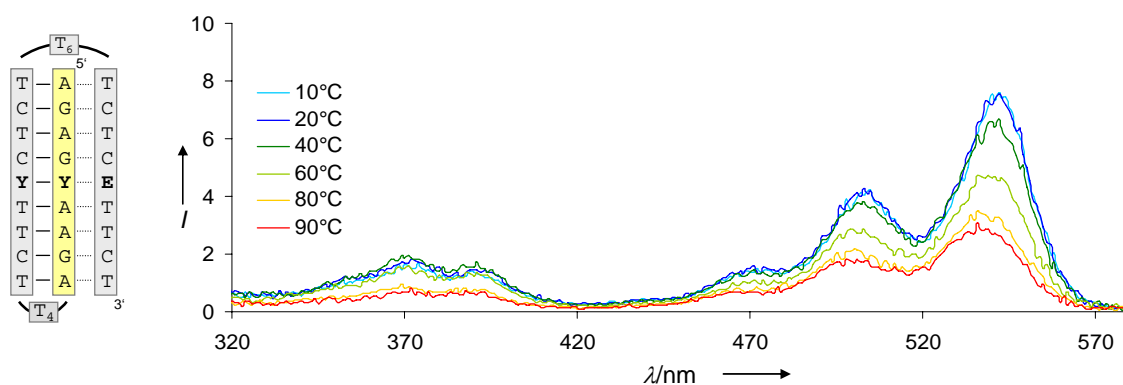


Figure 7.9. Temperature-dependent fluorescence excitation spectra of oligomer **I2**. Conditions: 0.1 μM single strand concentration, 10 mM sodium cacodylate buffer, pH 7.0, 100 mM NaCl, 20 mM MgCl_2 , λ_{em} : 597 nm, ex/em slit widths: 5/5 nm, PMT voltage: 600 V, equilibration time: 3 min.

Further investigation of the oligomers **I1** to **I4** were accomplished by temperature-dependent CD measurements. (Figure 7.10 and Figure 7.11). The signals for the alkynylpyrene unit appear between 300-430 nm whereas the PDI unit can be studied between 430-630 nm. [25;26;28;30;34;58-63] Upon heating, the dissociation of the building blocks is initiated and leads to signal decay. The oligomers containing only alkynylpyrene chromophores show similar CD signatures however the exciton coupled signal is best observed at 40°C for oligomer **I1** (Figure 7.10 top).

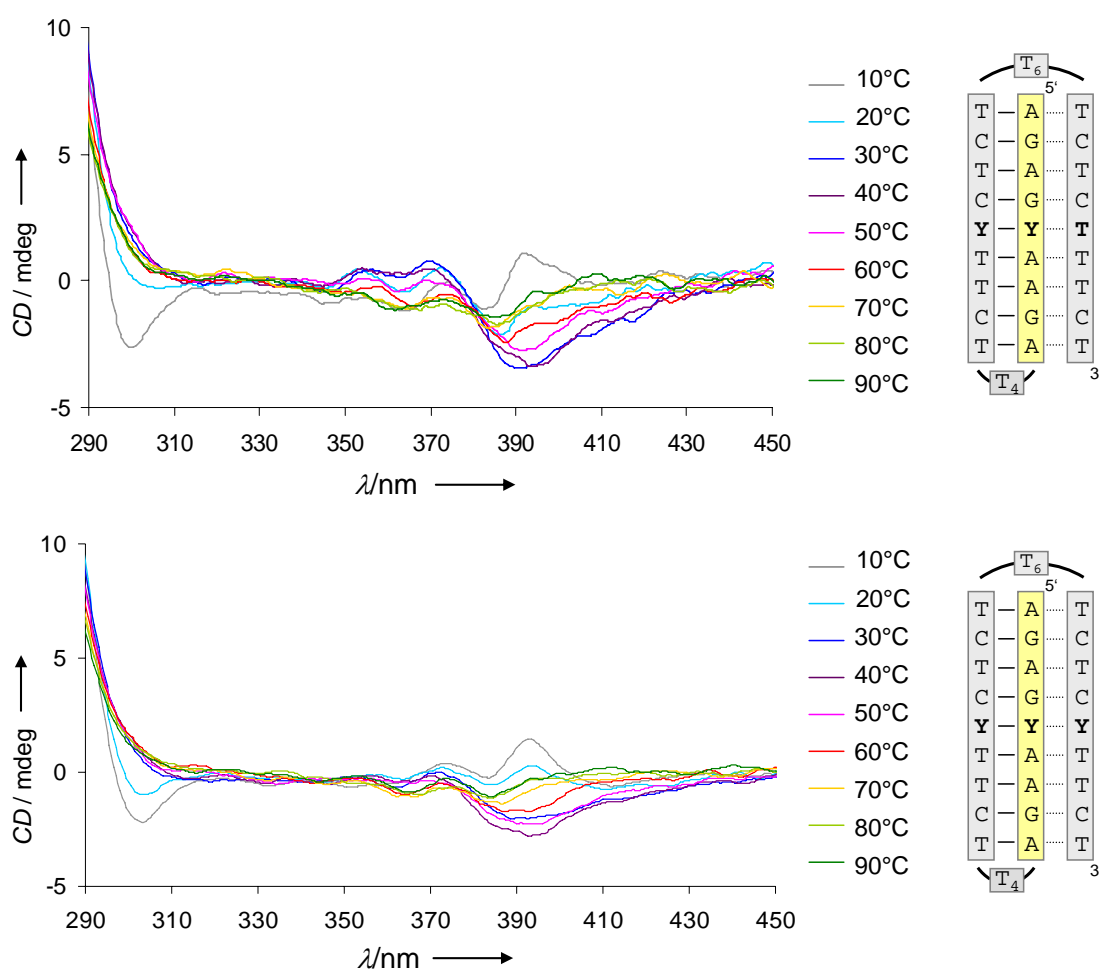


Figure 7.10. Temperature-dependent CD measurements of oligomer **I1** (top) and oligomer **I3** (bottom), temperature range from 10°C (grey) to 90°C (green) in 10°C increments. Conditions: 4.0 μM single strand concentration, 10 mM sodium cacodylate buffer, pH 7.0, 100 mM NaCl, 20 mM MgCl_2 , equilibration time: 3 min.

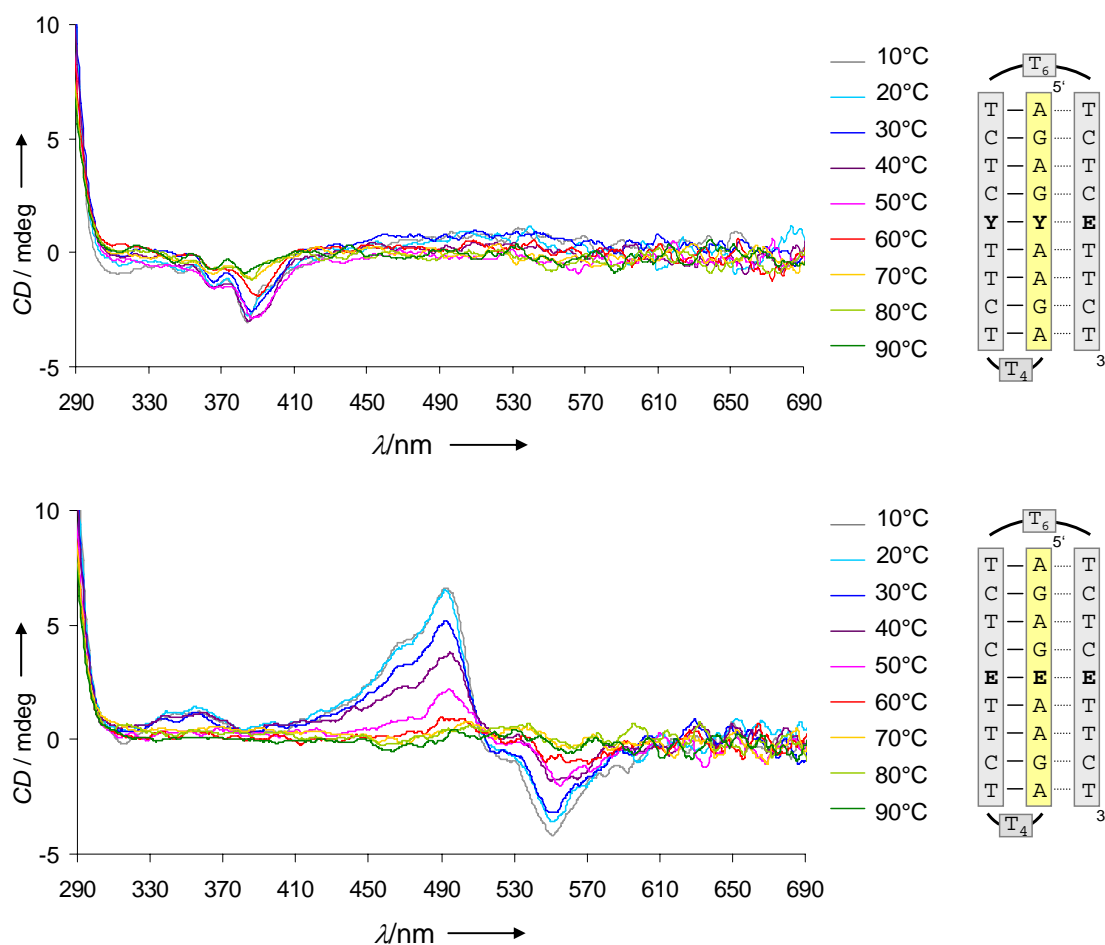


Figure 7.11. Temperature-dependent CD measurements of oligomer **I2** (top) and oligomer **I4** (bottom), temperature range from 10°C (grey) to 90°C (green) in 10°C increments. Conditions: 4.0 μ M single strand concentration, 10 mM sodium cacodylate buffer, pH 7.0, 100 mM NaCl, 20 mM $MgCl_2$, equilibration time: 3 min.

The CD data obtained for oligomer **I2** are in line with the previous conclusion of the possible presence of an exciplex (see fluorescence data). The transition moments of the alkynylpyrene and PDI units can be oriented in an in-line mode which results in no CD signal whereas the second alkynylpyrene unit can be arranged within the DNA frame resulting in an induced CD signal as it can be seen in Figure 7.11 top.^[59-60] Oligomer **I4** shows a signal signature as it is characteristic for aggregated PDI units embedded in DNA.^[61-63]

7.4 Conclusion

In conclusion the data show that a triple helix can be formed in presence of two respectively three incorporated polyaromatic building blocks. As a consequence the transitions from triplex to a hairpin structure can be followed upon fluorescence spectroscopy and absorbance measurements focused on the alkynylpyrene properties. On one side the change from monomer to excimer fluorescence emission and on the other side the change in the transition ratios ($A^{0\rightarrow0}/A^{0\rightarrow1}$) of the alkynylpyrene building blocks are characteristic for certain aggregation states. The next transition from hairpin to a random coil shows the opposite properties in fluorescence and absorbance experiments. In addition it could be shown that three polyaromatic building blocks are not able to proceed a well defined stacking arrangement in this strand design. Absorbance data for the oligonucleotide with three PDI units show a more dimer-like or aggregated state of the building blocks whereas the oligonucleotide with three alkynylpyrene units features a disaggregated state in UV/Vis measurements similar if two alkynylpyrenes and one PDI unit is incorporated. The latter indicates the formation of an alkynylpyrene-PDI exciplex. These findings lead to the suggestion that in the presence of two alkynylpyrenes and one PDI unit a mixture of a strong interaction between alkynylpyrenes and the PDI building block occurs. Nevertheless, this study shows the use of chromophores to follow the formation of intramolecular triple helices and the possible use of a triplex as a mould to investigate chromophoric interactions.

7.5 Experimental Part

Oligonucleotide synthesis. The required alkynylpyrene^[26] and PDI^[25] building blocks were synthesized according to published procedures. Commercial natural nucleoside phosphoramidites were used for oligonucleotide synthesis. Oligomers **I1** to **I4** were prepared *via* automated oligonucleotide synthesis by a standard synthetic procedure (2 min coupling time; ‘trityl-off’ mode) on a 394-DNA/RNA synthesizer (*Applied Biosystems*), except for the coupling step of the PDI phosphoramidite, an adapted activating step was proceeded. Cleavage from the solid support and final deprotection was done by treatment with 30% NH₄OH solution at 55°C overnight.

Oligonucleotide purification and mass determination. Purification was done by reverse phase HPLC (LiChrospher 100 *RP-18*, 5µm, Merck; *Kontron Instruments* device); eluent A = (Et₃NH)OAc (0.1 M, pH 7.4); eluent B = MeCN ([Table 7.2](#)).

Table 7.2. Purification performance and retention times (t_R s).

	Elution temperature	Elution gradient	Elution time	t_R
I1	50°C	5 – 50 %	30 min	17.5 min
I2	40°C	5 – 30 %	30 min	18.5 min
I3	50°C	5 – 50 %	30 min	18.1 min
I4	40°C	5 – 30 %	30 min	17.6 min

Mass spectrometry was performed with a Sciex QSTAR pulsar (hybrid quadrupole time-of-flight mass spectrometer, *Applied Biosystems*); ESI-TOF MS (negative mode, acetonitrile/H₂O/triethylamine) ([Table 7.3](#)).

Table 7.3. Specification of the investigated oligomers.

	<i>Molecular formula</i>	<i>calcd. avg. mass</i>	<i>found avg. mass</i>
I1	C ₃₉₂ H ₄₇₆ N ₁₀₀ O ₂₃₂ P ₃₆	11415.56	11492.46
I2	C ₄₁₂ H ₄₈₄ N ₁₀₀ O ₂₃₃ P ₃₆	11679.84	11680.57
I3	C ₄₀₆ H ₄₈₀ N ₉₈ O ₂₂₉ P ₃₆	11511.73	11510.87
I4	C ₄₂₄ H ₄₉₂ N ₁₀₄ O ₂₄₁ P ₃₆	12016.05	11896.70

Oligonucleotide analysis. Temperature-dependent UV/Vis spectra were carried out on a *Varian Cary-100 Bio-UV/Vis* spectrophotometer equipped with a *Varian Cary-block* temperature controller and data were collected with *Varian WinUV* software. Fluorescence spectra were recorded on a *Varian Cary Eclipse* fluorescence spectrophotometer equipped with a *Varian Cary-block* temperature controller using 1 cm x 1 cm quartz cuvettes. *Varian Eclipse* software was used to process the data. CD spectra were recorded on a *JASCO J-715* spectrophotometer using quartz cuvettes with an optic path of 1 cm.

7.6 References

- [1] E. T. Kool, *Chem.Rev.* **1997**, 97, 1473-1487.
- [2] F. J. M. Hoeben, P. Jonkheijm, E. W. Meijer, A. P. H. J. Schenning, *Chem.Rev.* **2005**, 105, 1491-1546.
- [3] N. L. Rosi, C. A. Mirkin, *Chem.Rev.* **2005**, 105, 1547-1562.
- [4] N. C. Seeman, *Mol.Biotechnol.* **2007**, 37, 246.
- [5] V. L. Malinovskii, D. Wenger, R. Häner, *Chem.Soc.Rev.* **2010**, 39, 410-422.
- [6] F. Wojciechowski, C. J. Leumann, *Chem.Soc.Rev.* **2011**, 40, 5669-5667.
- [7] S. Keller, A. Marx, *Chem.Soc.Rev.* **2011**, 40, 5690-5697.
- [8] C. Dohno, K. Nakatani, *Chem.Soc.Rev.* **2011**, 40, 5718-5729.
- [9] N. Dai, E. T. Kool, *Chem.Soc.Rev.* **2011**, 40, 5756-5770.
- [10] H. Asanuma, T. Ito, T. Yoshida, *Angew.Chem.Int.Ed.* **1999**, 38, 2393-2395.
- [11] N. Amann, E. Pandurski, T. Fiebig, H. A. Wagenknecht, *Chem.Eur.J.* **2002**, 8, 4877-4883.
- [12] E. T. Kool, *Acc.Chem.Res.* **2002**, 35, 936-943.
- [13] P. M. Wengel, *Trends in Biotechnol.* **2003**, 21, 74-81.
- [14] C. Beuck, I. Singh, A. Bhattacharya, W. Hecker, V. S. Parmar, O. Seitz, E. Weinhold, *Angew.Chem.Int.Ed.* **2003**, 42, 3958-3960.
- [15] S. Bevers, S. Schutte, L. W. McLaughlin, *J.Am.Chem.Soc.* **2000**, 122, 5905-5915.
- [16] M. Balaz, B. C. Li, J. D. Steinkruger, G. A. Ellestad, K. Nakanishi, N. Berova, *Org. Biomol.Chem.* **2006**, 4, 1865-1867.
- [17] T. A. Zeidan, R. Carmieli, R. F. Kelley, T. M. Wilson, F. D. Lewis, M. R. Wasielewski, *J.Am.Chem.Soc.* **2008**, 130, 13945-13955.
- [18] S. M. Langenegger, R. Häner, *Helv.Chim.Acta* **2002**, 85, 3414-3421.
- [19] A. Stutz, S. M. Langenegger, R. Häner, *Helv.Chim.Acta* **2003**, 86, 3156-3163.
- [20] S. M. Langenegger, R. Häner, *Chem.Commun.* **2004**, 2792-2793.
- [21] S. M. Langenegger, R. Häner, *ChemBioChem* **2005**, 6, 2149-2152.
- [22] I. Trkulja, R. Häner, *Bioconjugate Chem.* **2007**, 18, 289-292.
- [23] V. L. Malinovskii, F. Samain, R. Häner, *Angew.Chem.Int.Ed.* **2007**, 46, 4464-4467.
- [24] I. Trkulja, S. M. Biner, S. M. Langenegger, R. Häner, *ChemBioChem* **2007**, 8, 25-27.

- [25] N. Bouquin, V. L. Malinovskii, R. Häner, *Chem. Commun.* **2008**, 1974–1976.
- [26] H. Bittermann, D. Siegemund, V. L. Malinovskii, R. Häner, *J. Am. Chem. Soc.* **2008**, *130*, 15285–15287.
- [27] F. Samain, V. L. Malinovskii, S. M. Langenegger, R. Häner, *Bioorg. Med. Chem.* **2008**, *16*, 27–33.
- [28] R. Häner, S. M. Biner, S. M. Langenegger, T. Meng, V. L. Malinovskii, *Angew. Chem. Int. Ed.* **2010**, *49*, 1227–1230.
- [29] D. Wenger, V. L. Malinovskii, R. Häner, *Chem. Commun.* **2011**, *47*, 3168–3170.
- [30] S. M. Biner, D. Kummer, V. L. Malinovskii, R. Häner, *Org. Biomol. Chem.* **2011**, *9*, 2628–2633.
- [31] F. Garo, R. Häner, *Angew. Chem. Int. Ed.* **2011**, *in press* DOI: 10.1002/ange.201103295
- [32] M. Probst, D. Wenger, S. M. Biner, R. Häner, *Org. Biomol. Chem.* **2012**, *10*, 755–759.
- [33] A. L. Nussbaumer, D. Studer, V. L. Malinovskii, R. Häner, *Angew. Chem. Int. Ed.* **2011**, *24*, 5490–5494.
- [34] S. M. Biner, R. Häner, *ChemBioChem* **2011**, *12*, 2733–2736.
- [35] G. Felsenfeld, D. R. Davies, A. Rich, *J. Am. Chem. Soc.* **1957**, *79*, 2023–2024.
- [36] T. Le Doan; L. Perrouault, D. Praseuth, N. Habhouh, J. L. Decout, N. T. Thuong, J. Lhomme, C. Hélène, *Nucl. Acids Res.* **1987**, *15*, 7749–7760.
- [37] M. D. Frank-Kamenetskii, C. M. Mirkin, *Annu. Rev. Biochem.* **1995**, *64*, 65–95.
- [38] J. R. Goñi, X. de la Cruz, M. Orozco, *Nucl. Acids Res.* **2004**, *32*, 354–360.
- [39] J. R. Goñi, J. M. Vaquerizas, J. Dopazo, M. Orozco, *BMC Genomics* **2006**, *7*: 63.
- [40] B. P. Belotserkovskii, E. De Silva, S. Tornaletti, G. Wang, K. M. Vasquez, P. C. Hanawalt, *J. Biol. Chem.* **2007**, *282*, 32433–32441.
- [41] S. Kaushik, M. Kaushik, F. Svinarchuk, C. Malvy, S. Femandjian, S. Kukreti, *Biochemistry* **2011**, *50*, 4132–4142.
- [42] S. Steenken, J. P. Telo, H. M. Novais, L. P. Candeias, *J. Am. Chem. Soc.* **1992**, *114*, 4701–4709.
- [43] M. Manoharan, K. L. Tivel, M. Zhao, K. Nafisi, T. L. Netzel, *J. Phys. Chem.* **1995**, *99*, 17461–17472.
- [44] M. Rist, N. Amann, H. A. Wagenknecht, *Eur. J. Org. Chem.* **2003**, 2498–2504.

- [45] C. E. Crespo-Hernández, D. M. Close, L. Gorb, J. Leszczynski, *J.Phys.Chem.B*, **2007**, 111, 5386-5395.
- [46] J. N. Wilson, C. Younjin, S. Tan, A. Cuppoletti, E. T. Kool, *ChemBioChem* **2008**, 9, 279-285.
- [47] H. Kashida, T. Takatsu, K. Sekiguchi, H. Asanuma, *Chem.Eur.J.* **2010**, 16, 2479-2486.
- [48] H. Langhals, R. Ismael, *Eur.J.Org.Chem.* **1998**, 1915-1917.
- [49] F. Würthner, C. Thalacker, S. Diele, C. Tschierske, *Chem.Eur.J.* **2001**, 7, 2245-2253.
- [50] A. D. Q. Li, W. Wang, L. Q. Wang, *Chem.Eur.J.* **2003**, 9, 4594-4601.
- [51] W. Wang, L. S. Li, G. Helms, H. H. Zhou, A. D. Q. Li, *J.Am.Chem.Soc.* **2003**, 125, 1120-1121.
- [52] F. M. Winnik, *Chem.Rev.* **1993**, 93, 587-614.
- [53] K. Fujimoto, H. Shimizu, M. Inouye, *J.Org.Chem.* **2004**, 69, 3271-3275.
- [54] P. Conlon, C. J. Yang, Y. Wu, Y. Chen, K. Martinez, Y. Kim, N. Stevens, A. A. Marti, S. Jockusch, N. J. Turro, W. Tan, *J.Am.Chem.Soc.* **2008**, 130, 336-342.
- [55] Y. Saito, Y. Shinohara, S. S. Bag, Y. Takeuchi, K. Matsumoto, I. Saito, *Tetrahedron* **2009**, 65, 934-939.
- [56] H. Kashida, T. Takatsu, T. Fujii, K. Sekiguchi, X. G. Liang, K. Niwa, T. Takase, Y. Yoshida, H. Asanuma, *Angew.Chem.Int.Ed.* **2009**, 48, 7044-7047.
- [57] Y. N. Teo, J. N. Wilson, E. T. Kool, *Chem.Eur.J.* **2009**, 15, 11551-11558.
- [58] D. E. Callahan, T. L. Trapane, P. S. Miller, P. O. Tso, L. S. Kan, *Biochemistry* **1991**, 30, 1650-1655.
- [59] N. Berova, K. Nakanishi, R. W. Woody, *Circular Dichroism – Principles and Applications*, Wiley-VCH: New York, **2000**.
- [60] S. E. Boiadjiev, D. A. Lightner, *Monatsheft für Chemie* **2005**, 136, 489-508.
- [61] W. Wang, W. Wan, H. H. Zhou, A. Niu, A. D. Q. Li, *J.Am.Chem.Soc.* **2003**, 125, 5248-5249.
- [62] Y. Zheng, H. Long, G. C. Schatz, F. D. Lewis, *Chem.Commun.* **2005**, 4795-4797.
- [63] T. E. Kaiser, V. Stepanenko, F. Würthner, *J.Am.Chem.Soc.* **2009**, 131, 6719-6732.

8. Organization of Oligopyrene Foldamers in a Bi-Segmental DNA Strand Design

8.1 Abstract

Stacking interactions and helical organization of oligopyrene foldamers inside a bi-segmental strand design able to adapt double- and triple-helical structures were investigated. The structural arrangement of the non-nucleosidic, polyaromatic building blocks was analyzed within a double- and triple-stranded DNA/pyrene chimera.

8.2 Introduction

Previous studies about bi- and tri-segmental hybrids based on double-stranded DNA/pyrene chimeras have shown interesting structural properties in the modified oligonucleotide part.^[1;2] There, the self-organization of oligopyrene foldamers was described and claimed to be an intrinsic property of the oligoaryl part independent from the natural, unmodified part of the oligomer (Figure 8.1).

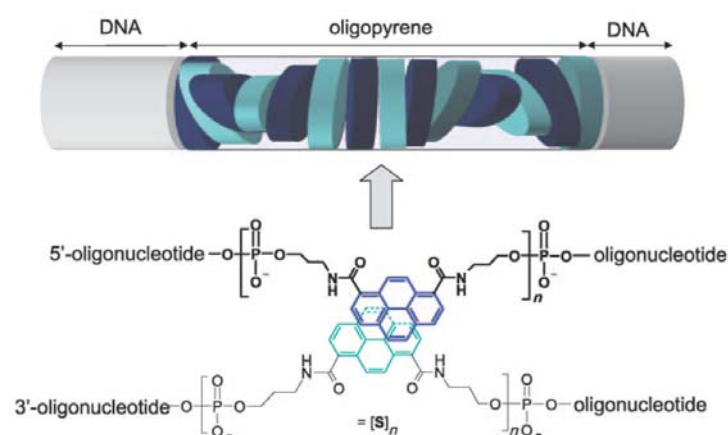


Figure 8.1. Schematic illustration of a tri-segmental DNA/pyrene chimera and the helical arrangement of the achiral pyrene units.^[2] The structure of the pyrene derivative is shown in the centre of the illustration.

A bi-segmental chimera was presented possessing the most pronounced helical arrangement of the pyrenylstack itself (Figure 8.2).

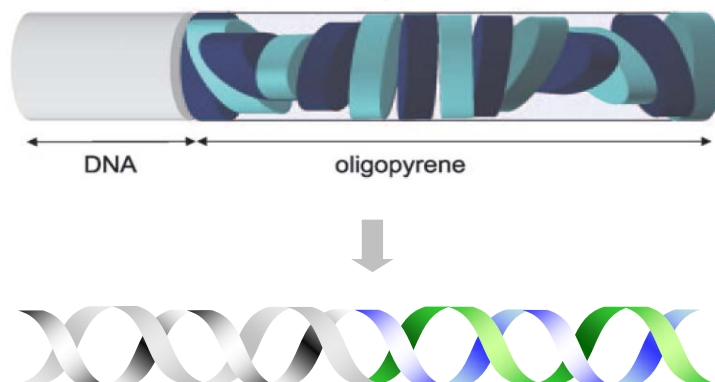


Figure 8.2. Two illustrations of a bi-segmental DNA/pyrene chimera and the helical arrangement of the achiral non-nucleosidic pyrene units in an intermolecular stacking mode. Further schematic illustrations of investigated structures inside this chapter are represented with the lower scheme type.

In this study the structural arrangement by adding a third bi-segmental strand able to form a triple-helical structure was investigated. The natural part of the oligomers contains seven natural bases whereas seven 1,8-carboxamidepyrenes (**S**) build up the modified part of the sequence (Table 8.1).

Table 8.1. Modified oligonucleotide and reference sequences.

Modified strands	S1	5'	CCTTCTC SSSSSSS
	S2	3'	GGAAGAG SSSSSSS
	S3	3'	CCTTCTC SSSSSSS
References	R1	5'	CCTTCTC
	R2	3'	GGAAGAG
	R3	3'	CCTTCTC
	R4	5'	CCTTCTCTCCTT
	R5	5'	GGAAGAGAGGAA
	R6	3'	CCTTCTCTCCTT

8.3 Spectroscopic study of bi-segmental, double- and triple-stranded structures

Thermal denaturation experiments were performed to test the temperature-dependent stability of possible structures formed by the bi-segmental oligomers, based on two or three strands. The data obtained for 260 nm are shown in Figure 8.3. The absorption at 260 nm can be attributed to a superposition of both units, natural and modified. Melting temperatures of 55.3°C for hybrid **S1*S2** and 53.5°C for hybrid **S1*S2*S3** were determined. The dissociation of the Hoogsteen strand in hybrid **S1*S2*S3** could not be observed; indicating that the transition occurred is due to melting of the double-helical structure. A sharp transition occurs, which is mostly a hint for a high level of cooperativity during the melting process.^[3-10] But nevertheless, the determined hyperchromicity is not that strong.

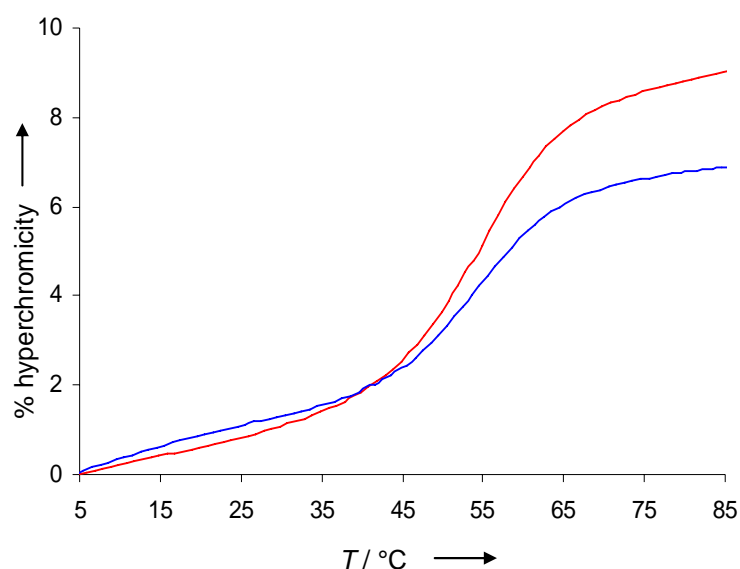


Figure 8.3. Temperature-dependent absorbance measurements of hybrids **S1*S2** (red) and **S1*S2*S3** (blue). Conditions: 5.0 μM single strand concentration, 10 mM sodium cacodylate buffer, pH 7.0, 100 mM NaCl, 20 mM MgCl_2 , absorbance was recorded at 260 nm, performance of three ramps (90-5°C / 5-90°C / 90-5°C), heating/cooling rate: 0.5°C/min, only the 2nd cooling ramp is shown.

The incorporated non-nucleosidic building blocks influence the stability of the hybrids. Compared to the reference hybrids, the addition of seven pyrene units increases the melting temperatures of approx. 30°C (Table 8.2).

Table 8.2. T_m -values.

	T_m [°C] ^a	ΔT_m [°C]		T_m [°C] ^a	ΔT_m [°C]
S1*S2	55.3		S1*S2*S3	53.5	
R1*R2	22.7	32.6	R1*R2*R3	21.3	32.2
R4*R5	52.7	2.6	R4*R5*R6	52.7	0.8

^aConditions: 5.0 μM single strand concentration, 10 mM sodium cacodylate buffer, pH 7.0, 100 mM NaCl, 20 mM MgCl_2 , estimated error $\pm 1^\circ\text{C}$.

This increase in stability arises from stacking interaction of the polyaromatic base surrogates and implies intermolecular arrangement of the pyrene units. Under aqueous conditions the structural arrangement is mainly driven by hydrophobic interactions. For further information about the structural organization inside the bi-segmental chimeras, temperature-dependent UV/Vis measurements were performed. Data recorded for hybrid **S1*S2** show clear hyperchromic effects in certain areas characteristic for DNA/pyrene chimeras (Figure 8.4).^[6;7;10-25] Apart from that, two isosbestic points could be determined.

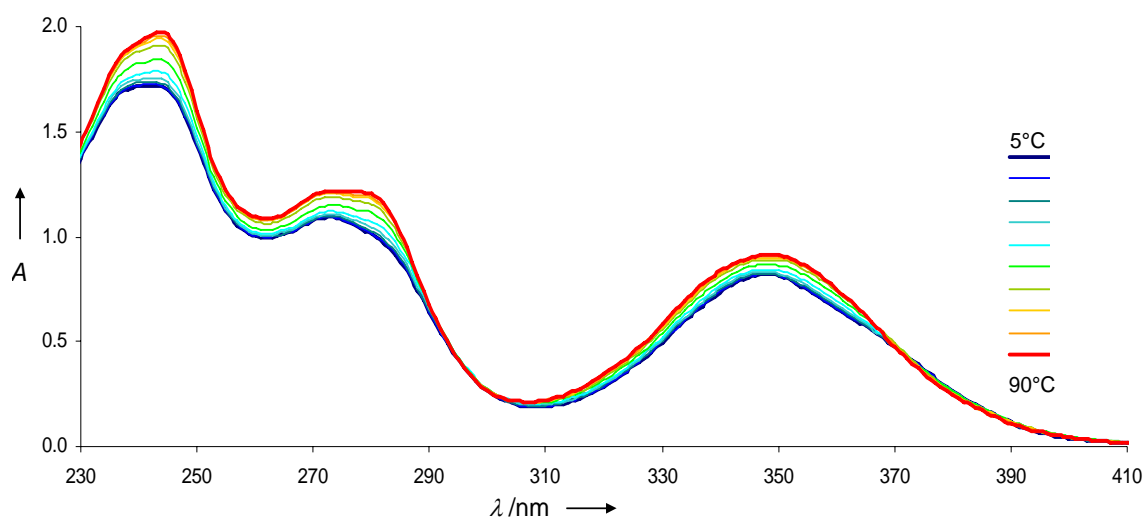


Figure 8.4. Temperature-dependent absorbance spectra of the double-stranded hybrid **S1*S2**. Conditions: 5.0 μM single strand concentration, 10 mM sodium cacodylate buffer, pH 7.0, 100 mM NaCl, 20 mM MgCl_2 , equilibration time: 10 min.

Figures 8.5 and Figure 8.6 present a closer look at the region between 410 to 310 nm that is only attributed to pyrene absorbance. Two isosbestic points at 371 nm and 362 nm are observable. Upon increasing the temperature from 5°C (dark blue -) to 60°C (light green -) a first change occurs (371 nm) verifying the transition from double to single stranded structures (Figure 8.5).^[1;2;6;10] The oligopyrene strands can not any longer interact in an intermolecular way.

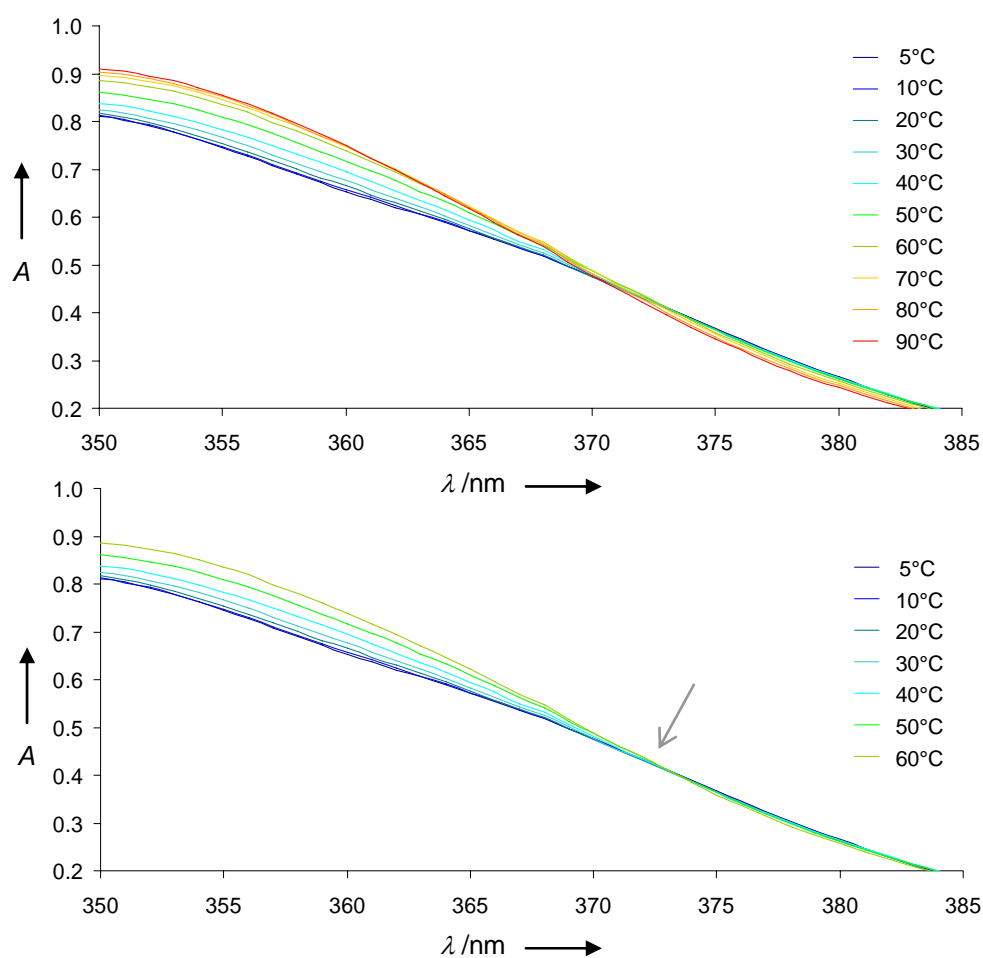


Figure 8.5. Detailed view on the first isosbestic point observed for the double-stranded hybrid **S1*S2**. Conditions: see Figure 8.4.

However, intramolecular arrangement inside the single bi-segmental strands takes place. These intramolecular interactions fade away by a further increase in temperature attested by the second isosbestic point at 362 nm (Figure 8.6).

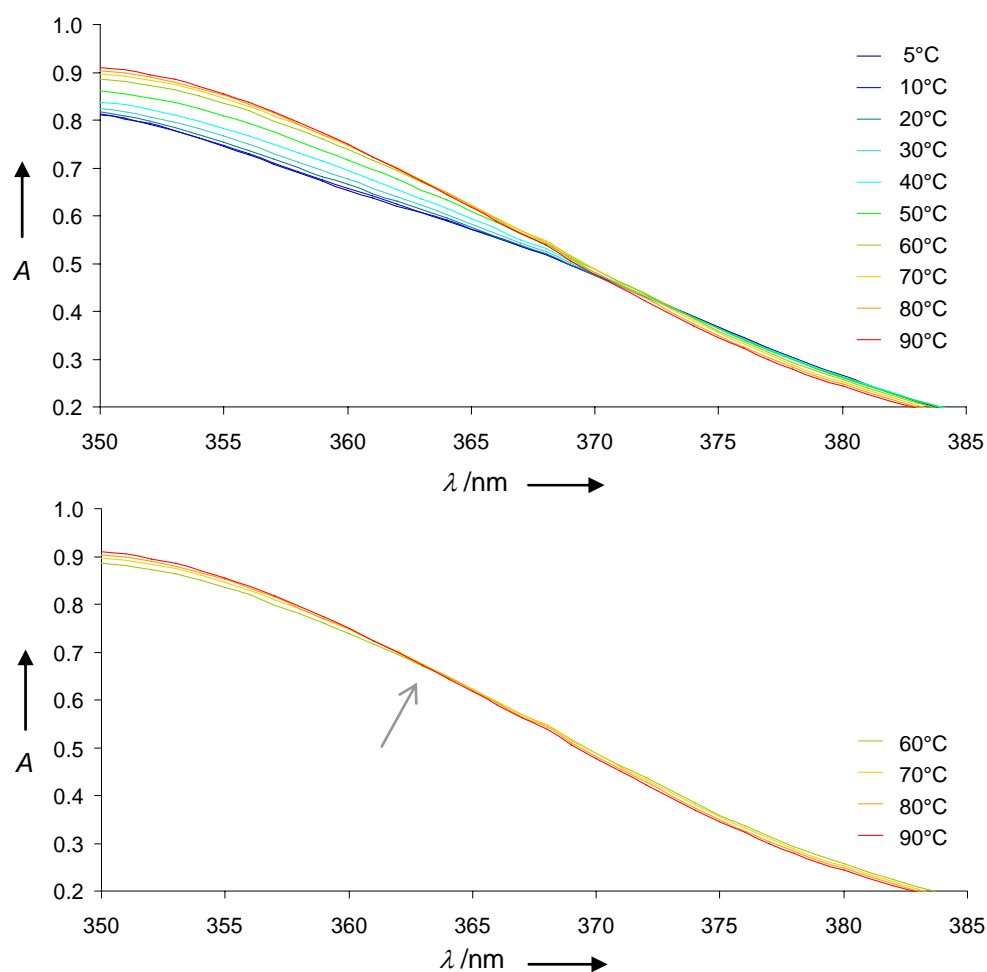


Figure 8.6. Detailed view on the second isosbestic point observed for the double-stranded hybrid **S1*S2**. Conditions: see [Figure 8.4](#).

The data gained from hybrid **S1*S2** contain additional evidences for interstrand stacked pyrene units, namely the changes in the vibronic band structure ([Figure 8.7](#)). The signal recorded between 290–260 nm is broadening based on an increase of the signal developing at 283 nm compared to the signal at 272 nm. Similar observations can be done for the signal between 250–230 nm. The vibronic band structure at low temperatures is a consequence of the pyrene arrangement that implies a reduction of rotational freedom of the aromatic units in contrast to a broadening of signals upon dissociation of the strands and so a disaggregation of the pyrene stack.^[1;2;6;10;26]

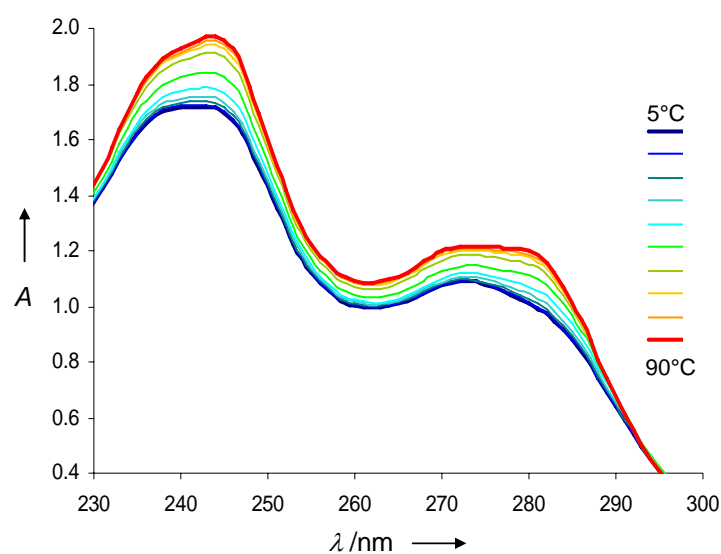


Figure 8.7. UV/Vis spectra of the double-stranded hybrid **S1*S2** with a detailed view on the region between 300 to 230 nm. Conditions: see [Figure 8.4](#).

Hybrid **S1*S2*S3** was investigated in the same procedure. [Figure 8.8](#) shows the temperature-dependent UV/Vis data obtained for the three stranded, bi-segmental sample.

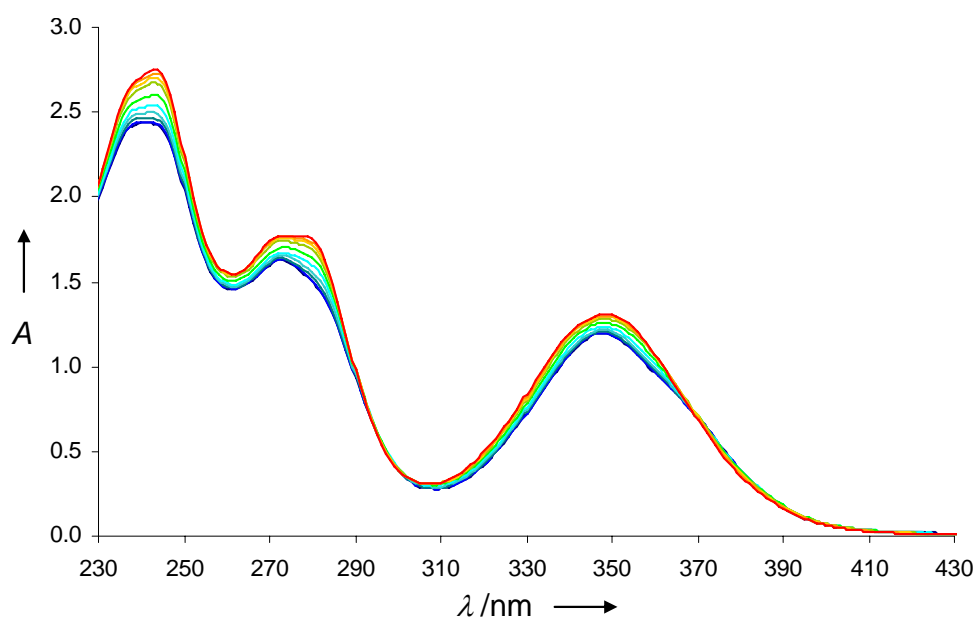


Figure 8.8. Temperature-dependent absorbance spectra of the triple-stranded hybrid **S1*S2*S3**. Conditions: 5.0 μM single strand concentration, 10 mM sodium cacodylate buffer, pH 7.0, 100 mM NaCl, 20 mM MgCl_2 , equilibration time: 10 min.

Equal to the double-stranded, bi-segmental hybrid **S1*S2** hyperchromic effects are detected in different areas. However, the changes in the vibronic band structure seem to be more pronounced for this hybrid (Figure 8.9).

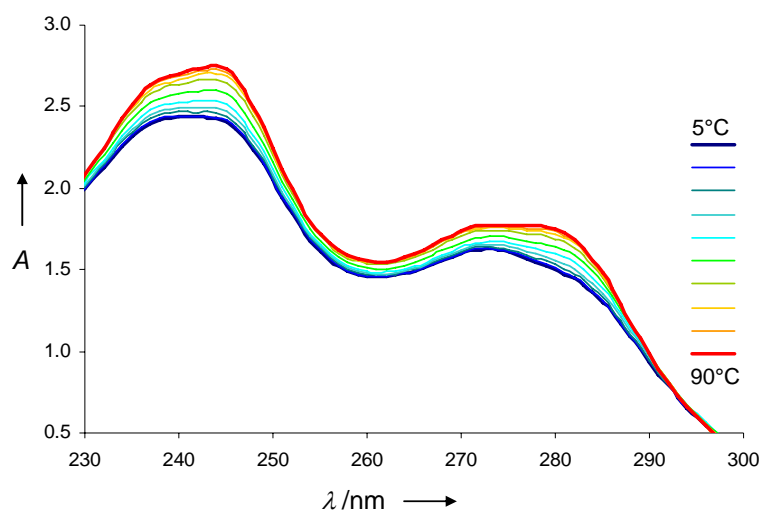


Figure 8.9. A detailed view in the region between 300 to 230 nm of the temperature-dependent absorbance spectra of the triple-stranded hybrid **S1*S2*S3**. Conditions: see Figure 8.8.

Both hybrids possess a broad signal in fluorescence emission measurements. This signal occurs from the formation of pyrene excimers either intra- or intermolecular.^[1;2;7-10;19;20;24;26-28] Monomer emission is completely no present. The organization of the oligopyrene strand in bi-segmental oligomers was studied with fluorescence spectroscopy over a certain period of time. Figure 8.10 summarizes the date gained for hybrids **S1*S2** and **S1*S2*S3** over a time period of six days.

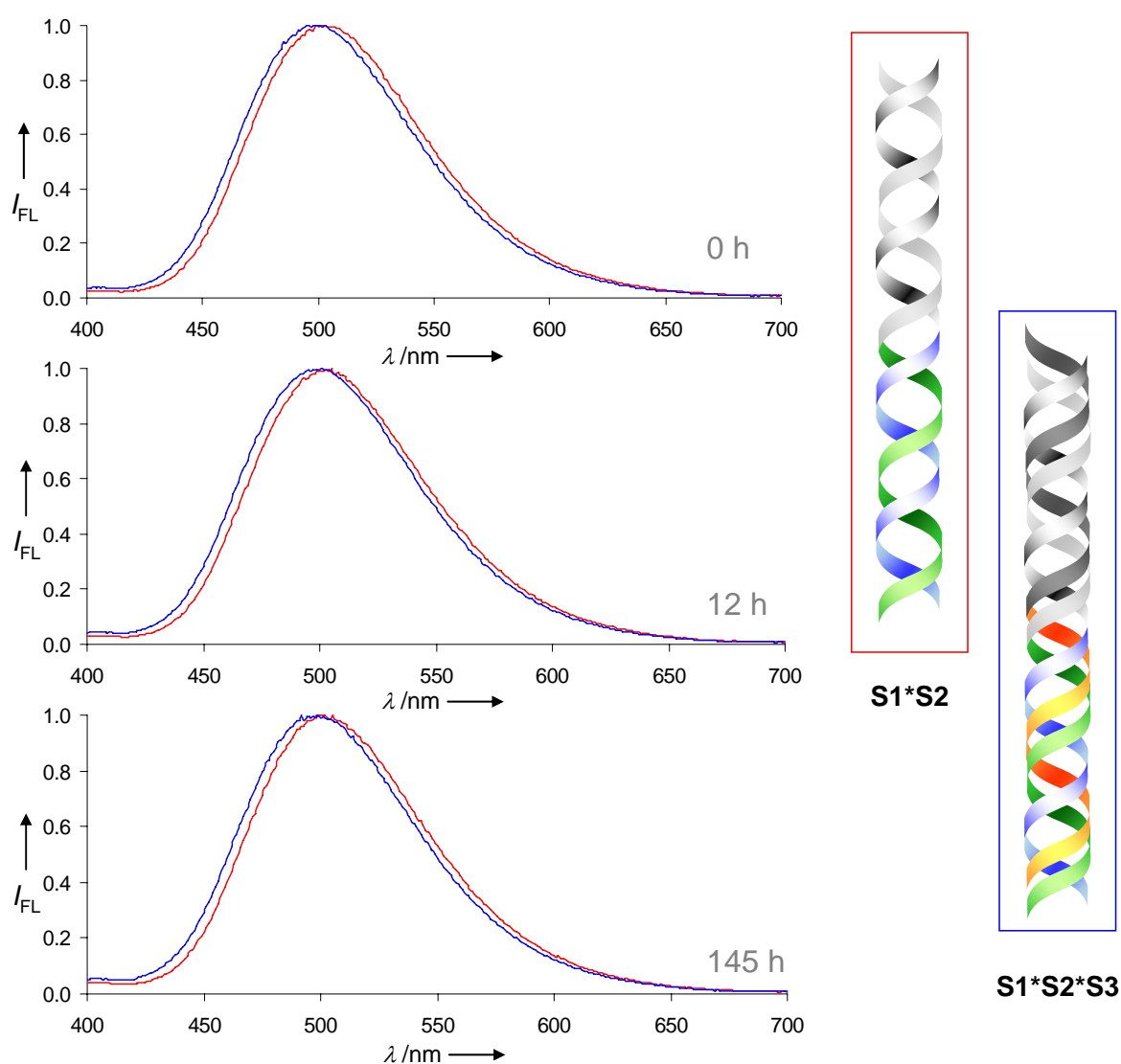


Figure 8.10. Time-dependent pyrene excimer emission (normalized) for bi-segmental double- and triple stranded DNA/pyrene chimeras. Conditions: 5.0 μ M single strand concentration, 10 mM sodium cacodylate buffer, pH 7.0, 100 mM NaCl, 20 mM $MgCl_2$, equilibration time: 10 min.

The broad excimer signals for both hybrids are not completely super imposable. There is a slight blue-shift of the excimer signal obtained for the triple-stranded chimera. In general, a blue-shift is a hint for a loss in rotational freedom of the polyaromatic units based on a constrained conformation of the pyrenes.^[1,2,26,27] The wavelength change of the emission maxima over time is illustrated in Figure 8.11.

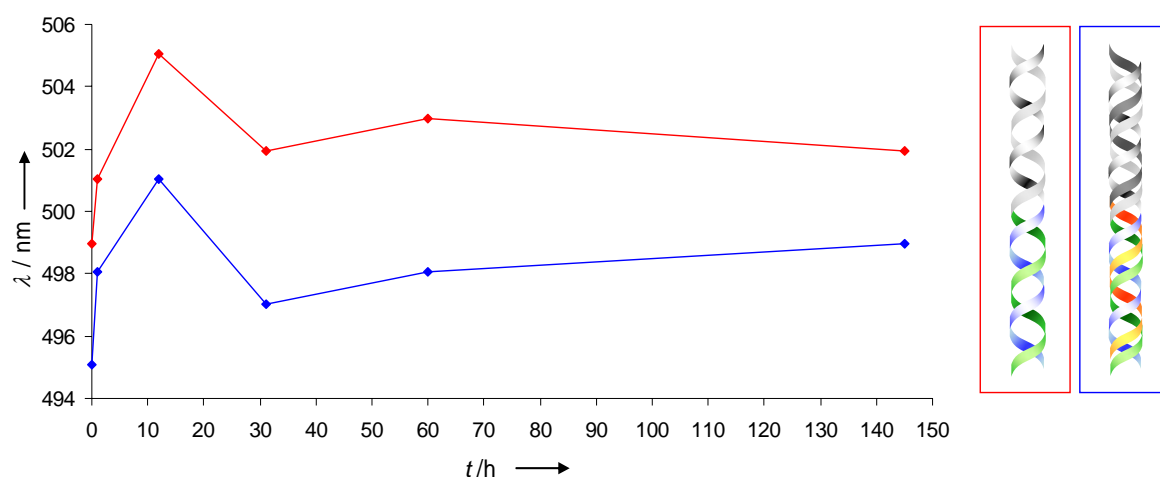


Figure 8.11. Wavelength shift of the excimer emission maxima for both hybrids **S1*S2** (red) and **S1*S2*S3** (blue). Conditions: see [Figure 8.10](#).

The blue-shift is observable through the whole data range. Both curves indicate a process of rearrangement until a final organization is achieved. A red-shift during the first 12 hours occurs (**S1*S2**: 499 nm to 505 nm and **S1*S2*S3**: 495 nm to 501 nm) followed by a blue-shift (**S1*S2**: 505 nm to 503 nm and **S1*S2*S3**: 501 nm to 499 nm). The reason therefore could be a relaxation of the arrangement before moving into their favoured organization; from a random assembly to a rearranged organized structure.

Any helical organization inside the polypyrene stack however is not yet identified ([Figure 8.12](#)).^[1;2;28] Consequently additional investigations were proceeded concerning the use of circular dichroism (CD) measurements.

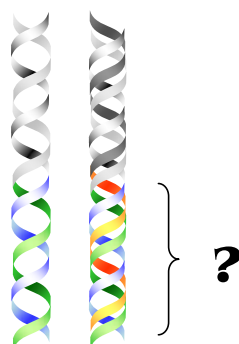


Figure 8.12. Schematic representation of a helical organization of the achiral pyrene units.

In parallel to the time-dependent fluorescence emission measurements CD data were recorded (Figure 8.13). Data directly obtained (0 h) for the double-stranded hybrid (**S1*S2**, red) verifies the formation of a helical organization inside the pyrenyl stack. A positive Cotton-effect implements a right-handed orientation of a structure. The exciton coupled CD signal for the triple-stranded chimera (**S1*S2*S3**, blue), seems to be inverted compared to hybrid **S1*S2**.

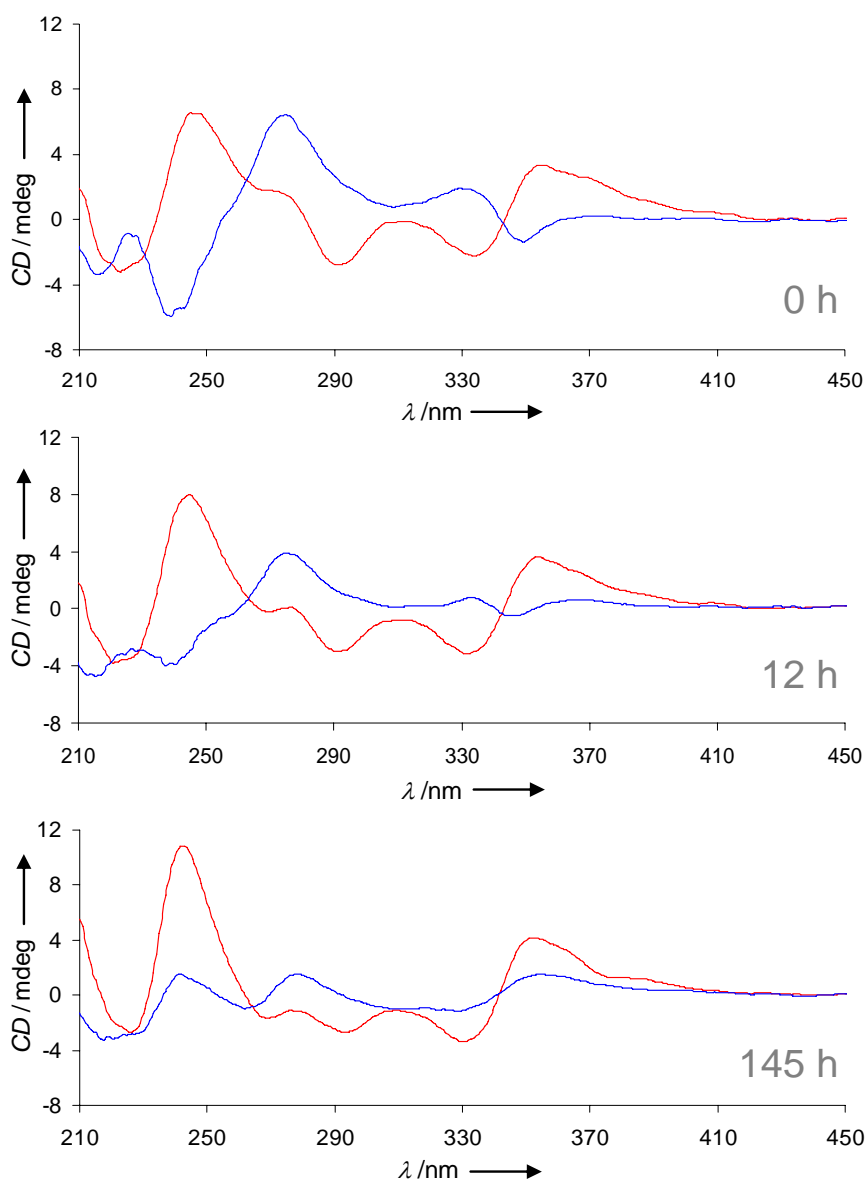


Figure 8.13. Time-dependent CD spectra recorded for the bi-segmental double- and triple-stranded DNA/pyrene chimeras, **S1*S2** (red) and **S1*S2*S3** (blue). Conditions: 5.0 μM single strand concentration, 10 mM sodium cacodylate buffer, pH 7.0, 100 mM NaCl, 20 mM MgCl_2 , equilibration time: 10 min.

However, both hybrids show changes in their CD signature over time. To get a detailed view on the signal development the time-dependent data of the two hybrids **S1*S2** and **S1*S2*S3** were presented separately (Figure 8.14).

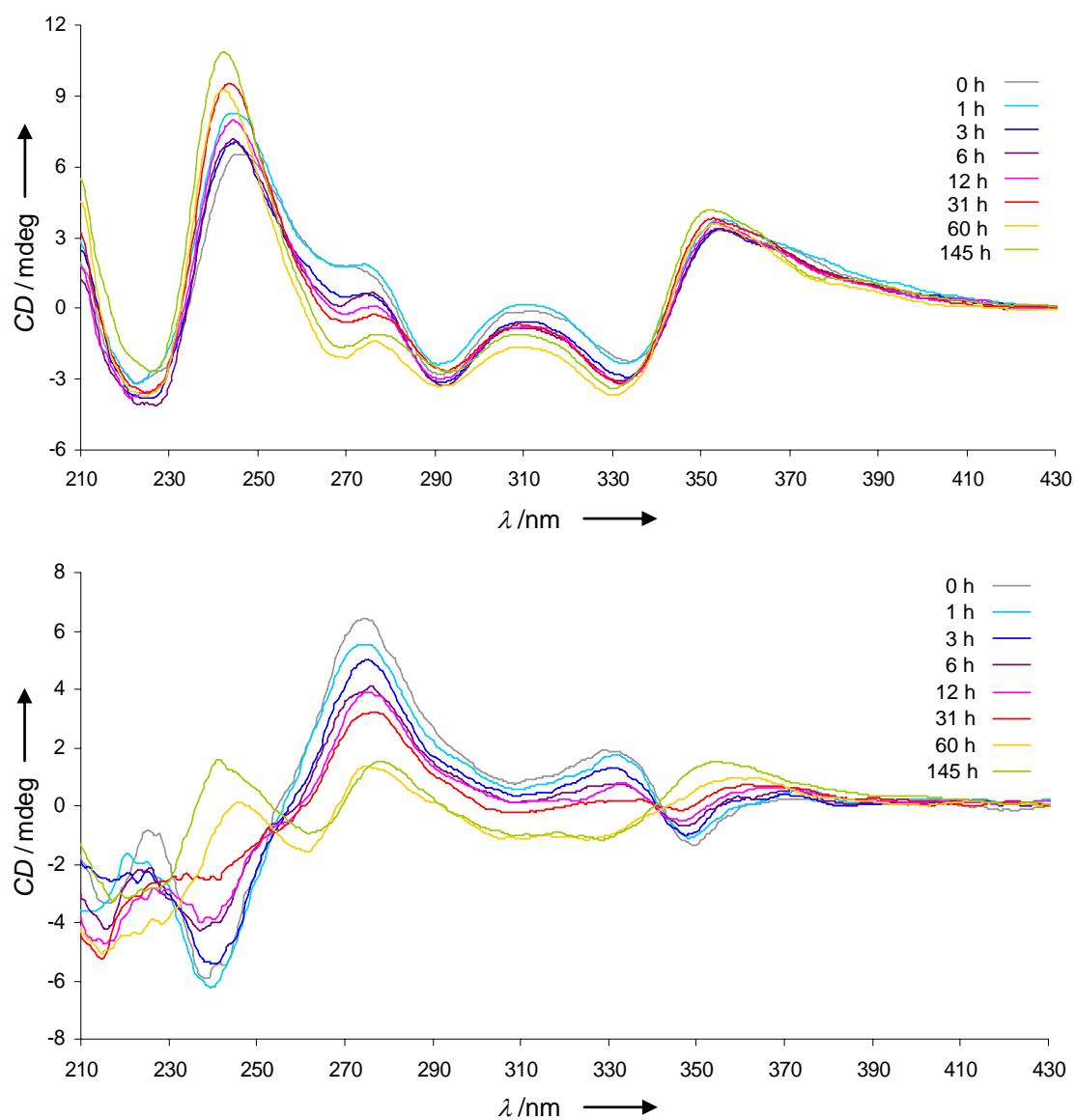


Figure 8.14. Time-dependent CD spectra recorded for hybrid **S1*S2** (top) and hybrid **S1*S2*S3** (bottom). Conditions: 5.0 μM single strand concentration, 10 mM sodium cacodylate buffer, pH 7.0, 100 mM NaCl, 20 mM MgCl_2 , equilibration time: 10 min.

The oligopyrene stack in hybrid **S1*S2** shows an exciton coupled CD signal in the region of 410 – 310 nm.^[1;2;6;8;19;28-34] This signal undergoes only minor changes during time, whereas the signal between 280–260 nm changes from a positive (273 nm) to a negative (267 nm) maxima. The triple-stranded chimera behaves similar in this region (280–260 nm) but the positive maximum is more pronounced. The characteristic signal for a triple-helical arrangement (negative band between 230–210 nm) is not distinct and vanishes almost completely after 145 h. Nevertheless, most dramatic are the changes in the pyrene only region. There, the negative Cotton-effect passes into a positive Cotton-effect within a broadening of the signal. As suggested already based on the fluorescence emission data, a previous rearrangement within the pyrenyl stack and an ensuing self-organization of the polyaromatic units could be the reason.

8.4 Conclusion

The arrangement in an oligopyrene stack inside a bis-segmental oligomer was investigated (Figure 8.15). Further the addition of a third DNA/pyrene containing bi-segmental strand and possible formation of triple-helical structures were studied.

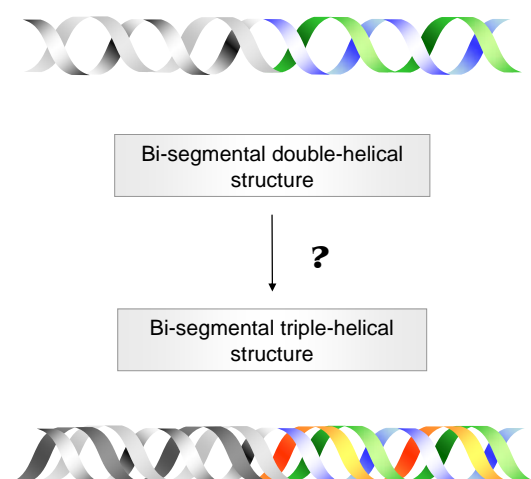


Figure 8.15. Schematic illustration of possible structures with two or three pyrene containing strands.

The interactions either inter- or intramolecular could be followed by UV/Vis and fluorescence experiments. Bi-segmental double-stranded DNA/pyrene chimeras show nicely observable changes if the interactions undergo a transition from inter- to a more intramolecular way and further to disaggregated assembly of pyrene units. Changes in the vibronic band structure of the 1,8-carboxamidepyrene give evidence for an aggregated or disaggregated state upon increasing the temperature and in consequence a disruption of the structure.

The orientation and structure inside the pyrenyl part could not be finally assigned within both hybrids (Figure 8.15). Whereas for the double-stranded hybrid a self-organization and a helical arrangement of the pyrene units could be determined, but the data gained for three strands were not completely convincing that a triple-helical arrangement and a helical organization of all three polypyrene segments are mainly subsisting. Nevertheless, some first evidence for complete triple-helical structures inside bi-segmental DNA/pyrene chimeras could be attained for further studies.

8.5 Experimental Part

Oligonucleotide synthesis. The required 1,8-carboxamide pyrene^[6] building block was synthesized according to published procedures. Commercial natural nucleoside phosphoramidites were used for oligonucleotide synthesis. Oligonucleotide **R1** to **R6** were purchased from Microsynth, Balgach, Switzerland. Oligomers **S1** to **S3** were prepared *via* automated oligonucleotide synthesis by a standard synthetic procedure (2 min coupling time; ‘trityl-off’ mode) on a 394-DNA/RNA synthesizer (*Applied Biosystems*). Cleavage from the solid support and final deprotection was done by treatment with 30% NH₄OH solution at 55°C overnight and for oligomer **S1** at 80°C for two days.

Oligonucleotide purification and mass determination. Purification was done by reverse phase HPLC (LiChrospher 100 *RP-18*, 5µm, Merck; *Shimadzu LC-20AT*); eluent *A* = (Et₃NH)OAc (0.1 M, pH 7.4); eluent *B* = MeCN ([Table 8.2](#)).

Table 8.2. Purification performance and retention times (t_R s).

	Elution temperature	Elution gradient	Elution time	t_R
S1	30°C	4 – 35 %	20 min	22.6 min
S2	30°C	4 – 35 %	20 min	22.3 min
S3	30°C	4 – 35 %	20 min	22.7 min

Mass spectrometry was performed with a Sciex QSTAR pulsar (hybrid quadrupole time-of-flight mass spectrometer, *Applied Biosystems*); ESI-TOF MS (negative mode, acetonitrile/H₂O/triethylamine) ([Table 8.3](#)).

Table 8.3. Specification of the investigated oligomers.

	<i>Molecular formula</i>	<i>calcd. avg. mass</i>	<i>found avg. mass</i>
S1	C ₂₃₄ H ₂₄₉ N ₃₂ O ₈₅ P ₁₃	5272.36	5272.66
S2	C ₂₃₈ H ₂₄₆ N ₄₉ O ₇₉ P ₁₃	5459.50	5457.45
S3	C ₂₃₄ H ₂₄₉ N ₃₂ O ₈₅ P ₁₃	5272.36	5272.52

Oligonucleotide analysis. Temperature-dependent UV/Vis spectra were carried out on a *Varian Cary-100 Bio-UV/Vis* spectrophotometer equipped with a *Varian Cary-block* temperature controller and data were collected with *Varian WinUV* software. Fluorescence spectra were recorded on a *Varian Cary Eclipse* fluorescence spectrophotometer equipped with a *Varian Cary-block* temperature controller using 1 cm x 1 cm quartz cuvettes. *Varian Eclipse* software was used to process the data. CD spectra were recorded on a *JASCO J-715* spectrophotometer using quartz cuvettes with an optic path of 1 cm.

8.6 References

- [1] V. Malinovskii, F. Samain, R. Häner, *Angew.Chem.Int.Ed.* **2007**, 46, 4464-4467.
- [2] R. Häner, F. Samain, V. Malinovskii, *Chem.Eur.J.* **2009**, 15, 23, 5701-5708.
- [3] S. M. Langenegger, R. Häner, *Helv.Chim.Acta* **2002**, 85, 3414-3421.
- [4] S. M. Langenegger, R. Häner, *Tetrahedron Lett.* **2004**, 45, 9273-9276.
- [5] S. M. Langenegger, R. Häner, *Chem.Biodiv.* **2004**, 1, 259-264.
- [6] S. M. Langenegger, R. Häner, *Chem.Commun.* **2004**, 2792-2793.
- [7] S. M. Langenegger, R. Häner, *ChemBioChem* **2005**, 6, 2149-2152.
- [8] I. Trkulja, R. Häner, *J.Am.Chem.Soc.* **2007**, 129, 7982-7989.
- [9] I. Trkulja, S. M. Biner, S. M. Langenegger, R. Häner, *ChemBioChem* **2007**, 8, 25-27.
- [10] F. Samain, V. L. Malinovskii, S. M. Langenegger, R. Häner, *Bioorg.Med.Chem.* **2008**, 16, 27-33.
- [11] M. N. Dioubankova, A. D. Malakhov, D. A. Stetsenko, M. J. Gait, P. E. Volynsky, R. G. Efremov, V. A. Korshun, *ChemBioChem* **2003**, 4, 841-847.
- [12] A. Okamoto, T. Ichiba, I. Saito, *J.Am.Chem.Soc.* **2004**, 126, 8364-8365.
- [13] K. Fujimoto, H. Shimizu, M. Inouye, *J.Org.Chem.* **2004**, 69, 3271-3275.
- [14] P. J. Hedlicka, B. R. Babu, M. D. Sorensen, J. Wengel, *Chem.Commun.* **2004**, 1478-1479.
- [15] V.V. Filichev, B. Vester, L. H. Hansen, E. B. Pedersen, *Nucl.Acids Res.* **2005**, 33, 7129-7137.
- [16] M. Nakamura, Y. Ohtoshi, K. Yamana, *Chem.Commun.* **2005**, 5163-5165.
- [17] Y.J. Cho, E. T. Kool, *ChemBioChem* **2006**, 7, 669-672.
- [18] E. Mayer-Enthart, H. A. Wagenknecht, *Angew.Chem.Int.Ed.* **2006**, 45, 3372- 3375.
- [19] I. Trkulja, R. Häner, *Bioconjugate Chem.* **2007**, 18, 289-292.
- [20] N. Bouquin, V. L. Malinovskii, R. Häner, *Chem.Commun.* **2008**, 1974-1976.
- [21] S. Werder, V. L. Malinovskii, R. Häner, *Org.Lett.* **2008**, 10, 2011-2014.
- [22] R. Häner, S. M. Biner, S. M. Langenegger, T. Meng, V. L. Malinovskii, *Angew.Chem.Int.Ed.* **2010**, 49, 1227-1230.

- [23] S. M. Biner, D. Kummer, V. L. Malinovskii, R. Häner, *Org.Biomol.Chem.* **2011**, 9, 2628-2633.
- [24] M. Probst, D. Wenger, S. M. Biner, R. Häner, *Org.Biomol.Chem.* **2012**, 10, 755-759.
- [25] S. M. Biner, R. Häner, *ChemBioChem* **2011**, 12, 2733-2736.
- [26] F. M. Winnik, *Chem.Rev.* **1993**, 93, 587-614.
- [27] M. Nakamura, Y. Fukunaga, K. Sasa, Y. Ohtoshi, K. Kanaori, H. Hayashi, H. Nakano, K. Yamana, *Nucleic Acids Res.* **2005**, 33, 5887-5895.
- [28] A. L. Nussbaumer, D. Studer, V.L. Malinovskii, R. Häner, *Angew.Chem.Int.Ed.* **2011**, 24, 5490-5494.
- [29] A. Ueno, I. Suzuki, T. Osa, *J.Am.Chem.Soc.* **1989**, 111, 6391-6397.
- [30] H. Mihara, J. Hayashida, H. Hasegawa, H. I. Ogawa, T. Fujimoto, N. Nishino, *J. Chem.Soc.Perkin. Trans. 2*, **1997**, 517-522
- [31] N. Berova, K. Nakanishi, R. W. Woody, *Circular Dichroism – Principles and Applications*, Wiley-VCH: New York, **2000**.
- [32] S. Yagi, H. Kitayama, T. Takagishi, *J Chem.Soc.Perkin. Trans. 1*, **2000**, 925-932
- [33] O. Shoji, D. Nakajima, M. Ohkawa, Y. Fujiwara, M. Annaka, M. Yoshikunu, T. Nakahira, *Macromolecules* **2003**, 36, 4557-4566.
- [34] M. Nakamura, Y. Ohtoshi, K. Yamana, *Chem.Commun.* **2005**, 5163-5165.

9. Outlook

The presented projects in this work have given a brief insight into possible applications of chromophoric aggregations within a DNA framework as signal control systems. Besides the applicability in molecular diagnostic tools the introduced chromophores can also be set in for the construction of DNA architectures. In modern house construction the bricks to build up walls need to be fixed with cement. In our case, the strong stacking properties of the polyaromatic building blocks act as cement. The “bricks” for our constructions are made up with branched DNA structures, in particular *four-way junctions* (4WJ) (Figure 9.1). The 5'-end of each of the four different strands are either *blunt ends* or *sticky ends*. The blunt-ended strands are the stop-units, whereas the sticky-ended sequences assure a continuous growing of the assembly. The sticky ends are either three natural nucleotides or two polyaromatic units. Table 9.1 summarizes the oligonucleotide sequences synthesized for this study.

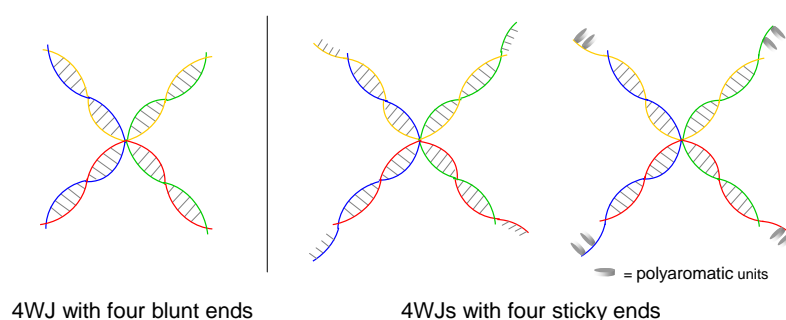


Figure 9.1. Schematic illustration of the three unmixed 4WJs.

Table 9.1. DNA sequences to form 4WJs with either blunt (-) or sticky 5'-ends.

	Sequence (5'-3')	5'- ends
1	TGA TGT GGC TGC	- / GCTC / E / Y / S
2	GCA GCC TGT ACG	- / GCAC / E / Y / S
3	CGT ACA CCG TAC	- / GAGC / E / Y / S
4	GTA CGG ACA TCA	- / GTGC / E / Y / S

The artificial DNA part consists of two 3,4,9,10-perylenetetracarboxylic diimide (PDI, **E**), 1,8-dialkynylpyrene (**Y**) or 1,8-dicarboxamidepyrene (**S**) building blocks (Figure 9.2).

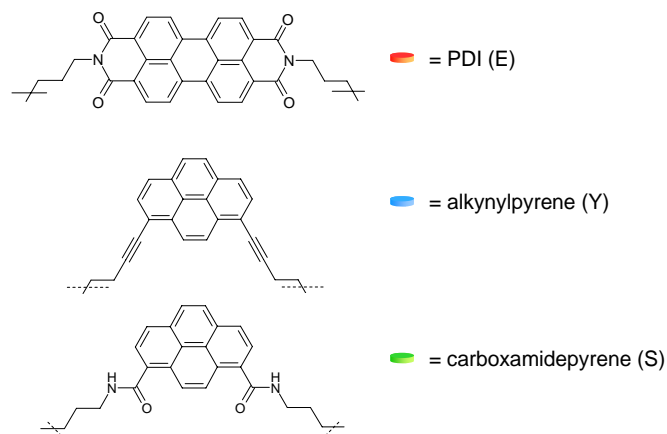


Figure 9.2. Molecular structure of the incorporated building blocks: PDI, (**E**) and the two pyrene derivatives alkylnylpyrene (**Y**) and carboxamidepyrene (**S**).

Depending on the composition of the formed aggregation characteristic fluorescence emission should be detected (Figure 9.3). The interaction between sticky ends with PDI molecules should lead to a non-fluorescent complex, whereas pyrene-pyrene complexes should emit fluorescence.

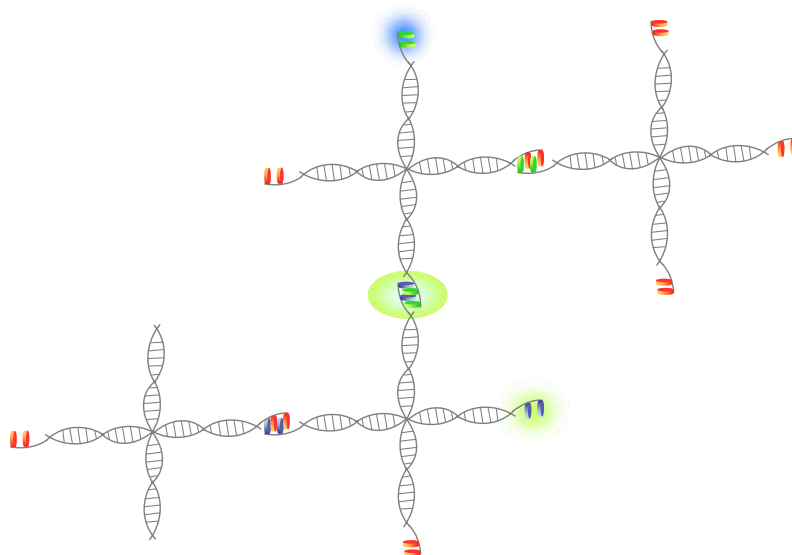


Figure 9.3. Assembly of 4WJs. Excimer signals are highlighted in blue and light green, a possible exciplex formation is represented with both colors and if quenching occurs or a non-fluorescent complex is formed no highlighting spot is drawn.

In mixed pyrene complexes exciplex or excimer formation can occur. However, both aggregation forms should be fluorescent. In contrast to a multichromophoric complex containing PDI units, there it is supposed that the fluorescence is quenched.

The use of DNA as a scaffold for nano-architectures was pioneered by *N. C. Seeman* and co-workers.^[1-3] The aim of our study is to investigate a potential approach to follow the formation of such DNA assemblies and to find out the limits of our design.

References

- [1] N. C. Seeman, *DNA and Cell Biology*. **1991**, 10, 475-486.
- [2] N. C. Seeman, N. R. Kallenbach, *Annu.Rev.Biophys.Biomol.Struct.* **1994**, 23, 53-86.
- [3] N. C. Seeman, *Acc.Chem.Res.* **1997**, 30, 357-363.

APPENDIX

The appendix contains information concerning the presented work and the author of the thesis:

- A.1 List of Abbreviations**
- A.2 List and Collection of the Publications presented in this Work**
- A.3 Curriculum Vitae**
- A.4 Erklärung**

A.1 List of Abbreviations

A	absorption
A	adenine base
A-T	adenine – thymine base pair
BHQ TM	black hole quencher TM
BODIPY	4,4-difluoro-4-bora-3a,4a-diaza-s-indacene
C	cytosine base
CD	circular dichroism
Cy5	cyanine dye
C1'	numbered carbon atom of the ribose molecule
C3'	numbered carbon atom of the ribose molecule
C5'	numbered carbon atom of the ribose molecule
D-A	donor-acceptor complex
D-A-D	donor-acceptor-donor complex
DNA	deoxyribonucleic acid
Dabcyl <i>acid</i>	4-((4-(dimethylamino)phenyl)azo)benzoic acid
E	PDI / 3,4,9,10-perylenetetracarboxylic diimide
(Et ₃ NH)OAc	triethyl amine acetic acid buffer
ESI-TOF MS	electrospray ionization – time of flight mass spectrometry
EDANS <i>acid</i>	5-[(2-aminoethyl)amino]naphthalene-1-sulfonic acid
EtBr	ethidium bromide
eq.	equivalents
ex/em	excitation / emission
F	fluorescence signal
F _{buffer}	fluorescence signal of the corresponding buffer-solution
F _{hybrid}	fluorescence signal of the MB*target hybrid
F _{MB}	fluorescence signal of the MB
FAM	6-carboxy-fluorescein
FITC	fluorescein isothiocyanate
FRET	fluorescence resonance energy transfer

G	guanine base
G-C	guanine- cytosine base pair
H ₂ O	water (deionized, <i>Millipore – ultrapure ionex cartridge 18MΩcm⁻¹</i>)
HPLC	high-performance liquid chromatography
IAEDANS <i>acid</i>	5-({2-[(iodoacetyl)amino]ethyl} amino)naphthalene-1-sulfonic acid
<i>I_{FL}</i>	intensity of the fluorescence signal
LOD	limit of detection
MeCN	acetonitrile
MB	molecular beacon
Mg ₂ Cl	magnesium chloride
<i>N</i>	<i>North</i> conformation of the ribofuranose
NaCl	sodium chloride
NH ₄ OH	ammonium hydroxide
N1	numbered nitrogen atom of the bases molecule
N9	numbered nitrogen atom of the bases molecule
PDI	3,4,9,10-perylenetetra-carboxylic diimide
PMT	photomultiplier tube
PNA	peptide nucleic acid
PCR	polymerase chain reaction
qPCR	quantitative polymerase chain reaction
Q	quenching efficiency
RET	resonance energy transfer
RNA	ribonucleic acid
rRNA	ribosomal ribonucleic acid
R ²	coefficient of determination
T	thymine base
T _m	melting temperature
t _R	retention time
TD	DNA target
TR	RNA target
TTS	triple-helix target site

S	<i>south</i> conformation of the ribofuranose
S/B	signal to background
U	uracil base
UV/Vis	ultraviolet and visible spectroscopy
Y	1,8-dialkynylpyrene
Φ	quantum yield
λ	wavelength
λ_{em}	emission wavelength
λ_{ex}	excitation wavelength
σ	standard deviation
3WJ	three-way junction
4WJ	four-way junction
5WJ	five-way junction

A.2 List and Collection of the Publications presented in this Work

Robert Häner, Sarah M. Biner, Simon M. Langenegger, Tao Meng and Vladimir L. Malinovskii, **A Highly Sensitive, Excimer-Controlled Molecular Beacon**, *Angew. Chem. Int. Ed.* **2010**, 49, 1227–1230.

Sarah M. Biner, Dominic Kummer, Vladimir L. Malinovskii and Robert Häner, **Signal Control by Self-Assembly of Fluorophores in a Molecular Beacon – A Model Study**, *Org. Biomol. Chem.* **2011**, 9, 2628-2633.

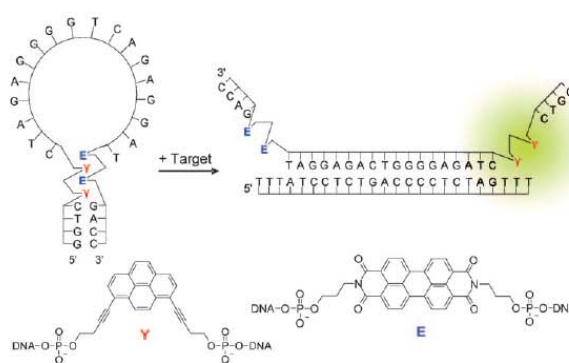
Sarah M. Biner and Robert Häner, **A Two-Color, Self-Controlled Molecular Beacon**, *ChemBioChem* **2011**, 12, 2733-2736.

Molecular Beacons

A Highly Sensitive, Excimer-Controlled Molecular Beacon**

Robert Häner,* Sarah M. Biner, Simon M. Langenegger, Tao Meng, and Vladimir L. Malinovskii

Molecular beacons (MBs) are widely used hairpin probes for the specific detection of DNA and RNA targets.^[1–8] First proposed by Tyagi and Kramer,^[1] the concept of a MB is based on the interaction between a fluorescent and a quenching molecule. In the absence of the target, the MB adopts a hairpin structure resulting in close proximity of the two terminally attached chromophores and, hence, fluorescence quenching, whereas hybridization of the target to the MB loop region leads to spatial separation of fluorophore and quencher and concomitant signal appearance. The choice of the stem is a crucial aspect in the design of MBs. Its stability must be finely tuned to ensure close proximity of the dyes in the native form (\rightarrow low background signal) and, at the same time, allow efficient hybridization with the target (\rightarrow high sensitivity). Additionally, it should not take part in unintended target hybridization, which might adversely affect selectivity, or interfere with formation of the hairpin structure, for example, by binding to the loop sequence which may also lead to an increase in background or a loss in signal intensity. Several types of stem-modified beacons have been presented to address these issues.^[9–15] Incomplete fluorescence quenching in the hairpin form is a well-recognized drawback, and different directions have been described to overcome this problem, including the use of time-resolved fluorescence techniques,^[16] wavelength-shifted^[17–19] or super-quenched beacons,^[20] the formation of triple-helical stems,^[21,22] and stemless peptide nucleic acid beacons.^[23] We propose here a molecular beacon in which signal control is accomplished by formation of a donor–acceptor (D–A) complex.^[24–28] As illustrated in Figure 1, the stem contains pairs of non-nucleosidic pyrenes (Y) and perylene-diiimides (PDIs, E) that can interact by interstrand stacking.^[29–31] In the native structure this leads to efficient signal suppression, whereas the hybridized form is characterized by an excimer signal^[32–35] produced by the two adjacent pyrenes.^[36] Additionally, the formation of a stable D–A complex



MB: 5' GGT **CYY** CTA GAG GGG TCA GAG GAT **EEG** ACC
 TD1: 3' TTT GAT CTC CCC AGT CTC CTA TTT
 TD2: 3' TTT **TAT** CTC CCC AGT CTC CTA TTT
 TD3: 3' TTT GAT CTC **ACC** AGT CTC CTA TTT
 TD4: 3' TTT GAT CTC CCC **ATT** CTC CTA TTT
 TR1: 3' UUU GAU CUC CCC AGU CUC CUA UUU
 TR2: 3' UUU **UAU** CUC CCC AGU CUC CUA UUU
 TR3: 3' UUU GAU CUC **ACC** AGU CUC CUA UUU
 TR4: 3' UUU GAU CUC CCC **AUU** CUC CUA UUU

Figure 1. Top: Illustration of an excimer-controlled molecular beacon; excimer formation between pyrene derivatives (Y) is prevented by D–A complex formation with PDI (E) in the native form. Upon hybridization with the target, PDI and pyrene units are separated whereby excimer formation is enabled. Bottom: MB and target DNA and RNA sequences; bold: target region, bold and underlined: mismatches.

helps to minimize the number of natural bases in the stem, thus reducing the chances of unwanted base-pairing interactions.

The oligomers used in this study are shown in Figure 1. An 18-mer target sequence was chosen arbitrarily. In our molecular beacon **MB** the two pairs of pyrenes and PDIs are located immediately adjacent to either side of the loop region. 1,8-Dialkynylpyrene **Y** is used because it forms a strongly fluorescent excimer with both a large extinction coefficient and a high quantum yield.^[37,38] Moreover, the extension of the pyrene aromatic core with two triple bonds renders this pyrene a particularly electron-rich component for a D–A complex. With four additional base pairs, the stem is of comparable length to that in conventional MBs (5–7 base pairs). D–A interstrand stacking interactions between the electron-rich pyrenes and the electron-poor PDIs support a highly stable secondary structure (see the Supporting Information). This interaction prevents excimer formation and fluorescence emission. Upon titration of our **MB** with the fully matched DNA target **TD1**, a strong excimer signal

[*] Prof. Dr. R. Häner, M. Sc. S. M. Biner, Dr. S. M. Langenegger, Dr. T. Meng, Dr. V. L. Malinovskii
 Department of Chemistry and Biochemistry, University of Bern
 Freiestrasse 3, 3012 Bern (Switzerland)
 Fax: (+41) 31-631-8057
 E-mail: robert.haener@ioc.unibe.ch
 Homepage: <http://www.dcb-server.unibe.ch/groups/haener>

[**] This work was supported financially by the Swiss National Foundation (grant 200020-117617).

Supporting information for this article is available on the WWW under <http://dx.doi.org/10.1002/anie.200905829>.

Communications

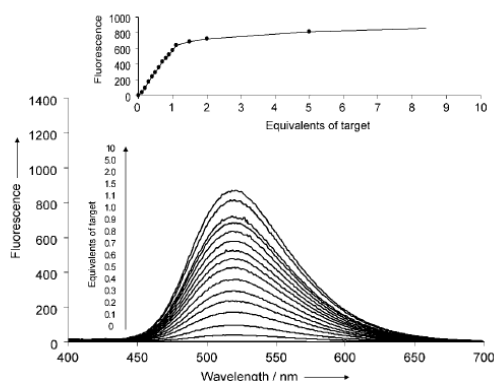


Figure 2. Fluorescence read-out obtained with MB (10^{-6} M) on hybridization with the DNA target TD1 (0 to 10 equiv, in steps as indicated). Conditions: Excitation at 370 nm, slits 10/5 nm; 10 mM phosphate buffer, pH 7.0, 100 mM NaCl, 37 °C. Inset: Concentration-dependent signal intensities at 520 nm. Signal-to-background (S/B)^[39] at 520 nm: 434; quenching efficiency (Q): 99.8%.

around 520 nm is generated, which increases linearly up to 1 equivalent ($R^2=0.997$) of target before leveling off (Figure 2).

The excimer-controlled MB efficiently differentiates between matched and mismatched DNA and RNA targets (Table 1). Mismatches located near the middle of the target

Table 1: Melting temperatures of MB hybridized to DNA and RNA targets obtained from fluorescence measurements (see Figure 3).

DNA hybrid ^[a]	T_m [°C] ^[a]	RNA hybrid ^[a]	T_m [°C] ^[b]
MB-TD1	55	MB-TR1	47
MB-TD2	51	MB-TR2	41
MB-TD3	50	MB-TR3	35
MB-TD4	44	MB-TR4	28

[a] Conditions are given in Figure 3. [b] Estimated error ± 1 °C.

sequence or at the pyrene-bearing end were tested (Figure 1). Temperature-variable fluorescence curves (Figure 3) show a loss of signal intensity with all mismatched targets at substantially lower temperatures than with the matched target. The quantum yield of excimer fluorescence (ϕ) of MB (1×10^{-6} M concentration) in the presence of 1 equivalent of DNA target TD1 was 0.12 (see the Supporting Information). Together with the high absorptivity of the two bis-alkynylpyrenes ($\epsilon \approx 70000 \text{ L mol}^{-1} \text{ cm}^{-1}$)^[37] this translates to a brightness of approximately $8400 \text{ L mol}^{-1} \text{ cm}^{-1}$. Spectral overlap between excimer emission and PDI absorbance is excellent and may, therefore, lead to a partial reduction in signal intensity by means of a FRET mechanism. This potential signal loss, however, is compensated by the high bis-pyrenyl absorptivity.

Fluorescence quenching in conventional MBs is described in the literature as dynamic (FRET mechanism) or static (ground-state complex) quenching.^[40,41] Both static and

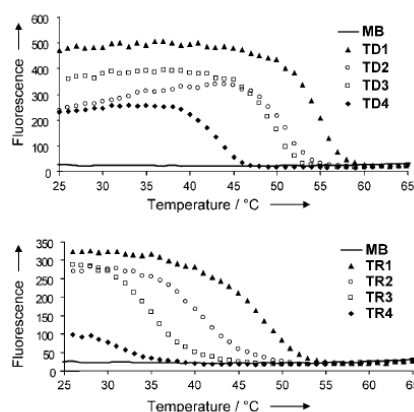


Figure 3. MB excimer signal intensities obtained in the presence of 1 equiv of matched and mismatched DNA (top; TD1–TD4) and RNA (bottom; TR1–TR4) targets. Conditions: MB (1×10^{-7} M), target (1×10^{-7} M); excitation at 370 nm, emission at 520 nm, slits 5/5 nm; 10 mM phosphate buffer, pH 7.0, 100 mM NaCl; only heating ramps are shown.

dynamic quenching are often incomplete, resulting in a strong background signal, which is a major drawback for the detection of target molecules at low concentrations.^[2,6] In the present type of beacon, the excimer signal from the YY dimer that appears in the open form is entirely cancelled in the hairpin structure because of the formation of a D–A complex in the stem with two PDIs.^[42–44] Based on the spectroscopic data formation an EY EY complex seems most likely. UV/Vis and circular dichroism (CD) spectroscopy indicate the stacking of PDI and pyrene units. PDIs are involved in stacking interactions over the whole temperature range (20–90 °C, see the Supporting Information) as indicated by the vibronic band pattern.^[45] The vibronic band pattern of the pyrenes significantly differs from those of previously reported pyrene dimeric stacks.^[37] Furthermore, direct PDI–PDI (E–E) interactions are unlikely because of very weak exciton-coupled CD in the closed form (see the Supporting Information). In the presence of the target (open form) the two PDI units are in direct proximity, and this is accompanied by an increase in the CD couplet. Taken together, these data suggest that an EY EY complex is dominant in the closed form of the beacon.

Fluorescence in the present beacon is suppressed by the physical separation of the two pyrenes. This chromophoric system results in very robust signal characteristics: high signal intensity, largely red-shifted emission, and low background fluorescence. These features allow the detection of the DNA target TD1 at low nanomolar concentrations (Figure 4). In the presence of 10^{-7} M MB, a resolved signal is still obtained at 1×10^{-9} M. Thus, the target is detectable at a concentration corresponding to 1% of the beacon concentration. The calculated detection limit corresponds to a value of 0.3 nM (see the Supporting Information).^[15] To the best of our knowledge such sensitivity has not been reported for molecular beacons in a simple hybridization assay.

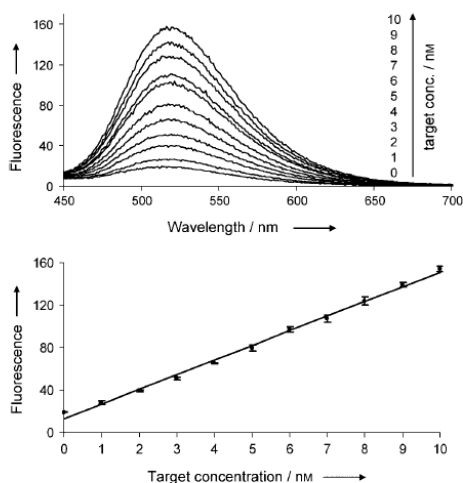


Figure 4. Top: Fluorescence intensities obtained with MB (1×10^{-7} M) in the presence of the DNA target TD1 (1×10^{-8} to 1×10^{-9} M). Bottom: Concentration dependence of the fluorescence signal ($R^2 = 0.996$, independent triplicate experiments); fluorescence measurements were taken after 10 min. Conditions: Excitation at 370 nm, slits 10/5 nm; 10 mM phosphate buffer, pH 7.0, 100 mM NaCl, 37°C.

In conclusion, we have presented an excimer-controlled molecular beacon in which the interaction between two pairs of non-nucleosidic chromophores (pyrene and peryleneimide) located in the stem is used for signal control. Excimer fluorescence is effectively inhibited by formation of a donor-acceptor complex between pyrene and PDI units that prevent the formation of an excited pyrene dimer. The high efficiency of excimer inhibition allows target detection in the presence of a large excess of beacon. In combination with the bright excimer fluorescence of the alkylnylpyrene used, this enables the detection of target sequences at low nanomolar concentrations. The excellent sensitivity renders this type of beacon attractive for cellular imaging as well as for screening applications without prior amplification.

Received: October 16, 2009

Revised: November 19, 2009

Published online: January 12, 2010

Keywords: DNA · donor–acceptor systems · fluorescence · molecular beacons · RNA

- [1] S. Tyagi, F. R. Kramer, *Nat. Biotechnol.* **1996**, *14*, 303–308.
- [2] R. T. Ranasinghe, T. Brown, *Chem. Commun.* **2005**, 5487–5502.
- [3] A. P. Silverman, E. T. Kool, *Trends Biotechnol.* **2005**, *23*, 225–230.
- [4] S. A. E. Marras, S. Tyagi, F. R. Kramer, *Clin. Chim. Acta* **2006**, *363*, 48–60.
- [5] N. Venkatesan, Y. J. Seo, B. H. Kim, *Chem. Soc. Rev.* **2008**, *37*, 648–663.
- [6] K. M. Wang, Z. W. Tang, C. Y. J. Yang, Y. M. Kim, X. H. Fang, W. Li, Y. R. Wu, C. D. Medley, Z. H. Cao, J. Li, P. Colon, H. Lin, W. H. Tan, *Angew. Chem.* **2009**, *121*, 870–885; *Angew. Chem. Int. Ed.* **2009**, *48*, 856–870.
- [7] W. H. Tan, K. M. Wang, T. J. Drake, *Curr. Opin. Chem. Biol.* **2004**, *8*, 547–553.
- [8] P. Santangelo, N. Nitin, G. Bao, *Ann. Biomed. Eng.* **2006**, *34*, 39–50.
- [9] O. Seitz, *Angew. Chem.* **2000**, *112*, 3389–3392; *Angew. Chem. Int. Ed.* **2000**, *39*, 3249–3252.
- [10] H. Kuhn, V. V. Demidov, J. M. Coull, M. J. Fiandaca, B. D. Gildea, M. D. Frank-Kamenetskii, *J. Am. Chem. Soc.* **2002**, *124*, 1097–1103.
- [11] C. Crey-Desbiolles, D. R. Ahn, C. J. Leumann, *Nucleic Acids Res.* **2005**, *33*, e77.
- [12] L. Wang, C. Y. J. Yang, C. D. Medley, S. A. Benner, W. H. Tan, *J. Am. Chem. Soc.* **2005**, *127*, 15664–15665.
- [13] Y. Saito, Y. Shinohara, S. S. Bag, Y. Takeuchi, K. Matsumoto, I. Saito, *Tetrahedron* **2009**, *65*, 934–939.
- [14] Y. Ueno, A. Kawamura, K. Takasu, S. Komatsuzaki, T. Kato, S. Kuboe, Y. Kitamura, Y. Kitade, *Org. Biomol. Chem.* **2009**, *7*, 2761–2769.
- [15] E. Socher, D. V. Jarikote, A. Knoll, L. Roglin, J. Burmeister, O. Seitz, *Anal. Biochem.* **2008**, *375*, 318–330.
- [16] P. Conlon, C. J. Yang, Y. Wu, Y. Chen, K. Martinez, Y. Kim, N. Stevens, A. A. Marti, S. Jockusch, N. J. Turro, W. Tan, *J. Am. Chem. Soc.* **2008**, *130*, 336–342.
- [17] S. Tyagi, S. A. E. Marras, F. R. Kramer, *Nat. Biotechnol.* **2000**, *18*, 1191–1196.
- [18] P. Zhang, T. Beck, W. H. Tan, *Angew. Chem.* **2001**, *113*, 416–419; *Angew. Chem. Int. Ed.* **2001**, *40*, 402–405.
- [19] A. Tsourkas, M. A. Behlke, Y. Q. Xu, G. Bao, *Anal. Chem.* **2003**, *75*, 3697–3703.
- [20] C. J. Yang, H. Lin, W. Tan, *J. Am. Chem. Soc.* **2005**, *127*, 12772–12773.
- [21] T. N. Grossmann, L. Roglin, O. Seitz, *Angew. Chem.* **2007**, *119*, 5315–5318; *Angew. Chem. Int. Ed.* **2007**, *46*, 5223–5225.
- [22] Y. Xiao, K. J. I. Plakos, X. H. Lou, R. J. White, J. R. Qian, K. W. Plaxco, H. T. Soh, *Angew. Chem.* **2009**, *121*, 4418–4422; *Angew. Chem. Int. Ed.* **2009**, *48*, 4354–4358.
- [23] E. Socher, L. Bethge, A. Knoll, N. Jungnick, A. Herrmann, O. Seitz, *Angew. Chem.* **2008**, *120*, 9697–9701; *Angew. Chem. Int. Ed.* **2008**, *47*, 9555–9559.
- [24] C. A. Hunter, J. K. M. Sanders, *J. Am. Chem. Soc.* **1990**, *112*, 5525–5534.
- [25] W. Y. Zhang, W. R. Dichtel, A. Z. Stieg, D. Benitez, J. K. Gimzewski, J. R. Heath, J. F. Stoddart, *Proc. Natl. Acad. Sci. USA* **2008**, *105*, 6514–6519.
- [26] F. Würthner, *Chem. Commun.* **2004**, 1564–1579.
- [27] J. J. Reczek, B. L. Iverson, *Macromolecules* **2006**, *39*, 5601–5603.
- [28] Z. Merican, K. D. Johnstone, M. J. Gunter, *Org. Biomol. Chem.* **2008**, *6*, 2534–2543.
- [29] a) S. M. Langenegger, R. Häner, *Bioorg. Med. Chem. Lett.* **2006**, *16*, 5062–5065; b) S. M. Langenegger, R. Häner, *Chem. Commun.* **2004**, 2792–2793.
- [30] V. L. Malinovskii, F. Samain, R. Häner, *Angew. Chem.* **2007**, *119*, 4548–4551; *Angew. Chem. Int. Ed.* **2007**, *46*, 4464–4467.
- [31] V. L. Malinovskii, D. Wenger, R. Häner, *Chem. Soc. Rev.* **2010**, DOI: 10.1039/B910030J.
- [32] F. M. Winnik, *Chem. Rev.* **1993**, *93*, 587–614.
- [33] F. Samain, V. L. Malinovskii, S. M. Langenegger, R. Häner, *Bioorg. Med. Chem.* **2008**, *16*, 27–33.
- [34] R. Häner, F. Samain, V. L. Malinovskii, *Chem. Eur. J.* **2009**, *15*, 5701–5708.
- [35] V. A. Galievsky, V. L. Malinovskii, A. S. Stasheuski, F. Samain, K. A. Zachariasse, R. Häner, V. S. Chirvony, *Photochem. Photobiol. Sci.* **2009**, *8*, 1448–1454.
- [36] For alternative approaches using pyrene excimer formation in molecular beacons, see: a) K. Fujimoto, H. Shimizu, M. Inouye,

Communications

- J. Org. Chem.* **2004**, *69*, 3271–3275; b) I. Trkulja, S. M. Biner, S. M. Langenegger, R. Häner, *ChemBioChem* **2007**, *8*, 25–27; c) K. Yamana, Y. Ohshita, Y. Fukunaga, M. Nakamura, A. Maruyama, *Bioorg. Med. Chem.* **2008**, *16*, 78–83; d) P. Conlon, C. J. Yang, Y. Wu, Y. Chen, K. Martinez, Y. Kim, N. Stevens, A. A. Marti, S. Jockusch, N. J. Turro, W. Tan, *J. Am. Chem. Soc.* **2008**, *130*, 336–342; e) S. Thurley, L. Roglin, O. Seitz, *J. Am. Chem. Soc.* **2007**, *129*, 12693–12695; f) E. Mayer, L. Valis, C. Wagner, M. Rist, N. Amann, H. A. Wagenknecht, *ChemBioChem* **2004**, *5*, 865–868; g) I. V. Astakhova, V. A. Korshun, J. Wengel, *Chem. Eur. J.* **2008**, *14*, 11010–11026; thiazole orange as fluorophore: h) S. Berndt, H. A. Wagenknecht, *Angew. Chem.* **2009**, *121*, 2454–2457; *Angew. Chem. Int. Ed.* **2009**, *48*, 2418–2421; exciplex-based probe: i) A. Gbaj, L. Walsh, M. C. Rogert, A. Sardarian, E. V. Bichenkova, L. L. Etchells, D. Whitcombe, K. T. Douglas, *Biosci. Rep.* **2008**, *28*, 1–5; ends-free molecular beacons: j) Y. Saito, Y. Shinohara, S. S. Bag, Y. Takeuchi, K. Matsumoto, I. Saito, *Tetrahedron* **2009**, *65*, 934–939; k) H. Kashida, T. Takatsu, T. Fujii, K. Sekiguchi, X. G. Liang, K. Niwa, T. Takase, Y. Yoshida, H. Asanuma, *Angew. Chem.* **2009**, *121*, 7178–7181; *Angew. Chem. Int. Ed.* **2009**, *48*, 7044–7047.
- [37] H. Bittermann, D. Siegemund, V. L. Malinovskii, R. Häner, *J. Am. Chem. Soc.* **2008**, *130*, 15285–15287.
- [38] S. Uno, C. Dohno, H. Bittermann, V. L. Malinovskii, R. Häner, K. Nakatani, *Angew. Chem.* **2009**, *121*, 7498–7501; *Angew. Chem. Int. Ed.* **2009**, *48*, 7362–7365.
- [39] J. A. M. Vet, S. A. E. Marras in *Oligonucleotide Synthesis: Methods and Applications*, Humana, Totowa, NJ, **2004**, p. pp. 273–290.
- [40] S. A. E. Marras, F. R. Kramer, S. Tyagi, *Nucleic Acids Res.* **2002**, *30*, 122e.
- [41] T. Förster, *Naturwissenschaften* **1946**, *33*, 166–175.
- [42] C. A. Hunter, K. R. Lawson, J. Perkins, C. J. Urch, *J. Chem. Soc. Perkin Trans. 2* **2001**, 651–669.
- [43] E. A. Meyer, R. K. Castellano, F. Diederich, *Angew. Chem.* **2003**, *115*, 1244–1287; *Angew. Chem. Int. Ed.* **2003**, *42*, 1210–1250.
- [44] N. Bouquin, V. L. Malinovskii, R. Häner, *Chem. Commun.* **2008**, 1974–1976.
- [45] R. Carmieli, T. A. Zeidan, R. F. Kelley, Q. Mi, F. D. Lewis, M. R. Wasielewski, *J. Phys. Chem. A* **2009**, *113*, 4691–4700.

Signal control by self-assembly of fluorophores in a molecular beacon—a model study†

Sarah M. Biner, Dominic Kummer, Vladimir L. Malinovskii and Robert Häner*

Received 7th December 2010, Accepted 14th January 2011

DOI: 10.1039/c0ob01132k

Pyrene excimer fluorescence is efficiently regulated through formation of π -stacked aggregates between dialkynylpyrene (Y) and peryleneimide (E) residues located in the stem region of a molecular beacon (MB). The building blocks form organized, multichromophoric complexes in the native form. Hybridization to the target results in a conformational reorganization of the chromophores. The nature of the aggregates was investigated by changing the number of chromophores and natural base pairs in the beacon stem. The formation of different types of complexes (EY EY \rightarrow YEY \rightarrow EY) is revealed by characteristic spectroscopic changes. The data show that signal control is an intrinsic property of the interacting chromophores. The directed assembly of non-nucleosidic chromophores can be used for the generation of an *on/off* switch of a fluorescence signal. The concept may find applications in various types of light-based input/output systems.

Introduction

Molecular beacons (MBs) are hairpin-shaped oligonucleotide probes, in which the loop region contains the target recognition sequence and the stem part enables the generation of a fluorescent diagnostic signal.^{1–4} The composition of the stem represents an essential aspect for the successful design of a MB. The stability of the stem has to be balanced to ensure the complete suppression of fluorescence in the closed form and, on the other hand, an efficient formation of the target-beacon complex.^{4–8} Fluorescence quenching in hairpin-type MBs is based on the formation of a non-fluorescent ground state complex between fluorophore and quencher or *via* resonance energy transfer (FRET), corresponding to static and dynamic quenching, respectively.^{9,10} Incomplete quenching of the signal in the closed form is one of the major drawbacks of MBs for highly sensitive applications. Therefore, the development of new fluorophores and/or quenchers^{11–21} as well as innovative fluorophore–quencher systems is in continuous progress.^{18,22–31} Improved spectroscopic properties as well as hybridization behaviour were also observed with stem modified MBs.^{32–38}

In the course of our work on non-nucleosidic DNA building blocks,^{39–47} we have shown that alkynyl- and triazole-substituted pyrenes^{48–50} possess excellent fluorescence properties. Large extinction coefficients and quantum yields result in a high brightness of these fluorophores. Excimer fluorescence of these pyrenes is nearly environment independent⁵⁰ and may, therefore, be used as a robust

output signal in sensor applications.^{51,52} Recently, we reported that the placement of two peryleneimide (PDI) units opposite to two pyrenes led to very efficient suppression of the excimer signal.^{26,53} The very low background observed with this stem design opens the possibility of using the beacon in a considerable excess over the target, which is often not possible due to incomplete quenching.

This article provides an extended study on the origin of this remarkable signal suppression. The present type of MB possesses a detection system based on the formation of a donor–acceptor (D–A) type complex between 1,4-dialkynylpyrenes and PDI units (Scheme 1).²⁶ The combination of this chromophore complex with natural base pairs renders this stem a valuable module for fluorogenic detection systems. Control of fluorescence is based on specific interactions between the two types of chromophores. The organization of this multichromophoric complex is the reason for the excellent signal control. Since this type of π -stacked architecture^{54–69} can also be applied to other sensor systems, we studied the chromophore organization in more detail. Here, we demonstrate that the supramolecular self-assembly of donor–acceptor π -aggregates serves as a highly reliable and robust system for the control of fluorescence and represents an alternative to the classic MB design.

Results and discussion

For the study of the PDI–pyrene interaction, a set of MBs (MB1 to MB5) varying in the composition of the stem was synthesized (Table 1). Both chromophores possess a strong absorptivity and exhibit a high sensitivity towards stacking interactions which can conveniently be followed by changes in the relative vibronic band intensities ($A^{0\rightarrow0}/A^{0\rightarrow1}$ transitions).^{49,70–72} Since the longest wavelength absorption of the two different chromophores appears

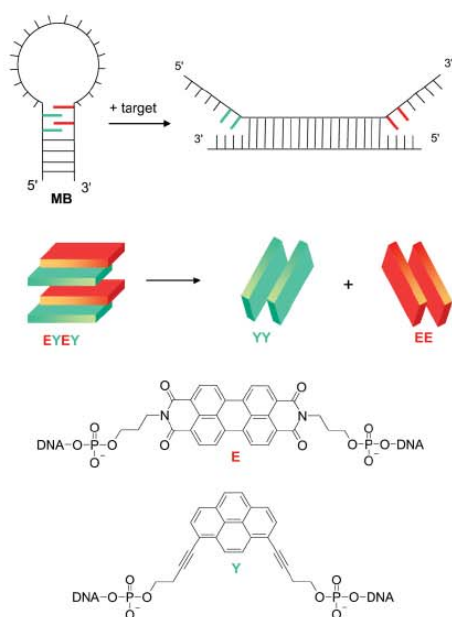
Department of Chemistry and Biochemistry, University of Bern, Freiestrasse 3, 3012, Bern, Switzerland. E-mail: Robert.haener@ioc.unibe.ch

† Electronic supplementary information (ESI) available: Synthetic and analytical details; additional UV/Vis, fluorescence and CD spectra. See DOI: 10.1039/c0ob01132k

Table 1 Sequences of molecular beacons (MB1 to MB5) and targets (T1 to T4)

	Sequence
MB1	5' GGT CYY CTA GAG GGG TCA GAG GAT EEG ACC
MB2	5' T CYY CTA GAG GGG TCA GAG GAT EEG A
MB3	5' YY CTA GAG GGG TCA GAG GAT EE
MB4	5' T CYY CTA GAG GGG TCA GAG GAT EGA
MB5	5' GGT CTY CTA GAG GGG TCA GAG GAT EAG ACC
T1	3' TTT GAT CTC CCC AGT CTC CTA TTT
T2	3' TTT TAT CTC CCC AGT CTC CTA TTT
T3	3' TTT GAT CTC <u>ACC</u> AGT CTC CTA TTT
T4	3' TTT GAT CTC CCC <u>ATT</u> CTC CTA TTT

The chromophores alkylnylpyrene (Y) and PDI (E) are highlighted in bold and the mismatches are underlined.



Scheme 1 Illustration of signal control through self-assembly of aromatic chromophores in a molecular beacon (MB). Generation of the fluorescence signal is regulated by conformational rearrangement of multichromophoric assembly of alkylnylpyrene (Y) and PDI (E) building blocks.

in separate regions of the UV/Vis spectra (dialkylnylpyrene, Y: 330–420 nm; PDI, E: 420–650 nm) conformational changes and aggregation processes can be followed for each type of the chromophores independently.

Fig. 1 shows the changes in vibronic band intensities between open (presence of 1.2 eq. of T1) and closed (absence of target) form of MB1. A high degree of PDI stacking is revealed by the strong intensity of the 0→1 transition in the open form, in which the PDI units are in close proximity. In the closed form, the PDI–PDI interaction is significantly reduced. This suggests the formation of a different molecular complex. The same pattern is observed in the pyrene area: the vibronic band intensity ratio varies strongly between open and closed form, showing pronounced pyrene–pyrene interactions in the presence of the target. Intensity ratios

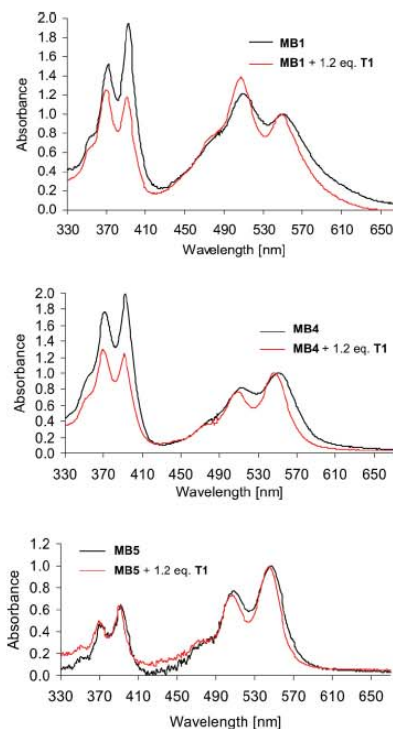


Fig. 1 Normalized UV/Vis absorption spectra at 20 °C of MB1 (top), MB4 (middle) and MB5 (bottom), MB (black line) and with 1.2 equivalents of the target T1 (red line, normalized at the 0→0 transition band of PDI).

of the vibronic bands are listed in Table 2. These observations are compatible with interstrand stacking interactions between PDI and dialkylnylpyrene units in an alternating mode (EYEY) in the stem part of the closed beacon. These findings correlate with the well-described effects of hydrophobic stacking interactions between PDI derivatives in a polar environment.^{73–76} Furthermore, they are in best agreement with the described distance dependence of vibronic band intensity ratios in DNA–PDI constructs.⁷⁷ The same qualitative behaviour was also observed for beacons MB2 and MB3 (Table 2 and SI). In MB4 and MB5 (Fig. 1), which contain only a single PDI, the ratio of A^{0→0}/A^{0→1} transitions indicates non-aggregated PDIs in both closed and open form. Therefore, we can conclude that the significant increase of the

Table 2 Absorption ratios of the 0→0 to the 0→1 transition at 20 °C^a

	A ^{0→0} /A ^{0→1} alkylnylpyrenes ^b		A ^{0→0} /A ^{0→1} PDI ^c	
	No target (closed)	1.2 eq. T1 (open)	No target (closed)	1.2 eq. T1 (open)
MB1	1.28	0.94	0.84	0.72
MB2	1.19	0.90	0.74	0.71
MB3	1.19	1.06	0.76	0.73
MB4	1.12	0.96	1.22	1.31
MB5	1.39	1.29	1.30	1.36

^a Conditions: 100 mM NaCl, 10 mM sodium phosphate buffer, pH 7.0; ^b 330–420 nm; ^c 420–650 nm.

0→1 transition is primarily due to PDI–PDI and not to PDI–pyrene interactions. Pyrene aggregation is observed for all beacons containing two adjacent pyrenes in the open form. The pyrene vibronic band ratios observed for **MB4** suggest that the same conclusions can also be drawn for the pyrene building block, *i.e.* the pyrene 0→1 transition is most sensitive to pyrene–pyrene interactions, but not for pyrene–PDI interactions (see Fig. 1, **MB5**). The results support the model shown in Scheme 1, in which mixed aggregates (**EY**EY) are present in the closed form and, upon opening of the stem part, self-aggregates (**EE** and **YY**) are formed (see Scheme 1).

Further insight into chromophore organization was obtained by circular dichroism (CD) spectroscopy. Variable temperature spectroscopy of **MB2** (Fig. 2) shows a signal signature for the pyrene units [394 nm (+), 382 nm (–) and 362 nm (–)] and the PDI building blocks [561 nm (+), 499 nm (–)]. The spectra at long wavelengths show a positive bisignate signal characteristic for an exciton coupling^{78,79} between the PDI units. The signal of the alkynylpyrene building blocks at shorter wavelengths indicates that exciton coupling also takes place between the pyrene units. However, the CD signal originating from alkynylpyrene interactions is different from the one observed previously in a DNA hybrid in which two alkynylpyrenes were placed in close contact leading to a **YY** interaction.⁴⁹ This difference in CD signature can be attributed to the separation of the alkynylpyrenes by PDI units that leads to an alternating **EY**EY π -stack. The CD signatures in the 300–600 nm region gradually disappear with increasing temperature.

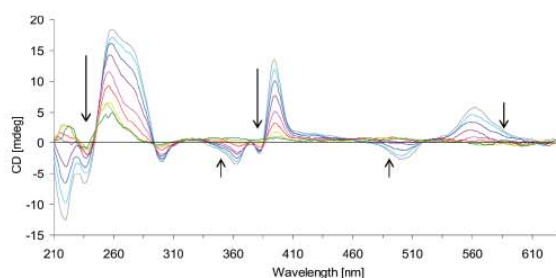


Fig. 2 Variable temperature CD spectroscopy of **MB2** from 10 to 90 °C in 10 °C increments. Arrows indicate increasing temperature. Conditions: 5.0 μ M **MB2**, 100 mM NaCl, 10 mM sodium phosphate buffer, pH 7.0.

The spectra of **MB1** in the presence and the absence of target **T1** are shown in Fig. 3. Addition of **T1** leads to gradual change of this pyrene CD signal (from $A = +100$ to $A = -15$), whereas the strength of the PDI couplet is increasing (from $A = +26$ to $A = +64$). This finding is explained by the strong hydrophobic PDI interactions in an aqueous environment.

The formation of **EY**EY aggregates follows the well-documented pattern of donor–acceptor π -interactions.^{60,80–84} such as arene–perfluoroarene^{85–89} or pyrene–naphthalenediimide aromatic interactions.^{90–95} The present pyrene–PDI aggregation seems to proceed after this motif.

A worthy goal in the design of MBs consists in the reduction of the stem to a minimal length. The difference between **MB1** and **MB2** is a reduction of the stem length from four to two natural base pairs. Fig. 4 shows the fluorescence curves obtained upon hybridization to the target. The quenching efficiency in the

Table 3 Quenching efficiency ($Q\%$) values for **MB1**–**MB5** in presence of 1 eq. target^a

	MB1 ²⁶	MB2	MB3	MB4	MB5
Q (%)	99.7	97.2	53.1	91.5	36.9

^a Conditions: 100 mM NaCl, 10 mM sodium phosphate buffer, pH 7.0; 37 °C, excitation: 370 nm; values were determined at emission maxima.

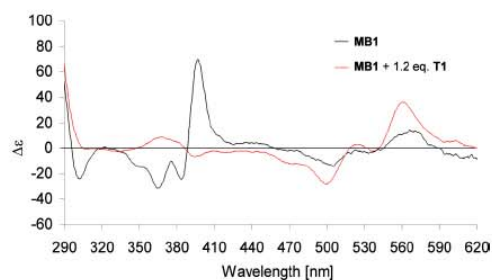


Fig. 3 CD spectra of **MB1** at 20 °C (black line) and with 1.2 equiv. of target **T1** (red line). Conditions: 100 mM NaCl, 10 mM sodium phosphate buffer, pH 7.0.

absence of the target is approx. 97% (Table 3), which is excellent in view of the shortness and simplicity of the stem. In addition, **MB2** exhibited a mismatch discrimination comparable to **MB1** (SI) when hybridized to control oligomers **T2**–**T4**.

Further simplification was tested with **MB3** containing no natural base pairs in the stem. Formation of a stem–loop structure can be expected through intramolecular stacking interactions between the two alkynylpyrene and PDI building blocks that are located at the ends of the oligomer. The UV/Vis spectrum shows PDI and dialkynylpyrene aggregation also for this MB. However, the degree of quenching in the absence of the target is greatly diminished (SI). Furthermore, the CD spectra (Fig. 5) exhibit a remarkable temperature dependent behaviour in the PDI area (410–510 nm). These changes may well be due to PDI-mediated formation of dimers or larger aggregates at low temperature. It is likely that individual molecules associate also *intermolecularly* through stacking interactions between the PDI and/or pyrene residues located at their ends. The formation of interstrand assemblies of DNA conjugates through interaction of sticky ends formed with porphyrine⁶⁶ or PDI⁶⁷ derivatives was recently demonstrated. The intensity of the broad, unstructured band between 410 nm and 510 nm is significantly reduced on increasing the temperature, which may indicate thermal disaggregation. Therefore, we attribute the broadening of this band to partial intermolecular PDI aggregation.

In the presence of target **T1** (Fig. 6), substantial temperature dependent CD changes are observed in the pyrenyl area of **MB3**. The negative Cotton-effect in the alkynylpyrene signature including an intense negative signal at ~390 nm indicates a change in the aggregation state of the building blocks. These changes may have their origin in competing intra- and intermolecular aggregation of the stemless beacon: at low temperature, interactions between PDI and pyrene sticky ends predominate and at high temperature, after dissociation from the target, the pyrenes adopt the same **EY**(Y) conformation as observed with the beacons containing additional base pairs (**MB1** and **MB2**). In the PDI region, the CD

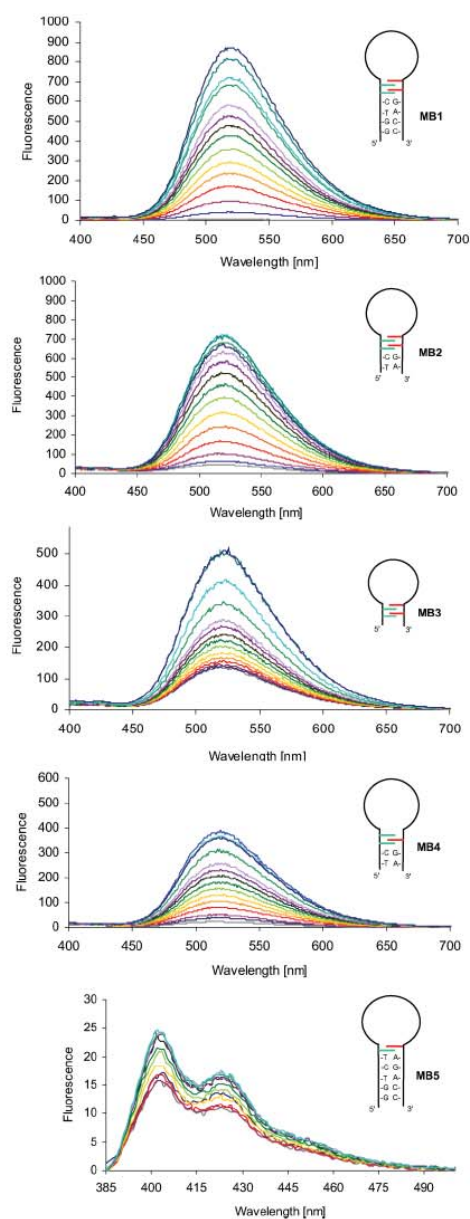


Fig. 4 Fluorescence spectra of MB1–MB5. Conditions: MB1, MB2, MB3, MB4 1.0 μM , T1 0 to 10 equiv., MB5 0.1 μM , T1 0 to 2 equiv., (lines correspond to: 0, 0.1, 0.2, 0.3, 0.4, 0.5, 0.6, 0.7, 0.8, 0.9, 1.0, 1.5, 2.0, 5.0, 10 equiv.), 10 mM sodium phosphate buffer pH 7.0, 100 mM NaCl. Excitation: 370 nm; Temp.: 37 $^{\circ}\text{C}$.

spectrum shows a negative Cotton-effect and a broadening of the band at shorter wavelengths. These observations can be due to a dangling PDI unit at the 3'-end of the stem while the PDI closer to the loop region can interact as described above with the two alkynylpyrenes. These findings support the occurrence of donor–acceptor interactions among the chromophores in MB3 but they also suggest that this type of (stemless) beacon is less suitable for

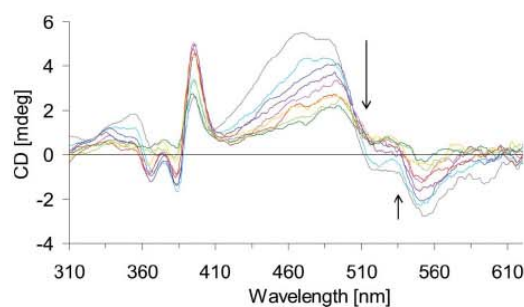


Fig. 5 Variable temperature CD spectroscopy of MB3 from 10 to 90 $^{\circ}\text{C}$ in 10 $^{\circ}\text{C}$ increments. Arrows indicate increasing temperature. Conditions: 5.0 μM MB3, 100 mM NaCl, 10 mM sodium phosphate buffer, pH 7.0.

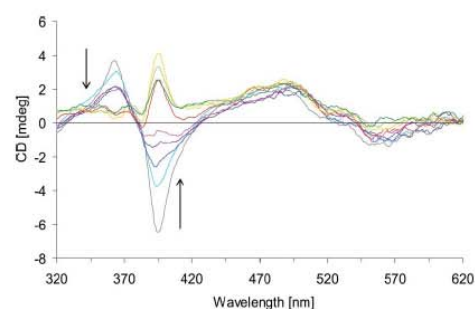


Fig. 6 Temperature-dependent CD spectra for MB3 in presence of T1 from 10 to 90 $^{\circ}\text{C}$ in 10 $^{\circ}\text{C}$ increments. Arrows indicate spectral changes with increasing temperature. Conditions: 5.0 μM MB3, 6.0 μM T1, 100 mM NaCl, 10 mM sodium phosphate buffer, pH 7.0.

practical use due to the increased competition between inter- and intramolecular stacking of the aromatic chromophores.

The fluorescence data obtained with MB4 (Fig. 4) are quite remarkable. This MB contains only a single PDI yet the excimer signal is largely suppressed in the closed form (Table 3). The excellent signal control can be attributed to the formation of a YEY (donor–acceptor–donor) complex. MB5 contains only a single pyrene and a single PDI and allows, therefore, a direct comparison between monomer and excimer based sensing systems. The findings reveal the high value of the pyrene excimer read-out. In comparison to beacons MB1–MB4, which are all based on excimer formation, MB5 shows (i) a very weak (monomer) signal (Fig. 4, bottom) and (ii) very poor signal quenching in the absence of the target (Table 3).

The UV/Vis and CD data obtained for MB1, MB2 and MB3 (see also SI) were quite similar despite significantly differing numbers of natural bases in the stem. This indicates that the organization of the PDI/pyrene complex is an intrinsic property of the chromophoric building blocks and largely independent from the DNA part. Therefore, in the context of supramolecular chemistry, the loop of the MB may be regarded as a flexible linker between the components of the directed assembly. The target sequence serves as an external factor that induces a conformational reorganization of the supramolecular complex under isothermal conditions. Furthermore, it should also be mentioned that this study allows the direct comparison of optical properties and stacking interactions of both types of chromophores (pyrene and

PDI) in a single experiment at equal conditions. The UV/Vis and CD effects are comparable for the two types of compounds. Pyrene interactions lead to pronounced fluorescence signals while the PDI aggregates are basically non-fluorescent.

Conclusions

We have demonstrated that the directed assembly of chromophores can be used as an *on/off* switch for a fluorescence signal. Pyrene excimer fluorescence is efficiently regulated by formation of π -stacked aggregates between non-nucleosidic dialkynylpyrenes and PDI residues located in the stem region of the MB. By varying the numbers of pyrene (Y) and PDI (E) residues we could show that the two types of chromophores interact in a donor–acceptor fashion in the closed form. The formation of various types of complexes ($EY E Y \rightarrow Y E Y \rightarrow E Y$) is revealed by characteristic changes in CD, UV/Vis and fluorescence spectra. Conformational changes induced by target recognition lead to direct pyrene–pyrene interaction and, thus, efficient excimer fluorescence. Highest quenching efficiency was obtained with two PDIs placed opposite two pyrenes in MB1 and MB2. A single PDI, however, showed also surprisingly strong excimer signal inhibition (MB4). A longer stem gave better quenching efficiencies (MB1 vs. MB2 vs. MB3). Finally, the approach of using aromatic π -stacking works largely better for control of excimer than of monomer suppression (e.g. MB1 vs. MB5). The data show that signal control is an intrinsic property of the interacting chromophores. Therefore, the concept described herein represents a functional module that may find applications not only in MBs but also in other input/output systems using light as the source of information.^{96–98}

Experimental section

Synthetic and analytical procedure

The building blocks alkynylpyrene (Y)⁹⁹ and PDI (E)⁹⁹ were synthesized as previously described. The oligonucleotide T1 was obtained commercially from Microsynth, Balgach, Switzerland. MB1 to MB5 were prepared *via* automated oligonucleotide synthesis by an adapted synthetic procedure on a 394-DNA/RNA synthesizer (Applied Biosystems). Cleavage from the solid support and final deprotection was done by treatment with 30% NH₄OH solution at 55 °C overnight. Purification was performed by reverse phase HPLC (LiChrospher 100 RP-18, 5 μ m, Merck; Shimadzu LC-20AT and Kontron). Mass spectrometry was done with a Sciex QSTAR pulsar (hybrid quadrupole time-of-flight mass spectrometer, Applied Biosystems); ESI-TOF MS (negative mode, acetonitrile–H₂O–triethylamine). Temperature-dependent UV/Vis spectra were measured on a Varian Cary-100 Bio-UV/Vis spectrophotometer equipped with a Varian Cary-block temperature controller and data were collected with Varian WinUV software over the range of 200–700 nm between 10 and 90 °C. CD spectra were recorded on a JASCO J-715 spectrophotometer using quartz cuvettes with an optic path of 1 cm. Fluorescence spectra were measured on a Varian Cary Eclipse fluorescence spectrophotometer equipped with a Varian Cary-block temperature controller using 1 cm \times 1 cm quartz cuvettes. Excitation wavelength: MB1 to MB5 370 nm. Varian Eclipse software was used to investigate the fluorescence data at

a wavelength range of 375–700 nm in the temperature range of 20–90 °C. All measurements were performed in 10 mM sodium phosphate buffer pH 7.0 and 100 mM NaCl.

Acknowledgements

This work was supported by the Swiss National Foundation (200020-132581).

Notes and references

- S. Tyagi and F. R. Kramer, *Nat. Biotechnol.*, 1996, **14**, 303–308.
- R. T. Ranasinghe and T. Brown, *Chem. Commun.*, 2005, 5487–5502.
- B. Juskowiak, *Anal. Bioanal. Chem.*, 2010, DOI: 10.1007/s00216-010-4304-5.
- K. M. Wang, Z. W. Tang, C. Y. J. Yang, Y. M. Kim, X. H. Fang, W. Li, Y. R. Wu, C. D. Medley, Z. H. Cao, J. Li, P. Colon, H. Lin and W. H. Tan, *Angew. Chem., Int. Ed.*, 2009, **48**, 856–870.
- A. P. Silverman and E. T. Kool, *Trends Biotechnol.*, 2005, **23**, 225–230.
- S. A. E. Marras, S. Tyagi and F. R. Kramer, *Clin. Chim. Acta*, 2006, **363**, 48–60.
- N. Venkatesan, Y. J. Seo and B. H. Kim, *Chem. Soc. Rev.*, 2008, **37**, 648–663.
- P. Santangelo, N. Nitin and G. Bao, *Ann. Biomed. Eng.*, 2006, **34**, 39–50.
- S. A. E. Marras, F. R. Kramer and S. Tyagi, *Nucleic Acids Res.*, 2002, **30**, e122.
- T. Förster, *Naturwissenschaften*, 1946, **33**, 166–175.
- K. Fujimoto, H. Shimizu and M. Inouye, *J. Org. Chem.*, 2004, **69**, 3271–3275.
- P. Conlon, C. J. Yang, Y. Wu, Y. Chen, K. Martinez, Y. Kim, N. Stevens, A. A. Marti, S. Jockusch, N. J. Turro and W. Tan, *J. Am. Chem. Soc.*, 2008, **130**, 336–342.
- E. Socher, L. Bethge, A. Knoll, N. Jungnick, A. Herrmann and O. Seitz, *Angew. Chem., Int. Ed.*, 2008, **47**, 9555–9559.
- I. V. Astakhova, V. A. Korshun and J. Wengel, *Chem.–Eur. J.*, 2008, **14**, 11010–11026.
- V. V. Filichev, I. V. Astakhova, A. D. Malakhov, V. A. Korshun and E. B. Pedersen, *Chem.–Eur. J.*, 2008, **14**, 9968–9980.
- H. Kashida, T. Takatsu, T. Fujii, K. Sekiguchi, X. G. Liang, K. Niwa, T. Takase, Y. Yoshida and H. Asanuma, *Angew. Chem., Int. Ed.*, 2009, **48**, 7044–7047.
- Y. Ueno, A. Kawamura, K. Takasu, S. Komatsuzaki, T. Kato, S. Kuboe, Y. Kitamura and Y. Kitade, *Org. Biomol. Chem.*, 2009, **7**, 2761–2769.
- Y. Saito, Y. Shinohara, S. S. Bag, Y. Takeuchi, K. Matsumoto and I. Saito, *Tetrahedron*, 2009, **65**, 934–939.
- R. Varghese and H. A. Wagenknecht, *Org. Biomol. Chem.*, 2010, **8**, 526–528.
- U. Förster, C. Grunewald, J. W. Engels and J. Wachtveitl, *J. Phys. Chem. B*, 2010, **114**, 11638–11645.
- K. Giessler, H. Griesser, D. Gohringer, T. Sabirov and C. Richert, *Eur. J. Org. Chem.*, 2010, 3611–3620.
- T. N. Grossmann, L. Roglin and O. Seitz, *Angew. Chem., Int. Ed.*, 2007, **46**, 5223–5225.
- J. N. Wilson, Y. J. Cho, S. Tan, A. Cuppoletti and E. T. Kool, *ChemBioChem*, 2008, **9**, 279–285.
- I. Trkulja, S. M. Biner, S. M. Langenegger and R. Häner, *ChemBioChem*, 2007, **8**, 25–27.
- I. V. Nesterova, S. S. Erdem, S. Pakhomov, R. P. Hammer and S. A. Soper, *J. Am. Chem. Soc.*, 2009, **131**, 2432–2433.
- R. Häner, S. M. Biner, S. M. Langenegger, T. Meng and V. L. Malinovskii, *Angew. Chem., Int. Ed.*, 2010, **49**, 1227–1230.
- M. E. Ostergaard, J. Maity, B. R. Babu, J. Wengel and P. J. Hrdlicka, *Bioorg. Med. Chem. Lett.*, 2010, **20**, 7265–7268.
- Y. V. Gerasimova, A. Hayson, J. Ballantyne and D. M. Kolpashchikov, *ChemBioChem*, 2010, **11**, 1762–1768.
- S. P. Sau, T. S. Kumar and P. J. Hrdlicka, *Org. Biomol. Chem.*, 2010, **8**, 2028–2036.
- Y. N. Teo, J. N. Wilson and E. T. Kool, *J. Am. Chem. Soc.*, 2009, **131**, 3923–3933.
- F. Seela and S. A. Ingale, *J. Org. Chem.*, 2010, **75**, 284–295.
- L. Wang, C. Y. J. Yang, C. D. Medley, S. A. Benner and W. H. Tan, *J. Am. Chem. Soc.*, 2005, **127**, 15664–15665.

- 33 C. Crey-Desbiolles, D. R. Ahn and C. J. Leumann, *Nucleic Acids Res.*, 2005, **33**, e77.
- 34 K. Yamana, Y. Ohshita, Y. Fukunaga, M. Nakamura and A. Maruyama, *Bioorg. Med. Chem.*, 2008, **16**, 78–83.
- 35 P. P. Sheng, Z. Y. Yang, Y. M. Kim, Y. R. Wu, W. H. Tan and S. A. Benner, *Chem. Commun.*, 2008, 5128–5130.
- 36 J. Chen, T. W. B. Liu, P. C. Lo, B. C. Wilson and G. Zheng, *Bioconjugate Chem.*, 2009, **20**, 1836–1842.
- 37 K. Matsumoto, Y. Shinohara, S. S. Bag, Y. Takeuchi, T. Morii, Y. Saito and I. Saito, *Bioorg. Med. Chem. Lett.*, 2009, **19**, 6392–6395.
- 38 L. Bethge, I. Singh and O. Seitz, *Org. Biomol. Chem.*, 2010, **8**, 2439–2448.
- 39 S. M. Langenegger and R. Häner, *Helv. Chim. Acta*, 2002, **85**, 3414–3421.
- 40 S. M. Langenegger and R. Häner, *Chem. Commun.*, 2004, 2792–2793.
- 41 S. M. Langenegger and R. Häner, *ChemBioChem*, 2005, **6**, 2149–2152.
- 42 S. M. Langenegger and R. Häner, *Bioorg. Med. Chem. Lett.*, 2006, **16**, 5062–5065.
- 43 V. L. Malinovskii, F. Samain and R. Häner, *Angew. Chem., Int. Ed.*, 2007, **46**, 4464–4467.
- 44 I. Trkulja and R. Häner, *J. Am. Chem. Soc.*, 2007, **129**, 7982–7989.
- 45 R. Häner, F. Samain and V. L. Malinovskii, *Chem.–Eur. J.*, 2009, **15**, 5701–5708.
- 46 R. Häner, F. Garo, D. Wenger and V. L. Malinovskii, *J. Am. Chem. Soc.*, 2010, **132**, 7466–7471.
- 47 D. Wenger, V. L. Malinovskii and R. Häner, *Chem. Commun.*, 2011, DOI: 10.1039/c0cc05125j.
- 48 V. L. Malinovskii and R. Häner, *Eur. J. Org. Chem.*, 2006, 3550–3553.
- 49 H. Bittermann, D. Siegmund, V. L. Malinovskii and R. Häner, *J. Am. Chem. Soc.*, 2008, **130**, 15285–15287.
- 50 S. Werder, V. L. Malinovskii and R. Häner, *Org. Lett.*, 2008, **10**, 2011–2014.
- 51 V. A. Galievsky, V. L. Malinovskii, A. S. Stasheuski, F. Samain, K. A. Zachariasse, R. Häner and V. S. Chirvony, *Photochem. Photobiol. Sci.*, 2009, **8**, 1448–1454.
- 52 S. Uno, C. Dohno, H. Bittermann, V. L. Malinovskii, R. Häner and K. Nakatani, *Angew. Chem., Int. Ed.*, 2009, **48**, 7362–7365.
- 53 N. Bouquin, V. L. Malinovskii and R. Häner, *Chem. Commun.*, 2008, 1974–1976.
- 54 C. A. Hunter and J. K. M. Sanders, *J. Am. Chem. Soc.*, 1990, **112**, 5525–5534.
- 55 E. A. Meyer, R. K. Castellano and F. Diederich, *Angew. Chem., Int. Ed.*, 2003, **42**, 1210–1250.
- 56 J. Rebek, *Acc. Chem. Res.*, 2009, **42**, 1660–1668.
- 57 H. J. Schneider, *Angew. Chem., Int. Ed.*, 2009, **48**, 3924–3977.
- 58 N. Sakai, J. Mareda and S. Matile, *Acc. Chem. Res.*, 2008, **41**, 1354–1365.
- 59 J. D. Badjic, A. Nelson, S. J. Cantrill, W. B. Turnbull and J. F. Stoddart, *Acc. Chem. Res.*, 2005, **38**, 723–732.
- 60 J. K. Klosterman, Y. Yamauchi and M. Fujita, *Chem. Soc. Rev.*, 2009, **38**, 1714–1725.
- 61 V. L. Malinovskii, D. Wenger and R. Häner, *Chem. Soc. Rev.*, 2010, **39**, 410–422.
- 62 S. Grimme, *Angew. Chem., Int. Ed.*, 2008, **47**, 3430–3434.
- 63 I. Trkulja and R. Häner, *Bioconjugate Chem.*, 2007, **18**, 289–292.
- 64 F. Samain, V. L. Malinovskii, S. M. Langenegger and R. Häner, *Bioorg. Med. Chem.*, 2008, **16**, 27–33.
- 65 K. I. Shaikh, C. S. Madsen, L. J. Nielsen, A. S. Jorgensen, H. Nielsen, M. Petersen and P. Nielsen, *Chem.–Eur. J.*, 2010, **16**, 12904–12919.
- 66 A. Mammanna, G. Pescitelli, T. Asakawa, S. Jockusch, A. G. Petrovic, R. R. Monaco, R. Purrello, N. J. Turro, K. Nakanishi, G. A. Ellestad, M. Balaz and N. Berova, *Chem.–Eur. J.*, 2009, **15**, 11853–11866.
- 67 P. P. Neelakandan, Z. Pan, M. Hariharan, Y. Zheng, H. Weissman, B. Rybtchinski and F. D. Lewis, *J. Am. Chem. Soc.*, 2010, **132**, 15808–15813.
- 68 A. W. I. Stephenson, N. Bomholt, A. C. Partridge and V. V. Filichev, *ChemBioChem*, 2010, **11**, 1833–1839.
- 69 I. Bouamaied, T. Nguyen, T. Ruhl and E. Stulz, *Org. Biomol. Chem.*, 2008, **6**, 3888–3891.
- 70 H. Langhals and R. Ismael, *Eur. J. Org. Chem.*, 1998, 1915–1917.
- 71 A. D. Q. Li, W. Wang and L. Q. Wang, *Chem.–Eur. J.*, 2003, **9**, 4594–4601.
- 72 Y. Zheng, H. Long, G. C. Schatz and F. D. Lewis, *Chem. Commun.*, 2005, 4795–4797.
- 73 W. Wang, L. S. Li, G. Helms, H. H. Zhou and A. D. Q. Li, *J. Am. Chem. Soc.*, 2003, **125**, 1120–1121.
- 74 T. E. Kaiser, V. Stepanenko and F. Würthner, *J. Am. Chem. Soc.*, 2009, **131**, 6719–6732.
- 75 M. A. Abdalla, J. Bayer, J. O. Radler and K. Müllen, *Angew. Chem., Int. Ed.*, 2004, **43**, 3967–3970.
- 76 F. Würthner, C. Thalacker, S. Diele and C. Tschierske, *Chem.–Eur. J.*, 2001, **7**, 2245–2253.
- 77 T. A. Zeidan, M. Hariharan, K. Siegmund and F. D. Lewis, *Photochem. Photobiol. Sci.*, 2010, **9**, 916–922.
- 78 N. Berova, K. Nakanishi and R. W. Woody, *Circular Dichroism – Principles and Applications*, 2nd edn, Wiley-VCH, New York, 2000.
- 79 N. Berova, L. Di Bari and G. Pescitelli, *Chem. Soc. Rev.*, 2007, **36**, 914–931.
- 80 D. B. Amabilino and J. F. Stoddart, *Chem. Rev.*, 1995, **95**, 2725–2828.
- 81 K. M. Guckian, B. A. Schweitzer, R. X. F. Ren, C. J. Sheils, D. C. Tahmassebi and E. T. Kool, *J. Am. Chem. Soc.*, 2000, **122**, 2213–2222.
- 82 C. A. Hunter, K. R. Lawson, J. Perkins and C. J. Urch, *J. Chem. Soc., Perkin Trans. 2*, 2001, 651–669.
- 83 J. J. Rezek and B. L. Iverson, *Macromolecules*, 2006, **39**, 5601–5603.
- 84 A. L. Sisson, N. Sakai, N. Banerji, A. Furstenberg, E. Vauthey and S. Matile, *Angew. Chem., Int. Ed.*, 2008, **47**, 3727–3729.
- 85 F. Cozzi, F. Ponzini, R. Annunziata, M. Cinquini and J. S. Siegel, *Angew. Chem., Int. Ed. Engl.*, 1995, **34**, 1019–1020.
- 86 G. W. Coates, A. R. Dunn, L. M. Henling, D. A. Dougherty and R. H. Grubbs, *Angew. Chem., Int. Ed. Engl.*, 1997, **36**, 248–251.
- 87 A. P. West, S. Mecozzi and D. A. Dougherty, *J. Phys. Org. Chem.*, 1997, **10**, 347–350.
- 88 F. Ponzini, R. Zaghera, K. Hardcastle and J. S. Siegel, *Angew. Chem., Int. Ed.*, 2000, **39**, 2323–2325.
- 89 G. Mathis and J. Hunziker, *Angew. Chem., Int. Ed.*, 2002, **41**, 3203–3205.
- 90 N. S. S. Kumar, M. D. Gujrati and J. N. Wilson, *Chem. Commun.*, 2010, **46**, 5464–5466.
- 91 H. M. Colquhoun, Z. X. Zhu and D. J. Williams, *Org. Lett.*, 2003, **5**, 4353–4356.
- 92 B. W. Greenland, S. Burattini, W. Hayes and H. M. Colquhoun, *Tetrahedron*, 2008, **64**, 8346–8354.
- 93 T. Murase, K. Otsuka and M. Fujita, *J. Am. Chem. Soc.*, 2010, **132**, 7864–7865.
- 94 S. Bhosale, A. L. Sisson, P. Talukdar, A. Furstenberg, N. Banerji, E. Vauthey, G. Bollot, J. Mareda, C. Roger, F. Würthner, N. Sakai and S. Matile, *Science*, 2006, **313**, 84–86.
- 95 S. V. Bhosale, C. H. Jani and S. J. Langford, *Chem. Soc. Rev.*, 2008, **37**, 331–342.
- 96 V. Balzani, A. Credi, F. M. Raymo and J. F. Stoddart, *Angew. Chem., Int. Ed.*, 2000, **39**, 3349–3391.
- 97 W. R. Browne and B. L. Feringa, *Nat. Nanotechnol.*, 2006, **1**, 25–35.
- 98 E. R. Kay, D. A. Leigh and F. Zerbetto, *Angew. Chem., Int. Ed.*, 2007, **46**, 72–191.
- 99 N. Rahe, C. Rinn and T. Carell, *Chem. Commun.*, 2003, 2120–2121.

DOI: 10.1002/cbic.201100651

A Two-Color, Self-Controlled Molecular Beacon

Sarah M. Biner and Robert Häner*^[a]

The reliable detection of DNA and RNA sequences is of major interest for the design of future diagnostic tools. The use of hybridization probes, such as molecular beacons (MBs), to quantify or localize genes is widespread in the biological and medicinal sciences.^[1–4] The principle of the classical MB, first proposed by Tyagi and Kramer,^[5,6] is based on a stem-loop structure containing terminally attached fluorophore and quencher moieties that form a FRET pair. The interplay of the two dyes is controlled by the secondary structure of the beacon and results in the diagnostic read-out.^[1–3,6–11] The quality of the signal depends on several factors including the sequence of the beacon, the choice of the dye molecules and the stability of the stem-loop structure. Any unwanted dissociation of the fluorophore–quencher pair will directly lead to a loss in sensitivity and specificity of the beacon. Therefore, the design of the stem is of particular importance for the success of the MB. Several approaches addressing this issue have been proposed over the past years.^[12–28] We present herein a MB with two different fluorophores, 1,8-dialkynylpyrene (Y) and perylene-3,9,10,10-tetracarboxylic diimide (PDI, E),^[25,26,29] arranged in a triple-helical stem.^[30–34] In the closed form, the dyes engage in a donor–acceptor–donor (Y–E–Y) interaction^[35–44] resulting in a mutual quenching of the two fluorophores. Binding of the beacon to the target sequence disrupts the triple helix^[13] and generates a two-color fluorescent hybrid. The principle is illustrated in Figure 1.

The triple-helical stem design involves the formation of one C+GC and two TAT base triplets. In this setup, the PDI is embedded in a stretch of thymidines, whereas the pyrenes are attached to the 5'-end of the MB. The stacking interaction between PDI and pyrenes in the closed form is demonstrated by UV/Vis spectroscopy (Figure 2). A clear blue-shift is observed upon melting of the triple-helical stem in the PDI region (440–600 nm). Hyperchromicity is observed for both PDI and for pyrene (320–420 nm). The A^{0-0}/A^{0-1} ratio, which serves as a measure for the aggregation state of PDI^[45–49] and 1,8-dialkynylpyrene,^[26,50] changed in accordance with our expectations (Supporting Information).

As mentioned, the two fluorophores quench each other in the closed form of the MB. Separation of the dyes results in an increase in PDI and pyrene fluorescence. Figure 3 shows the emission spectra resulting from hybridization of the MB with the target. Both fluorophores exhibit fluorescence emission proportional to the target concentration. For pyrene (Figure 3, top) both, monomer and excimer fluorescence are observed.

[a] S. M. Biner, Prof. Dr. R. Häner
Department of Chemistry and Biochemistry, University of Bern
Freiestrasse 3, 3012 Bern (Switzerland)
E-mail: robert.haener@ioc.unibe.ch

Supporting information for this article is available on the WWW under <http://dx.doi.org/10.1002/cbic.201100651>.

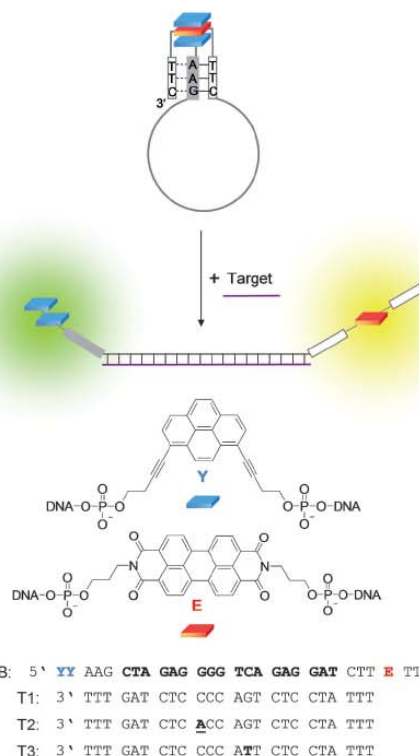


Figure 1. Top: Illustration of a dual-labeled, self-controlled molecular beacon; in the native form, a triple-helical stem supports the formation of a nonfluorescent pyrene–PDI–pyrene (Y–E–Y) stack. Disruption of the stem generates two fluorescence signals (pyrene excimer and PDI). Bottom: MB (bold: target region) and target DNA sequences T1–T3; (bold and underlined: mismatches).

The monomer contribution (380–460 nm) is comparatively large.^[26] This may be due to increased flexibility arising from the terminal location of the two pyrenes compared to a situation where the pyrenes are located at internal positions.^[26] Nevertheless, the excimer signal (emission maximum 520 nm) grows proportionally with the concentration of the target. The same behaviour is observed for PDI (530–680 nm). Also for this fluorophore, the signal increases with the concentration of the target. In the presence of 1.2 equivalents of target, a quantum yield (Φ_f) of approximately 0.028 is obtained (Supporting Information). This is in strong contrast to mixed sequences, in which context PDI is usually entirely quenched.^[29] In the current design of the triple-helical stem, the PDI is placed in between several thymidines,^[51] which has a similar effect to unnatural insulators.^[52] The simultaneous, hybridization-based ap-

CHEMBIOCHEM

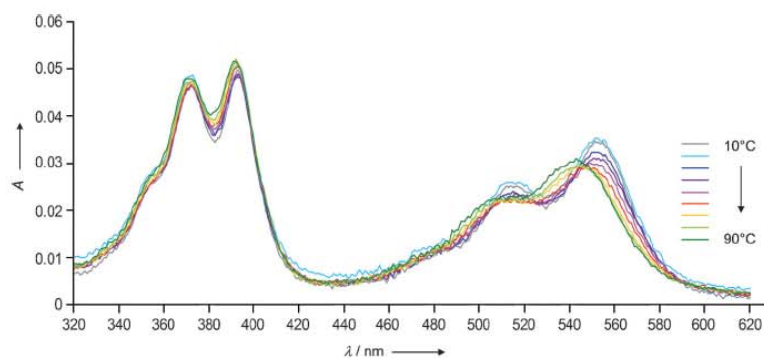


Figure 2. Temperature-dependent UV/Vis read-out obtained with MB (10^{-6} M). Conditions: acetate buffer (sodium acetate (10 mM), NaCl (100 mM), $MgCl_2$ (20 mM), pH 5.0).

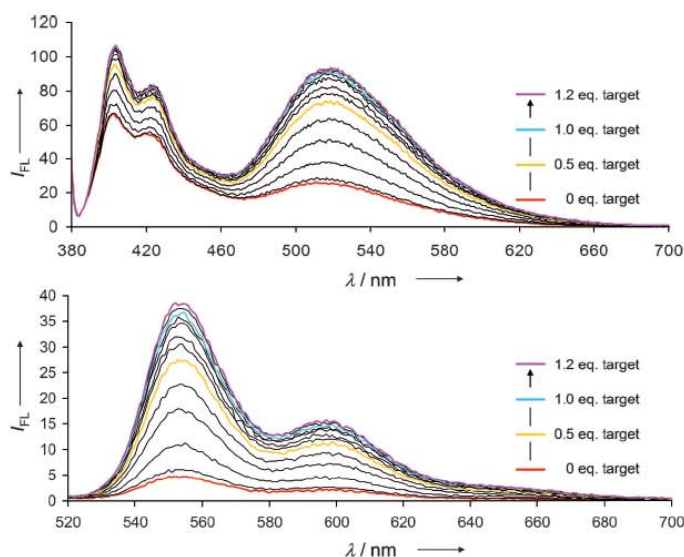


Figure 3. Fluorescence intensities obtained with MB (10^{-6} M) on hybridization with the target T1 (0.1 equiv increments). Conditions: see Figure 2. Instrument set-up: $\lambda_{ex}=370$ (top) and 505 nm (bottom), slit widths: 10/5 nm, 15 °C.

pearance of two independent fluorescence signals (pyrene and PDI) provides an efficient way of eliminating false positive signals. Thus, the two labels act not only as mutual suppressors in the closed form but also as internal references for each other in the presence of the target.

Thermal denaturation of the beacon shows the expected increase of both signal intensities upon heating. Melting of the triple-helical structure leads to the deaggregation of the chromophore stack, resulting in the parallel growth of the pyrene excimer and PDI signals (Supporting Information).

This system represents a self-controlled chromophoric system of two fluorescent labels that function as mutual quenchers. The quenching efficiencies are 64% (pyrene excimer) and 84% (PDI). Figure 4 shows the target-response curves of the beacon for the two chromophores. Both signals increase

with target concentration and reach a maximum at one equivalent.

The hybridization kinetics of molecular beacons is an important aspect which has been discussed in the literature.^[53] Triple helix formation^[54] is considerably slower than duplex formation. In order to ensure fast hybridization of the MB to the target, the triple-helical stem was kept as short as possible, that is, three base triplets. As shown in Figure 5, the signal response is very fast. The signal intensity of both labels reaches 80–90% (PDI: 81%; pyrene: 86%) of the maximum read-out immediately (<1 min) after addition of the target to the MB at 20 °C.

The selectivity of the molecular beacon was studied by temperature-variable fluorescence measurements in the presence of different targets (Figure 6). The hybrids containing mismatched targets (T2 and T3) show a loss in fluorescence intensity at lower temperature than the matched target sequence (T1).

In conclusion, a molecular beacon with a two-color read-out signal has been described. Signal control involves a triple-helical stem design. In the closed form, 1,8-dialkynylpyrene and PDI are arranged in a π -stacked complex and the two chromophores act as mutual fluorescence quenchers. Hybridization of the probe to a target sequence disrupts the chromophore complex resulting in two independent fluorescence sig-

nalities.

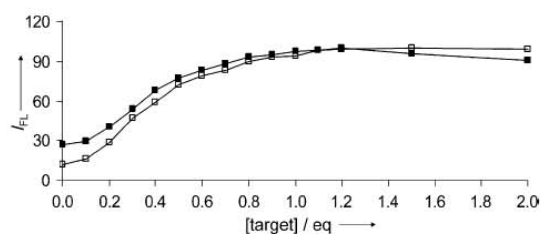


Figure 4. Concentration-dependent normalized signal intensities at 520 nm ($\lambda_{ex}=370$ nm, ■) and 553 nm ($\lambda_{ex}=505$ nm, □). Conditions: see Figure 2; instrumental set-up: see Figure 3.

COMMUNICATIONS

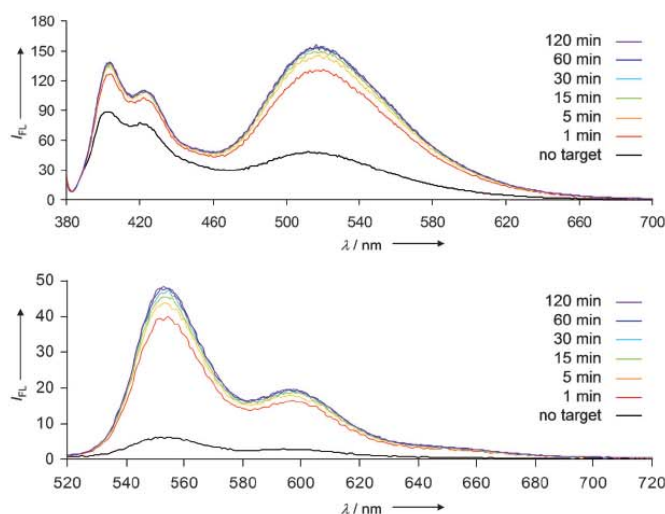


Figure 5. Time-dependent fluorescence read-out obtained with MB (10^{-6} M) upon hybridization with DNA target T1 (1.2 equiv). Conditions: see Figure 2. Instrument set-up: $\lambda_{\text{ex}}=505$ nm, slit widths: 10/5 nm, 20 °C.

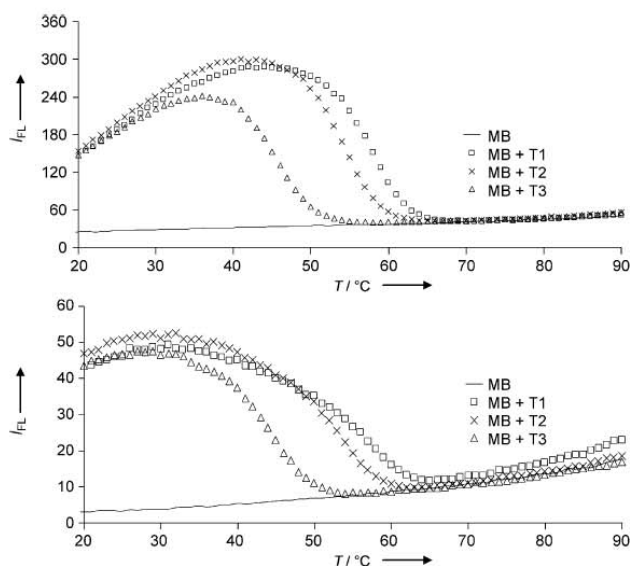


Figure 6. MB pyrene excimer emission (top) and PDI fluorescence read-out (bottom) in presence of matched (T1) and mismatched (T2, T3) targets. Conditions: MB (10^{-6} M), target (10^{-6} M). Instrumental set-up: $\lambda_{\text{ex1}}: 370$ nm (pyrene), $\lambda_{\text{em1}}: 520$ nm (top), $\lambda_{\text{ex2}}: 505$ nm (PDI), $\lambda_{\text{em2}}: 552$ nm (bottom), slit widths: 10/5 nm, PMT: 600 V.

nals. The combination of two detectable individual signals and their mutual quenching properties introduces a “self-control” feature, which might help to eliminate false positive signals in imaging and screening applications.

Experimental Section

The required pyrene^[50] and PDI^[55] building blocks were synthesized according to published procedures. Commercial natural nucleoside phosphoramidites were used for oligonucleotide synthesis. The target oligonucleotides (T1, T2 and T3) were purchased from Microsynth (Balgach, Switzerland). MB was prepared by automated oligonucleotide synthesis by a standard synthetic procedure (2 min coupling time; “trityl-off” mode) on a 394-DNA/RNA synthesizer (Applied Biosystems), except for the coupling step of the PDI phosphoramidite; an adapted activating step was used. Cleavage from the solid support and final deprotection was achieved by treatment with 30% NH_4OH solution at 55 °C overnight. Purification was achieved using reversed-phase HPLC (LiChrospher 100 RP-18, 5 μm , Merck; Kontron HPLC device; eluent A: $(\text{Et}_3\text{N})\text{OAc}$ (0.1 M, pH 7.4); eluent B: MeCN; elution at 40 °C; gradient 5–50% B over 30 min). Low resolution ESI-MS was performed with a Sciex QTrap (Applied Biosystems) in negative mode (acetonitrile/ H_2O (1:1) + 1% triethylamine). Fluorescence spectra were recorded on a Varian Cary Eclipse fluorescence spectrophotometer equipped with a Varian Cary block temperature controller using 1 x 1 cm quartz cuvettes. Varian Eclipse software was used to process the data. Temperature-dependent UV/Vis spectra were measured on a Varian Cary-100 Bio-UV/Vis spectrophotometer equipped with a Varian Cary block temperature controller and data were collected with Varian WinUV software, over the range of 200–700 nm at 10–90 °C in 10 °C increments.

Acknowledgements

Financial support by the Swiss National Foundation (Grant 200020–132581) is gratefully acknowledged.

Keywords: fluorescence · molecular beacon · perylenediimide · pyrene · triplex

- [1] R. T. Ranasinghe, T. Brown, *Chem. Commun.* **2005**, 5487–5502.
- [2] P. Santangelo, N. Nitin, G. Bao, *Ann. Biomed. Eng.* **2006**, *34*, 39–50.
- [3] K. M. Wang, Z. W. Tang, C. Y. J. Yang, Y. M. Kim, X. H. Fang, W. Li, Y. R. Wu, C. D. Medley, Z. H. Cao, J. Li, P. Colon, H. Lin, W. H. Tan, *Angew. Chem.* **2009**, *121*, 870–885; *Angew. Chem. Int. Ed.* **2009**, *48*, 856–870.
- [4] B. Juskowiak, *Anal. Bioanal. Chem.* **2011**, *399*, 3157–3176.
- [5] S. Tyagi, D. P. Bratu, F. R. Kramer, *Nat. Biotechnol.* **1998**, *16*, 49–53.
- [6] S. Tyagi, F. R. Kramer, *Nat. Biotechnol.* **1996**, *14*, 303–308.
- [7] A. P. Silverman, E. T. Kool, *Trends Biotechnol.* **2005**, *23*, 225–230.
- [8] S. A. E. Marras, S. Tyagi, F. R. Kramer, *Clin. Chim. Acta* **2006**, *363*, 48–60.
- [9] N. Venkatesan, Y. J. Seo, B. H. Kim, *Chem. Soc. Rev.* **2008**, *37*, 648–663.

CHEMBIOCHEM

- [10] W. H. Tan, K. M. Wang, T. J. Drake, *Curr. Opin. Chem. Biol.* **2004**, *8*, 547–553.
- [11] Y. V. Gerasimova, A. Hayson, J. Ballantyne, D. M. Kolpashchikov, *ChemBioChem* **2010**, *11*, 1762–1768.
- [12] O. Seitz, *Angew. Chem.* **2000**, *112*, 3389–3392; *Angew. Chem. Int. Ed.* **2000**, *39*, 3249–3252.
- [13] T. N. Grossmann, L. Roglin, O. Seitz, *Angew. Chem.* **2007**, *119*, 5315–5318; *Angew. Chem. Int. Ed.* **2007**, *46*, 5223–5225.
- [14] E. Socher, L. Bethge, A. Knoll, N. Jungnick, A. Herrmann, O. Seitz, *Angew. Chem.* **2008**, *120*, 9697–9701; *Angew. Chem. Int. Ed.* **2008**, *47*, 9555–9559.
- [15] H. Kuhn, V. V. Demidov, J. M. Coull, M. J. Fiandaca, B. D. Gildea, M. D. Frank-Kamenetskii, *J. Am. Chem. Soc.* **2002**, *124*, 1097–1103.
- [16] K. R. Fox, T. Brown, *Quart. Rev. Biophys.* **2005**, *38*, 311–320.
- [17] L. Wang, C. Y. J. Yang, C. D. Medley, S. A. Benner, W. H. Tan, *J. Am. Chem. Soc.* **2005**, *127*, 15664–15665.
- [18] C. Crey-Desbiolles, D. R. Ahn, C. J. Leumann, *Nucleic Acids Res.* **2005**, *33*, e77.
- [19] Y. W. Lin, H. T. Ho, C. C. Huang, H. T. Chang, *Nucleic Acids Res.* **2008**, *36*.
- [20] Y. Saito, Y. Shinohara, S. S. Bag, Y. Takeuchi, K. Matsumoto, I. Saito, *Tetrahedron* **2009**, *65*, 934–939.
- [21] Y. Ueno, A. Kawamura, K. Takasu, S. Komatsuzaki, T. Kato, S. Kuboe, Y. Kitamura, Y. Kitade, *Org. Biomol. Chem.* **2009**, *7*, 2761–2769.
- [22] Y. Xiao, K. J. I. Plakos, X. H. Lou, R. J. White, J. R. Qian, K. W. Plaxco, H. T. Soh, *Angew. Chem.* **2009**, *121*, 4418–4422; *Angew. Chem. Int. Ed.* **2009**, *48*, 4354–4358.
- [23] H. Kashida, T. Takatsu, T. Fujii, K. Sekiguchi, X. G. Liang, K. Niwa, T. Takase, Y. Yoshida, H. Asanuma, *Angew. Chem.* **2009**, *121*, 7178–7181; *Angew. Chem. Int. Ed.* **2009**, *48*, 7044–7047.
- [24] I. Trkulja, S. M. Biner, S. M. Langenegger, R. Häner, *ChemBioChem* **2007**, *8*, 25–27.
- [25] R. Häner, S. M. Biner, S. M. Langenegger, T. Meng, V. L. Malinovskii, *Angew. Chem.* **2010**, *122*, 1249–1252; *Angew. Chem. Int. Ed.* **2010**, *49*, 1227–1230.
- [26] S. M. Biner, D. Kummer, V. L. Malinovskii, R. Häner, *Org. Biomol. Chem.* **2011**, *9*, 2628–2633.
- [27] C. Holzhauser, H. A. Wagenknecht, *Angew. Chem.* **2011**, *123*, 7406–7410; *Angew. Chem. Int. Ed.* **2011**, *50*, 7268–7272.
- [28] J. Ren, H. Qin, J. Wang, N. Luedtke, E. Wang, J. Wang, *Anal. Bioanal. Chem.* **2011**, *399*, 2763–2770.
- [29] N. Bouquin, V. L. Malinovskii, R. Häner, *Chem. Commun.* **2008**, 1974–1976.
- [30] G. Felsenfeld, D. R. Davies, A. Rich, *J. Am. Chem. Soc.* **1957**, *79*, 2023–2024.
- [31] I. Trkulja, R. Häner, *Bioconjugate Chem.* **2007**, *18*, 289–292.
- [32] I. Trkulja, R. Häner, *J. Am. Chem. Soc.* **2007**, *129*, 7982–7989.
- [33] N. T. Thuong, C. Helene, *Angew. Chem.* **1993**, *105*, 697–723; *Angew. Chem. Int. Ed. Engl.* **1993**, *32*, 666–690.
- [34] H. E. Moser, P. B. Dervan, *Science* **1987**, *238*, 645–650.
- [35] C. A. Hunter, J. K. M. Sanders, *J. Am. Chem. Soc.* **1990**, *112*, 5525–5534.
- [36] R. S. Lokey, B. L. Iverson, *Nature* **1995**, *375*, 303–305.
- [37] G. Mathis, J. Hunziker, *Angew. Chem.* **2002**, *114*, 3335–3338; *Angew. Chem. Int. Ed.* **2002**, *41*, 3203–3205.
- [38] S. Bhosale, A. L. Sisson, P. Talukdar, A. Furstenberg, N. Banerji, E. Vauthey, G. Bollot, J. Mareda, C. Roger, F. Wurthner, N. Sakai, S. Matile, *Science* **2006**, *313*, 84–86.
- [39] J. J. Reczek, B. L. Iverson, *Macromolecules* **2006**, *39*, 5601–5603.
- [40] E. A. Meyer, R. K. Castellano, F. Diederich, *Angew. Chem.* **2003**, *115*, 1244–1287; *Angew. Chem. Int. Ed.* **2003**, *42*, 1210–1250.
- [41] W. Y. Zhang, W. R. Dichtel, A. Z. Stieg, D. Benitez, J. K. Gimzewski, J. R. Heath, J. F. Stoddart, *Proc. Natl. Acad. Sci. USA* **2008**, *105*, 6514–6519.
- [42] Z. Merican, K. D. Johnstone, M. J. Gunter, *Org. Biomol. Chem.* **2008**, *6*, 2534–2543.
- [43] J. K. Klosterman, Y. Yamauchi, M. Fujita, *Chem. Soc. Rev.* **2009**, *38*, 1714–1725.
- [44] S. Shirai, S. Iwata, T. Tani, S. Inagaki, *J. Phys. Chem. A* **2011**, *115*, 7687–7699.
- [45] H. Langhals, *Helv. Chim. Acta* **2005**, *88*, 1309–1343.
- [46] F. Würthner, *Chem. Commun.* **2004**, 1564–1579.
- [47] A. D. Q. Li, W. Wang, L. Q. Wang, *Chem. Eur. J.* **2003**, *9*, 4594–4601.
- [48] Y. Zheng, H. Long, G. C. Schatz, F. D. Lewis, *Chem. Commun.* **2005**, 4795–4797.
- [49] M. A. Abdalla, J. Bayer, J. O. Radler, K. Müllen, *Angew. Chem.* **2004**, *116*, 4057–4060; *Angew. Chem. Int. Ed.* **2004**, *43*, 3967–3970.
- [50] H. Bittermann, D. Siegemund, V. L. Malinovskii, R. Häner, *J. Am. Chem. Soc.* **2008**, *130*, 15285–15287.
- [51] Y. Paukku, G. Hill, *J. Phys. Chem. A* **2011**, *115*, 4804–4810.
- [52] a) J. N. Wilson, Y. J. Cho, S. Tan, A. Cuppoletti, E. T. Kool, *ChemBioChem* **2008**, *9*, 279–285; b) H. Kashida, K. Sekiguchi, H. Asanuma, *Chem. Eur. J.* **2010**, *16*, 11554–11557.
- [53] A. Tsourkas, M. A. Behlke, S. D. Rose, G. Bao, *Nucleic Acids Res.* **2003**, *31*, 1319–1330.
- [54] V. N. Soyfer, V. N. Potaman, *Triple-Helical Nucleic Acids*, Springer, New York, **1996**.
- [55] N. Rahe, C. Rinn, T. Carell, *Chem. Commun.* **2003**, 2119–2121.

Received: October 17, 2011

Published online on November 11, 2011

A.3 Curriculum Vitae

Personal details

Contact: Sarah Maria BINER
Feld 51
3924 St.Niklaus (VS)
sarah.biner@ioc.unibe.ch

Date of birth: 16th of december 1981

Nationality: Swiss



Education

02/08 – 03/12 Ph.D work in the group of Prof. Dr. Robert Häner
Department of Chemistry and Biochemistry / University of Bern

10/06 – 12/07 „Master of Science in Chemistry and Molecular Science“ (M Sc).
Main modul: Material Science – Physical Chemistry

12/07 Masterthesis: *Investigation of mercury (Hg) behaviour in seasonal snow cover at the Jungfraujoch.*
At the Department of Chemistry and Biochemistry / University of Bern and in the Laboratory for Radiochemistry and Environmental Chemistry at the Paul Scherrer Instituts (PSI) in Villigen.
Supervisor: Prof. Dr. Heinz W. Gäggeler

10/03 – 06/06 „Bachelor of Science in Chemistry and Molecular Science“ (B Sc).
06/06 Bachelorthesis: *DNA Triplex Mimics: Excimer forming clamps.*
At the Department of Chemistry and Biochemistry / University of Bern.
Supervisor: Prof. Dr. Robert Häner

08/99 – 07/03 Matura, at the „Kollegium Spiritus Sanctus“ in Brig, VS
Major subject: Chemistry and Biology
Minor subject: Sculptural design and art history

A.4 Erklärung**Erklärung**

gemäß Art. 28 Abs. 2 RSL 05

Name/Vorname: BINER Sarah Maria

Matrikelnummer: 03-102-910

Studiengang: Chemie & Molekulare Wissenschaften

Bachelor Master Dissertation


Titel der Arbeit: DNA-mediated Arrangement of Chromophores - Potential Use for Diagnostic Applications

LeiterIn der Arbeit: Prof. Dr. Robert HÄNER

Ich erkläre hiermit, dass ich diese Arbeit selbständig verfasst und keine anderen als die angegebenen Quellen benutzt habe. Alle Stellen, die wörtlich oder sinngemäss aus Quellen entnommen wurden, habe ich als solche gekennzeichnet. Mir ist bekannt, dass andernfalls der Senat gemäss Artikel 36 Absatz 1 Buchstabe o des Gesetzes vom 5. September 1996 über die Universität zum Entzug des auf Grund dieser Arbeit verliehenen Titels berechtigt ist.

Bern, 21.02.2012

Ort/Datum


Unterschrift

The End
